POLYTECHNIQUE MONTRÉAL

affiliée à l'Université de Montréal

The Biopigment Eumelanin in the Sustainability Challenge: Interfaces with Metal Electrodes, UV-Absorption Enhancement of Plastics and its Biodegradability

EDUARDO DI MAURO

Département de génie physique

Thèse présentée en vue de l'obtention du diplôme de *Philosophiae Doctor*

Génie physique

Mai 2019

POLYTECHNIQUE MONTRÉAL

affiliée à l'Université de Montréal

Cette thèse intitulée :

The Biopigment Eumelanin in the Sustainability Challenge: Interfaces with Metal Electrodes, UV-Absorption Enhancement of Plastics and its Biodegradability

présentée par **Eduardo DI MAURO**

en vue de l'obtention du diplôme de *Philosophiae Doctor*

a été dûment acceptée par le jury d'examen constitué de :

Alain ROCHEFORT, président

Clara SANTATO, membre et directrice de recherche

Fabio CICOIRA, membre et codirecteur de recherche

Noémie-Manuelle DORVAL COURCHESNE, membre

Rafael A. AURAS, membre externe

ACKNOWLEDGEMENTS

RÉSUMÉ

L'Organisation des Nations Unies (ONU) définit le développement durable comme la capacité d'une génération de satisfaire ses propres besoins « sans compromettre la possibilité des générations suivantes de satisfaire les leurs ». Le domaine de l'électronique est marqué par la croissance effrénée des déchets d'équipements électriques et électroniques (DEEE) et par l'épuisement des ressources nécessaires à la fabrication des EEE. L'utilisation de matériaux organiques (constitués de carbone) naturels (biosourcés), biodégradables et traités à l'aide de solvants non toxiques, est alors une solution à considérer pour réduire l'empreinte écologique de l'électronique.

L'eumélanine, sous-catégorie noire/marron de la mélanine (pigment omniprésent dans la faune et la flore), présente une absorption optique étendue sur les spectres ultraviolet (UV) et visible, une réponse électrique dépendante du niveau d'hydratation, des propriétés de chélation des métaux et de piégeage des radicaux ainsi qu'une structure moléculaire qui comporte des groupements fonctionnels redox.

L'eumélanine est donc un matériau prometteur dans l'électronique organique verte. L'électronique organique utilise des matériaux conducteurs ou semiconducteurs à base de carbone, qui présentent une alternance de liaisons simples et doubles carbone-carbone (systèmes conjugués). Ces matériaux, outre leur flexibilité mécanique, peuvent être traités en solution. Les dispositifs à base de matériaux organiques se distinguent, par conséquent, par leur faible énergie intrinsèque (l'énergie consommée pendant leur fabrication), comparés à la majorité des dispositifs à base de matériaux inorganiques pour lesquels le processus de fabrication implique de hautes températures et des très baisses pressions (vide élevé).

Les efforts pour rendre le développement plus durable concernent aussi les matériaux organiques isolants (plastiques) pour les emballages et leurs additifs nécessaires pour améliorer certaines propriétés telles que la stabilité thermique et l'absorption des rayons UV.

Le cœur de cette thèse est consacré à l'étude de plusieurs propriétés fonctionnelles de l'eumélanine dans le cadre d'une utilisation potentielle dans les technologies liées à l'électronique organique verte ainsi que dans le domaine des additifs plus respectueux de l'environnent pour les plastiques.

Le Chapitre 1 présente la mélanine, avec une attention particulière portée à l'eumélanine et ses propriétés. Le Chapitre 2 concerne l'état de l'art des potentielles applications de l'eumélanine qui

ont été prouvées dans la littérature. Les objectifs de la thèse sont énumérés dans le Chapitre 3 : l'étude des interfaces eumélanine/métal sous tension, l'évaluation de l'eumélanine comme additif pour un matériau plastique utilisé dans les emballages ainsi que l'étude de la biodégradation du biopigment. Le Chapitre 4 explique brièvement les techniques de caractérisation utilisées.

Dans les Chapitres 5 et 8 de cette thèse, les interfaces entre une électrode métallique (Au, Pd, Cu, Ni et Fe) et une couche d'eumélanine (synthétique et naturelle) hydratée ont été étudiées en configuration planaire (métal/eumélanine/métal), sous tension électrique, à différents degrés d'humidité relative, par microscopie à force atomique, microscopie électronique à balayage et spectrométrie de masse des ions secondaires en temps de vol. Ces interfaces ont une importance primordiale dans l'électronique verte : pour bien caractériser la réponse électrique intrinsèque des couches d'eumélanine, la stabilité de ces interfaces est indispensable (absence de phénomènes électrochimiques). L'étude des interfaces entre les couches de mélanine hydratées à un degré d'humidité relative de 90%, avec une teneur en chlorure similaire à celle de l'eumélanine naturelle, et les électrodes métalliques a révélé une dissolution possible de l'électrode ainsi que la formation de structures conductrices qui établissent un contact entre les électrodes dans le cas de l'Au, du Pd et du Cu. Une teneur en chlorure plus faible et un degré d'humidité relative plus bas causent l'absence de dissolution pour le Pd et Cu. Dans le cas de l'or, le changement de résistivité se produisant lorsqu'une structure établit un contact entre les électrodes peut être modulé par l'humidité relative. Le Ni présent, quant à lui, une forte dissolution localisée, mais aucune structure conductrice établissant un contact entre les électrodes n'est visible. Les électrodes de Fe présentent des instabilités sur de larges portions des électrodes, sans qu'il y ait formation de structures établissant un contact entre les électrodes. En résumé, les électrodes de Pd et Ni peuvent être utilisées pour la caractérisation de la réponse électrique de l'eumélanine à un degré d'humidité relative inférieure à 90%.

Dans le Chapitre 6, deux types d'eumélanine synthétiques et une naturelle ont été étudiées dans l'objectif d'améliorer l'absorption UV d'un copolymère commercial (éthylène-acétate de vinyle, EVA) utilisé dans les emballages. Avant d'être mélangée avec le polymère, l'eumélanine a subi un traitement chimique (*Melanin Free Acid*) pour augmenter sa dispersion dans le polymère et réduire son absorption dans le visible. De plus, les effets de l'exposition prolongée aux rayons UV ont été évalués par un test de vieillissement UV. Comme les polymères commerciaux incluent des additifs antioxydants, les effets synergétiques ou antagonistes de l'eumélanine avec l'antioxydant présent

dans l'EVA commercial (le butylhydroxytoluène) ont été étudiés à l'aide de l'analyse thermogravimétrique. L'ajout d'eumélanines synthétiques et d'eumélanine naturelle ont permis d'augmenter l'absorption UV du polymère commercial EVA. Toutefois, en raison de la réduction de la capacité à piéger les radicaux, causée par le traitement *Melanin Free Acid*, et de la génération de dérivés réactives de l'oxygène sous UVA, l'eumélanine a aussi fonctionné comme un photo pro-oxydant (elle a favorisé la photo-dégradation). L'optimisation du traitement chimique *Melanin Free Acid* est à considérer pour conserver la capacité de piéger les radicaux, afin que l'eumélanine puisse augmenter l'absorption UV et être un photo-stabilisant (empêcher la photo-dégradation).

Dans l'électronique, les matériaux et les dispositifs ont toujours été conçus de façon à privilégier leurs performances, avec peu d'attention accordée à leur devenir après utilisation. En revanche, dans l'électronique organique verte, la biodégradation comme possible scenario après utilisation est d'importance primordiale. Dans le Chapitre 7, nous avons réalisé une étude de biodégradabilité de l'eumélanine extraite de l'encre de seiche mélangée à du compost provenant de déchets municipaux, en conditions mésophiliques (25°C) et thermophiliques (compostage, 58°C). L'étude a aussi concerné deux matériaux synthétiques bien connus en électronique organique : la phtalocyanine de cuivre (Cu-PC) et le sulfure de polyphénylène (PPS). L'eumélanine a atteint un degré de biodégradation de 37% en conditions de compostage en 100 jours, alors que le Cu-Pc et PPS n'ont montré aucune biodégradation. Ce résultat a confirmé que recourir à des matériaux biosourcés est une option à considérer pour l'écoconception de dispositifs électroniques organiques biodégradables. Cependant, le seuil (90% de biodégradation en 6 mois) imposé par la norme ASTM D6400 (conçue pour les plastiques pour emballer et servir la nourriture) n'a pas été passé. Établir une norme internationale pour mesurer la biodégradabilité des matériaux de l'électronique organique serait primordial. Enfin, le degré presque négligeable de biodégradation de l'eumélanine à 25 °C (conditions similaires à un écosystème naturel) a démontré le besoin de confier les déchets organiques à des installations de compostage industrielles.

Pour conclure, dans cette thèse, trois différentes facettes du biopigment eumélanine ont été étudiées : ses interfaces avec électrodes métalliques sous tension, son utilisation comme additif pour les plastiques et sa biodégradabilité. Notre travail suggère que clarifier les liens structure moléculaire-propriétés, ainsi que contrôler la composition chimique des matériaux biosourcés, est primordial pour leur intégration dans des technologies plus vertes.

ABSTRACT

The United Nations define sustainability as the ability to meet one generation's needs "without compromising the ability of future generations to meet their own needs". The field of electronics features a dramatic increase of waste electrical and electronic equipment (WEEE) and the depletion of key elements necessary for EEE fabrication. The use of biodegradable organic (carbon-based) materials extracted from natural sources (bio-sourced) and processed with non-toxic solvents represents a valuable option to alleviate the environmental footprint of the electronic sector.

Eumelanin, a dark-brown subcategory of melanins (a ubiquitous biopigment in flora and fauna), features broad ultraviolet-visible absorption, hydration-dependent electrical response as well as metal chelation, radical scavenging and redox activity. Eumelanin is a promising candidate in the field of green (sustainable) organic electronics. Organic (plastic) electronics is based on carbon-based conducting and semiconducting polymers and small molecules that feature conjugation (alternance of single and double carbon-carbon bonds) in their molecular structure. In addition of being mechanically flexible, devices based on organic electronic materials can be solution-processable and thus stand for their lower embodied energy (i.e. "energy spent in the production phase and stored in the inner constituents") with respect to most inorganic ones, which are processed at high-temperature and under high-vacuum conditions.

Sustainability is an issue also in the field of (non-conducting) plastics for packaging, where it concerns not only the packaging polymers but also the additives needed to enhance certain properties, such as thermal stability or ultraviolet (UV) radiation absorption.

The core of this PhD thesis is devoted to the study of a number of functional properties of eumelanin in view of its use in sustainable organic electronic technologies as well as a greener additive for plastic packaging.

Chapter 1 gives an overview on melanins, with a focus on the subcategory eumelanin and its properties. Chapter 2 provides a review of the state of the art of the potential applications of eumelanin demonstrated in the literature. Chapter 3 details the targets of the research: the investigation of eumelanin-metal interfaces under bias, the study of eumelanin as an additive for plastics and the assessment of eumelanin's biodegradability. Chapter 4 briefly explains the characterization techniques used.

Chapters 5 and 8 of this thesis deal with interfaces between metal electrodes (Au, Pd, Cu, Ni and Fe) and hydrated films of different types of eumelanin (synthetic and natural). These interfaces are of paramount importance for applications in green electronics: the proper characterization of the intrinsic electrical response of eumelanin films requires indeed interface stability (absence of electrochemical processes). The metal/melanin interfaces were investigated in planar configuration (metal/eumelanin/metal), at different RH (relative humidity) levels, by atomic force microscopy (AFM), scanning electron microscopy (SEM) and time-of-flight secondary ion mass spectrometry (ToF-SIMS), after transient current measurements. We found that electrode dissolution and formation bridging structures take place at the interface with eumelanin films, with a chloride content similar to natural eumelanin, and hydrated at 90% RH, in the case of Au, Pd and Cu electrodes. Reducing the RH level and chloride content rules out the occurrence of dissolution for Pd and Cu. For Au, varying the RH level allows to modulate the change in resistivity that takes place when bridging structures connect one electrode to the other. Ni presented only very localized dissolution, with no formation of bridging structures. Fe presented instabilities over large sections of the electrodes, with no formation of bridging structures. All in all, Pd and Ni electrodes can be used for the characterization of eumelanin's electrical response, for RH levels lower than 90%.

In Chapter 6, synthetic as well as natural eumelanins were investigated as UV absorption enhancers of a commercial grade packaging polymer (ethylene-vinyl acetate copolymer, EVA). Prior to melt compounding with the polymer, eumelanin underwent the Melanin Free Acid (MFA) treatment to improve its dispersion in the polymer matrix and reduce its visible absorption. The effect of long-term UV exposure was evaluated by means of a UV-aging test. As commercial grade polymers contain anti-oxidants, possible synergistic or antagonistic effects between eumelanin and the anti-oxidant present in the commercial grade EVA (butylated hydroxytoluene) were studied using thermogravimetric analysis (TGA). Both synthetic and natural eumelanin proved to work as UV-absorption enhancers for the commercial grade EVA. However, due the reduced radical scavenging ability related the MFA treatment concomitant to reactive oxygen species (ROS) production under UVA irradiation, eumelanin also worked as a photo-prooxidant (i.e. favoring photodegradation). The optimization of the MFA treatment has to be envisaged, to keep the radical scavenging properties of eumelanin, so that it can work as UV-absorption enhancer and photostabilizer (i.e. hindering photodegradation).

In the field of electronics, materials and devices have been designed, so far, focusing mainly on the performance, with limited attention to the scenarios after service (end of life). As opposed to that, green organic electronics puts great emphasis on one of the possible end-of-life scenarios of materials and devices, i.e. biodegradation. In Chapter 7 we conducted a biodegradability study of eumelanin extracted from cuttlefish ink (Sepia Melanin) blended with compost from municipal waste, both under mesophilic (25 °C) and thermophilic (composting, 58 °C) conditions. The investigation under composting conditions was extended to two well-investigated synthetic organic electronic materials, copper (II) phthalocyanine (Cu-Pc) and poly(p-phenylensulphide) (PPS). Eumelanin reached a level of biodegradation of 37% in composting conditions in 100 days, strikingly higher than Cu-Pc and PPS, that showed no biodegradation. This result confirmed that recurring to bio-sourced materials can be a valuable option to eco-design biodegradable organic electronic devices. However, the threshold (90% in 6 months) set by the standard ASTM D6400 (that addresses plastics for packaging and food serving) was not passed. It would be paramount to have an international protocol to assess the biodegradability of organic electronic materials. The low level of biodegradation at 25 °C (conditions similar to a natural ecosystem) highlighted the need of sending organic waste to industrial composting facilities.

In conclusion, in this thesis, three different aspects of the biopigment eumelanin were investigated: metal/eumelanin interfaces under bias, its use as an additive for plastics and its biodegradability. Our work confirmed that elucidating the molecular structure-property relationship of bio-sourced materials and controlling their chemical composition (after extraction from natural sources) is paramount for their integration in greener technologies.

TABLE OF CONTENTS

LIST OF TABLES

LIST OF FIGURES

LIST OF SYMBOLS AND ABBREVIATIONS

AFM	Atomic force microscopy
ATR	Attenuated total reflection
BHT	Phenol, 2,6-bis(1,1-dimethylethyl)-4-methyl- or butylated hydroxytoluene
BLS®531	2-hydroxy-4-(octyloxy) benzophenone
Cu-Pc	Copper (II) phthalocyanine
DHI	5,6-dihydroxyindole
DHICA	5,6-dihydroxyindole-2-carboxylic acid
DMSO	Dimethyl sulfoxide
ECMs	Electrochemical metallization memory cells
EDX	Energy-dispersive X-ray spectroscopy
EVA	Ethylene-vinyl acetate copolymer
FT-IR	Fourier transform infrared spectroscopy
L-dopa	L-3-(3,4-dihydroxyphenyl)-alanine
NAA	Neutron activation analysis
NIR	Near infrared
NM	Neuromelanin
PC	Bisphenol A polycarbonate
PCL	Poly-ε-caprolactone
PE	Polyethylene
PHB	Polyhydroxy Butyrate
PI	Polyimide
PLA	Poly(lactic acid)
PMMA	Poly(methyl methacrylate)

PON   Peroxynitrate

PP   Polypropylene

PPS   Poly(p-phenylene sulphide)

PS   Polystyrene

PTT   Photothermal therapeutic agent

PVA   Poly(vinyl alcohol)

ReRAM   Resistive random access memories

RH   Relative humidity

ROS   Reactive oxygen species

SEM   Scanning electron microscopy

TGA   Thermogravimetric analysis

ToF-SIMS   Time of flight-secondary ion mass spectrometry

UV   Ultraviolet

WEEE   Waste electrical and electronic equipment

LIST OF APPENDICES

CHAPTER 1   INTRODUCTION

In our daily life, we might have already noticed black spots on moldy bread, black incrustations on shower curtains, dark parts of banana peels or the different complexations of human skin: in all such occasions, we came across melanin, a vast category of natural pigments [1], [2]. Even melanin's absence cannot pass unnoticed: albino animals have fascinated humans for centuries [3]. Melanins are biopigments present in humans, animals, plants and microorganisms, such as fungi and bacteria [2].

1.1 Classification

The first scientist to use the term *melanin* was the Swedish chemist Berzelius, in 1840, referring to black animal pigments [4]. The first classification categorized melanins based on the living beings where they could be found [5]: (i) eumelanin (from ancient Greek εὖ=well and μέλας=black) and pheomelanins (from ancient Greek φαιός=dusky, grey) present in humans and animals; (ii) allomelanins, present in plants and microorganisms.

The second classification, however, puts more emphasis on the chemistry of the pigments [2]. Melanins are "pigments of diverse structure and origin derived by the oxidation and polymerization of tyrosine in animals or phenolic compounds in lower organisms" (Figure 1.1, A) [2]. Several subgroups can be identified:

1. *Eumelanins* are "a black-brown subclass of insoluble melanin pigments derived at least in part from the oxidative polymerization of L-3-(3,4-dihydroxyphenyl)-alanine (L-dopa) from 5-6 dihydroxyindole (DHI) intermediates" [2] (Figure 1.1, B-D).
2. The term *pheomelanins* denotes a yellow to reddish-brown subgroup of melanin pigments containing sulfur. They are alkali-soluble, obtained from the oxidation of cysteinyl-dopa precursors (Figure 1.1, E) [2]. Their building blocks are benzothiazine and benzothiazole (Figure 1.1, F-G) [6].
3. The dark pigment *neuromelanin* (NM) forms from the oxidation of dopamine and other catecholamine[1] precursors within neurons [2] (Figure 1.1, H).

---

[1] Catecholamine = an amine covalently bonded to a benzene with two hydroxyl side groups at carbons 1 and 2.

4. *Pyomelanins* are "dark pigments produced by microorganisms mainly, but not exclusively, from 2,5-dihydroxyphenyl-acetate (homogentisate)" [2] (Figure 1.1, I).

Eumelanin, the type of melanin most studied by materials scientists, is the focus of this thesis.
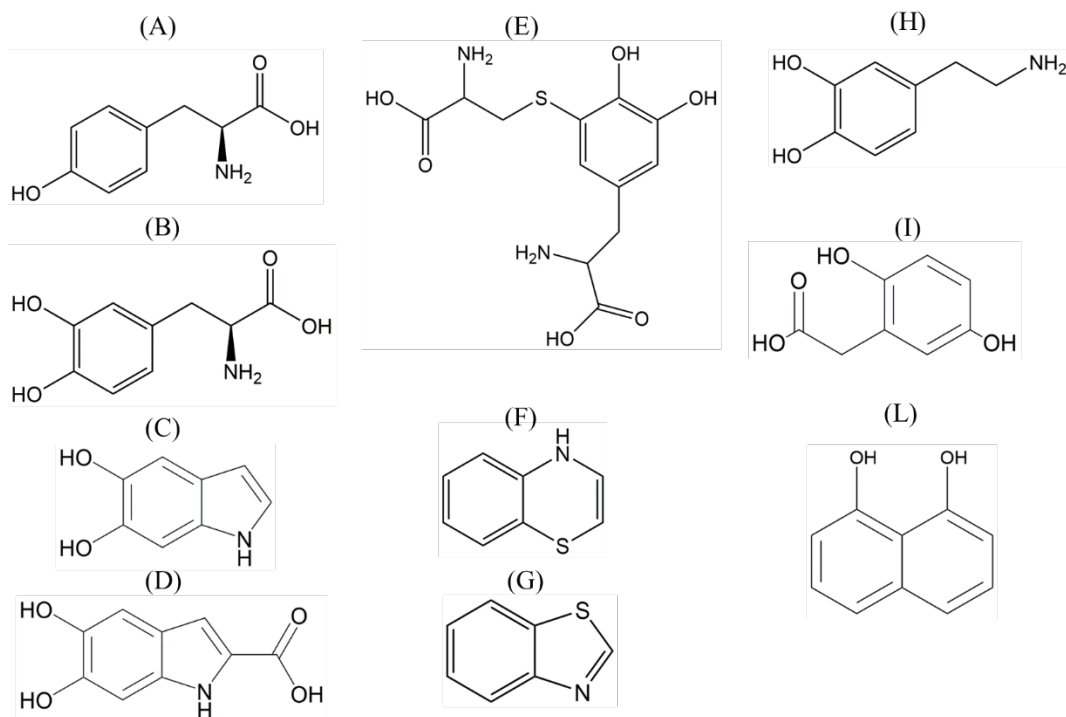
Figure 1.1: (A) 4-hydroxyphenylalanine, tyrosine; (B) L-3-(3,4-dihydroxyphenyl)-alanine, L-dopa; (C) 5-6 dihydroxyindole, DHI; (D) 5,6-dihydroxyindole-2-carboxylic acid, DHICA; (E) cynsteinyl-dopa; (F) benzothiazine; (G) benzothiazole; (H) 3,4-dihydroxyphenethylamine, dopamine; (I) homogentisic acid, (2,5-Dihydroxyphenyl)acetic acid); (L) 1,8-dihydroxynaphthalene, DHN.

1.2 Eumelanin

1.2.1 Eumelanin in the Biosphere

In vertebrates, eumelanins can be found in the epidermis, in the eyes, in the hairs, as well as in several internal parts of the body (spleen, liver, kidney, inner ear, lung, connective tissues, heart, peritoneum, muscles) [7] (Figure 1.2). NM is present in the brain of humans and large primates [8] (Figure 1.2).
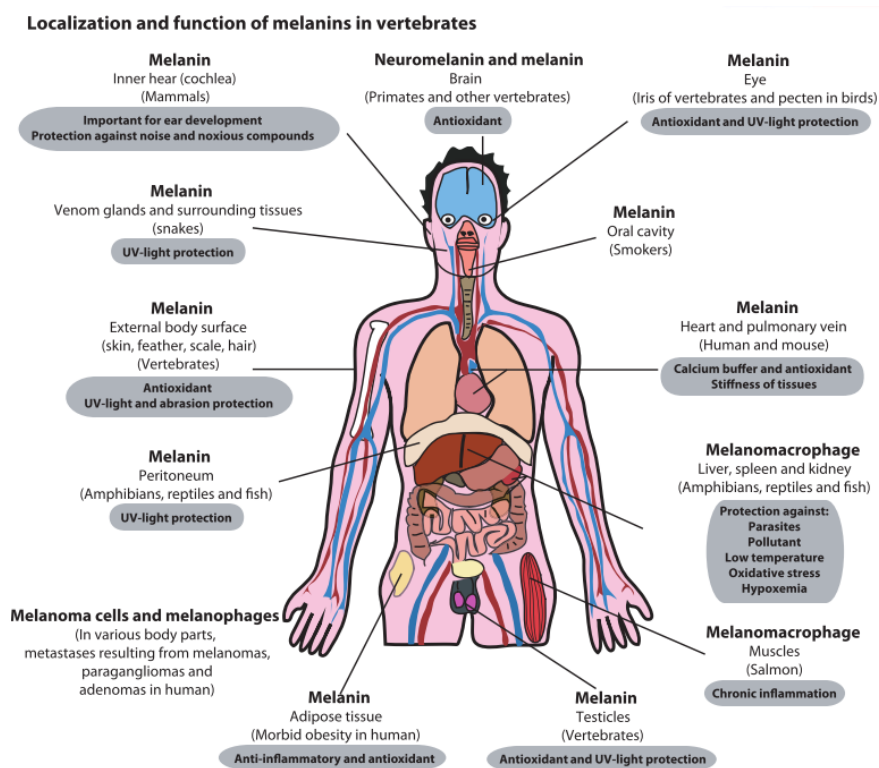
Figure 1.2 Localization and function of melanins in vertebrates. Reprinted with permission from Ref. [7].

Eumelanin can be found in invertebrates, too: cephalopods eject black ink to escape from predators. The black color is due to the presence of eumelanin. One of the most studied natural eumelanins is indeed Sepia Melanin, extracted from the ink sac of the cephalopod *Sepia officinalis* (cuttlefish) [9].

1.2.2 Skin Complexations

As melanins are the only pigments to be endogenously synthesized in humans (apart from hemoglobin), eumelanin synthesis has become synonym of pigmentation [10]. Melanogenesis in human epidermis is controlled by a very complex regulatory system [11]. Eumelanin in humans' epidermis blocks harmful ultraviolet (UV) radiation that can cause damage to the DNA as well as skin cancer and mitigates the effects of the radicals formed because of UV light [12]. However, the syntheses of the vitamin D_3 and some endorphins are mediated by UV light, so that a minimum amount of UV radiation is beneficial for the human body [12]. Consequently, depending on the

latitude (i.e. on the exposure to UV radiation), the human body developed an amount of eumelanin in the skin that is a trade-off between the need to block harmful UV radiation from one side, and, from the other, the need to absorb some UV radiation in the skin to promote the aforementioned photo-mediated syntheses. This trade-off explains why humans living at different latitudes developed differently pigmented skins: from eumelanin-rich pigmentations near the Equator (high levels of UV radiation exposure) to eumelanin-devoid skins outside of tropical latitudes (low levels of UV radiation exposure) [1]. As early as the IV century BC, Aristotle and his followers in their "climatic theory" had already mentioned an association between dark skin pigmentation with intense sunshine and heat [1].

1.2.3 Synthetic Pathways and Redox Forms

In humans, eumelanin is synthesized in specialized organelles of the cytoplasm (melanosomes), belonging to cells known as melanocytes [13]. Eumelanin's precursor is tyrosine (Figure 1.1, A), an amino acid. During eumelanin biosynthesis, tyrosine is oxidized to dopaquinone by the enzyme tyrosinase. From the intramolecular cyclization of dopaquinone, cyclodopa is formed which, following redox exchange with dopaquinone itself, produces dopachrome and L-dopa (Figure 1.1, B). This latter can be further enzymatically oxidized to dopaquinone (Figure 1.3).
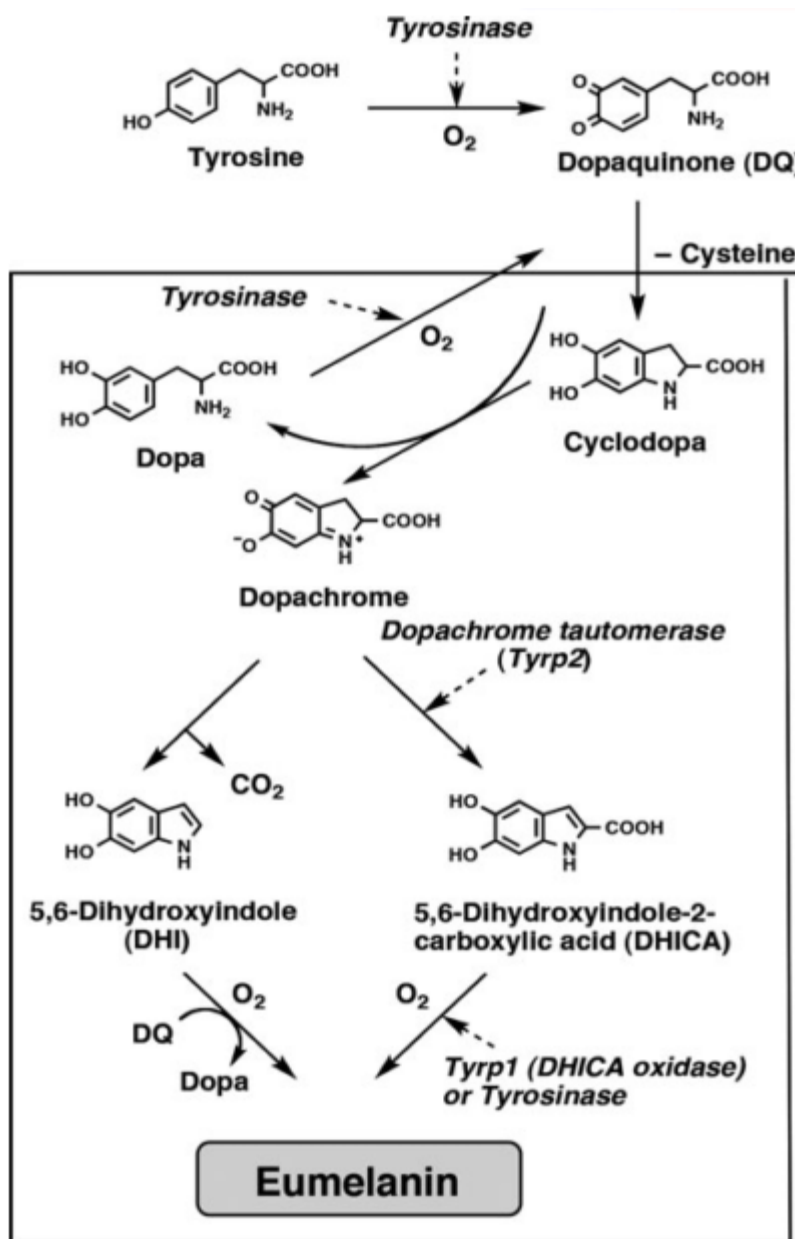
Figure 1.3 Biosynthetic pathway of eumelanin. Reprinted with permission from Ref. [14].

In presence of the enzyme dopachrome tautomerase (also known as tyrosine-related protein 2, Tyrp2), dopachrome isomerizes to DHICA (5,6-dihydroxyindole-2-carboxylic acid, Figure 1.1, D). In absence of enzymatic assistance, a spontaneous decarboxylation takes place to give DHI (5-6 dihydroxyindole) [15], [16] (Figure 1.1, C). The building blocks of eumelanin are thus DHI and DHICA [2].

Isolation of natural eumelanins has proven to be a challenging task [17]; nonetheless, it is possible to mimic their formation by synthetic procedures *in vitro* [18]. The oxidative polymerization of synthetic melanins does not stop until monomers are still available: already-polymerized eumelanin is always able to integrate in its structure new monomers, thus it acts as a "living bio-polymer" [19].

As early as in 1939, Figge reported about the redox properties of eumelanin as a natural reversible oxidation-reduction system and an intracellular redox indicator dye (i.e., its change in color indicates whether redox reactions related to certain enzymes' activity took place) [20]. Eumelanin was demonstrated to be an efficient electron transfer agent in various reduction-oxidation systems [21]. DHI and DHICA are indeed catecholic subunits, that can be reversibly oxidized into the corresponding orto(o)-quinone forms in two processes of one-electron one-proton removal process [22], [23]. Various redox forms of the building blocks coexist in eumelanin [24] (Figure 1.4).
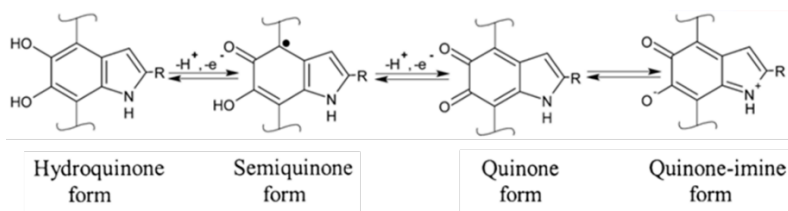
Figure 1.4 Redox forms of eumelanin's building blocks, R=H for DHI and R=COOH for DHICA. Reprinted with permission (granted by co-authorship) from Ref. [25].

1.2.4 Supramolecular Structure

The supramolecular buildup of eumelanin largely determines its properties. Its monomers (DHI and DHICA) form oligomers of up to a few tens of monomers [26]–[31]. The oligomers stack one on the other via π-π stacking; the characteristic d-spacing is of 3.4 Å [26]–[31]. The oligomeric sheets form protoparticles. Such protoparticles then arrange in an onion-like structure and densify into spherical particles and finally undergo aggregation in larger spherical particles [32]. Consistently, Sepia Melanin is constituted of 150 nm-sized aggregates [33] that assemble into granules.
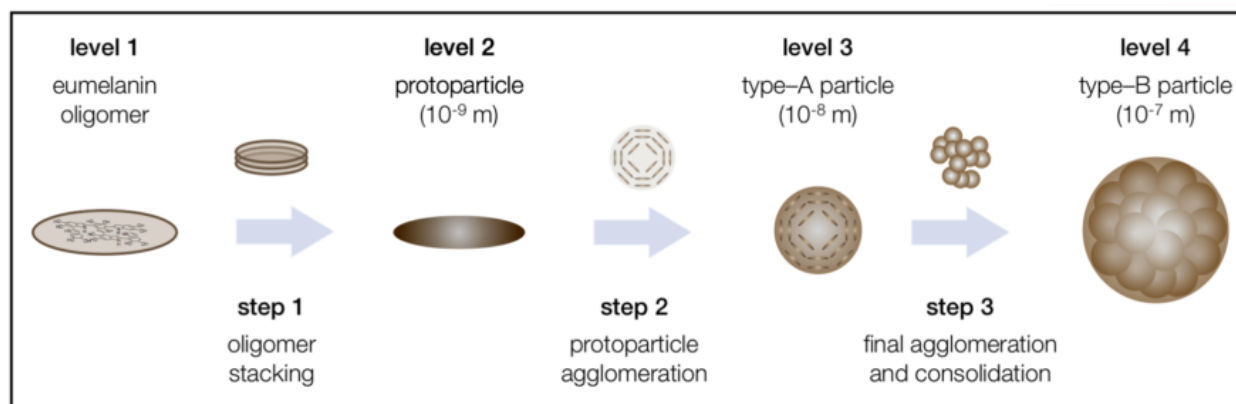
Figure 1.5 Supramolecular buildup of eumelanin. Reprinted with permission (granted by Creative Commons Attribution License of Open Access) from Ref. [32].

Molecular dynamics simulations and first-principles density-functional theory (DFT) calculations were recently used by Antidormi *et al.* to simulate the polymerization of DHI and DHICA in methanol. Such a work confirmed that the oligomer size of 10 units is the most likely to occur for eumelanin [34]. To gain more insights into eumelanin polymerization, a bottom-up approach was adopted by De Marchi *et al.* They studied the self-assembled monolayer networks of DHI and DHICA on Au and Ag surfaces using scanning tunneling microscopy (STM) [35], [36].

It was also demonstrated that the supramolecular buildup can be stopped at each level by enzymatic oxidation *in vitro* [37]. Cations and small molecules are able to influence the supramolecular aggregation of eumelanin [38]. Belitsky *et al.* recently investigated the ability of small molecules to influence aggregation of dopa-melanin during its polymerization and aggregation (measured considering the acceleration or delay in the appearance of macroscopic particles) [38].

1.3 Other Types of Melanin

1.3.1 Pheomelanin

In presence of cysteine, tyrosine oxidation leads to the formation of pheomelanin. A weakly acidic pH in melanosomes renders pheomelanogenesis favored over eumelanogenesis. Not only red hairs, but also black and brown hairs contain pheomelanin [39]. The ratio of eumelanin/pheomelanin in hairs can be measured by electron spin resonance [40].

Pheomelanin has poor photoprotective properties compared to eumelanin [41]. It acts as photosensitizer, generating reactive oxygen species (ROS) upon UV irradiation [41], [42].

1.3.2 Neuromelanin

Neuromelanin is present only in the brain of humans and large primates. This complicates the ethics of procurement, so that Sepia Melanin is used as a NM simulant [8], [43]. In humans, NM piles up within the dopaminergic neurons of the *substantia nigra* and in the neurons of the *locus coeruleus* of the brain [44]. NM is largely depleted in patients with Parkinson's disease through a selective loss of NM-containing neurons, suggesting that NM may be involved in the neurodegenerative processes of Parkinson's disease [45]. In Parkinsonian brains, after neuronal death, NM is released in the extracellular environment. As it is insoluble, it can remain for a long time acting as a pro-inflammatory stimulus leading to further neuronal damage [44]. NM may have both a beneficial and a detrimental role (Figure 1.6). An example of the beneficial role is the chelation of iron and other potentially toxic metals with formation of non-redox active species as well as the binding of environmental toxins, such as pesticides. The detrimental role can occur, for example, when high iron levels are present. In such a scenario, NM accumulates iron in low affinity binding sites where iron remains redox active [44], [46].
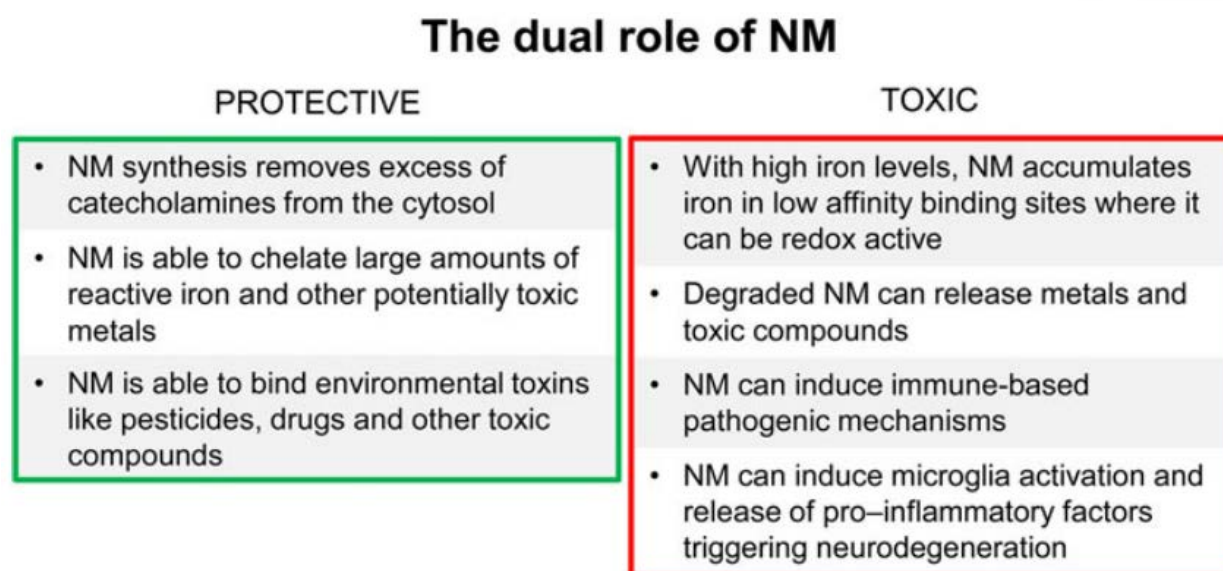
Figure 1.6 The dual role of NM. Reprinted with permission from Ref. [44].

1.3.3 Melanins in Insects, Microorganisms and Plants

Melanins are present in insects, too, where they play several roles: wound healing, defense reactions, cuticular coloration, and camouflage. Melanins in insects originate from dopamine, hence the term dopamine-melanin [47].

The building block of most (but not all [48], [49]) fungal melanins is DHN, 1,8-dihydroxynaphthalene (often referred to as DHN-melanin)[2] (Figure 1.1, L) [6]. Melanins in fungi are located in the cell walls or secreted into the environment, while eumelanins in animals are synthesized and maintained almost entirely as melanosomes as well as granules within melanocytes [50]. In fungi, melanins provide mechanical strength and chemical resistance to the cell, protection against the detrimental effects of UV radiation, high concentrations of salts and heavy metals [51]. They also allow fungi to tolerate extreme conditions, from the Earth's poles to deserts [52]. The exposure of certain fungi to gamma rays lead to increased production of melanin [53]. Melanized fungi have been found in Chernobyl's reactors, responding to ionizing radiation with enhanced growth [54]. Such a response lead to the intriguing hypothesis that fungal melanin is able to transduce radiation into metabolic energy in a sort of radiotropism [54]. In pathogenic fungi, melanin contributes to virulence, promoting tissue invasion and inactivation of the plant defense system [55]. Lately, interest in the electrical conductivity of fungal melanin has grown, too [56]. Fungi have been studied for the production of melanin from food or agricultural waste, such as wheat extracts [57]–[60]. However, in such cases, the pigment extraction from cell walls proved to be cumbersome. Recently, Ribera *et al.* demonstrated a scalable method to obtain eumelanin from a fungus that secretes the pigment in the surrounding liquid environment, thus facilitating its extraction [61].

Bacteria associated with darkly pigmented sponges [62] and other bacteria [63] have been studied as a source of melanin, too.

---

[2] Fungi: "Eukaryotic microorganisms of the kingdom Fungi, that possess cell walls and lack chlorophyll. Some species are pathogens of humans, animals and plants. Certain fungi are used commercially (e.g. in the production of enzymes and fermented foods)." [529]

Melanins extracted from plants are also based on oligomers: their building blocks can be either conventional eumelanin-like indoles [64] or phenolic units (such as p-cumaric acid for black oat hull [65]). Natural melanins in plants contribute to the defense mechanisms against pathogens and to the strengthening of the cell walls [65]. Melanin can be extracted from waste such as sunflower husk [66], flesh fruit [67] and fruit kernel skin [68].

1.4 Physical and Chemical Properties of Eumelanin

Eumelanin presents a vast set of properties such as UV-visible absorption, radical scavenging, hydration dependent electrical conduction [69], and metal ion chelation [70].

In a biological environment, an anti-oxidant can be defined as ''any substance that, when present at low concentrations compared to that of an oxidizable substrate, would significantly delay or prevent oxidation of that substrate'': radical scavengers, metal ion chelators and reducing agents fall within this definition [71]–[73]. Consequently, eumelanin is often defined as an anti-oxidant [69].

Eumelanin is available from natural sources and environmentally-friendly extraction routes (e.g. from natural fibers, such as fleece from alpaca [74]): eumelanin is therefore considered a carbon-based bio-sourced material.

1.4.1 UV-visible Absorption and Photoprotection

Eumelanin presents a featureless UV-visible absorption spectrum (Figure 1.7), in virtue of which it plays the role of photoprotector [75]. If there had been any gaps in the spectrum, the living organisms deploying eumelanin for protection against UV-radiation would have been left vulnerable to these specific wavelengths of the sun's radiation [76].
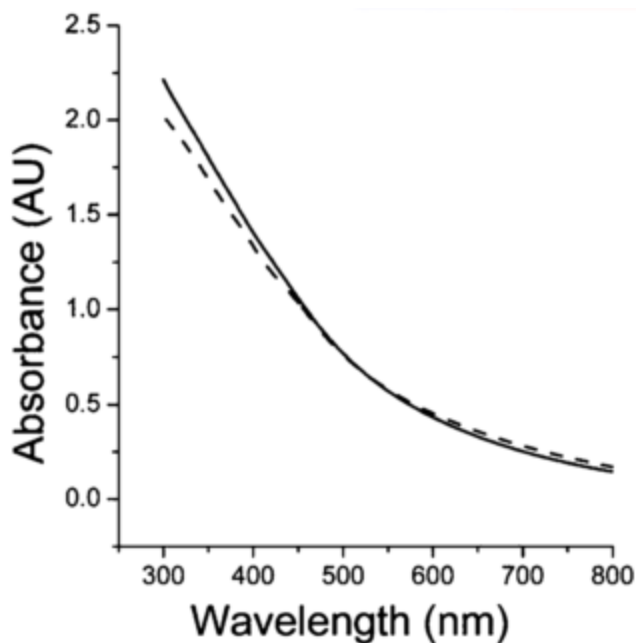
Figure 1.7 Absorbance spectra of synthetic dopa-melanin in water, pH 7 (dotted line) and in dimethyl formamide (dashed line), 0.005% (w/w). Reprinted with permission from Ref. [27].

The main photoprotection path entails that eumelanin converts the energy of the photons into heat (rotational and vibrational energy), in the so called "photothermal effect" (which is the main contribution of the "photoacoustic effect", so that eumelanin is often defined to have "photoacoustic properties") [77], [78]. Such a property is not affected by temperature until 80 °C [79].

The featureless absorption spectrum of eumelanins has been explained with the chemical disorder model. According to this model, eumelanin is constituted of several chemically distinct species, i.e. oligomers that differ by number of monomers, type of monomers and polymerization sites. Its broadband absorption spectrum would thus result from the averaging over the spectra of these species (superposition principle) [75]. The inconsistencies of such a model were summarized in a recent study by Chen *et al.* [76]. *Inter alia*, the chemical disorder model did not explain the reason for the monotonic increase of the spectrum toward lower wavelengths [76]. Furthermore, interactions among eumelanin oligomers can significantly affect the spectrum so that the superposition principle does not hold [80]. The work by Chen *et al.* does not stress the focus on the chemical heterogeneity but rather on the geometric disorder: the stacked eumelanin oligomers

differ by size and are randomly oriented, so that peculiar excitonic interactions take place among them [76].

The ratio DHI/DHICA monomers in eumelanin dramatically influences light absorption (as well as other properties such as paramagnetic and redox behavior, particle morphology, surface properties and metal chelation) [81]. These differences can be understood studying synthetic eumelanins made up of only one of the two monomers, DHI-melanin and DHICA-melanin. The oligomers of DHI-melanin are planar, with a high level of stacking and inter-unit π-conjugation. DHICA features carboxyl groups that cause steric hindrance, so that DHICA forms non-planar oligomers, with limited inter-unit π-conjugation [18]. The negative charge of the deprotonated carboxyl groups can further limit efficient stacking, so that rod-shaped assemblies form [77] (Figure 1.8).
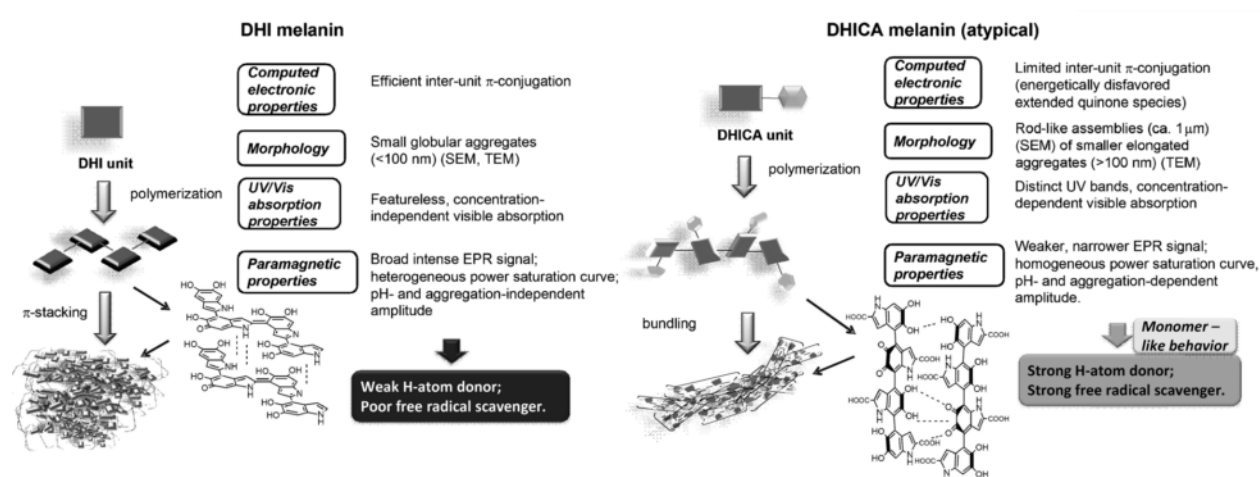
Figure 1.8 Differences in structure and properties between DHI-melanin and DHICA-melanin. Reprinted with permission from Ref. [77].

In general, stacking increases the visible absorption [80], so that a higher content in DHICA decreases visible absorption [81], [82]. The light absorbing properties and redox behavior are intimately connected: it has been suggested that the nonradiative decay processes of DHI can lead to DHI in a different oxidation state [83].

1.4.2 Binding of Metals and Organic Compounds

In the fields of dermatology, materials chemistry and physics many scientists have advanced arguments that melanin does not play a merely pigmentary role [84]. Eumelanin can bind both organic compounds [85], [86] and metal ions [70], [87]. The binding capacity of melanin towards metal ions is large but finite [88]: it depends on the cation, on the pH and on the binding site [89]. When eumelanin binds reactive metals, it mitigates their potential role in inducing oxidative stress [70]. A detailed literature review concerning the binding of eumelanin towards metal ions is provided in Article 5 [89].

1.4.3 Radical Scavenging

Eumelanin is a radical scavenger[3] [69] and its redox state determines its radical scavenging ability. Eumelanin must be in a reduced state to donate electrons to scavenge oxidative radicals or must be oxidized to receive electrons from reductive radicals [90].

Eumelanin's photoprotective role is strongly related to the radical scavenging properties. In particular, it has been suggested that the reactive oxygen species (ROS) generated as an inflammatory response to UV radiation may be scavenged by eumelanin [91].

However, eumelanin itself, under UV irradiation, can form ROS [92]–[94], thus explaining the dichotomous role (photoprotective and photodamaging) played by its light-absorbing properties [95], [96]. The factors that determine whether the photoprotective or photodamaging effect of the UV-visible absorption properties prevails are the radiation wavelength [78], [84], the UV exposure time [97], [98] and the pigment's aggregation [99], [100].

It has been suggested that the main photoprotective mechanism, the photothermal conversion, may take place at long wavelengths, i.e. UVB, i.e. 280–320 nm, UVA, i.e. 320–400 nm and visible [78]. Conversely, at short wavelengths (UVC, i.e. 220–280 nm) eumelanin may become cytotoxic by generating radicals [84].

---

[3] A radical is a molecular entity with an unpaired electron; in this thesis, the term "free radical", belonging to an old nomenclature, but still sometimes used in the literature, will be avoided, following IUPAC recommendations [530].

In the human eye, eumelanin has a supportive role in the visual process: it reduces intraocular light scatter [101]. However, a prolonged exposure to UVA could lead to its photodegradation and photoaging [92], with the loss of its radical scavenging abilities [102], [103]. In that case, eumelanin of the retinal pigment epithelium (RPE) can even become an efficient pro-oxidant [97].

It was proved that small particles of natural eumelanin are involved in UVA-induced photochemical processes that can lead to the DNA damage in skin cells [104]. Conversely, large particles efficiently dissipate UVA energy through the nonradiative decay processes (the aforementioned photothermal conversion). It is thus clear that aggregation limits ROS photoproduction related to UV irradiation, suggesting that the aggregation of the biopigment and the integrity of melanosomes in tissues is another factor determining whether the photoprotective or the photodamaging behavior prevails in nature [99], [100].

The radical scavenging property, too, is influenced by the DHI/DHICA ratio [81]. In DHICA-melanin, relatively homogeneous radical species, spatially confined within restricted segments of the polymers, are present [81]. On the contrary, DHI-melanin is characterized by a large variety of radical species that could be generated within the delocalized π-electron systems [81]. DHICA-melanin was also found to be a more efficient hydroxyl radical-scavenger: its aggregates would indeed be more accessible to radicals compared to compact π-π stacked DHI-melanin [81]. Recently, the ability to scavenge radicals by natural and synthetic eumelanins, as well as by their precursors DHI and DHICA, has been quantified [105]. Such ability is higher in the monomers with respect to synthetic DHICA-melanin and DHI-melanin, as polymerization involves the oxidation of some building blocks from the catechol to the quinone form, reducing the amount of OH groups involved in radical scavenging [105]. In agreement with the literature, DHICA-melanin proved to have superior radical scavenging than DHI-melanin, as explained above [105].

Furthermore, it was proved by Agapito and Cabral that the enthalpy of formation of the OH· radical from the hydroxyl groups of catechol subunits is lower in the DHI monomer than in DHICA. The lower "energetic cost" for OH· formation in DHI than in DHICA could potentially explain why DHI-melanin features superior ROS generation rates than DHICA-melanin [42].

The differences in ROS generation between DHI and DHICA could also tentatively explain why nature "opts" for an enzymatically-controlled pathway to DHICA instead of leveraging on the spontaneous, biologically "low cost" process of DHI formation (Figure 1.3) [81].

1.4.4 Electrical Properties

Eumelanin is one of the first biomaterials whose electrical properties have been investigated [106]. Eumelanin's electrical conductivity ranges from 10^{-3} S cm^{-1} in the fully hydrated state to 10^{-8} S cm^{-1} in the dehydrated state [107], [108].

It was defined a "mixed semiconductor" in 1970 by Powell and Rosenberg, with a proton to electron ratio of $\approx$1:2: the experiment was carried out on synthetic melanin (dopa-melanin) powders, placed in a sandwich cell made of platinum foil and such a ratio did not change in the hydration range 10 – 35% wt. [106]. Bistable switching behavior depending on eumelanin's hydration was reported by McGinness *et al.* in 1974 [109], leading to the definition of eumelanin as an amorphous semiconductor. The investigation of the parameters related to the amorphous semiconductor model followed: optical band gap [110], band structure and charge carrier density [111], [112].

In 2012, a new model was suggested: a hydration-dependent electronic–ionic conduction [113]. The comproportionation equilibrium, already known since the 70s [22] (Figure 1.9), was used to explain the conductivity increase with the amount of water. The presence of two indole moieties in different oxidation states (catechol and quinone) together with adsorbed water would bring about the (thermodynamically favorable) generation of semiquinone moieties and protons, responsible for the doping of electrons and ions into the system (Figure 1.9) [113].
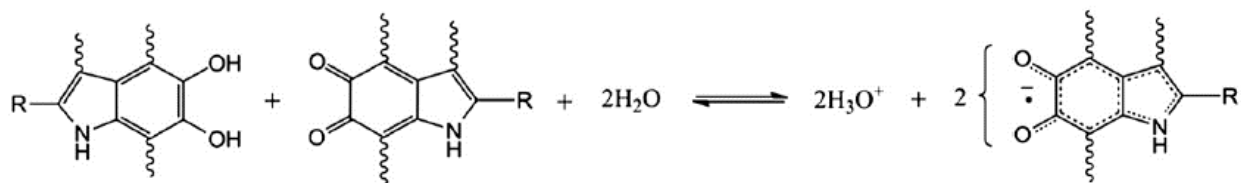
Figure 1.9 Comproportionation equilibrium. Reprinted with permission (granted by noncommercial educational use) from Ref. [113].

Further experiments involving D_2O (heavy water, an oxide of the hydrogen isotope deuterium), in presence of which the forward reaction of Figure 1.9 is more favored than the backward one, were provided to corroborate such model [114].

However, the same authors who postulated the hybrid electronic–ionic conduction theory very recently demonstrated that the main component of eumelanin's hydration dependent conductivity is actually protonic [115].

Other important properties are photoconductivity [110], [113], [116]–[118] and permanent paramagnetism [119]. The photoconductivity of eumelanin has been explained within the frame of the comproportionation equilibrium, too [120]. DHI-melanin was recently demonstrated to be a photocatalytic material, capable of reducing oxygen to hydrogen peroxide upon irradiation [121].

1.4.5 Other Proprieties of Eumelanin

Eumelanin is hydrophilic [122]: Sepia Melanin can absorb an amount of water equal to its mass in a water vapor saturated environment in 24 hours [123]. Studies on the water sorption of synthetic melanin (dopa-melanin) thin films, exposed at different vapor pressures of H_2O and D_2O, revealed that water is taken up thoroughly through the films [124].

Eumelanin is biocompatible [125] and bioresorbable [126]. Tyrosine-melanin implants *in vivo* located nearby a peripheral nerve tissue caused a foreign body response similar to silicone and were almost fully eroded and bioresorbed after 8 weeks [126].

1.5 Context of the Investigation: Green electronics, Compostability and Additives for Packaging

1.5.1 Organic Electronics, Bioelectronics and Green Electronics

Electronics have become indispensable in our daily routine. A great part of the electronic equipment that surrounds us belongs to what is known as conventional electronics, based on inorganic materials such as silicon and gallium arsenide [127].

However, with the life of the electric and electronic equipment becoming shorter and shorter, two major issues arise for both the scientific community and municipalities: the increasing amount of Waste of Electrical and Electronic Equipment (WEEE) and the depletion of natural resources [127], [128]. The United Nations define sustainability as the ability of satisfying one generation's needs "without compromising the ability of future generations to meet their own needs" [129]. It is thus evident that the electronics sector lacks sustainability, at least so far [127]. Consequently, great

attention has been given to green (sustainable) electronics in the last years, having as core values (i) the use of abundant and low-cost precursors, (ii) the use of biodegradable materials, leveraging on processing routes that (iii) lack toxic solvents as well as toxic waste and (iv) are low cost. Sustainable electronics envisages devices with low embodied energy, i.e. "energy spent in the production phase and stored in the inner constituents" [128].

Organic electronics is based on organic (carbon-based) materials as the core semiconductor element. Such materials, polymers or small molecules, are characterized by conjugation, i.e. alternance of single and double carbon-carbon bonds. Organic electronics features solution processability, printability and tunable optical and electronic properties with chemical synthesis [130]. The feature of being solution-processable (printable) adds to organic electronic devices the further advantage of lower embodied energy with respect to their inorganic counterparts, that are processed by high-vacuum and high-temperature techniques [128].

Organic bioelectronics is a branch of organic electronics, which has the specific aims of "implementing biocompatible materials in different electronic architectures at the interface with living tissues" [131]. The main challenge of organic bioelectronics is to transduce signals between biology, featuring predominantly ionic signals, and semiconductors electronics, featuring electronic signals [132].

1.5.2 Electrochemical Metallization Memory Cells: towards Green Electronics

Electrochemical metallization memory cells (ECMs), also known as conductive bridge random access memories [133], belong to *Resistive Random Access Memories* (ReRAMs) [134], a subgroup of non-volatile memories, NVM [135]. ECM working mechanism entails the formation, under bias, of conductive filaments. As the active electrode dissolves, cations migrate through a solid electrolyte (ion conductor) and accumulate on the counter electrode (CE), where the conductive bridge starts growing [135]. Once the filament grows over the entire inter-electrode distance, it connects one electrode to the other, causing the system's resistivity to plummet [135]. The advantages of ReRAMs are good reliability [133], low power consumption [134], [136]–[138], fast response time [133], [136], multilevel data storage [133], [136], [139], and high density [134].

Albeit initially constituted entirely of inorganic materials, ECMs have witnessed the use of organic synthetic materials for the ion conductive layer since 2011 [140]. The use of natural (bio-sourced)

organic materials ensued in the last few years [141]. Organic and polymeric switching memories feature flexibility [142]–[148], optical transparency [144], printability [142], [149], electrical and physical properties tunable by means of molecular design and chemical synthesis [150], [151], which provide a potential for high density memory applications [135], [152]. Conductive bridge memories have been obtained using conductive polymers well-established in the field of organic electronics, polymers loaded with salts, small molecules and dyes [153]–[160].

Interest regarding biomaterials and bio-sourced materials for memories (Bio-ReRAMs) has increased, too [141]. Examples of natural materials used as ion conductors in ECMs are: dead leaves [161], lignin loaded with Au nanoparticles [162], eggshells [163], pectin extracted from orange peels [164], a DNA-based biomaterial [165], [166], electro-spun cellulose fibers [167], nano-cellulose [168], gelatin [169], [170], *Aloe vera* gel [171], [172], chicken [173] and duck [174] egg albumen, silk fibroin [175]–[179], glucose [180] and carrageenan, a polysaccharide from seaweeds [181]. Natural materials investigated as dielectrics for ECMs are chicken egg albumen [182], gelatin [183] and human hair keratin [184]. Further examples of biomaterials for Bio-ReRAMs can be found in the review by Raeis-Hosseini and Lee [141].

1.5.3 Biodegradation as an Option for Waste Disposal

At the end of life of materials, their biodegradability plays a key role in the challenge to achieve sustainability [127], [185]. Biodegradation is "the metabolic breakdown of materials into simpler components by living organisms" [186]. When a material is defined biodegradable, the conditions and the time range have to be specified, too [187].

In municipal waste management, composting (aerobic biodegradation, i.e. in presence of O_2) has been identified as a valuable disposal pathway [188]. During composting, the temperature is of ~ 60 °C is reached because of the microbial activity [189]. The ultimate end products of composting are CO_2, minerals and water [187]. Composting has several advantages, such as reducing the volume of waste for landfilling and incineration, avoiding methane production and release in the atmosphere (differently from anaerobic biodegradation) and providing a product that can be used for crop growth. Standard test methods have been developed for plastic materials used for food packaging and serving in order to evaluate their compostability, that is, biodegradability in composting conditions (e.g. CAN/BNQ 0017-088/2010 in Canada, ASTM D5338 and ASTM D6400 in the USA, EN 13432 and EN 14995 in the European Union as well as ISO 14855-1:2005).

Examples of compostable materials are polylactic acid (PLA) and poly-ε-caprolactone (PCL) [190]. It is worthy of note that bio-based material does not necessarily imply biodegradability: for example, poly-ε-caprolactone is petroleum-based and biodegradable while nylon 11 is bio-based but not biodegradable [191].

1.5.4 Additives for Packaging

Stabilizers are needed in plastic polymers since UV radiation, heat and oxygen cause their physical and chemical degradation during processing and service [192].

During a prolonged exposure of plastics to UV light, radicals form, that, in presence of oxygen bring about photo-oxidative degradation [193], [194]. Furthermore, when dealing with plastic polymers for packaging applications, screening UV-radiation is crucial in order to mitigate damage on the material wrapped by the packaging (e.g. food) in the storage or end-use environments [193]. Consequently, UV absorbers are added to plastics, in order to enhance their UV-absorption and photostability [193].

In addition, plastics are exposed, during processing, to both heat and oxygen that can cause thermo-oxidative degradation. The additives used in this case are anti-oxidants for thermo-oxidative stabilization [193].

CHAPTER 2   LITERATURE REVIEW

2.1 Organic Electronics Applications of Eumelanin

Given the molecular properties of eumelanin, the pigment has been considered for organic electronic applications [195].

Filmability (i.e. high thin film stability) is a key factor for the use of eumelanin in organic electronics. The insolubility of eumelanin has rendered not only the investigation of its physico-chemical properties but also its processability in thin film form complex. Great efforts have been made towards the achievement of stable eumelanin thin films in the last decade [107]. Recently, the deposition by spin coating of homogeneous films from eumelanin suspensions in dimethyl sulfoxide (DMSO) has been demonstrated, with a surface roughness below 0.5 nm [196].

Apart from thin films, DHI-melanin was also fabricated in nano- and micro-tubes, by polymerization on electrospun poly(lactic acid) (PLA) fibers, eventually removed by organic solvent treatment. Such microtubular structures have potential applications in microfluidics and drug delivery [197].

An electrode based on DHI-melanin and commercial poly(3,4-ethylenedioxythiophene) with poly(styrenesulfonate) (PEDOT:PSS) was developed featuring (i) higher water stability and substrate adhesion with respect to a blank PEDOT:PSS film, thanks to eumelanin (ii) conductivity of the same order of magnitude of PEDOT:PSS (370 S/cm) (iii) optical transmittance of nearly 80%–90% in the range 400–600 nm. The electrode was used as an anode in an organic light emitting device that did not feature ITO (indium tin oxide), with performance comparable to reference ITO-free devices [198]. The presence of DHI-melanin increased the crystalline order of the PEDOT:PSS fraction [199].

Synthetic eumelanin (dopa-melanin) was also used as a gating medium for PEDOT:PSS based transistors; the modulation was achieved by controlling the water vapor pressure to which eumelanin was exposed [132]. Eumelanin was also capable of transducing proton-to-electronic currents [130]. Previously, the detection of DHI-melanin in colloidal suspensions was demonstrated using Organic Electrochemical Transistors (OECTs) making use of PEDOT:PSS as the active layer and the suspensions as the transistor gate; the detection was based on the redox reactivity of the DHI-melanin [200].

Synthetic and natural eumelanins have been used as cathode materials for magnesium-ion batteries [23] and anode materials in sodium-ion batteries [201]. Supercapacitors and flexible micro-supercapacitors on flexible polyethylene terephthalate (PET) featuring eumelanin-based electrodes were also demonstrated. Such devices work in aqueous electrolytes and can be fabricated at room temperature [25].

Furthermore, synthetic eumelanin (dopa-melanin) was used as active layer of electrolyte-gated field effect transistors for pH sensing [202].

The adhesion and the band alignment of DHI oligomers with respect to Si surfaces was studied with *ab initio* calculations for potential applications in photovoltaics, and a prevalence of quinone moieties was found to favor adhesion and band alignment with Si [203]. Such results were then experimentally confirmed [204]. Eumelanin, extracted from squid ink thanks to a proteolytic enzyme [205] and from Antarctic bacteria [206], was used as a natural dye in dye-sensitized solar cells (DSSCs) based on TiO_2 nanotubes and nanoparticles. It proved to successfully sensitize the TiO_2 providing interesting power conversion efficiency [205]; however, DSSCs based on TiO_2 and matrix-assisted pulsed laser evaporation (MAPLE) deposited melanin did not show a reliable operation [207]. Tyrosine-melanin, enzymatically produced *in situ*, was also used to enhance the performance of photoelectrochemical cells [208]. Functionalization of photoanodes of α-Fe_2O_3 (hematite) with phycocyanin, a light harvesting protein, and eumelanin lead to an increase in the photocurrent density [208].

Eumelanin-inspired molecules (i.e. based on an indole unit) were synthetized from vanillin, from which polymers with extended conjugation can be obtained, thus being promising candidates as organic semiconductors [209].

2.2 Interfaces between Eumelanin and Metal Electrodes

Wuensche *et al.* demonstrated that gold dendrites form in hydrated thin films of eumelanin, confined between metal electrodes in a planar configuration, at a distance of 10 μm, under bias (1 V) [210]. The process was explained with a chloride mediated dissolution of the positive electrode: gold nano-aggregates, formed after the electrode dissolution, migrate within the eumelanin layer towards the negative electrode, with the catecholic units binding the gold ions. Once the gold nano-aggregates reach the negative electrode, dendrites nucleate and grow towards the positive electrode.

When one gold dendrite connects one electrode to the other, the resistivity plummets (resistive switch); the ON/OFF ratio, i.e. the ratio between the current after the resistive switch and the current before the resistive switch, amounts to ~10^4-10^5 [210]. The similarity between the working mechanism of ECMs and the dendrite formation process of hydrated eumelanin thin films points to a potential use of eumelanin as ion conductor in Bio-ReRAMs.

2.3 Melanin's Biodegradability: Not to Be Taken for Granted

Due to the confusion that surrounds the terms bioresorbable and biodegradable, eumelanin has often been defined biodegradable in studies that referred to a work where its bioresorbability was proven [126].

Studies on melanosomes outlined the resistance of the pigment to degradation *in vivo* [211]–[213]. Preserved eumelanin was also reported in the orbit of a 54 million year-old fish fossil [214], in a 160 million year-cephalopod [215], and in other fossils [216], [217].

Proper biodegradability evaluations on natural eumelanin (from human hair, buried in laboratory and field settings) [218] and synthetic melanin (dopa-melanin in presence of a mixed bacterial culture [219] and tyrosine-melanin in potting soil [220]) revealed negligible biodegradation. Conversely, fungi were demonstrated to be able to biodegrade eumelanin from human hair [221] and human skin [222]. The fungus *Aspergillus Fumigatus* is able to fully biodegrade natural eumelanins from insects, aged banana skin, human hair, octopus' ink as well as synthetic dopa-melanin and tyrosine-melanin. Such fungus is also able to develop its own form of fungal melanin [223].

The biodegradability of fungal melanins gained attention as the pigment represents an aesthetic damage that forms in humid environments on the surface of wood works of art [224], [225]. Fungal melanin can also be present in non-tolerable concentrations in waste waters of the industrial fermentation of antibiotics [226]. Much work suggests that fungal melanin, too, is rather reluctant to biodegradation [227]–[231]. Furthermore, certain fungal melanins are so resistant to biodegradation that they can protect the polysaccharides of the cell walls of certain fungi or cellulosic waste from biodegradation [220], [232]–[245]. Melanin's protection of the polysaccharides of the cell walls was explained as physical barrier and/or proper enzyme inhibition [220], [232]–[245]. This entails that the presence of melanin in cell walls becomes a virulence

factor in some phytopathogenic fungi. In other words, such fungi use melanin to protect themselves against the defense mechanisms of the host (as explained in the paragraph regarding <u>fungal melanins</u>) [246]. Other fungal melanins featured a higher tendency to biodegrade [247], transforming into humic substances [248]. For the treatment of the fungal melanin-rich waste waters of industrial fermentation of antibiotics, *Acrostaphylus* was suggested, as it is able to biodegrade fungal melanin [226]. White rot fungi can biodegrade fungal melanin and synthetic dopa-melanin [224], [246], [249].

Synthetic and fungal melanin were both reported to be resistant to biodegradation in some works [219], [220], [227]–[231] and biodegradable in others [221]–[223]: this points out how much different parameters such as the type of melanin, melanin's supramolecular structure, the type of soil, the availability of nutrients and the type of microorganisms can lead to different conclusions.

2.4 Biodegradability in Green Electronics

Although biodegradability is a paramount feature of materials for green organic electronics, so far organic electronics has focused almost entirely on device performance [250]. Until now, no international standard test method has been conceived to assess the biodegradability of organic electronic materials and devices. This points to the need to elaborate protocol specifically designed to claim an organic electronic device to be biodegradable [251]. In most of the works where the biodegradability of organic electronic devices is investigated, such devices are put in contact with aqueous solutions similar to the human body fluid [252]–[255].

Lei *et al.* produced a thin film transistor (TFT) fully biocompatible and "disintegrable" (i.e., degraded in a solution containing cellulase, the enzyme able to decompose cellulose back to the monomeric form), based on cellulose, iron electrodes and a semiconducting polymer. Such a biodegradable polymer was designed *ad hoc*, i.e. a copolymer of isoindigo (diketopyrrolopyrrole) (DPP) and phenylenediamine (PD), PDPP-PD [256]. Pan *et al.* produced a biodegradable triboelectric nanogenerator (TENG) composed of gelatin film and an electrospun PLA nanofiber membrane; the degradation was tested in water [257]. Zhang *et al.* produced a TENG based on silk fibroin proteins, wherein the biodegradation of silk can be followed monitoring optical diffraction and the triboelectric performance [258]. Salvatore *et al.* fabricated temperature sensors with reliable electrical performance and dissolvable in water, based on magnesium, silicon dioxide and

silicon nitride nanometric thin films, and using a compostable polymer as the encapsulant, i.e. poly(butylene adipate terephthalate) (PBAT) [259].

A battery capable to power electronic devices (1.5-3 V), i.e. suitable for portable applications, fully biodegradable, was demonstrated by Esquivel *et al.* The battery is based on cellulose, carbon, beeswax, and a quinone-based redox material. The battery is biodegradable in anaerobic conditions (in absence of oxygen and at 35 °C). Such conditions were chosen as they represent a worse-case scenario with respect to aerobic biodegradation, that is faster than the anaerobic one [260].

Jeong *et al.* proved how starch paper modified with poly(vinyl alcohol) (PVA) and a crosslinker could work as a biodegradable substrate in flexible organic electronic devices. The biodegradability was tested by means of a fungus in fish bowl water [261].

2.5 Eumelanin as an Additive for Plastic Polymers

Natural and synthetic eumelanin, fungal melanin as well as dopamine-melanin (a eumelanin-like synthetic material [262]) have been evaluated as additives to improve the UV-blocking properties [263], [264] and the photostability [263] of polymers such as PVA and bisphenol A polycarbonate (PC) [265] as well as the thermal stability of PVA [266], [267], PLA [266], [268], poly(methyl methacrylate) (PMMA), polypropylene (PP) [269], polyhydroxy butyrate (PHB) [270], and of a bio-sourced polymer, carrageenan, extracted from red seaweeds [271] (Table 2.1). Sepia Melanin was also used to stabilize (i.e. to avoid agglomeration) of ZnO nanoparticles, used as an antimicrobial agent in carrageenan films [272].

Table 2.1. Literature regarding eumelanin added to polymers as a UV-absorber and/or anti-oxidant.

Polymer and corresponding reference	Additive	UV-Visible Absorption or Transmission (% wt. of additive causing the effect)		Increase of onset of decomposition temperature, °C) (% wt. of additive causing the effect)
Poly(methyl methacrylate) (PMMA) [269]	DMSO-melanin	80% transmission kept (1% wt.)		≈ 70 (5% wt.)
	Sepia Melanin	N/A		≈ 50 (5% wt.)
Polypropylene (PP) [269]	Sepia Melanin	N/A		≈ 50 (5% wt.)
Polystyrene (PS) [269]	Sepia Melanin	N/A		No effect (5% wt.)
Poly(vinyl alcohol) (PVA) [263]	Sepia Melanin	Absorption (%) (0.5% wt.)*		N/A
		UVC	100	
		UVB	> 98.5	
		UVA	30	
		Visible	Transparency close neat PVA	
		Absorption (%) (2 % wt.)*		
		$\lambda < 340$ nm	≈ 100	
		Visible	Transparency deceased	
PVA [264]	Dopamine-Melanin Hollow Nanoparticles (Dpa-h NPs)	$\approx 100\%$ absorption * in UV region $(200 - 400$ nm). With wall thickness ~ 8 nm maintained relatively high transparency to visible light		N/A
PVA [266]	Dopa-melanin	N/A		≈ 80
Poly(lactic acid) (PLA) [266]	Dopa-melanin	N/A		No effect (PLA does not generate radicals during thermal decomposition)
PVA [267]	Dopamine-Melanin	N/A		87 (0.5% wt.) – 110 (2% wt.)
Fluorinated Anhydride-Terminated Copolyimides (PI) [194]	Sepia Melanin modified with a silane coupling agent	Absorption (%) (0.5% wt.) **		The temperature at which 5 % weight loss takes place increases of 10 °C (0.5 % wt.)
		< 400 nm	100	
		Transmission (%) (0.5% wt.)		
		800 nm	72.6	
PLA [268]	Fungal melanin	Transmittance (%) (0.2 % wt.)		Not affected
		> 250 nm	7 - 8% lower than neat	

Polyhydroxy Butyrate (PHB) [270]	Melanin from a marine sponge	N/A		Highly thermostable crystalline polymer (degradation peak at 292.94 °C)
Bisphenol A polycarbonate (PC) [265]	Sepia Melanin	Absorption (%) *** (0.5% wt.)		N/A
		300 nm	50	
		Absorption (2% wt.)		
		280 nm	All radiation shielded	
		Transmission (%) (2% wt.)		
		550 nm	40	
	Dopamine-Melanin	Nanoparticles 240 nm		
		Transmission (%) (1% wt.)		
		< 270 nm	0	
		Visible	50	
		Nanoparticles 15 nm		
		Transmission (%) (1% wt.)		
		< 340 nm	0	
		Visible	83	
Copolymer of α-(1–3)-D-galactose and β-(1–4)-3,6-anhydro-D- or L-galactose, carrageenan (extracted from certain species of red seaweeds, *Rhodophyta*) [271]	Sepia Melanin	Nanoparticles 98 ± 22 nm		Main decomposition temperature increased of 7 °C (2% wt.)
		Transmittance (%) (2% wt.)		
		280 nm	2.6	
		660 nm	12.5	
PP [273]	Dopamine-melanin	N/A	N/A	14.5 (1% wt.)

* with respect to the absorbance of pristine rhodamine B solution.

** with respect to the absorbance of pristine methylene blue solution.

*** with respect to the blank polymer.

2.6 Biomedical Applications of Eumelanin

Eumelanin has been investigated for biomedical applications thanks to its biocompatibility [125], bioresorbability [126], photothermal conversion of radiations [274] as well as binding affinity with respect to organic compounds and metals [275].

Bettinger *et al.* demonstrated that physically crosslinked hydrogels loaded with Sepia Melanin could be disintegrated upon UV irradiation, thanks to the photothermal conversion of eumelanin. Such hydrogels could be used in biotechnology (e.g. controlled drug release and regenerative medicine) [274]. As a matter of fact, a few years later Sepia Melanin-releasing hydrogels were tested to reduce inflammation in skin wound healing [276]. Microparticles of the polysaccharide alginate were loaded with synthetic eumelanin and used as drug delivery carrier, where the drug delivery would be mainly induced by the photothermal conversion of melanin upon NIR (near infrared) irradiation. Natural eumelanin was used as a photothermal therapeutic agent (PTT), able to kill tumor cells by hyperthermia when irradiated with NIR radiation [277], [278]. The research about eumelanin as a PTT agent also focused on avoiding recognition and clearance by the immune system: red blood cell membrane-camouflaged melanin nanoparticles were successfully tested as *in vivo* PTT agents and photoacoustic imaging (PAI) agents for tumor imaging [279]. The same research group later improved such camouflage, using a hybrid biomimetic coating constituted of red blood cell membrane and tumor cell membrane. The presence of the tumor cell membrane entailed enhanced tumor targeting of the melanin nanoparticles, with consequent improved PTT efficacy *in vivo* [280].

Eumelanin has been considered as a biomarker to detect diseases such as melanoma [281]. Eumelanin's ability to bind drugs and metals (radioactive $^{64}Cu^{2+}$, Fe^{3+}) combined to its photoacoustic properties were leveraged to produce nanoparticles (functionalized with polyethylene glycol (PEG)) that would work not only as a drug delivery system but also for multimodality imaging (positron emission tomography (PET) and PAI) guided therapy [275], [282]. Hybrid synthetic eumelanin-Fe_3O_4 nanoparticles were used as PTT agents as well as magnetic resonance and photoacoustic contrast agents [283]. Analogously, biocompatible Au nanoparticles were grown on Sepia Melanin for imaging-guided photothermal tumor ablation. The so-obtained nanocomposites allowed the detection of tumors by X-ray computed tomography (CT), photoacoustic and thermal imaging and their ablation by photothermal therapy [284]. Eumelanin's

ability of binding organic compounds could be harnessed to test the phototoxicity of pharmaceuticals [285].

Sepia Melanin nanoparticles, functionalized with dopamine-melanin, showed potential as antibiotic delivery systems [286]. Sepia Melanin was also used as a drug-delivering coating for glass-ceramic scaffolds studied as prosthetic materials [287]. Sepia Melanin – PVA coatings were also used to reduce the anti-inflammatory response to ITO electrodes, with excellent electrochemical activity and durability [288].

The possibility of producing synthetic eumelanin films (DHI-melanin) as biocompatible platform for stem cell growth was demonstrated by Pezzella *et al.* [289]. Aligned silk fibroin scaffolds containing eumelanin were used as neural regeneration substrates, showing anti-oxidant properties and biocompatibility [290].

DHICA-melanin/TiO_2 hybrid nanostructures showed antimicrobial activity under UV and visible radiation, thanks to the formation of ROS species by both components (only partially quenched by the synthetic melanin) [291], [292]. Conversely, hybrid nanoparticles silica/DHICA-melanin showed protecting effects against hydrogen peroxide-induced oxidative stress and cytotoxicity [293].

Eumelanin was proven to be able to protect the liver against alcohol-induced stress [294] and for prevention and management of high fat diet-induced hyperlipidemia in mice [295].

Melanins can interact with drugs in manners that may influence their activity, metabolism and toxicity. A synthetic melanin biomimicking neuromelanin and Sepia Melanin have been reported to act as electron donor vs drugs and paraquat, an environmental toxin (a pesticide which has been linked to Parkinson's disease) [296], [297].

Further applications of eumelanin in the biomedical field can be found in the review by Solano [298].

2.7 Further Diverse Applications of Eumelanin

Sepia Melanin, added to the polymer poly(ethylene-alt-maleic anhydride) by solubilization and lyophilization, in a weight ratio 1/1, was studied as an adsorbent for purification of waters polluted by the methylene blue dye [299]. The metal chelating properties of eumelanin can be also used for

the same purpose. Tripathi and Melo prepared agarose-chitosan low density biopolymers functionalized with dopa-melanin that showed high sorption affinity towards uranium (the uranyl oxycation) and could be reused multiple times after elution with HCl [300]. The surface roughness (and, by result, the surface area) was later increased by the incorporation of colloidal silica nanoparticles [301]. Similarly, melanin-covered *Escherichia coli* were used to remove the model pharmaceutical chloroquine from water [302].

Eumelanin was also used as a support for palladium nanoparticles working as catalysts for Suzuki coupling reactions, thanks to the pigment's affinity towards the metal [303]. Eumelanin was encapsulated in mesoporous metal-organic frameworks in order to improve their binding affinity towards carbon dioxide [304].

Thanks to its anti-oxidant properties, films of DHI-melanin were investigated as potential sacrificial electrodes for the detection of peroxynitrate (PON) in solution, as both their electrochemical response and absorbance characteristics changed in presence of PON [305].

Cuttlefish ink was also directly used to create vivid colors with tunable hues that cover the entire visible spectrum. The method implies simply mixing monodisperse polystyrene (PS) particles with the ink and subsequent drop-coating of substrates such as paper, glass and plastic followed by drying at ambient temperature and humidity. The drop-coated substrates could then be ground into powders to obtain pigments [306].

The surface of wool fabrics was functionalized with composite particles of natural melanin extracted from alpaca fibers and rutile TiO_2. Such melanin/TiO_2 composites were used to increase the photostability of the fabrics [307].

2.8 Diverse Synthetic Melanins

DMSO-melanin is a synthetic eumelanin obtained from the synthesis in DMSO so that eumelanin's building blocks partly feature sulfonated groups ($=SO_2CH_3$) [308]–[310]. With respect to synthetic and natural eumelanin, sulfonated melanin derivatives show greater solubility in DMSO [308], higher photoluminescence in the visible [311] and good thin film stability [308]. DMSO-melanin is also biocompatible [312]. A synthetic eumelanin-like material obtained from the polymerization of the methyl ester of DHICA was shown to exhibit superior anti-oxidant properties with respect to DHICA-melanin, good solubility in alcoholic or other common organic solvents as well as

resistance to photoaging. Such properties suggested its use as an anti-oxidant ingredient for dermocosmetic formulations [313].
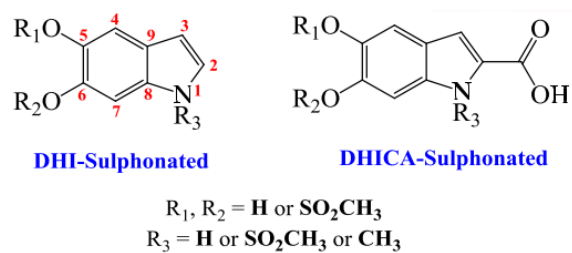
Figure 2.1 DMSO-melanin's building blocks. Reprinted with permission from Ref. [311].

CHAPTER 3   OBJECTIVES

In spite of the intense research efforts of materials scientists, engineers, physicists and dermatologists during the last decades, fundamental aspects of the physico-chemical properties of eumelanin have still to be fully understood [89]. In addition to that, the use of eumelanin for technological applications still features key challenges. For instance, in the field of green electronics, the stability of the interfaces between metal electrodes and eumelanin films under bias (i.e. absence of electrochemical processes resulting in electrode dissolution) is paramount. Such stability is important both for the proper characterization of the intrinsic electrical response of eumelanin and for the functioning of any eumelanin-based device. As previously mentioned, the only exception is represented by ReRAMS, systems where the electrode dissolution is desirable. As pointed out by Wuensche *et al.* [210], the stability of the metal electrode-eumelanin interface is not to be taken for granted even when dealing with supposedly inert metals, such as gold. Bio-sourced materials can indeed have traces of salts still present after their extraction from their biological medium. Such salts can trigger electrochemical processes at the eumelanin-metal electrode interface under bias in wet environments. Given the hygroscopicity of eumelanin [123], the presence of water in eumelanin films cannot be ruled out at ambient conditions. It is thus evident that identifying the conditions under which the electrode dissolution does/does not take place is crucial for the electrical characterization of eumelanin and its potential applications as bio-sourced material in green electronics.

Furthermore, in the plastics industry, the endeavor towards sustainability has concerned not only plastics themselves, but also their additives [190]. Eumelanin can thus be explored as a bio-sourced UV-absorption enhancer for plastic polymers, as the works developed in parallel with this thesis confirmed [194], [263], [265], [268], [271]. In this context, in order to reduce the gap between the demonstration of the UV-absorption enhancement provided by the biopigment to a polymer and a potential use of eumelanin as a commercial additive, important challenges are be tackled such as (i) the improvement of eumelanin's dispersion in the polymer matrix (ii) elucidating the effects of long exposure to UV radiation, given the dichotomous role (i.e. photoprotective vs photodamaging) of eumelanin's UV-absorption properties (iii) clarifying if any synergistic or antagonistic effects occur with respect to anti-oxidants inevitably present in commercial grade polymers.

In addition, as aforementioned, eumelanin's bioresorbability (biodegradability in contact with body fluids) was proven [126], but no studies were carried out in compost from municipal waste, at room temperature or composting conditions (58 °C). Clarifying the environments and the conditions under which the biopigment undergoes biodegradation is a further key aspect both in the context of materials for green electronics, as biodegradability is one of its pillars, and in the field of additives for polymers.

Given all these considerations, the targets of this work are:

1) Determining the conditions under which electrochemical processes (metal electrode dissolution) take place at the interfaces between hydrated eumelanin films and metal electrodes. In Article 1, we clarified the effect of the relative humidity on the eumelanin-metal electrode interface in the case of Au. In Article 4, a systematic study including metals other than Au (Pd, Cu, Fe and Ni) was carried out in order to try to "map" the conditions where the electrode dissolution does/does not take place.

2) Assessing the possibility of using eumelanin as an additive for plastic polymers, that could work as UV-absorption enhancer and evaluating the effects of a long-term UV irradiation. In Article 2 we studied the UV-absorption enhancement provided by both synthetic and natural eumelanin to a commercial grade of ethylene-vinyl acetate copolymer (EVA), a polymer for packaging applications. The effects of prolonged UV exposure were studied, too. Eumelanin's performance was compared to a commercial UV stabilizer (2-hydroxy-4-(octyloxy) benzophenone or BLS®531 from Mayzo).

3) Shedding light on eumelanin's biodegradability in compost from municipal waste, at room temperature (25 °C) and in composting conditions (58 °C);

a. Given that proper assessments of the biodegradability of materials for organic electronics have lacked so far [250], the case study of the biodegradability in composting conditions was extended to two materials representative of organic electronics: a solution-processable polymer whose electrical conductivity can be increase by 16 orders of magnitude by chemical doping [314], investigated in photovoltaics [315], namely poly(p-phenylene sulphide) (PPS), and a molecular dye featuring semiconducting properties that was assessed as the active layer of transistors and photovoltaic cells [316]–[318], namely copper (II) phthalocyanine (Cu-Pc) (Figure 3.1). This investigation is reported in Article 3.

(A)

(B)
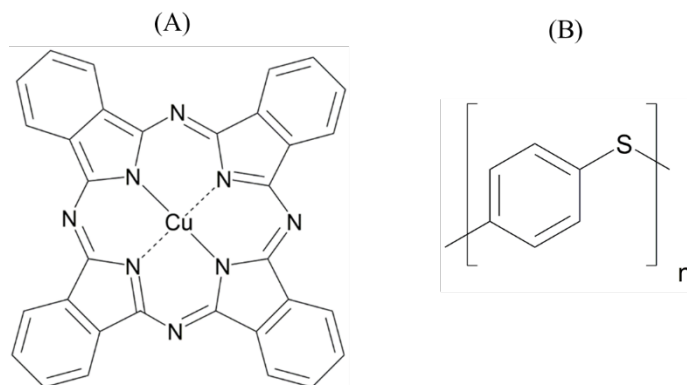
Figure 3.1 (A) Cu (II) phthalocyanine; (B) monomer of poly(p-phenylene sulphide).

CHAPTER 4   METHODOLOGY

4.1 Atomic Force Microscopy

The atomic force microscope (AFM), also known as the scanning force microscope (SFM), belongs to a larger family of instruments termed the scanning probe microscopes (SPMs) [319].

An AFM instrument is based on a sharp probe (tip), mounted at the apex of a flexible microcantilever arm (Figure 4.1). In turn, the cantilever itself is mounted on a piezocrystal which allows the position of the probe to be moved with respect to the surface of interest [319], [320].
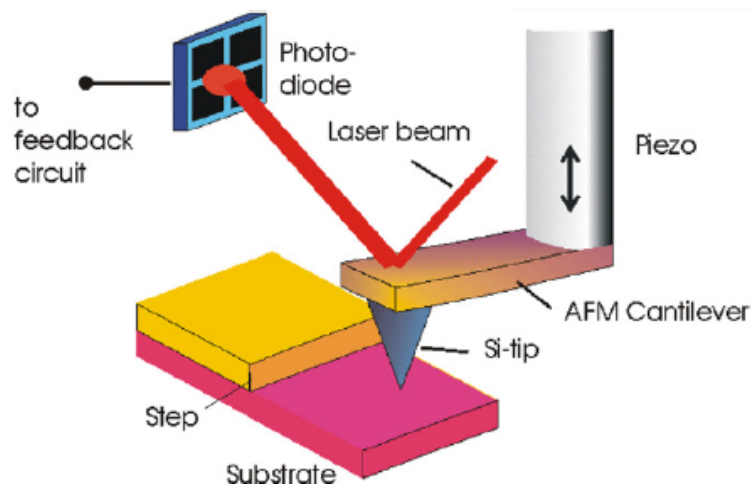
Figure 4.1 Basic AFM set-up. Reprinted with permission from Ref. [320].

A three-dimensional picture of the topography of such surface can be obtained to a nanometric or sub-nanometric resolution, by raster-scanning this probe across the surface of interest. As the probe meets the topographic features present on the surface, the deflection of the cantilever is monitored. From the reverse (uppermost) side of the cantilever, a laser beam is reflected onto a position-sensitive photodetector. The deflection of the cantilever brings about a change in the position of the laser spot on the photodetector, so that changes of such deflection are monitored (Figure 4.1) [319], [320].

In "static" AFM modes, such as contact mode, the probe remains in constant contact with the sample while in "dynamic" modes the cantilever is oscillating, such as with the intermittent

(tapping) or non-contact modes [319]–[321]. Tapping mode was conceived to reduce lateral forces and drag while the probe is scanned across the surface. The cantilever oscillates at a frequency close to its resonant value with fixed amplitude. The probe repeatedly engages and disengages with the surface when approaching a sample [319], [320]. Consequently, the amplitude of oscillation will be restricted as the probe encounters differing topography. By using a feedback mechanism to maintain a constant amplitude (by changing the height of the piezocrystal), an image of the topography of the surface is obtained. Differences in the mechanical and adhesive properties of areas of the same surface can cause a change in the frequency of oscillation, in turn bringing about a shift in the phase signal between the frequency with which the cantilever is actually oscillating and the drive frequency. This phenomenon has been leveraged to obtain phase images in parallel with topographic images [319], [320].

Commercially manufactured probes and cantilevers are mostly made of silicon nitride or silicon [319], [320].

AFM in tapping mode was used to study the interface between eumelanin thin films and metal electrodes as well as the 10 μm interelectrode distance, after the transient electrical measurements, in Article 1 and Article 4.

4.2 Scanning Electron Microscopy and Energy-Dispersive X-ray Spectrometry

The components of a scanning electron microscope (SEM) are: an electron gun, a column with electromagnetic lenses, an electron detector, the sample chamber as well as a computer and display to view the images [322] (Figure 4.2).
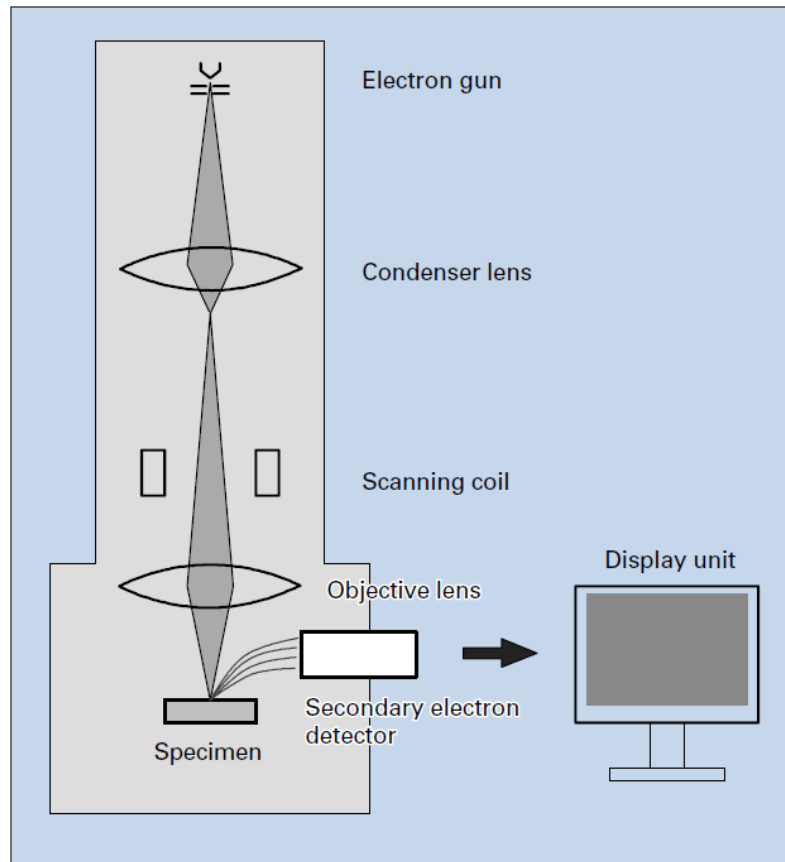
Figure 4.2 Basic components of a SEM. Reprinted with permission of JEOL USA Inc. from Ref. [323].

The sample is mounted on a stage in the chamber area; both the column and the chamber are kept under vacuum by a combination of vacuum pumps. At the top of the column, the electron gun generates electrons and accelerates them to an energy in the range 0.1-30 keV [322]. The electrons travel down the column, passing through a combination of lenses that produces a focused electron beam. Such a beam (diameter lower than 10 nm) reaches the surface of the sample. A deflection system (scan coils) controls the position of the electron beam on the sample, allowing it to sweep across the specimen. The interaction between the electron beam and the sample generates several signals, that are detected by appropriate detectors, to form images which are then displayed on the computer screen. In particular, images can be taken either in secondary electron mode or in backscattered electron mode [322].

Secondary electrons are defined as "the loosely bound outer shell electrons from the constituent atoms of the specimen, which receive sufficient kinetic energy from the beam electrons to be ejected from the atom" [322]. Those generated near the top surface of the specimen are emitted outside of it. The emission of secondary electrons depends on the incident angle of the electron beam and a secondary electron mode image gives information on the surface topography [322].

The interaction between the beam electrons and the specimen atoms can also cause elastic scattering of the beam electrons with no energy loss, i.e. backscattered electrons. The volume of interaction in the specimen has an approximately half-sphered shape, with its diameter inversely proportional to the atomic number of the constituent atoms. The probability of elastic scattering increases with the atomic number. A higher yield of backscattered electrons from one area with respect to another is due to atoms with a higher atomic number, with one area appearing brighter than another in the backscattered electron mode image [322].

The maximum resolution obtainable in an SEM depends on several factors, such as the electron spot size and interaction volume of the electron beam with the sample; some SEMs can achieve resolution below 1 nm [322].

SEM analytical capabilities are based on the interactions between the electron beam and the specimen's volume beneath the beam, from which X-ray photons are generated. If an X-ray spectrometer is added to the microscope, EDS or EDX (Energy-Dispersive X-Ray Spectrometry) can be carried out to obtain a localized chemical analysis. The electron beam bombardment can cause the ejection of an inner shell electron from the atom, creating a vacancy. The transition of an electron from a more external shell to the inner shell with such vacancy brings about the emission of an X-ray photon with a specific energy. As the energy differences between electron shells are characteristic for each element, the X-rays characteristic of each element (characteristic X-ray lines) can be inferred [322]. Another interaction electron beam-specimen is represented by the deceleration of the electron beam electrons in proximity of the Coulombic field of the specimen atoms. Such loss in kinetic energy implies the emission of other photons, which are not related to the specimen elements and give the continuum background of the spectrum [322].

SEM was used to study the interface between hydrated eumelanin thin films and metal electrodes as well as the 10 μm interelectrode distance, after the application of an electrical bias, in Article 1 and Article 4. Images both in secondary electron mode and backscattered electron mode were

taken. EDX was used to have insights on the composition of the bridging structures that formed from the dissolution of the metal electrodes in the same two articles.

4.3 Time-of-Flight Secondary Ion Mass Spectrometry

Time-of-Flight secondary ion mass spectrometry (ToF-SIMS) is the combination of the analytical techniques SIMS (Secondary Ion Mass Spectrometry) and Time-of-Flight mass analysis (ToF). It provides detailed elemental and molecular information regarding the surface of a sample. It is used for semiconductors, polymers, paints, coatings, glass, paper, metals, ceramics, biomaterials, pharmaceuticals and organic tissues [324].

During a ToF-SIMS analysis, a solid surface is bombarded by primary ions of high (some keV) energy. The primary ions kinetic energy is dissipated through collision cascades in the near-surface region. While the primary ion is buried below the surface, bonds near the site of impact are broken allowing surface atoms, molecular fragments and molecules to overcome the surface binding energy, being ejected from uppermost three atomic layers [324]. The majority of the emitted particles are neutral in charge, but a small proportion is also positively or negatively charged. Only the charged species will be detected by the ion mass spectrometer. If the primary ion dose is lower than 10^{12} ions/cm^2, the SIMS investigation is called "static", as in ToF-SIMS, because it analyzes the original, non-modified surface composition; if the primary ion dose is higher, there is a significant probability that the emitted ions arise from a previously sputtered area, hence they are not representative of the virgin surface [324].

Among the different types of mass spectrometers, ToF has the advantage of very high mass resolution (several thousands of Da). A ToF spectrometer leverages on the feature that ions with the same energy but different masses travel with different velocities. An extraction field of few thousand volts accelerates the generated ions with a fixed kinetic energy. The accelerated ions then travel over a drift path to the detector, with the velocity inversely proportional to the mass. From the measurement of the flight time of each ion, its mass can be inferred [324].

ToF-SIMS was used to gain insights into the composition of eumelanin-Au complexes of the dendrites forming in the interelectrode distance, after the application of an electrical bias, in Article 1.

4.4 UV-visible-NIR Spectroscopy

UV-visible-NIR spectroscopy provides a quantitative measurement of the interaction of ultraviolet (UV) (220–400 nm), visible (400–800 nm), and near infrared (NIR, 800–2500 nm) radiation with a material. This type of spectroscopy can be used to probe the intrinsic properties of a material, e.g. its absorption coefficient.

The interaction of light with a material's electrons, which results in electronic transitions between different energy levels, is responsible for the appearance of absorption in the UV, visible and NIR ranges [325]. In the present thesis, the instrument used for UV-visible-NIR spectrophotometry was a Lambda1050 spectrophotometer from PerkinElmer. Such an instrument provides monochromatic light by means of a monochromator over a wavelength range of 170 nm to 2500 nm; a deuterium lamp covers the UV spectrum and a tungsten-halogen lamp covers the visible-NIR spectrum. Using a combination of two detectors (a photomultiplier and an InGaAs-based detector) sensitive over the range of interest, a spectrophotometric curve is obtained by comparison of the signal measured after interaction of the monochromatic light with the sample and the signal recorded without the sample in the measurement beam (reference beam) [325]. In particular, the instrument used here is a double-beam spectrophotometer: the radiation produced by the source is split into two beams, one of which will encounter the sample whereas the other reaches the detector following a sample-free (reference) path [326]. Such a set-up allows for a continuous comparison between the intensity (power per unit area) of the two beams and, as a result, avoids erroneously attributing system fluctuations (e.g. light source intensity changes) to the sample.

In the case of an ideal non-scattering material, the measurement of the reflected or transmitted light beam is relatively straightforward, as both the reflected and transmitted beam travel along a single-well defined direction (Figure 4.3). The radiation passing through the material will face a change of direction according to Snell's law, and will be transmitted along a single direction as well (specular transmission) (Figure 4.3).

In the case of a scattering material, both reflected and transmitted light are redirected in all directions (Figure 4.3). Consequently, measuring diffusive samples is not a trivial task [326]. It is for these applications that integrating sphere methods become important, to collect and measure part of the diffusely transmitted and/or reflected radiation.
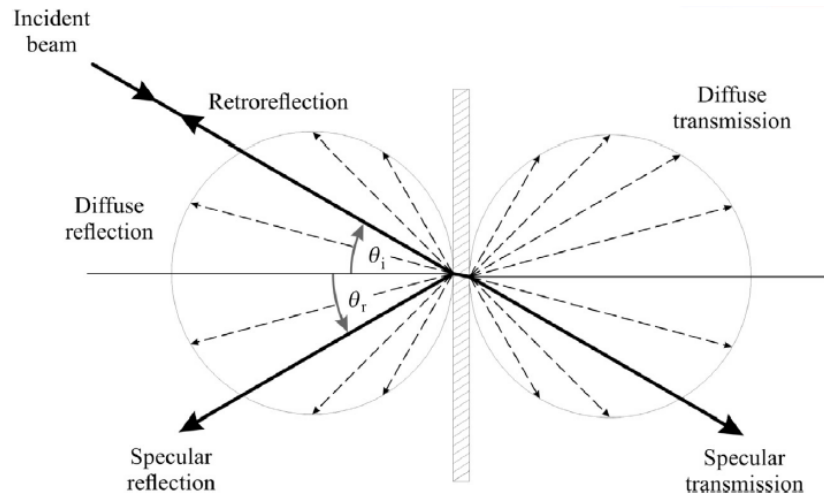
Figure 4.3 Schematic representation of reflection and transmission from a scattering material. Reprinted with permission from Ref. [326].

An integrating sphere, also called an Ulbricht sphere, is an optical device for photometric measurements featuring a hollow sphere covered inside with a white highly reflective and uniformly diffusing (Lambertian) coating (e.g. Spectralon®). The set-up brings about many diffuse internal reflections of the entering radiation (Figure 4.4, A). The sphere generally presents two or more small openings, the ports, for introducing the light beam or attaching detectors. Baffles that prevent the detector from directly viewing the light source or the area of the sphere wall directly illuminated by the light source are usually present [326] (Figure 4.4).

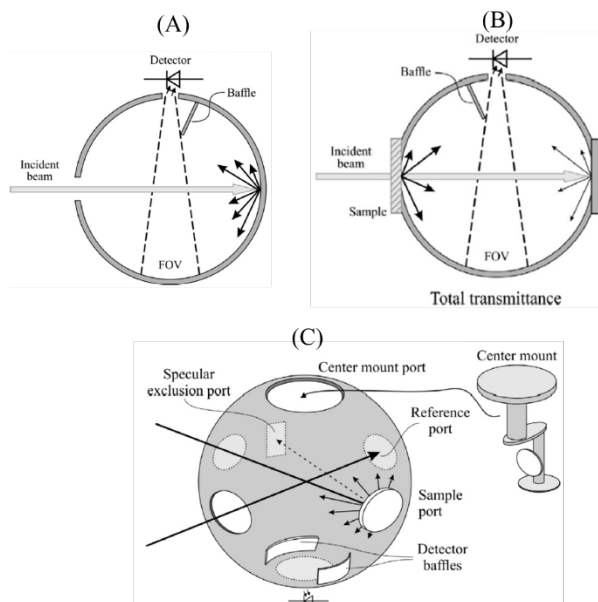
Figure 4.4 (A) Typical layout of an integrating sphere; FOV stands for field of view of the detector; (B) set-up of an integrating sphere system for total transmittance measurements; (C) commercial integrating sphere with the center-mount set-up. Reprinted with permission from Ref. [326].

An important class of accessory for diffuse reflectance and diffuse transmittance measurements with integrating spheres is represented by center-mount sample holders (Figure 4.4, C). In this type of sphere design, cuvettes or thin films are held in the middle of the sphere; the angle of incidence can be varied thanks to the rotation of the attached holder. Using the center-mount approach allows to measure simultaneously the diffusive transmittance τ and reflectance ρ. Absorptance can then be inferred as it is the complementary to 1 with respect to $\tau + \rho$.

The UV-visible-NIR Lambda1050 spectrophotometer equipped with an integrating sphere with center-mount set-up was used in Article 2 to compare the UV-visible absorption of the control plastic films with respect to the films containing eumelanin and the commercial benzophenone. In addition, it was deployed to check the effects of prolonged UV irradiation (UV-aging test) on the UV-visible spectra of the plastic films.

4.5 Infrared Spectroscopy

The absorption of electromagnetic radiation of the infrared region by a molecule promotes transitions between quantized vibrational energy levels of the ground (lowest) electronic energy state. Vibrational modes can range from bond stretching to various types of vibrations [327], [328]. An infrared (IR) spectrum reports bands related to the frequencies of excitation of vibrational modes. As such frequencies are characteristic of specific chemical bonds or functional groups, the presence of specific chemical bonds or functional groups in a sample can thus be established from the IR spectrum. Furthermore, the absorption is proportional to the concentration of such functional groups. The predominant technique nowadays is represented by Fourier transform infrared spectroscopy (FT-IR). Mid-infrared spectra typically cover the range between 4000 cm^{-1} (2.5 μm) and 500 cm^{-1} (20 μm) [327], [328].

The frequency of vibration of certain functional groups slightly varies from one molecule to another containing that same functional group: these modes belong to the "fingerprint" region of the spectrum (1200-700 cm^{-1}) which makes each spectrum unique and proves useful in establishing the identity of a compound [327], [328].

In transmission mode, the IR radiation is focused on the sample in a cone-shaped beam, where it will be partly absorbed. The transmitted IR light is then focused on the detector for measurement [329]. If the sample is not self-supported, an IR-transparent window has to be used. Powder samples can be dispersed and pressed in KBr pellets, as KBr is transparent to IR radiation (cutoff wavelength is 388 cm^{-1}).

Another FT-IR sampling technique is represented by the attenuated total reflection (ATR). In the ATR technique, the sample is placed in intimate contact with a crystal of a material featuring a high-refractive index, the internal reflection element (IRE) (Figure 4.5) [327], [328]. When two materials with different refractive indices are put in contact, the one featuring the lower index is named the optical rare medium (in an ATR configuration, the sample), while the other one is called the optically dense medium (in an ATR configuration, the IRE) [328]. The IRE is transparent to IR radiation: ZnSe, Si, diamond, and Ge are the most used materials. If the beam of the IR radiation is directed into the IRE with an angle of incidence above a critical value, total internal reflection occurs at the IRE internal surface [327], [328]. The IR beam can then face one (as in the instrument used for this work) or several (as in Figure 4.5) internal reflections as it travels along the crystal and is then passed to the detector in the IR spectrometer, generating an IR spectrum [327], [328].

The working principle of the ATR technique is that the internal reflectance is identically equal to 1 if the optically rare material (the sample) does not feature any absorption [328]. Even if the beam is confined into the IRE, it gives rise to an evanescent wave at the interface with the sample, as the electromagnetic field of a photon is perpendicular to its propagation direction. Such an evanescent wave can interact with the sample over a distance named depth of penetration (defined as the depth at which the strength of the field decays to 1/e of its intensity at the surface) [327]–[329]. The depth of penetration depends on the radiation wavelength, the refractive index of the IRE and of the sample as well as on the angle of incidence [327]–[329]. At the wavelengths where functional groups of the sample feature absorption, the evanescent wave becomes attenuated: the measurement of such an attenuation as a function of wavelength brings to the infrared spectrum of the sample [327]–[329].

ATR accessories usually feature a clamp, with a metallic, rubber or polymer pad, to ensure proper contact between the IRE and the sample [328].
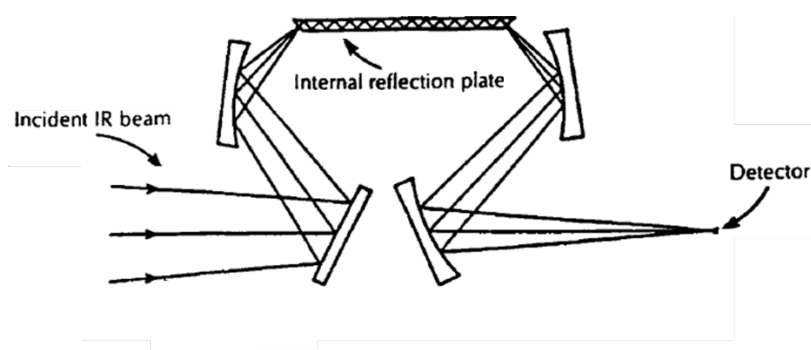
Figure 4.5 An ATR accessory. The sample is placed on the internal reflection plate assuring intimate contact. Adapted with permission from Ref. [327].

FT-IR in transmission mode was used in <u>Article 3</u> in order to compare eumelanin extracted from the cuttlefish ink to the commercially available counterpart, Sepia Melanin from Sigma-Aldrich. FT-IR in ATR mode was used in <u>Article 2</u> in order to identify the photo-degradation products forming during prolonged exposure of the polymer films to UV radiation.

4.6 Neutron Activation Analysis

Differently from most of chemical analysis methods that depend on the behavior of outer shell electrons, neutron activation analysis (NAA) is an elemental analysis method based on the properties of the nucleus. During NAA, a neutron bombardment of the nuclei of stable isotopes brings about the formation of radioactive isotopes, as some neutrons are captured by the nuclei [330]. A nuclear reactor is among the most practical neutron sources for NAA, producing neutrons via the nuclear fission process [330]. The radioactive isotopes emit characteristic γ-rays when they decay to stable nuclei (radioactive decay). The emitted radiations are used to characterize and quantify the constituent atoms of the specimen. The measurement is usually carried out with a high-resolution semiconductor detector [330], [331]. NAA has the advantage of being a non-destructive method. It allows for the characterization of more than 70 elements [332].

NAA was used to determine the amount of chlorine in natural and synthetic eumelanin in Article 1 as well as to measure the concentration of metals still present in traces after the extraction of Sepia Melanin from the cuttlefish ink in Article 3.

4.7 Thermogravimetric Analysis

During a thermogravimetric analysis (TGA), a sample (approximately 10 mg) is subjected to a controlled temperature program in a controlled atmosphere while its mass is measured by a balance as a function of temperature or time [333]. The atmosphere is controlled by flowing a purge gas through the balance. When gases such as nitrogen, argon, or helium are used, the atmosphere is inert (pyrolysis) while, if air or oxygen are used, it is oxidizing. A TGA measurement is usually visualized as a plot of residual mass (normalized with respect to the initial mass, so in percentage) versus temperature. The derivative with respect to temperature (DTG) is usually displayed, too [334], [335].

A TGA gives insights into the thermal decomposition of a material. Mass losses appear as steps in a TGA graph and are related to specific thermal degradation phenomena. For example, in the case of a polymer, volatile components such as low-molecular-mass additives and absorbed moisture are lost below 200 °C. Above such temperature, polymer degradation (chain scission, monomer unzipping and side group elimination) can take place by free radical processes initiated by bond

scission [334]. Regarding the DTG, its maxima represent the temperature of maximum rate of thermal degradation phenomena while its minima represent the end of such phenomena [334].

During processing and service, polymers are exposed to both heat and oxygen, so that a TGA in an oxidizing atmosphere better simulates the environment to which the polymer will be exposed. However, when a TGA is run in O_2 or air, a polymer can present an initial mass gain due to oxygen uptake, which can mask the onset of the degradation phenomena. In other words, the mass gain hides the mass loss due to the degradation onset and the polymer may then result, from the TGA graph, more thermally stable than it actually is [334]. TGAs in inert atmosphere, even if less close to simulate the real environment of service of the polymer, do not present the aforementioned artefact related to oxygen uptake and are consequently used as complementary tools to gain insights into the thermal stability of a polymer [334].

The standard ASTM E 2550-07 (*Standard Test Method for Thermal Stability by Thermogravimetry*) defines the onset degradation temperature of a polymer as "a point on the TG curve where a deflection is first observed from the established baseline prior to the thermal event": the deflection of the baseline can be determined by identifying the temperature at which the DTG attains a certain value (to be defined empirically case by case, e.g. 0.1 %/°C) [336].

Thermogravimetric analyses were used in Article 2 to evaluate potential synergistic or antagonistic effects between eumelanin and an anti-oxidant already present in the commercial grade polymer used. TGAs also helped gain insight into the effects of prolonged UV irradiation (UV-aging test) on the thermal stability of the polymers. In Article 3, the thermogravimetric analyses were used to compare the thermal decomposition of eumelanin extracted from cuttlefish ink to the commercially available counterpart, Sepia Melanin from Sigma-Aldrich. TGAs were also used to determine the dry mass and the ash content of the materials used for the biodegradability test in composting conditions. The dry solids represent the residual mass after heating the material at 105 °C until constant mass is reached, in inert atmosphere. The ash content represents the residual mass after heating the material at 550 °C until constant mass is reached, in air [337].

4.8 Biodegradation

4.8.1 Aerobic Biodegradation

When aerobic biodegradation takes place, the microorganisms present in the soil transform the carbon of the test material partly into gaseous products (CO_2, respired carbon) and partly into their biomass (assimilated carbon) [187]. The simplified biochemical reaction can be summarized as:

$$C_{TEST} + O_2 \rightarrow CO_2 + H_2O + C_{RESIDUE} + C_{BIOMASS} \qquad (1)$$

Where C_{TEST} is the carbon of the test material, $C_{RESIDUE}$ is the carbon not metabolized by the microorganisms and $C_{BIOMASS}$ is the carbon assimilated and transformed into their biomass by the microorganisms. From reaction (1) it is thus evident that the respiration of the microorganisms can be followed either by measuring the O_2 consumed or by measuring the CO_2 evolved. The ratio $CO_{2\ evolved}$ / $O_{2\ consumed}$ is called respiratory quotient (it was assumed to be 1 mol / mol in this work) [338].

However, it is worth noting that the microorganisms may, at the same time, biodegrade not only the carbon of the test material C_{TEST} but also the carbon of the organic matter already present in the compost ($C_{ORG\ MAT\ COMP}$) [338]. As a result, reaction (1) has to be written as:

$$C_{ORG\ MAT\ COMP} + C_{TEST} + O_2 \rightarrow (CO_{2\ from\ C\ ORG\ MAT\ COMP} + CO_{2\ from\ C\ TEST}) + H_2O + (C_{RESIDUE\ from\ C\ ORG\ MAT\ COMP} + C_{RESIDUE\ from\ C\ TEST}) + (C_{BIOMASS\ from\ C\ ORG\ MAT\ COMP} + C_{BIOMASS\ from\ C\ TEST}) \quad (1.1)$$
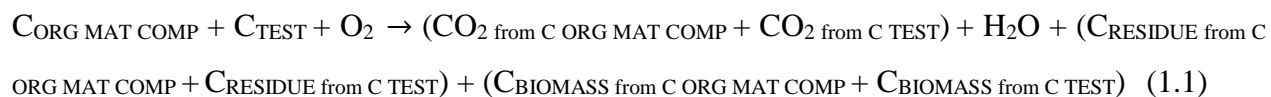
Consequently, it is always necessary to subtract the respiration activity of blank compost (plain compost without any test material), quantified with $CO_{2\ from\ C\ ORG\ MAT\ COMP}$, from the respiration activity of the compost containing the test material ($CO_{2\ from\ C\ ORG\ MAT\ COMP} + CO_{2\ from\ C\ TEST}$) in order to have a value related solely to the biodegradation of the test material ($CO_{2\ from\ C\ TEST}$) [339]. Apart from the monitoring the respiration activity of the blank compost, biodegradability tests generally involve also a biodegradable material (cellulose), called the positive control, and a non-biodegradable material (polyethylene, PE), called the negative control [339].

4.8.2 Quantifying the Biodegradation of a Material

The biodegradation percentage (mineralization) at a certain time is evaluated as follows [339]:

$$Mineralization\ (\%) = \frac{CO_2\ (material) - CO_2\ (blank\ compost)}{CO_2 (total)} * 100 \qquad (2)$$

Where *CO₂ (material)* is the measured mass of CO_2 evolved from the bioreactor containing the test material blended with or buried in the compost, *CO₂ (blank compost)* is the average measured mass of CO_2 evolved from the bioreactors containing blank compost, and *CO₂ (total)* is the total theoretical mass of CO_2 that would evolve if all the test material were completely respired by the compost's microbiota, as for the following equation:

$$CO_2\ (total)(g) = C_\% \ * m \ * \frac{44\ (CO_2\ molecular\ mass)}{12\ (C\ atomic\ mass)} \qquad (3)$$

where $C_\%$ is the mass percentage of carbon (inferred from the formula or measured by means of a CHN elemental analysis) and *m* is the sample mass.

ASTM D6400 (*Standard Specification for Labeling of Plastics Designed to be Aerobically Composted in Municipal or Industrial Facilities*) states that a plastic polymer can be defined biodegradable if it reaches 90% of mineralization, absolute or with respect to the positive control, in a time range between 45 and 180 days during the biodegradability test in composting conditions [339].

In Article 3, a biodegradability test under thermophilic conditions (composting, at 58 °C) was carried out using compost from municipal waste. The standard protocol ASTM D5338 (*Standard Test Method for Determining Aerobic Biodegradation of Plastic Materials Under Controlled Composting Conditions, Incorporating Thermophilic Temperatures*) was followed and the CO_2 evolving from the compost blended with the materials of interest was monitored for 98 days. A phytotoxicity test ensued (see next paragraph). Furthermore, in Article 3, a biodegradability test under mesophilic conditions (at 25 °C) was performed, too: the O_2 consumed by compost blended with the materials of interest was monitored for 97 days.

4.8.3 CHNS Elemental Analysis and Inorganic Carbon Analysis

The CHNS elemental analysis is a technique to determined carbon, hydrogen, nitrogen and sulphur in organic matrices in the field of pharmaceuticals, polymers as well as environmental and food science.

Such an analysis entails burning the sample in pure oxygen at 920 – 980 °C under static conditions (introduction of a fixed volume of oxygen). Carbon is converted to carbon dioxide, hydrogen to water vapor, nitrogen to nitrogen oxides (NO_x) and sulphur to sulphur dioxide. An inert gas such as helium sweeps the combustion gases out of the combustion chamber. Such gases pass over high

purity copper heated at approximately 600 °C, which assures the removal of any oxygen that did not react during the initial combustion as well as the conversion of any oxides of nitrogen to molecular nitrogen gas. Subsequently, the gases flow over absorbent traps in order to leave only carbon dioxide, water, molecular nitrogen and sulphur dioxide. If sulphur determination is not required (as in our case), its combustion products will be removed by the absorbents, too. The different gases are separated by gas chromatography and their amount is quantified by thermal conductivity detectors [340]. In Article 3, the CHN analysis, carried out by Galbraith laboratories (TN, USA), was used to determine the mass percentage of carbon ($C_\%$ of equation 3) of the materials of interest, for the computation of the biodegradation levels.

The Inorganic Carbon Analysis was carried out by Galbraith laboratories on Sepia Melanin extracted from cuttlefish ink, in Article 3. This analysis aimed at assuring that no traces of inorganic carbon (carbonates) were present in the pigment extracted, given the marine biological medium from which it was extracted. Such method determines bicarbonate ion and carbonate ion concentrations in a sample. Carbon dioxide evolves from the sample through acidification (1 N $HClO_4$ or 2 N H_2SO_4) and heating at approximately 50 °C, following a procedure established in the literature [341]. Carbon dioxide-free nitrogen sweeps the evolved carbon dioxide through a scrubber and into an absorption cell, which automatically titrates with a coulometer, as explained in [342].

4.8.4 Phytotoxicity Test

Biodegradability is only one of the three criteria to define a plastic material compostable, the other two being disintegration (maximum 10% of its original dry weight remains after sieving on a 2.0-mm sieve after 84 days of biodegradability test in composting conditions) and ecotoxicity. Ecotoxicity, also known as "terrestrial safety", refers to the impact that the material has on the quality of the compost as a fertilizer. To put it in simple terms, an ecotoxicity test evaluates whether the material "transferred toxicity" to the compost. It is based on two analyses carried out on the compost blended with the test material at the end of the ASTM D5338 test: the measurement of the concentration of certain elements (mostly metals) and a phytotoxicity test (planting seeds and evaluating the plant germination and growth) [343]. A phytotoxicity test was carried out, following an internal protocol of the Aquatic and Crop Resource Development Group of the Canadian Research Council, adapted from the OECD Guideline 208 (*Terrestrial Plant Test: 208: Seedling*

Emergence and Seedling Growth Test) in <u>Article 3</u>, to determine if the materials tested transferred toxicity to the compost during the biodegradability test at 58 °C.

CHAPTER 5   ARTICLE 1: RESISTIVE SWITCHING CONTROLLED BY THE HYDRATION LEVEL IN THIN FILMS OF THE BIOPIGMENT EUMELANIN

Article 1 has been published in the *Journal of Material Chemistry C* on September 21st, 2016. The Supplementary Information is provided in Appendix A.

5.1 Authors

Eduardo Di Mauro,[a] Olivier Carpentier,[a] Sergio Ivan Yáñez Sánchez,[a] Ndembi Ignoumba Ignoumba,[a] Myriam Lalancette-Jean,[a] Josianne Lefebvre,[a] Shiming Zhang,[b] Carlos F. O. Graeff,[c] Fabio Cicoira,[b] Clara Santato[a]

[a] *Department of Engineering Physics, Polytechnique Montréal, C.P. 6079, Succ. Centre-ville, Montréal, Québec, H3C 3A7 Canada.*

[b] *Department of Chemical Engineering, Polytechnique Montréal, C.P. 6079, Succ. Centre-ville, Montréal, Québec, H3C 3A7 Canada.*

[c] *DF-FC, Universidade Estadual Paulista, Av. Eng. Luiz Edmundo Carrijo Coube 14-01, 17033-360 Bauru, Brazil.*

5.2 Introduction

Melanins are abundant pigments in the biosphere [113], endowed with a vast set of interesting properties, notably thermoregulation, photoprotection, metal ion-chelation, and free radical quenching [344], as well as antioxidant functions [69].

Eumelanin is a black-brown subgroup of melanins [2], whose building blocks are 5,6-dihydroxyindole (DHI) and 5,6-dihydroxyindole-2-carboxylic acid (DHICA) [19], [31], [344]. Between four and eight of these building blocks form planar, covalently-bonded oligomers (protomolecules), which stack non-covalently via π-π interactions [27], [31], [345]–[347]. Its humidity dependent electrical conductivity, once studied in the context of amorphous semiconductivity [109], has been recently reinterpreted as an electronic-ionic (protonic) mixed

conduction [113], [114]. Other intriguing features are radioprotection [348], immunomodulatory activity [349], biodegradability and biocompatibility [126].

In humans, eumelanin can be found in the skin, hair, middle ear, retina and heart [350], [351].

Considerable attention has been paid to the involvement of eumelanin in the accumulation and release of metal cations in the human body [352]–[355]. Zinc [352], [354], [356]–[361], copper [356], [357], [359], [360], [362]–[364], calcium [353], [361], [365], manganese [366], [367], iron and heavy metals [359], [360], [368]–[372] bind *in vivo* to eumelanins. Depending on the pH and the type of eumelanin (natural or synthetic), the phenolic hydroxyls, amine or carboxylic groups of the indolic building blocks have been reported to be preferential binding sites for metal cations [28], [373]. Particular efforts have been made to understand the binding of iron to neuromelanin [374]–[383], a subclass of melanin that accumulates within the dopaminergic neurons of the *substantia nigra* of the brain [384], since iron has been reported in such neurons only in the case of Parkinson's disease [385].

While the interactions of eumelanin with free metal cations have been extensively studied [70], only recently attention has been paid to the interfaces between thin films of the pigment and metal electrodes [210], mainly due to the well-known limited solubility of eumelanin in common organic solvents [107]. The formation of tree-shaped electrically conductive bridges (dendrites) has been observed in hydrated eumelanin thin films included between gold electrodes, in planar configuration, under electrical bias [210]. Dendrites form by the dissolution of the positively biased Au electrode and migration of gold nanoclusters to the negative electrode, where they are reduced, forming dendrites, which grow towards the positive electrode. A dramatic drop in the resistivity takes place when the first dendrite bridges the electrodes (resistive switch, RS) [210].

Electrochemical metallization memory cells (ECMs), also called conductive bridge random access memories [133], are a class of Resistive Random Access Memories (ReRAM) [134], [135], which in turn are non-volatile memories [135]. The working mechanism of ECM is based on the formation of conductive filaments under bias: the active electrode dissolves generating cations that migrate through a solid electrolyte (ion conductor) to be reduced at the counter electrode, where the conductive filament nucleates [135]. The prospects of ReRAMs are low power consumption [134], [136]–[138], good reliability [133] as well as fast response time [133], [136], multilevel data

storage [133], [136], [139] and high density [134]. Furthermore, filamentary-based systems can lead to nanoscale memory devices, because the switching takes place in highly localized regions, highlighting the ease of miniaturization [386]. Organic and polymeric switching memories, a subclass of ReRAMs, have become an emerging technology that could complement conventional memory technologies [387]–[390]. They feature advantages such as stackability [391], scalability [149], flexibility [142]–[148], [392], optical transparency [144], printability [142], [149] and offer the possibility of tuning electrical and physical properties by means of molecular design and chemical synthesis [150], [151] for low-cost [153] and high density [135], [152] memory applications. Organic polymers, possibly including salts, well-established organic electronics polymers and small molecules have been used in conductive bridge memories [140], [153]–[157], [392]–[399].

Recently, interest in biomaterials for memories has increased in the context of green (sustainable) or biocompatible electronics [400]. Silk fibroin [400]–[403], egg albumen [404], cellulose [146], chitosan doped with Ag [145], [148] are examples of biomaterials that have been used in cells with conductive filament resistive switching. Interestingly, eumelanin presents both ion conduction [108] and metal binding properties [70], features that promote the formation of metal filaments in polymers included between metal electrodes [389].

The analogies between the phenomenon of dendrite growth in eumelanin films and the working mechanism of ECMs hints that the elucidation of metal-eumelanin interactions under bias may open technologically oriented studies e.g. where eumelanin can be used as ion conductor in ECMs with its characteristics of biodegradability [126] and biocompatibility [107].

In this work, we report on transient electrical measurements in planar configuration on eumelanin thin films (Au/eumelanin/Au systems) at different experimental conditions, such as different relative humidity (RH) levels and hydration times. Planar systems are crucial for the investigation of the filament growth and, consequently, for the future development of stacked (vertical) resistive switching devices [398]. Scanning electron microscopy (SEM), atomic force microscopy (AFM) and time of flight-secondary ion mass spectrometry (ToF-SIMS) gave insights on the morphology and chemical composition of the filaments that formed in the hydrated films upon electrical bias as well as on the different types of resistive switch observed.

5.3 Experimental

5.3.1 Sample Preparation

Synthetic (Sigma) eumelanin and natural (Sepia) eumelanin (extracted from the ink sac of a cuttlefish) were purchased from Sigma Aldrich (Canada) and had a chloride Cl^- content of respectively 0.83±0.04% wt. and 6.92±0.35% wt., as measured by nuclear activation analysis (NAA). DMSO-melanin was synthesized by the group of Prof. C. Graeff, São Paulo State University – UNESP following a procedure reported in the literature [310] (chloride Cl^- content of 0.10±0.01% wt., as measured by NAA).

Eumelanin was dissolved in dimethyl sulfoxide (DMSO) sonicated and filtered (0.1μm PTFE membrane with polypropylene housing, 25 mm diameter, PURADISC^{TM}), to yield suspensions of 15 mg/mL, *approximately* (as some eumelanin aggregates may have been trapped in the filter). NaCl was added to some of the 15mg/mL suspensions of eumelanin in DMSO in concentrations of 0.8mg/mL and 1.8mg/mL (Table S1).

The substrates (SiO_2 on Si) were purchased from Silicon Quest International (San Jose, California, USA), thickness 525±25μm. The Au electrodes were deposited by e-beam evaporation and photolitographically patterned on the substrates (5 nm of Ti as the adhesion layer and 30 nm of Au). The width of the electrodes was 4 mm, and the interelectrode distance was 10 μm. Prior to film deposition, the patterned substrates were cleaned in an ultrasonic bath with acetone, isopropanol, and de-ionized water, and then underwent a 10 min UV-ozone treatment. The thin films were spin coated (1 minute at 1000 rpm followed by 30 seconds at 4000 rpm) and hydrated in a Cole-Parmer Mini humidify/dehumidify chamber (03323-14), which includes an automatic humidity controller and an ultrasonic humidification system. Controlled humidity ranged from 5 to 95% with programmable controller set-points.

5.3.2 Electrical Measurements

The electrical measurements were performed with a Source Measure Unit (SMU), Agilent 2900A, with Quick IV Software for data recording. The confinement of the DMSO drops during transient current measurements was achieved by means of a well of Polydimethylsiloxane (PDMS). The evaluation of the resistance after 5-10 months of storage was made with voltage sweeps (each cycle

included three ramps: 0 V - maximum voltage, maximum voltage–minimum voltage, minimum voltage - 0 V) at combinations of the following conditions: 90% RH and at ambient RH (25%), at different sweep rates (0.2mV/s, 2 mV/s, 200 mV/s and 2 V/s), in different voltage ranges (- 1 V to 1 V, - 2.5 V to 2.5 V, -5 V to 5 V, -10 V to 10 V), and, for the fastest sweep rates (200mV/s and 2V/s) for 10^2 cycles.

5.3.3 Other Characterization Techniques

Atomic force microscopy images were taken with a Dimension 3100 with Nanoscope V (Digital Instruments, Santa Barbara, California, USA) with Si (model:ACTA) probes (tip radius <10 nm, spring constant 42 N m^{-1}) in tapping mode. The same microscope was used to measure the thickness: once a scratch had been done on the side of the interelectrode area, parallel to the channel, the thickness was then obtained from the profile of the scratch.

The measurements of the thickness by Spectral Reflectance were kindly carried out by the company Filmetrics (New York, USA), by means of a F40-Thin Film Analyzer.

Scanning electron microscopy was performed with a Microscope JEOL JSM7600F; all the images were taken in Secondary Electron Mode (SEM Voltage specified for each image). Samples were not metallized, unless otherwise stated. The EDX spectra were taken at the same microscope, Software: Aztec (Oxford), Detector: x-Max (80 mm^2) (Oxford), at 5kV.

Raman measurements were carried out using a Renishaw Invia reflex confocal Raman microscope with a CCD detector. Raman spectra were collected at room temperature with 10% of maximum laser power, 30 s exposure time and five accumulations in static mode. A 1800 lines mm^{-1} grating was used in conjunction with 25 mW, 488 nm laser lines, focused on the samples using a 50X objective lens.

Nuclear activation analysis was performed with a SLOWPOKE nuclear reactor (Atomic Energy of Canada Limited) and a Ge semiconductor gamma-ray detector (Ortec, GEM55185). The samples were irradiated for 600 s at a thermal neutron flux of 5.4×10^{11} cm^{-2} s^{-1}. Gamma rays were detected after 120 s, for 600 s, at a distance of 35 mm. Time-of-flight secondary ion mass spectrometry (ToF-SIMS) analyses were performed using a TOF-SIMS IV (IONTOF, GmbH, Münster, Germany). Bi^{3+} cluster ions at 25 keV were used as primary ions in burst alignment mode to obtain

high resolution ion mappings over areas of 50 μm x 50 μm. The pulsed ion current was 0.06 pA with a pulse width of 100 ns. Images were accumulated for 1000 s.

5.4 Results and discussion

5.4.1 Dendrite Formation Time

Transient current measurements performed at 1 V on films of synthetic eumelanin (hereinafter referred to as "Sigma eumelanin"), hydrated for 1 hour at 90% RH, revealed that, in about 40% of the cases, at least one dendrite bridged the interelectrode distance in a time range between 30 and 60 minutes. This standard resistive switch showed an ON/OFF ratio of ~10^4 (ratio between the electric current measured after (ON) and before (OFF) the electric resistive switch, Figures S1 and S2, Table S2). In the other cases, AFM and SEM images revealed that the process of dendrite formation was ongoing for biasing times longer than 1 hour. In particular, three different samples biased for times ≥3 hours (3 h, 15 h and 27 h) showed that the longer the biasing time, the closer was the sample to a resistive switch: after 15 hours, the dissolution of the positive electrode -and consequently the number of nanoclusters in the channel- was greater than after 3 hours and, after ≈ 28 hours, dendrites protruded from the negative electrode (Figure 5.1).

Although the average thickness of the samples where a resistive switch took place in the first hour of bias (27±7 nm) was higher than the average thickness of the remaining samples (18±10 nm), we could rule out the thickness as a factor determining a higher probability of resistive switch, due to (i) the absence of a trend of the thickness with respect to the time to resistive switch (Figure S3) and (ii) samples having a thickness in the same range showing different biasing effects (e.g. for 3 samples with 30 nm thickness, we observed a resistive switch after half an hour, a resistive switch after one hour and material migration still ongoing after 15 hours).

The key parameter that likely differentiate the two sets of thin films (one with resistive switch in a time scale of 1 hour and the others with dendrite formation process still ongoing over time scales as long as 28 hours) is the suspension from which they were spin coated. We can tentatively hypothesize that the time required for dendrite formation dramatically depends on the local film morphology (that is, the arrangement of eumelanin nanoaggregates that make up the film), which may vary from sample to sample depending upon the nature of the suspension. Indeed, different suspensions of eumelanin in the solvent DMSO, at a concentration of 15 mg/mL, may include

nanoaggregates with different supramolecular aggregation, size and shape [405], due to the well-established limited solubility of eumelanin in common organic solvents [107].
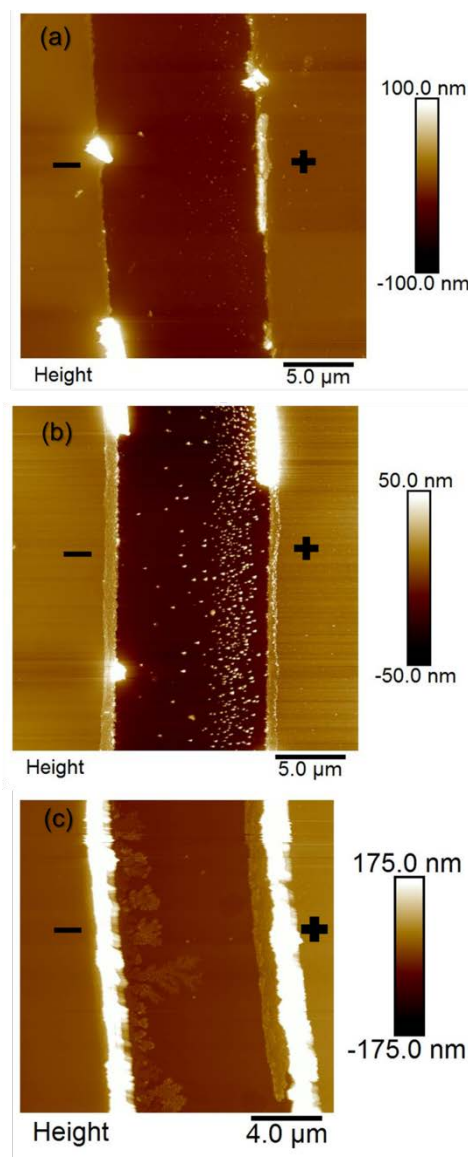
Figure 5.1 AFM images: (a) 25 μm × 25 μm, interelectrode area of a thin film of Sigma eumelanin, hydrated for 1 hour at 90% RH and biased at 1 V for 3 hours: nanoclusters form; (b) 25 μm × 25 μm, interelectrode area of a thin film of Sigma eumelanin, hydrated for 1 hour at 90% RH and biased at 1 V for 15 hours: nanoclusters migrate towards the negative electrode; (c) 18 μm × 18 μm, interelectrode area of a thin film of Sigma eumelanin, hydrated for 1 hour at 90% RH and biased at 1 V for ≈ 28 hours: dendrites grow from the negative electrode towards the positive electrode.

In some cases, the local morphology of the thin films may be more favorable to gold nanocluster formation and migration than others, providing a preferential direction for the growth of the dendrite (straight rather than lateral) (Figure S4). We can conclude that, for thin films of Sigma eumelanin, the phenomenon of dendrite formation takes place in each sample but its kinetics cannot easily be foreseen.

5.4.2 Effects of the Hydration Time

In order to study the influence of the hydration time on the process of formation of the dendrites, transient current measurements were performed on thin films hydrated for times longer than 1 hour. The time frame between the fabrication of the thin film and the start of the electrical measurements, during which the thin film is exposed to a certain RH level and consequently absorbs water, plays a major role in the dendrite formation: the longer is time, the higher is the uptake of water, up to a saturation limit, with a logarithmic increase [123].

The water content is expected to have a dichotomous role: up to a certain amount, a favorable effect, in terms of faster migration of metal cations [399], and above such amount a detrimental effect, in terms of instability (delamination) of the thin films.

A thin film obtained from the same suspensions that yielded slow dendrite formation was hydrated for 4½ days at 90% RH (instead of 1 h). The length of the largest dendrites was one half of the ones observed in a thin film hydrated for 1 hour (Figure S5). Between 1 hour of hydration and 4 ½ days, the logarithmic law that describes the water uptake for Sigma eumelanin powders at 90% RH [123] predicts that the water content increases from approximately 13% wt. to 19% wt. We tentatively propose that this increase in the water content triggers the onset of the destabilization of the films, in turn explaining the slower process.

The delamination phenomenon could also explain why a thin film with a hydration time of 14 days (water content foreseen of 21% wt.) does not show any dissolution of the positive electrode (Figure S6).

5.4.3 Effects of Chloride Content and Eumelanin Type (Natural Eumelanin and DMSO-melanin)

In order to investigate the influence of the chloride content, expected to play a role in the dissolution of the gold electrodes and intrinsically present in biological materials, transient current measurements were performed on thin films of Sigma eumelanin after addition of chlorides (Sigma eumelanin as received contains moderate amounts of chlorides, approximately 1% wt.). Intermediate and high chloride contents, respectively 4% wt. and 8% wt., were considered (Table S1). In contrast to as-received Sigma eumelanin, the time to resistive switch ranged between 6 and 14 minutes for films with intermediate Cl$^-$ amount and between 2 and 7 minutes for thin films with high Cl$^-$ amount. In this latter case, at points in the positive electrode facing dendrites growing from the negative electrode, it is visible that a dissolution is taking place, leaving "coves" (Figure 5.2).
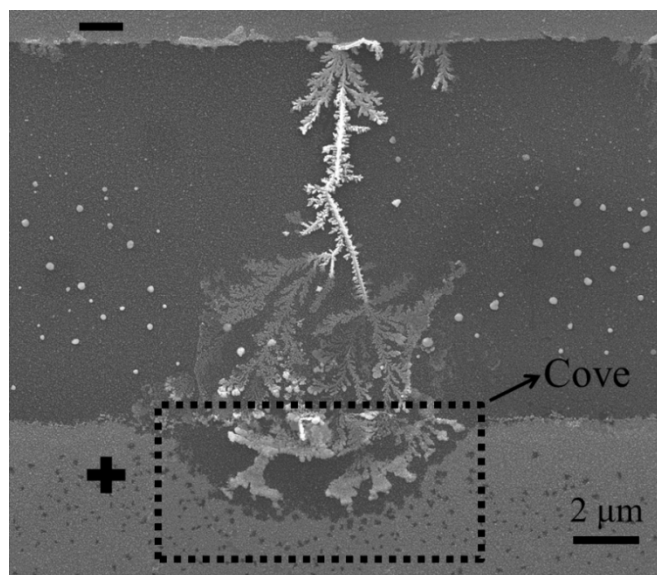
Figure 5.2 SEM image of the dendrite bridging one electrode to the other in a thin film of Sigma eumelanin with high Cl$^-$ content (1h½ hydration at 90% RH). The resistive switch took place after 3 minutes and the biasing voltage (1 V) was applied for 42 minutes. The sample was metallized (2 nm Au on the surface) prior to imaging. Image taken at 20 kV.

The chemical composition in the coves is similar to that of films in the middle of the interelectrode region, as indicated by Energy-dispersive X-ray spectroscopy (EDX). The EDX spectra show the

same intensity of the peaks of C, Si and O, and a negligible Au peak (most likely due to the metallization layer) compared to areas where there are structures made of gold (such as the body of the dendrites and the electrodes). Furthermore, the coves are surrounded by gold-free holes resulting from the migration of the oxidized gold. As the border of the coves expand with the advancement of the oxidation of Au, such holes may eventually merge with the coves contributing to their growth. The presence of coves at the positive electrode is similar to recent observations for planar Ag/AgClO$_4$-PEO/Ag [393] and Ag/AgClO$_4$-PEO/Pt [398] systems. For thin films with high chloride content, a few cases of late resistive switching pointed again to the role played by the local morphology of the films on the switching process (Figures S7-S8).

Transient current measurements at 1 V were also performed on Sepia eumelanin thin films. Sepia eumelanin has a content of Cl$^-$ of about 7% wt. As for synthetic eumelanin, the time to resistive switch varied depending on the suspension from which the thin film was spin coated (between 1.5 and 40 minutes). Sepia eumelanin thin films appeared to coexist with Sepia eumelanin granules (Figure S9), spherical or with a toroidal-like shape, with a bimodal size distribution (average diameters of 9±3 μm and 2±1 μm) [33], [406]. Such granules made the surface of Sepia eumelanin too rough for thickness measurements both by means of atomic force microscopy and spectral reflectance. Dendrites were observable within the interelectrode region in locations where granules were not present (Figure S10). It can be tentatively concluded that such granules are laying on a thin film of Sepia eumelanin. The film likely comprises fragments detached from the larger aggregates during the sonication; such a film was likely too thin to give a Raman spectroscopy signal but thick and continuous enough to promote the formation of the dendrites.

Sepia eumelanin showed, on average, longer times to resistive switch than Sigma eumelanin with high chloride content. As the two types of eumelanin have similar chlorides levels, this difference may be explained considering that Sepia eumelanin contains significant amounts of cations (Mg^{2+}, Ca^{2+}, Na$^+$ [406] as well as K$^+$ [407] and most of the first transition metals, especially Fe^{3+} [406], [408]) which may slow down the conductive bridge growth e.g. because the chelating sites may be already occupied.

Finally, it can be tentatively stated that the higher the chloride content, the more localized is the dissolution of the positive electrode and the faster is the resistive switch (Table S3).

The role of the catecholic hydroxyl groups of eumelanin was elucidated replacing, as the material in the channel, Sigma eumelanin with DMSO-melanin (that partially lacks such groups) [310] with intermediate and high Cl$^-$ levels. We found out that for biasing times as long as 12 hours there was no dissolution of the Au electrodes likely because of the low content of catecholic hydroxyl groups in DMSO-melanin (Figure S11) [310].

Concerning the effect of DMSO, the solvent used for film processing, transient current measurements carried out on drops of DMSO confined between Au electrodes revealed that a DMSO drop without any addition of Cl$^-$ does not cause the dissolution of the positive electrode, for biasing times as long as 19 hours at 1 V (Figure S12). However, for amounts of Cl$^-$ in DMSO similar to the high and intermediate amounts of Cl$^-$ studied for Sigma eumelanin, nanostructures made of little spheres and composed by Au and C (as revealed by EDX) protrude from the negative electrode (Figure S13). As these nanostructures do not resemble trees (dendrites), this may point out that in DMSO the growth of nanostructures is not diffusion limited, as it happens in eumelanin thin films (Table S4).

5.4.4 The Combined Effect of Cl$^-$ and Voltage

For a biasing voltage of 0.7 V, in the samples with intermediate Cl$^-$ concentration, the positive electrode was not dissolved or there was very little dissolution. For thin films of Sigma eumelanin with high chloride content, the dendrite formation process takes place at voltages as low as 0.7 V: dendrites may be observed after 3 hours of electrical bias (Figure 5.3). However, their morphology is different from that of dendrites formed at 1 V: their branches are very thin and very close together, to a point that the protruding structures have a bush-like, rather than a tree-like, shape.
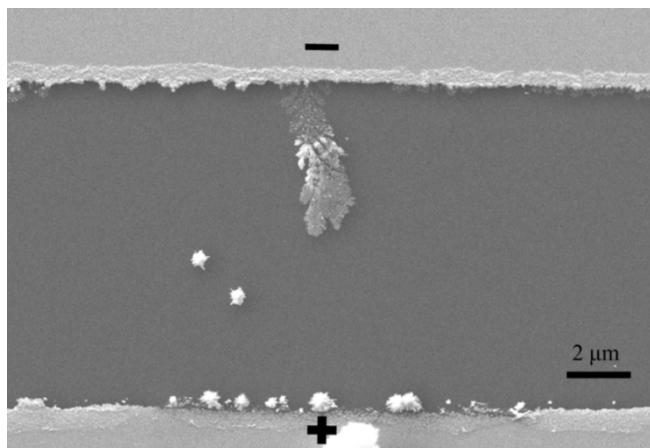
Figure 5.3 SEM image of a dendrite growing in a thin film of Sigma melanin (8% wt. Cl⁻), hydrated for 1 hour at 90% RH and biased at 0.7 V for 3 hours. No dendrite bridged the electrodes during the 3 hours of the measurement. Image taken at 10 kV.

5.4.5 The Combined Effect of Cl⁻ and Hydration Times Longer than 1 hour

The slowing down effect of hydration treatments longer than one hour is also confirmed for thin films with an intermediate Cl⁻ amount in Sigma eumelanin. A thin film hydrated for five days showed only nanocluster formation, no dendrite growth and no resistive switch. Nevertheless, for films of Sigma eumelanin with high chloride concentration, both after three hours of hydration and 24 hours of hydration (water content of respectively $14.8\pm0.1\%$ and $16.7\pm0.9\%$ wt.) [123], a resistive switch takes place in the same time range of that of most of the thin films hydrated for one hour (2-7 minutes). Sepia eumelanin behaved differently. After 3 hours of bias, no dendrite bridged the electrodes (but several were growing) for a thin film hydrated for 3 hours. This is in agreement with the higher tendency of Sepia eumelanin to absorb H_2O (Figure S15), which may promote a destabilization of the thin film for hydration times shorter than for Sigma eumelanin.

5.4.6 Different ON/OFF Ratios for Different Hydration Levels

In order to shed further light on the effect of the water uptake on the process of dendrite formation, transient current measurements at constant biasing voltage, 1 V, were carried out at relative humidity levels lower than 90% and hydration time of one hour on thin films of Sigma eumelanin with high chloride content and Sepia eumelanin. In particular, 48%, 60%, 70% and 80% RH levels were tested.

At 70% and 80%RH (water content of approximately 10.3±0.1%, and 10.8±0.3%, respectively) [123], a new type of resistive switch was observed (Figure 5.4). Whereas at 90% RH the ON/OFF ratio is ~10^4 (*standard* resistive switch), in this case the current increases by only 2-3 orders of magnitude (Table S2) and then follows a double exponential decay with two different time constants (Figure 5.4 c). We call this new type of behavior *hybrid* resistive switch.
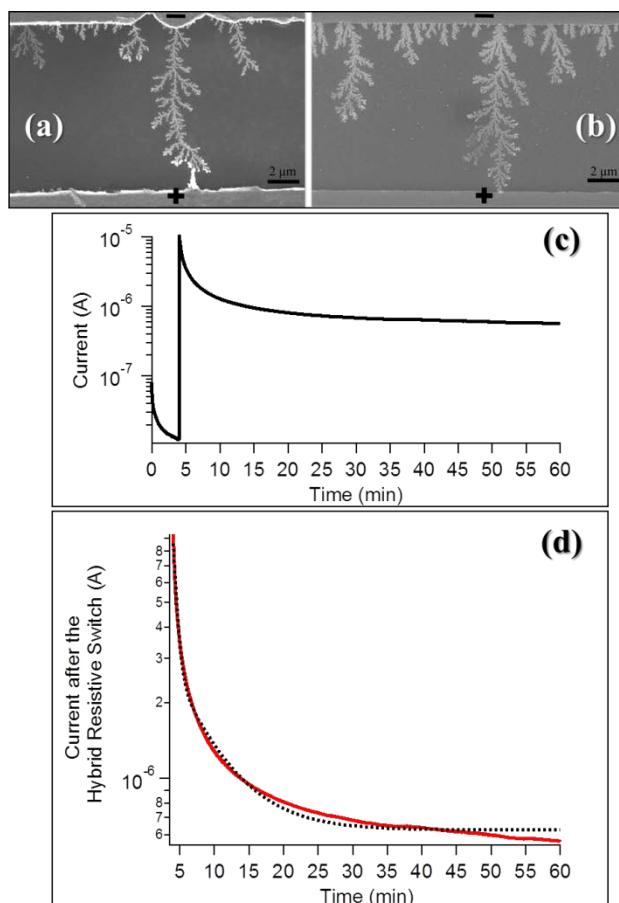
Figure 5.4 (a) and (b) SEM images of dendrites bridging the two electrodes in two thin films of Sigma eumelanin (8% wt. Cl⁻), hydrated for 1 hour at ≈ 80% RH and biased for 1 hour at 1 V. A hybrid resistive switch takes place after ≈4 minutes (a) and ≈12 minutes (b) of biasing. Images taken at 5 kV(a) and 10 kV (b); (c) Current-time plot for sample (a); (d) Zoom of the current-time diagram after the occurrence of the hybrid resistive switch: the dotted line represents the double exponential law that fits the trend $I(t)=I_0+I_1e^{[-(t-t_{rs})/\tau_1]} + I_2e^{[-(t-t_{rs})/\tau_2]}$, where I_0 is 6.2554e^{-7} A, I_1 is 5.8985e^{-6}A, τ_1 is 0.553 min, I_2 is 2.0187e^{-6} A, τ_2 is 5.892 min and t_{rs} is the time to the hybrid resistive switch (4.07 min).

In order to confirm that the hybrid resistive switch was related to the water uptake, we performed a transient current measurement at 1 V on a thin film of Sigma eumelanin (Cl⁻ 8% wt.) that had been hydrated for only half an hour at 90% RH (with a water content expected to be within the range of water absorbed after 1 hour at 70% and 80% RH, Table S5) [123]. The results confirmed a hybrid resistive switch after 11 minutes of bias (Figure S18). Approximately 12% wt. (water content after one hour-hydration at 90% RH) can be taken as the threshold amount below which the dendrites do not show four orders of magnitude of current increase (*standard* resistive switch).

To shed light on the phenomenon of the hybrid resistive switch, time-of-flight secondary ion mass spectrometry (ToF-SIMS) was used, to investigate the dendrite composition. We computed (i) the ratios of the intensities of the peaks related to eumelanin fragments (C_xN, CNO, C_3NH, C_6, $C_yH_3NO_2$, x=[2,3,5,7], y=[4,6,8]) to the intensity of the peak related to Au (Au⁻) and (ii) the peak intensity ratios MAu_x (x ≥ 2)/MAu (where MAu_x is a eumelanin-Au complex, that is $CNAu_x$, $CNOAu_x$, C_3NAu_x, with x≥2). Both ratios (i) and (ii) were higher for the dendrite that showed a hybrid resistive switch than for the dendrite that caused a standard resistive switch (Figure S19, Table S6 and Table S7). In other words, the dendrites that sustained higher current contain purer gold. As a consequence, it can be hypothesized that the dendrites that caused a *standard* resistive switch are able to sustain a higher current because they contain a more continuous metal backbone, whereas the other type of dendrites is more of a hybrid metallic-organic structure.

Sepia eumelanin show a *standard* resistive switch at RH levels as low as 70%; this result confirms that it is the relative humidity (and, as a consequence, the water content) which is responsible for the two different types of ON/OFF ratios: indeed, at 70% RH Sepia eumelanin absorbs more water than synthetic eumelanin does at 90% RH for the same hydration time (Figure S15) [123]. Results at RH levels lower than 70% are available in the SI (paragraph "Hydration at 48% and 60% RH", Figures S16 and S17). A synoptic image of the phenomena taking place at the interface between gold electrodes and eumelanin thin films under electrical bias as well as details of the ON/OFF ratio for the two types of resistive switch are provided in Figure 5.5 and Table S2.
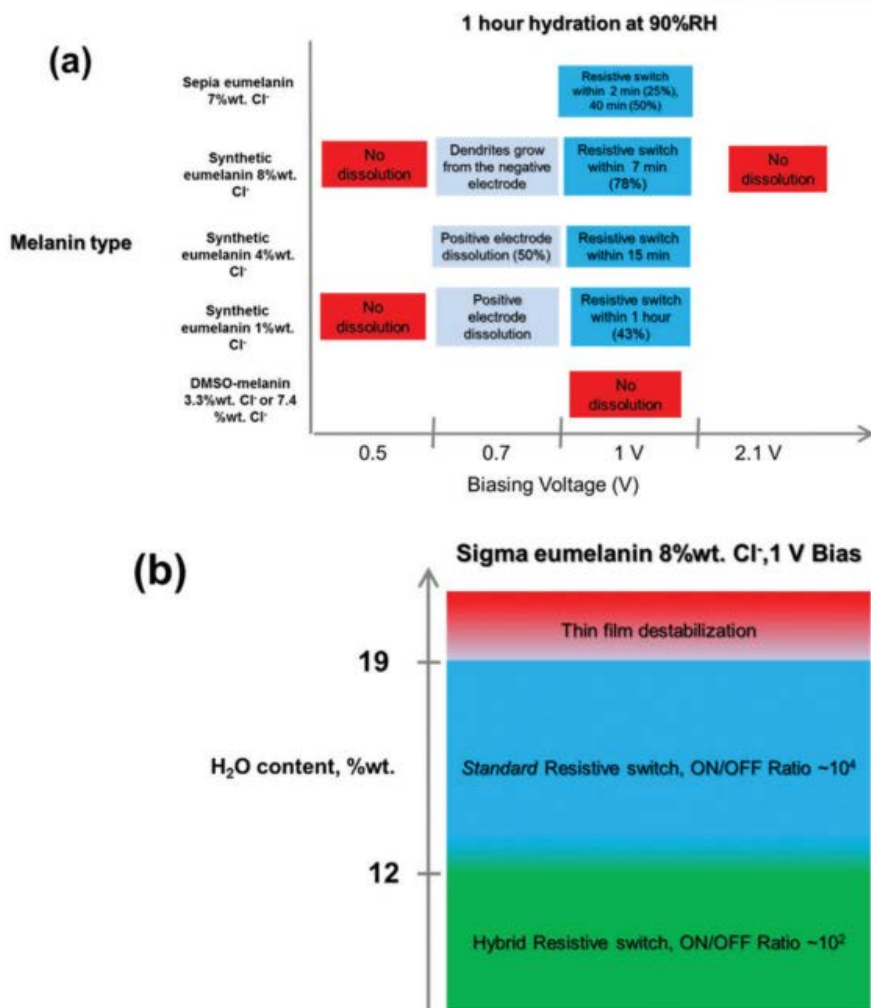
Figure 5.5 (a) Diagram of the phenomena taking place at the interface between thin films of different types of eumelanin and gold electrodes, for 1 hour-hydration at 90% RH, at different biasing voltages (in parentheses the probability). (b) Scheme representing how the water level influences the type of resistive switch for Sigma eumelanin with 8% wt. Cl⁻. Between approximately 12% wt. and 19% wt. a standard resistive switch occurs (ON/OFF ratio $\sim 10^4$); below 12% wt., a hybrid resistive switch takes place (ON/OFF ratio $\sim 10^2$) whereas, above 19% wt., the resistive switch is hindered by the thin film destabilization.

5.4.7 Attempt to Erase the Dendrites

For technological applications, the possibility of forming the conductive bridges is as important as that of annihilating them.

Attempts to erase the dendrites (that is, open them in order to interrupt the bridge between the electrodes) and bring the system back to the high resistive state were made. As the thin films of Sigma eumelanin with high chloride content had shown the best reproducibility in terms of time to resistive switch, they were used for the erasing attempt.

One test was chosen as representative: the thin film was hydrated for 1 hour at 90% RH, then biased for 12 minutes at 1 V (direct bias, during which the resistive switch occurred after 6 minutes) and finally for 12 hours at -1 V (reverse bias). The dendrites were not erased by reversing the biasing voltage. Nevertheless, some of them appeared partially consumed and discontinuous in some points along their bodies (Figure S20). The current during the reverse bias step was always of the order of mA (low resistive state after the resistive switch), confirming that only a fraction of the dendrites had been affected.

Moreover, some sides of the "branches" of the dendrites that were directly in front of the positive electrode after biasing voltage inversion look brighter in the SEM image, i.e. thicker, suggesting that the positive electrode after the biasing voltage inversion was dissolving and the material generated by its dissolution was accumulating on those branches (Figure S20). Small dendrites were nucleated on the negative electrode after biasing voltage inversion (Figure S21).

The results were confirmed by an experiment in which the dendrite formation was promoted by a sweeping (not constant) voltage (2 mV/s, initial and final voltage of each cycle = 0 V, max 2.5 V, min -2.5 V, 15 cycles), during which each electrode switched from positive to negative (and, consequently, from being the one consumed to the one towards which nanoclusters migrate) for 15 periods. In the interelectrode area dendrites protruding from both sides may be noted, some of which meet "half way" in the middle of channel. Rather than being akin to trees, these structures resemble leaves, perhaps due to the fact that they received nanoaggregates from both sides (both electrodes have been consumed) (Figure S22).

5.4.8 Retention Time

In order to evaluate the retention time, i.e. how long the system remained in the low resistive state, the samples for which a resistive switch occurred were biased again, with voltage ramps, after a period of 5-10 months at ambient temperature and 25% RH.

The results revealed that samples are able to keep the low resistive state for a period of time as long as 10 months, showing a perfect ohmic behaviour, up to voltages as high as |10| V for films ≥ ca. 25 nm. The resistance of the low resistive state proved to not be influenced by the RH level, sweep rates, voltage range and number of cycles (up to 100). This hints to a potential application for Write Once Read-Many-Times (WORM)-type memories. For thicknesses below ca. 25 nm, the low resistive state was lost. The film thickness, which did not play a role on the time to resistive switch, plays conversely a major role in determining the retention time: it can be hypothesized that it protects the thin dendrites from degradation due to the contact with the ambient atmosphere. Samples with a hybrid resistive switch lost their high conductive state after 10 months in agreement with our ToF-SIMS results: as their dendrites contain more eumelanin than the other type of dendrites, we suggest that the degradation of the pigment [2] causes the loss of the low resistive state.

5.4.9 Conclusions

We have found that it is possible to obtain two types of resistive switch, standard (ON/OFF ratio ~10^4) and hybrid (ON/OFF ratio ~10^2), in thin films of the biopigment eumelanin, in planar electrochemical metallization cell configuration.

Using eumelanins from synthetic and natural (the ink sac of the cuttlefish, Sepia) sources, we have revealed the complex interplay of factors determining the resistive switch process. These factors are: eumelanin hydration level (depending on relative humidity and hydration time), chelating groups in the molecular structure of the pigment, electrical bias and content of chlorides (commonly present in biological environments and known to promote the formation of gold complexes). In particular, if the hydration level is below a lower threshold (12% wt.) the hybrid dendrites form. Between 12 and 19% wt., we observe the standard resistive switch. For hydration levels higher than 19% wt., the process is slower or does not take place. Our results pave the way towards the demonstration of the use of eumelanin as the ionic conductor in electrochemical

metallization memory cells. With the aim to enhance the control over the cell switching characteristics, work is in progress to improve the chemical control of our eumelanin films, e.g. by solid state polymerization of the biopigment building block DHI [289]. Using a two-color electrode configuration (e.g. Pt and Au), we aim at demonstrating, in the near future, the possibility of erasing the dendrites. Nanoscale memory devices, with a vertical (stacked) configuration, are currently under investigation. In addition, the study of the interactions between eumelanin and metal electrodes may potentially shed light on the biological functions of the pigment as a metal ion chelator. Indeed, Sepia eumelanin has been proved to be a suitable model to study the binding properties of neuromelanin [8]. Therefore, the following steps of our research will be the inclusion of electrodes made of biologically relevant metals (such as Copper, Iron or Magnesium).

5.4.10 Acknowledgements

CHAPTER 6   ARTICLE 2: EUMELANIN FOR NATURE-INSPIRED UV-ABSORPTION ENHANCEMENT OF PLASTICS

Article 2 has been published in *Polymer International* on February 6th, 2019.

Optical images, additional graphs and tables of TGA, UV-visible spectroscopy as well as IR spectroscopy are provided in the Supporting Information, in <u>Appendix C</u>.

6.1 Authors

Eduardo Di Mauro[1], Matteo Camaggi[1,2], Nils Vandooren[1], Caleb Bayard[1], Jordan De Angelis[1,2], Alessandro Pezzella[3], Bill Baloukas[1], Richard Silverwood[4], Abdellah Ajji[4], Christian Pellerin[5], Clara Santato[1]

[1] *Département de Génie Physique, Polytechnique Montréal, C.P. 6079, Succ. Centre-ville, Montréal, Québec, H3C 3A7, Canada*

[2] *Department of Electrical Engineering (DEI), University of Bologna, Viale del Risorgimento, 2, Bologna, 40136, Italy*

[3] *Institute for Polymers, Composites and Biomaterials (IPCB), CNR, Via Campi Flegrei 34, Pozzuoli (Na), 80078, Italy*

[4] *CREPEC, Department of Chemical Engineering, Polytechnique Montréal, P.O. Box 6079, Station Centre-Ville, Montreal, Québec, H3C 3A7, Canada*

[5] *Département de chimie, Université de Montréal, C.P. 6128, Succ. Centre-Ville, Montréal, QC, H3C 3J7, Canada*

6.2 Abstract

In the human body, the black-brown biopigment eumelanin blocks the harmful ultraviolet (UV) radiation. In the plastics industry, additives are often added to polymers to increase their UV-absorption properties. We herein report an assessment of the biopigment eumelanin as a nature-inspired additive for plastics to enhance their UV-absorption. Since eumelanin is produced by natural sources and is non-toxic, it is an interesting candidate in the field of sustainable plastic

additives. In this work, eumelanin-including films of commercial ethylene-vinyl acetate copolymer (EVA), a plastic used for packaging applications, were obtained by melt-compounding and compression molding. The biopigment dispersion in the films was improved by means of the Melanin Free Acid treatment (MFA). It was observed that eumelanin amounts as low as 0.8% wt. cause an increase of the UV absorption, up to one order of magnitude in the UVA range. We also evaluated the effect of eumelanin on the thermal and photostability of the films: the biopigment proved to be double-edged, working both as UV-absorption enhancer and photo-prooxidant, as thermogravimetric analysis (TGA) and infrared (IR) spectroscopy revealed.

6.3 Introduction

The absorption in the ultraviolet (UV) region of plastics for packaging applications is paramount to protect the underlying wrapped material (e.g. food) [193]. Consequently, UV-absorbers are added in order to enhance the UV absorption of polymers and to stabilize them against UV-induced degradation [192]. In addition, the resistance to photodegradation is a requirement for plastics used in outdoor environments [192].

Nature has been confronted with the need of providing a UV-absorber to the organ that "wraps" the human body (the skin), as harmful UV rays are part of the solar radiation that reaches the Earth [1]. Such a natural UV-absorber, i.e. eumelanin, is a black-brown pigment that can be easily recognized, in our daily life, in the different skin complexations [1]. As a matter of fact, eumelanin exhibits featureless absorption in the UV and visible ranges (Figure 6.1-A) [409]. It derives from the oxidative polymerization of 5,6-dihydroxyindole (DHI) and 5,6-dihydroxyindole-2-carboxylic acid (DHICA) (Figure 6.1, B-C) [2]. DHI and DHICA form oligomers differing by number of units (up to tens), ratio DHI/DHICA and polymerization sites [75]. Such oligomers stack via π-π interactions, forming the so-called protomolecules, that, in turn, assemble in a complex supramolecular structure [37]. Eumelanin is widely investigated by both physicists and engineers [410]. The biopigment, indeed, features physico-chemical properties such as radical scavenging, redox activity, metal ion chelation, and hydration-dependent electrical conduction, all of interest for energy storage as well as bio and green electronics [2], [69], [70], [105], [127], [410]–[412].

The endeavor towards sustainability in the plastics field has involved not only the polymers but also their additives [190]. For instance, green tea extracts, α-tocopherol and other natural materials

were proved to be effective anti-oxidants in polymers [413], [414]. In this context, the advantages of eumelanin as a natural UV-absorber would be manifold. For instance, eumelanin is bio-sourced and non-toxic [125] (one of the requirements of additives for plastics [415]). These two features render the use of the biopigment greener with respect to several commercial additives [185]. Large scale production of melanin by microorganisms digesting food waste has been reported [416], and sustainable extraction from natural fibers (e.g. fleece from alpaca) has been demonstrated [74]. In addition, as eumelanin is formed of protomolecules [37], it would be less likely to leach from the matrix polymer than small molecule additives [269], [415].

Natural eumelanin (Sepia Melanin, extracted from the ink sac of a cuttlefish), fungal melanin and polydopamine (a eumelanin-like material) [262] have been assessed as additives to improve the UV-absorption properties of polyimide (PI) [194], poly(lactic acid) (PLA) [268] and poly(vinyl alcohol) (PVA) [264]. Other works regarding PVA [263] and bisphenol A polycarbonate (PC) [265] reported not only the improvement of the UV-absorption properties but also the long-term effects of UV irradiation. In such works, the polymer matrix embedding the pigment was protected by eumelanin against photodegradation under prolonged UV irradiation [263], [265]. Eumelanin was also assessed as a bio-sourced thermal stabilizer for PI [194], PVA [266], [267], polyhydroxybutyrate (PHB) [270], poly(methyl methacrylate) (PMMA) [269] and polypropylene (PP) [269], as it can scavenge the radicals that form during the thermal degradation of the polymers [69], [192].

In this work, we evaluated the biopigment eumelanin as an additive for the UV-absorption enhancement of a commercial grade of the copolymer ethylene-vinyl acetate, EVA (ELVAX®3128-1), used as plastic material for packaging applications (Figure 6.1-D) [417]. Both natural Sepia Melanin and two synthetic counterparts based on only one of the two building blocks (DHI-melanin and DHICA-melanin) were tested. The relevance of our efforts lays in the feature that eumelanin was not merely added as-polymerized or as-extracted nor functionalized [194]. Indeed, the dispersion of the biopigment in the polymer matrix was improved by the Melanin Free Acid (MFA) treatment. Such treatment opens the biopigment supramolecular structure and causes the reduction of the size of the oligomers [80], [418]. Both the π-π stacking featured by the supramolecular structure and the size of the oligomers affect the electronic delocalization [418]. An extended π-π stacking and a large oligomer size generate extended delocalization, in turn leading to the red shift of the optical absorption spectrum [80], [418]. The MFA treatment causes

therefore the shift of the eumelanin absorption towards the UV [80], [419]. The assessment included the evaluation of possible synergistic or antagonistic effects between eumelanin and the thermal stabilizer (butylated hydroxytoluene), already present in the commercial grade EVA [420]–[422]. Finally, eumelanin's UV-absorption properties in nature can have a dichotomous role, either photoprotective or photodamaging [95]. The latter effect was suggested to prevail after prolonged exposure of the biopigment to UVA radiation (320 – 400 nm) [98]. Consequently, we also assessed whether, in the polymeric matrix, the photoprotective or the photodamaging role of the biopigment prevails upon prolonged UV irradiation.
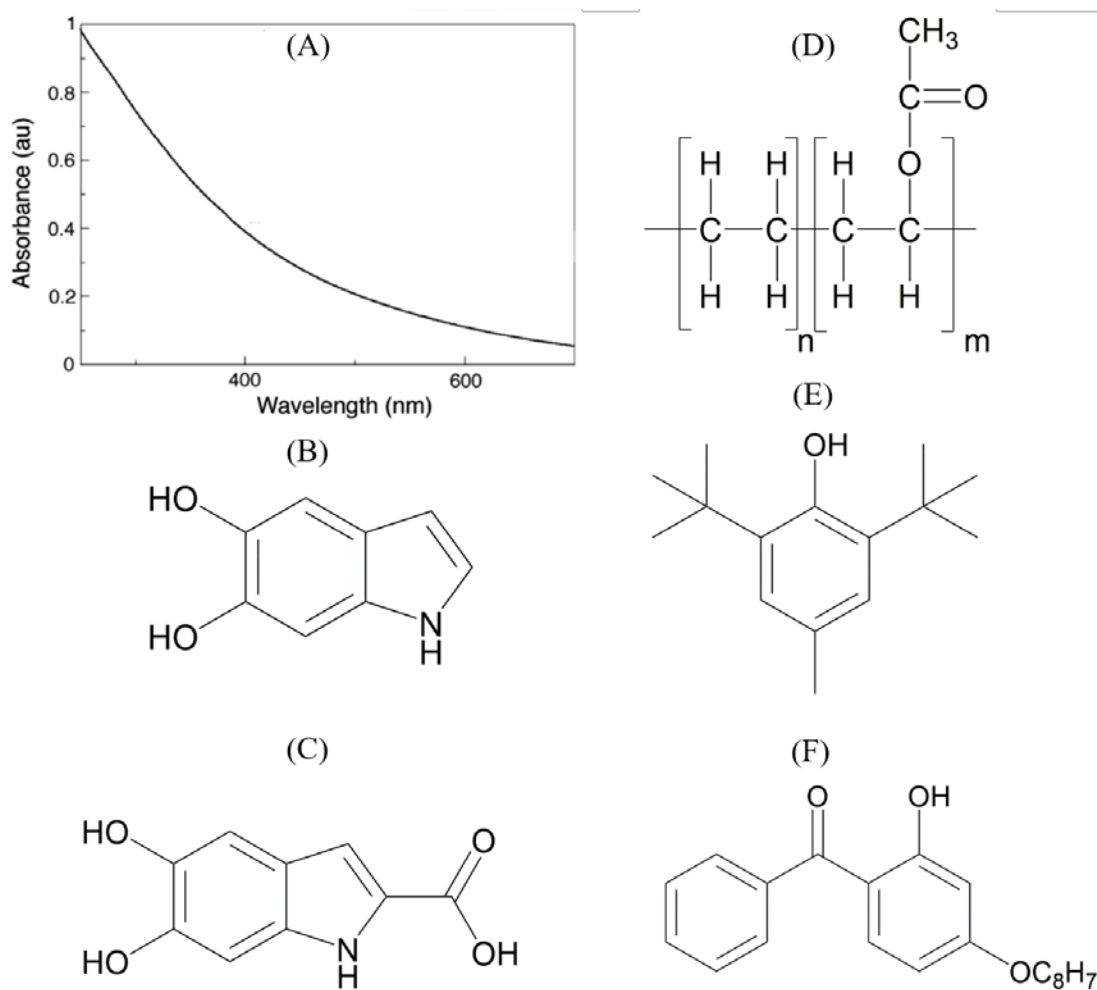
Figure 6.1 (A) Featureless UV-visible absorbance of eumelanin (adapted from [409]); Molecular structure of the building blocks of eumelanin, (B) DHI (5,6-dihydroxyindole) and (C) DHICA (5,6-dihydroxyindole-2-carboxylic acid); (D) Monomer of polyethylene-vinyl acetate copolymer, EVA; (E) Phenol, 2,6-bis(1,1-dimethylethyl)-4-methyl- or butylated hydroxytoluene (BHT), a

commercial anti-oxidant; (F) 2-hydroxy-4-(octyloxy) benzophenone or BLS®531, a commercial UV-absorber.

6.4 Materials and Methods

6.4.1 Materials and Processing

The plastic material studied was a commercial grade ethylene-vinyl acetate copolymer (EVA), namely ELVAX®3128-1 from DuPont[TM], containing butylated hydroxytoluene, BHT (Figure 6.1, D-E). The vinyl acetate content was 9.3% wt. and the melting point 99 °C.

ELVAX®3128-1 pellets were dried at 60 °C overnight prior to processing. Films of pure ELVAX®3128-1 were prepared from the pellets received from the company. The dried pellets were melted in a batch mixer (Brabender Plasticorder DDRV501), compression-molded in a hot press and stabilized in a cold press (Tables S1-S2-S3). The size of the so-obtained films was 20.1 cm × 15.0 cm. Such films will be from now on referred to as "control films".

Three types of eumelanins were used in this study, two synthetic and one bio-sourced. The two synthetic eumelanins were obtained from only one of the two monomers (DHI or DHICA), i.e. DHI-melanin and DHICA-melanin. Such synthetic eumelanins were synthesized by a solid-state polymerization method already reported in the literature [289]. Natural eumelanin was extracted from the ink sac of a cuttlefish (Sepia Melanin), following procedures established in the literature [423], [424] ("Sepia Melanin Extraction" in SI). Eumelanin was added to the polymers by melt compounding in the batch mixer. The processing parameters to obtain the eumelanin-including films were the same as the control films (Tables S1-S2-S3).

Prior to the addition of eumelanin to the plastics, the Melanin Free Acid (MFA) treatment of eumelanin was deemed necessary, in order to properly homogenize the product obtained by melt compounding commercial EVA and eumelanin in the batch mixer [425], [426]. The MFA treatment was carried out following existing protocols ("Melanin Free Acid Treatment" in SI and Figure S1) [426].

The lowest amount of eumelanin added to the plastic was 0.2% wt. Higher amounts (0.3% wt., 0.6% wt. and 0.8% wt.) were tested for synthetic DHICA-melanin that, compared to the other two

types (synthetic DHI-melanin and natural Sepia Melanin), has been reported to have lower visible absorption and more intense absorption in the UV region [77], [81].

For the sake of comparison, a commercial UV-absorber, 2-hydroxy-4-(octyloxy)benzophenone, also called BP12 [427] (commercial name BLS®531 from Mayzo), was also considered (Figure 6.1-F).

6.4.2 Characterizations

The absorption was measured using a PerkinElmer LAMBDA 1050 spectrophotometer equipped with a Labsphere integrating sphere on samples (approximately 2 cm × 3 cm) cut from the center of the compression-molded films and placed inside the sphere at a 20-degree angle with respect to the incident beam (5 samples for the control films, 3 samples for the films containing the different additives). This center-mount setup allowed for the total reflected R and transmitted T radiation to be measured simultaneously in the 250-800 nm range and the resulting absorption of the films obtained by posing $A = 1 - (R + T)$. As the films have different thicknesses, an equivalent absorption coefficient α was inferred by assuming a Beer-Lambert-like attenuation ("Equivalent absorption coefficient" and Figure S2 in SI). The equivalent absorption coefficient of the commercial EVA including eumelanin or the commercial benzophenone will be named α_{ADD} and the equivalent absorption coefficient of the control film α_{CON}. The ratio ${\alpha_{ADD}}/{\alpha_{CON}}$ thus indicates the relative increase of absorption provided by the additive in the films with respect to the control film.

Thermogravimetric analyses (TGAs) reveal whether the addition of the biopigment shifts the degradation temperature towards lower or higher temperatures, due to antagonistic or synergistic effects with the anti-oxidant butylated hydroxytoluene present in ELVAX®3128-1. Thermogravimetric analyses were carried out in argon and air atmosphere (90 cm^3 min^{-1}), at a heating rate of 10 °C min^{-1}, in the range of 25 – 600 °C, using a TA Instruments TGA 2950 thermogravimetric analyser. The onset degradation temperature, T_{on}, was calculated following ASTM E 2550-07, setting 0.1 %/°C as the value for which the initial plateau of the derivative of the TGA (DTG) was considered over. The temperature of the maximum rate of degradation is also reported. For the average values, 4 samples for the control films and 2 samples for all the other cases were considered.

To assess whether the absorption enhancement provided by eumelanin (MFA) prevents or favors photodegradation, a UV-aging test entailing prolonged UV exposure was carried out. Such test was conducted for 144 days in air, at 25 °C, using a lamp of ~10 W·m^{-2} in the 290 nm – 440 nm spectral range, with the films held at a 10 cm-distance from the lamp.

At day 48 and day 144 of UV irradiation, the possible presence of photodegradation products was assessed, by means of infrared spectroscopy (IR), UV-visible spectroscopy and thermogravimetric analyses. Optical images of the samples were taken at days 0, 48, 96 and 144 of UV irradiation.

IR spectra of the films were recorded in the attenuated total reflection (ATR) mode using a Bruker Optics Tensor 27 FT-IR spectrometer equipped with a HgCdTe detector. Samples were pressed against the silicon ATR element of a MIRacle accessory (Pike Technologies). All spectra were obtained with a resolution of 4 cm^{-1} by averaging at least 250 scans. Absorbance was normalized with respect to the maximum value of each spectrum.

6.5 Results and Discussion

We initially compared the UV-visible equivalent absorption coefficient (i.e. the absorption coefficient normalized by the thickness) of the control film (α_{CON}) with that of films including eumelanin (α_{ADD}). We used both natural Sepia Melanin and two synthetic counterparts based solely on one of the two building blocks (DHI-melanin and DHICA-melanin). The addition of 0.2% wt. eumelanin brings about a UV-absorption enhancement, with $\alpha_{ADD}/\alpha_{CON}$ = 6-8 in the UVA and UVB regions for the three types of eumelanin (Figure 6.2).

The peak located at about 285 nm is due to the presence of the anti-oxidant butylated hydroxytoluene in the control film (see "Materials and Methods"). Furthermore, two peaks located at ca. 320 nm and 370 nm are observable in the films containing eumelanin. Both peaks may result from the overlap of the absorption of collections of oligomers [419], [428]. A further contribution to the peak at 320 nm could be ascribed to polypyrroles resulting from the peroxidation of eumelanin during the MFA treatment [429], [430].
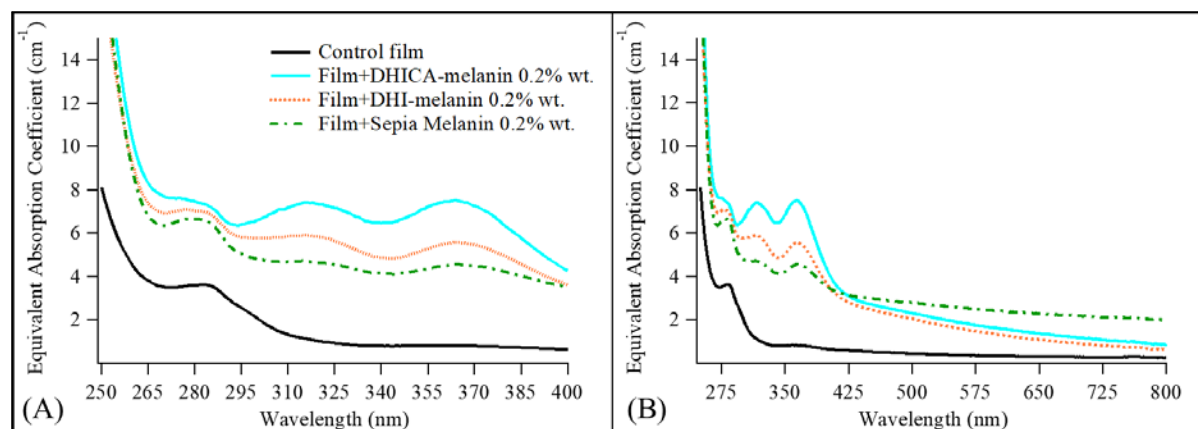
Figure 6.2 Equivalent absorption coefficient of the control film and films including different types of eumelanin 0.2% wt. (A) in the UV range and (B) in the UV and visible ranges.

For applications where color matters, a negligible absorption increase is ought in the visible range ($\alpha_{ADD}/\alpha_{CON}$ close to 1). In this context, DHICA-melanin and DHI-melanin perform better than Sepia eumelanin. For Sepia Melanin, $\alpha_{ADD}/\alpha_{CON}$ keeps increasing in the visible range, up to $\alpha_{ADD}/\alpha_{CON} = 8$ at 800 nm. On the other hand, for applications where a black color is desired, Sepia Melanin could represent a bio-sourced alternative to petroleum-based UV-absorbers (e.g. carbon black [431]).

The three types of eumelanin considered in this work were added to the commercial grade EVA after the MFA treatment. The MFA treatment causes the opening of eumelanin's supramolecular structure, by the dissociation of eumelanin aggregates into smaller protomolecules [425]. The treatment also reduces the oligomers' length [425]. Both effects reduce the absorption in the visible range [80], [419]. The more intense optical absorption in the visible region provided by Sepia Melanin with respect to the synthetic eumelanins may be due to the less complex initial supramolecular assembly of the synthetic eumelanins, which are easier to "open" by the MFA treatment with respect to Sepia [347]. This hypothesis is confirmed by the darker color of the pellets and films including Sepia Melanin with respect to its synthetic counterparts (Table S2). It is worthy of note that adding an as-polymerized synthetic powder (DHICA-melanin and DHI-melanin) or as-extracted natural powder (Sepia Melanin) to the batch mixer entailed films with black dots after compression molding.

As DHICA-melanin has been reported to have lower visible absorption and more intense absorption in the UV region [77], [81] with respect to the other two types of eumelanin (DHI-melanin and Sepia Melanin), higher concentrations of DHICA-melanin were also tested (0.6 and 0.8% wt.) (Figure 6.3).
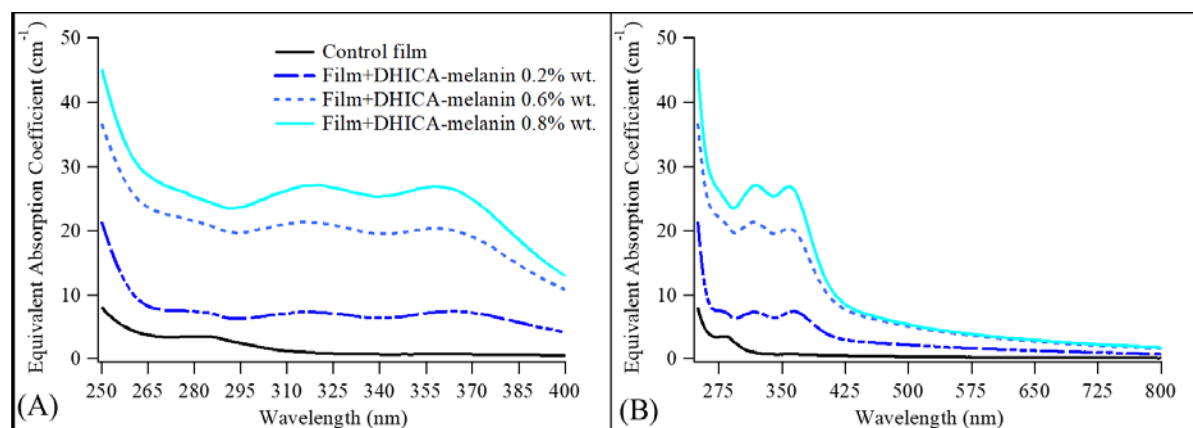
Figure 6.3 Equivalent absorption coefficient of the control film and films including different DHICA-melanin amounts (A) in the UV range and (B) in the UV and visible ranges.

The absorption coefficient increases more remarkably in the UV range than in the visible range with increasing DHICA-melanin amount from 0.2% to 0.8% wt. Such an increase is stronger in the UVA, where $\alpha_{ADD}/\alpha_{CON}$ = 27 for the 0.8% wt. concentration.

Overall, the results of Figure 6.2 and Figure 6.3 prove that eumelanin works as a UV-absorption enhancer for our commercial EVA. However, the absorption enhancement takes place also in the visible range, pointing to the residual presence of some oligomers with a high level of conjugation and still assembling via π-π stacking.

The thermogravimetry in inert atmosphere (Figure S3) of the commercial grade EVA shows an initial stage involving the deacetylation of the vinyl acetate fraction [432], with maximum rate at ≈ 355 °C. Such a step leaves a poly[ethylene-co-(acetylene)] backbone [432] and is followed by the degradation of the main chain, i.e. random splitting of the carbon skeleton, with maximum rate at ≈ 470 °C. In air, the thermo-oxidative degradation rate is faster. Indeed, the onset degradation temperature and the main degradation peak are located at lower temperatures with respect to the inert atmosphere (Figure S3) [433]. The thermo-oxidative degradation starts with an initial gain in

mass, ascribed to an oxygen uptake by the polyethylene fraction, bringing about the formation of alkyl-hydroperoxides [434]–[436]. The subsequent drop is due to the deacetylation [437] and thermo-oxidative cleavage of the backbone chains [434]–[436].

The addition of eumelanin to our commercial EVA, containing the anti-oxidant butylated hydroxytoluene, leaves both the onset degradation temperature and the main degradation peak unaltered (Figure S3). Eumelanin, in the MFA form, did not show any antagonistic nor synergistic effects with the butylated hydroxytoluene stabilizer, as it does not interfere with the thermal nor thermo-oxidative stabilization imparted by such a stabilizer. On the other hand, it has been reported that other polymers loaded with eumelanin presented higher degradation temperatures, suggesting thermal stabilization imparted by the biopigment [194], [266], [267], [269], [270]. As this effect was associated in the literature to the radical scavenging properties of the biopigment [194], [266], [267], [269], [270], we make the hypothesis that the Melanin Free Acid treatment reduced the radical scavenging power of eumelanin. This reduction following the MFA treatment has already been reported in the literature [90], [97], [438], [439].

The long-term effects on our commercial EVA of the UV-absorption enhancement were then evaluated by means of a UV-aging test. Findings from both medical doctors and physicists point to a dichotomous role, either photoprotective or photodamaging, conferred to eumelanin by its broad UV-absorption [95]. When eumelanin converts the energy of the photons into heat (photothermal effect), it can act as a photoprotector [78], [440]. This is the effect by which UV-absorbers protect polymers against photo-oxidation [420]. Another photoprotective path entails the quenching of reactive oxygen species (ROS) generated upon UVA irradiation [92]–[94]. However, a prolonged exposure to UV could lead to eumelanin photodegradation [92], [441], with fission of the indolequinone moiety. Such photo-induced chemical modification of eumelanin's building block can result in the loss of its radical scavenging abilities [98]. In that case, eumelanin can become a pro-oxidant [97].

To chemically identify possible photo-oxidation products in the control films during the UV-aging test, IR spectroscopy was used. The IR spectra revealed that the prolonged UV irradiation caused photodegradation of the control film, with the appearance of photo-oxidation products: in the first time range of UV-aging (48 days), only at 1715 cm^{-1} (carbonyl groups of ketones [442]–[448]), and, in the time frame 48 – 144 days, also at 1780 cm^{-1} (γ-lactone) [447], [449], 1170 cm^{-1} (C-O

stretching of a backbone ester) [450] and 909 cm^{-1} (vinyl groups) [450], [451] (Figure S4). Such photo-oxidation products are common to the photodegradation of the polyethylene fraction and to the UV-induced elimination of the vinyl acetate [452]. Because of such an elimination process, the intensity of the bands of the photo-oxidation products increases with time with respect to the intensity of the vinyl acetate band at 1740 cm^{-1}, which decreases with irradiation time (Table S4) [452].

In line with the IR results, the UV-visible absorption spectra of the control films, after UV-aging, feature a strong UV absorption increase, particularly in the UVC, peculiar of the photodegradation products (Figure 6.4) [453].
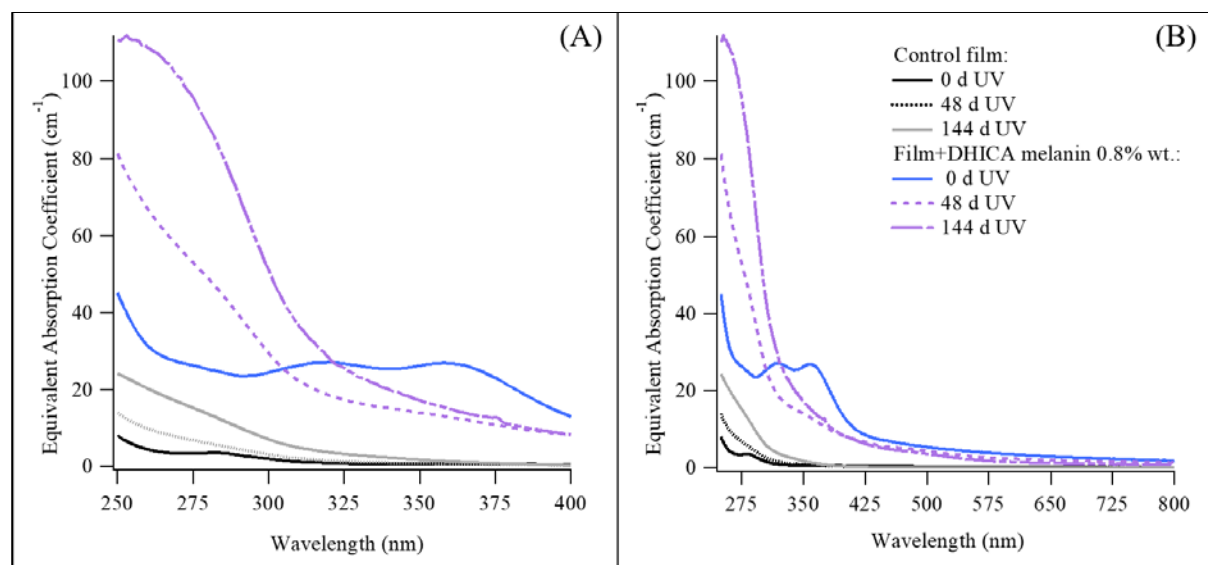
Figure 6.4 Equivalent absorption coefficient (A) in the UV range and (B) in the UV and visible ranges of the control film and films including DHICA-melanin 0.8% wt. at different times of UV-aging (0, 48 and 144 days).

IR spectra show that the films including the three types of eumelanin, 0.2% wt., after 48 days of UV irradiation, featured the same extent of photodegradation as the control film (Figure 6.5 and S5). Conversely, after 144 days, only the film containing natural Sepia Melanin showed the same extent of photo-oxidation as the control film. Films containing synthetic eumelanin underwent photo-oxidation to a higher extent with respect to the control counterparts (increased relative intensity of the bands at 1715, 1780, 1170 and 909 cm^{-1}) (Figure 6.5 and S5).

Increasing the DHICA-melanin amount entailed a more pronounced photo-oxidation (Figure 6.5). Mechanical embrittlement and surface crazing of the films with higher DHICA-melanin loadings, 0.6% and 0.8% wt. (Table S3), which are consequences of photo-oxidation, were also observed [454].
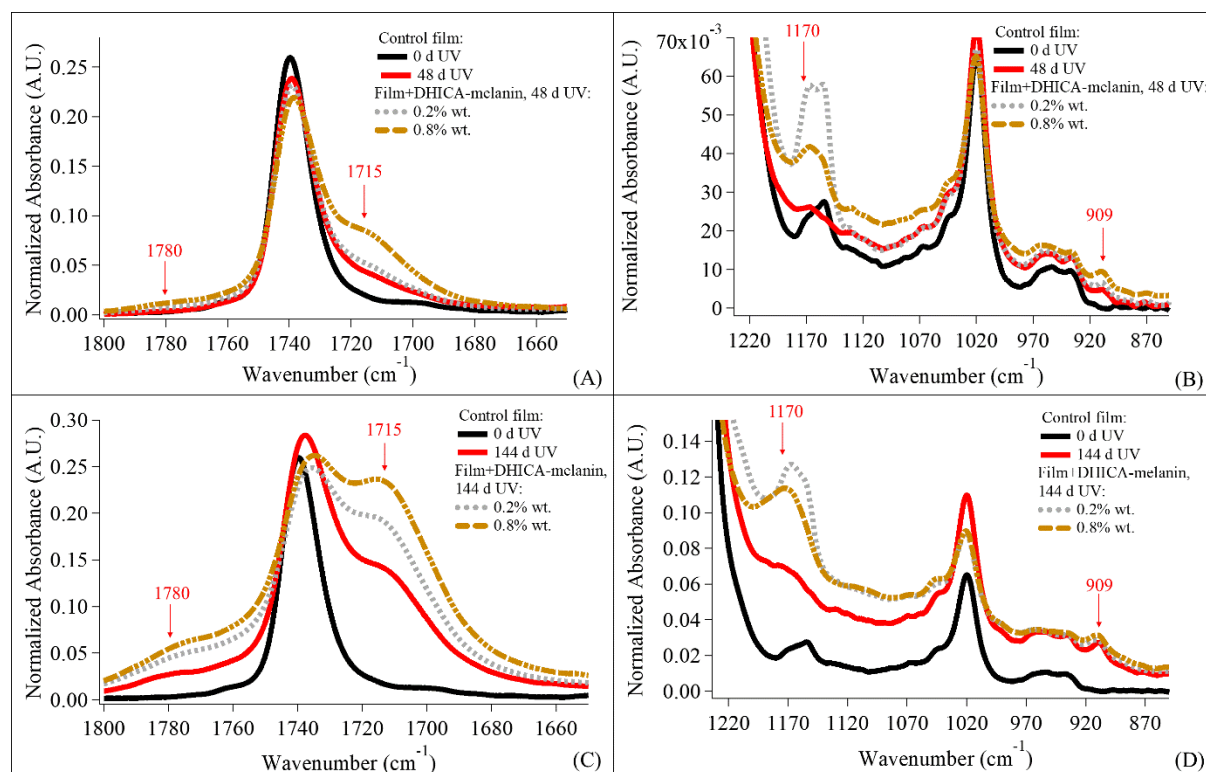
Figure 6.5 IR spectra of the control film and the films including different concentrations of DHICA-melanin at: 48 days of UV-aging in the range (A) 1800 cm^{-1} – 1650 cm^{-1} and (B) 1230 cm^{-1} – 850 cm^{-1}; 144 days of UV-aging, in the range (C) 1800 cm^{-1} – 1650 cm^{-1} and (D) 1230 cm^{-1} – 850 cm^{-1}. The control film at day 0 of UV-aging is reported for the sake of comparison.

In line with the IR results, after 144 days of UV-aging, films containing eumelanin showed higher absorption in the UVC and UVB than the non-UV-aged counterparts due to the presence of photo-oxidation products (Figure 6.4). In particular, the absorption at ca. 320 nm decreases during the first 48 days of UV-aging, but, then, in the time frame 48 – 144 days, it increases reaching values equal or higher than the non-UV-aged films (Table S5). This can be explained with an initial photo-degradation of the small oligomers and polypyrroles responsible for the peak at ca. 320 nm [455], followed by a rise in absorption related to the formation of photodegradation products of our

commercial EVA. Such photodegradation products feature a broad absorption in the UVB and UVC [453]. The decrease of the absorption peak at ca. 370 nm (resulting from collections of oligomers [419], [428]) after 144 days is in agreement with the UVA-induced oxidative degradation of eumelanin, with formation of pyrrole-2,3,5-tricarboxylic acid and fission of indolequinone [441]. Literature reports that, during prolonged UV irradiation of eumelanin in solution, concomitantly to the formation of such photodegradation products, reactive oxygen species (ROS) are also generated [92], [93], [98].

We make the hypothesis that the ROS formation takes place also when eumelanin is embedded in the polymer matrix. Considering that eumelanin was in the MFA form, with reduced radical scavenging ability, ROS cannot be efficiently quenched by eumelanin, contributing to the propagation of the photo-oxidation process of our commercial EVA [415]. This may explain the pro-oxidant behavior of eumelanin.

Thermogravimetry revealed that the onset degradation temperature (T_{on}) of films containing eumelanin decreases after UV-aging (Figures S6 and S7). The thermal decomposition of the photodegradation products can explain the lower thermal stability of the films. As a matter of fact, the decrease of T_{on} reaches a maximum for films with the highest eumelanin content (~ 17 °C in argon and ~ 83 °C in air). Such films feature the highest extent of photo-oxidation products, as revealed by IR spectroscopy. We cannot rule out chain scission as a further photodegradation path causing the T_{ON} decrease after UV-aging (Figures S6 and S7) [452], [456].

Finally, we compared the effects of the addition of eumelanin to a commercial synthetic UV-absorber, the benzophenone BLS®531. Such an additive belongs to a category of compounds that gave evidence of carcinogenic effects [457]–[459].

BLS®531 provides to our commercial EVA a one order of magnitude increase of the absorption coefficient in the UV range with a sharp absorption cut-off between the UV and the visible (Figure S8). BLS®531 limited, but did not completely avoid, the formation of photodegradation products after UV-aging, as shown by IR spectroscopy (Figure S9). As the UV-aging time elapses, the absorption coefficient in the UV-range of the film containing the commercial benzophenone decreases (by 10% - 20% after 48 days and by 20% - 50% after 144 days) (Table S5 and Figure S8), similarly to what happens to the eumelanin related absorption enhancement in the UVA. The

depletion of BLS®531 can be due both to its photodecomposition and to physical loss, because of its relatively low molecular weight [456].

6.6 Conclusions

We investigated the use of eumelanin, a dark-brown biopigment, as UV-absorber for packaging polymers. Three types of eumelanin were investigated: one bio-sourced (extracted from cuttlefish ink) and two synthetic (DHICA-melanin and DHI-melanin). In our work, eumelanin underwent the Melanin Free Acid treatment, prior to the addition to the commercial grade ethylene-vinyl acetate copolymer, EVA. The treatment aimed at dispersing the biopigment in the polymer matrix and limiting its absorption in the visible. The addition of amounts of eumelanin as low as 0.2% wt. caused a UV absorption increase, mainly in the UVA. Bringing the amount to 0.8% wt. for DHICA-melanin provided a substantial absorption increase (1 order of magnitude in the UVA). Such increase was partially lost during prolonged UV-irradiation, due to the additive depletion (mainly by indole fission), with photo-oxidation of the embedding polymeric matrix. Work is in progress to optimize the Melanin Free Acid treatment to favor the photo-stabilizing role of eumelanin through radical scavenging and to provide a sharp absorption cut-off between UV and visible ranges. Furthermore, the use of oligomers, not yet assembled in a supramolecular fashion, obtained by controlling eumelanin polymerization in its very early stages, is expected to selectively enhance the optical absorption in the sole UV range.

6.7 Funding Sources

6.8 Acknowledgment

CHAPTER 7   ARTICLE 3: BIODEGRADATION OF BIO-SOURCED AND SYNTHETIC ORGANIC ELECTRONIC MATERIALS: TOWARDS GREEN ORGANIC ELECTRONICS

Article 3 has been submitted to *Nature Sustainability* on December 20th, 2018. Supplementary Information is provided in <u>Appendix D</u>.

7.1 Authors

Eduardo Di Mauro[1], Denis Rho[2], Clara Santato[1]

[1] *Département de Génie Physique, Polytechnique Montréal, C.P. 6079, Succ. Centre-ville, Montréal, Québec, H3C 3A7, Canada*

[2] *Aquatic and Crop Resource Development, National Research Council Canada, 6100 Royalmount Avenue, Montréal, Québec, H4P 2R2, Canada*

7.2 Abstract

The ubiquitous use of electronic devices has led to the unprecedented increase of the related waste as well as to the depletion of the world reserves of key chemical elements required for their manufacturing. The use of biodegradable, abundant organic (carbon-based) electronic materials can contribute to alleviate the environmental impact of the electronic industry. The pigment eumelanin is a bio-sourced candidate for environmentally benign (green) organic electronics. The biodegradation of eumelanin extracted from cuttlefish ink was studied both at 25°C and under composting conditions (58°C) following ASTM D5338. The biodegradation under composting conditions of two synthetic organic electronic materials was comparatively evaluated. To evaluate if the materials transfer toxicity to the compost a phytotoxicity test was conducted. Eumelanin reached 37% biodegradation in 100 days, without phytotoxic effects. Conversely, the two synthetic materials were not biodegradable, causing also the inhibition of the microorganism activity or transferring toxicity to the compost.

7.3 Introduction

Electrical and electronic equipment has become ubiquitous in our everyday life. The increase of waste electrical and electronic equipment (WEEE, 44.6 Mt worldwide in 2016 [460]) and the depletion of chemical elements of key importance in the electronic industry (e.g. indium and gallium) [128] have put mounting pressure on the environment [128]. Limited attention has been dedicated to possible EEE end of life scenarios. The focus has been on device performance, as the technological advances of the last few decades confirm.

Refurbishment and recycling of electronic devices have been identified, among others, as economically and environmentally viable solutions to deal with WEEE [461]. Besides that, a promising route towards achieving sustainable (green) electronics is based on the use of abundant materials (e.g. biomolecules extracted from biomass feedstock), novel production schemes (e.g. involving non-toxic solvents) and eco-design of devices that includes biodegradation at the end of life [128].

In principle, organic (carbon-based) electronic materials are ideal candidates to explore such route [128]. Organic electronics is based on semiconducting molecules and polymers that feature electronic conjugation, i.e. the alternance of single and double carbon-carbon bonds [462]. Organic electronic devices, such as organic light-emitting diodes, photovoltaic cells, field-effect transistors and sensors, have been demonstrated [463], [464]. Organic devices stand out for their mechanical properties, such as flexibility, rollability and stretchability, of the highest interest for applications such as wearable electronics, imperceptible electronics and smart packaging [465]. Furthermore, being solution-processable (printable), organic electronic devices feature lower embodied energy (i.e. "energy spent in the production phase and stored in the inner constituents" [128]) with respect to their inorganic counterparts, processed by high-vacuum and high-temperature techniques [128].

Biodegradation is defined as the breakdown of materials into simpler and non-toxic components (e.g. CO_2, H_2O, minerals and humic matter) by living organisms, under specific environmental conditions, such as oxygen level, pH, temperature, C-N ratio, granulometry and water content [186], [187]. Composting (i.e. biodegradation in presence of oxygen under thermophilic conditions, at 58°C) is a disposal pathway identified by most municipalities as a valuable technology for the management of solid organic waste, all around the world [188]. Such organic

solid waste is streamed to industrial facilities, where it is converted into a non-toxic substratum that can be used in in agriculture and horticulture [188].

For the assessment of the biodegradability in composting conditions, the industrial sector of disposable plastics for food packaging and serving can leverage on standard test methods. Examples of such standards are CAN/BNQ 0017-088/2010 in Canada, ASTM D6400 in the USA, and EN 13432/EN 14995 in the European Union. Poly-ε-caprolactone (PCL) and polylactic acid (PLA) are among the most important biodegradable plastics in composting conditions [190]. Conversely, limited attention has been given to the biodegradability of materials and devices for organic electronics: no national or international standard exists to evaluate their biodegradability.

Melanins represent a vast category of pigments ubiquitous in nature and much noticeable in our daily life: from human skin color to black spots on moldy bread, from black incrustations on shower curtains to dark parts of banana peels [1], [2]. Melanin is an interesting candidate for green organic electronics because its molecular structure features conjugation and redox-active quinone groups [411]. Hydration-dependent electrical conduction has been reported for melanin pellets and films [108], [120]. Melanin-based supercapacitors [25], batteries [201] and organic electrochemical transistors [132] have been successfully developed.

Eumelanins are the subcategory of black-brown melanin pigments that originate from the oxidative polymerization of L-dopa [466], mostly present in animals. The building blocks of eumelanins are 5,6-dihydroxyindole (DHI) and 5,6-dihydroxyindole-2-carboxylic acid (DHICA) (Figure 7.1). Relevant properties of eumelanin are its broad UV-visible absorption, free-radical scavenging and hygroscopicity [123]. Biodegradability assessments on synthetic eumelanin (dopa-melanin in presence of a mixed bacterial culture [219] and tyrosine-melanin in soil [220]) and natural eumelanin (from human hair [218] in loamy soil) showed negligible biodegradation. Preserved eumelanin was also reported to be present in the orbit of a 54 million year-old fish fossil [214]. Conversely, the fungus *Aspergillus fumigatus* from a soil sample biodegraded different types of natural (from human hair [221], [223], human skin [222], banana peel [223], insects [223] and octopus ink [223]) and synthetic (tyrosine-melanin and dopa-melanin [223]) eumelanins.

Eumelanin is also biocompatible and bioresorbable [125], [126]. Differently from biodegradability in a compost medium, bioresorption is a process by which materials in contact in the physiological environment are degraded and the by-products are eliminated or completely bioabsorbed [467].
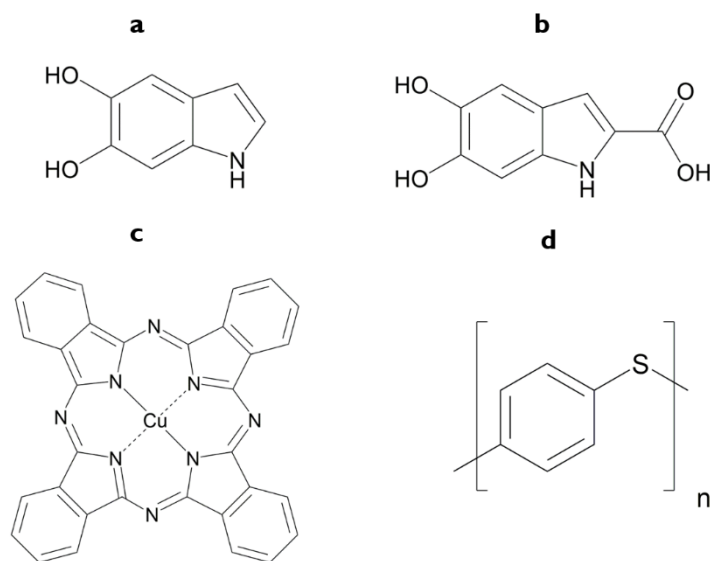
Figure 7.1 Organic electronic materials investigated. **a**, Molecular structure of DHI and **b** DHICA, the building blocks of the bio-sourced eumelanin. **c**, Cu (II) phthalocyanine. **d**, monomer of poly(p-phenylene sulfide).

In this work, we report on the aerobic biodegradability of natural eumelanin, extracted from the ink sac of cuttlefish (Sepia Melanin). Prior to the biodegradability studies, the extracted biopigment was characterized by infrared spectroscopy, thermogravimetric analysis, nuclear activation analysis, as well as elemental analyses of total carbon and total inorganic carbon. This is the first work where the biodegradability of Sepia Melanin blended with an industrial compost obtained from solid municipal waste was tested under mesophilic conditions and under thermophilic conditions (composting). The biodegradability test in composting conditions also included two synthetic organic electronic materials: copper (II) phthalocyanine (Cu-Pc) and poly(p-phenylensulphide) (PPS). Cu-Pc is a molecular dye featuring semiconducting properties and employed in organic field-effect transistors and photovoltaic cells [316]–[318]. PPS is a solution-processable polymer whose electrical conductivity can be increased by 16 orders of magnitude by chemical doping, investigated in photovoltaics [315].

An assessment of the potential transfer of toxicity from the test materials to the compost was also conducted, by means of plant germination and growth tests, following the 98-d incubation period under composting conditions.

7.4 Materials and Methods

7.4.1 Chemicals

Sepia Melanin was extracted from the ink sac of a cuttlefish (*Sepia officinalis*) following established extraction and purification procedures [423] ("Extraction of Sepia Melanin" in Supplementary Data). Sepia Melanin was characterized by infrared spectroscopy (IR), thermogravimetric analysis (TGA), nuclear activation analysis (NAA), as well as elemental analyses of total carbon (CHN analysis) and total inorganic carbon (TIC) ("Sepia Melanin Characterization", Supplementary Figures 1-2 and Tables S1-S2). Three chemicals were purchased from Sigma-Aldrich (Canada) and used as received: microcrystalline cellulose (20 μm powder), poly(p-phenylene sulfide) (powder, average M_n ~10,000), and copper(II) phtalocyanine (β-form, dye content 90% wt.). Polyethylene was purchased from ExxonMobil^{TM} (grade LL 6407.67).

7.4.2 Compost Characteristics

Compost from solid municipal waste (Englobe Corp.) was used as the *substratum* to conduct the biodegradation tests. The compost satisfied the requirements of the ASTM standard method D5338 (*Standard Test Method for Determining Aerobic Biodegradation of Plastic Materials Under Controlled Composting Conditions*) [339]: ash content 51.4%, pH 7.3, dry solids 46 ± 4 % wt., C/N ratio 24.3 with % C = 50% organic matter). The specific respiration rate of such blank compost, i.e. CO_2 evolved per g of volatile solids per day, met the criteria required by ASTM D5338 ("Blank Compost Characterization" in Supplementary Data) [339].

7.4.3 Biodegradability Test under Mesophilic Conditions

The aerobic biodegradability of Sepia Melanin, in the form of a powder, under mesophilic conditions (25°C), was tested over a 97-d incubation period. The respiration activity of the compost's microbiota was monitored by means of electrolytic respirometers. Such equipment measured continuously the O_2 consumed, 1 data point every 30 minutes (details in "Electrolytic

Respirometers" and "Biodegradability Test under Mesophilic Conditions" in Supplementary Data). The test also required the usage of a material biodegradable in the test conditions, the positive control, cellulose.

7.4.4 Biodegradability Test under Thermophilic Conditions

Under thermophilic conditions (composting, 58°C), over the 98-d incubation period, the respiration activity of the compost's microbiota was monitored measuring the CO_2 evolved (1 data point every 4 days). The equipment entailed a composting facility equipped with wet scrubbers for CO_2, (three $Ba(OH)_2$ traps in series after each bioreactor). The $Ba(OH)_2$ reacted with the CO_2. The CO_2 amount could be inferred by means of titrations of the $Ba(OH)_2$ traps (details in "Wet Scrubbers" and "Biodegradability Test, in Composting Conditions" in Supplementary Data). Titrations of two samples of 30 ml extracted from each trap were carried out and the average computed. The biodegradability test under thermophilic conditions involved Sepia Melanin, Cu-Pc, PPS, a positive control (cellulose) and a negative control, a non-biodegradable material under the test conditions, polyethylene, PE.

7.4.5 Statistics and Mineralization Computations

Both tests featured the same 1:6 weight ratio of test material to dry compost [339]. For both tests, duplicates or triplicates of bioreactors containing the same material blended or buried in the compost were used. The average and the standard deviation of the O_2 consumed or CO_2 evolved by the duplicates or triplicates of bioreactors containing the same material blended with the compost were computed. Only one side of the error bars is shown in all the graphs for the sake of clarity.

The biochemical reaction associated to the aerobic respiration of the compost's microbiota can be simplified as:

$$C_{TEST} + O_{2\ consumed} \rightarrow CO_{2\ respired} + H_2O + C_{RESIDUAL\ TEST} + C_{BIOMASS} \qquad (1)$$

Where C_{TEST} is the carbon of the test material at the beginning of the test; $C_{RESIDUAL\ TEST}$ is the carbon of the test material that is not biodegraded; and $C_{BIOMASS}$ is the carbon assimilated and transformed into the biomass (compost's microbiota) participating in the respiration process.

Consequently, the mineralization (i.e. biodegradation percentage) is evaluated as follow [339]:

$$Mineralization\ (\%) = \frac{CO_2\ (material)\ \text{-}\ CO_2\ (blank\ compost)}{CO_2(total)} \tag{2}$$

Where CO_2 *(material)* is the measured mass of CO_2 evolved from the bioreactor containing the test material blended with or buried in the compost; CO_2 *(blank compost)* is the average measured masses of CO_2 evolved from the bioreactors containing blank compost; and CO_2 *(total)* is the total theoretical mass of CO_2 that would evolve if all the test material was completely respired by the compost's microbiota, as for the following equation:

$$CO_2\ (total)(g) = C_\%\ * m\ * \frac{44\ (CO_2\ molecular\ mass)}{12\ (C\ atomic\ mass)} \tag{3}$$

Where *C%* is mass percentage of carbon in the test material; and *m* is the mass of the test material.

For the test under mesophilic conditions, based on the measurement of the O_2 consumed, the CO_2 respired (numerator of equation (2)) was computed following equation (1). The respiratory quotient CO_2 respired / O_2 consumed was assumed to be 1.0 mol/mol [338]. The standard deviation of the mineralization was computed following paragraph 12.3 of ASTM D5338 (details in "Mineralization" in Supplementary Data).

7.4.6 Phytotoxicity Test

Immediately after reaching the end point of the biodegradability test in thermophilic conditions [343], a germination and growth test was conducted to evaluate the (potential) phytotoxicity of the residual test material and, if any, of their biodegradation products. Such test is suggested in ASTM D6400 [343]. The procedure to conduct such test was adapted from the OECD Guideline 208 (*Terrestrial Plant Test: Seedling Emergence and Seedling Growth Test)* [468]. Samples were mixed with a wet sandy soil, then incubated for 19 days at 25°C. Two parameters were monitored: the seedling emergence of 20 seeds of a crop (Ryegrass), and the biomass production (wet weight of the resulting plants), after 19 days (details in "Phytotoxicity Test" in Supplementary Data). According to ASTM D6400, the phytotoxicity test is to be carried out with two plant species: consequently, our test has to be considered as a first indication of the phytotoxicity of the materials.

7.5 Results

7.5.1 Eumelanin: Biodegradability Test under Mesophilic Conditions (25°C)

Throughout the incubation period of the biodegradability test under mesophilic conditions, the respiration activity of the compost microbiota was monitored by electrolytic respirometers, measuring the amount of O_2 consumed. The cumulative O_2 consumed (i.e. the total O_2 consumed between the beginning of the test and a certain incubation time) was comparatively measured for Sepia Melanin blended with the compost, cellulose blended with the compost (positive control) as well as for the blank compost (baseline) (Figure 7.2, a). In the three cases, the O_2 consumed by the compost's microbiota increased steadily over the entire incubation period. Approximately 70% of the final value was consumed during the first 50 days (Δt_{0-50}). By the end of the biodegradability test, the O_2 respiration levels of Sepia Melanin (2731 mg) and cellulose (8835 mg) are 1.3x and 4.0x higher than the baseline level (2194 mg). After subtraction of the cumulative O_2 respired by the blank compost from the cumulative O_2 respired by Sepia Melanin and cellulose (Figure 7.2, b), by means of equations (2) and (3), the mineralization levels were computed (Figure 7.2, c). These levels amounted to 4% for Sepia Melanin and 71% for cellulose, at the end of the incubation period.
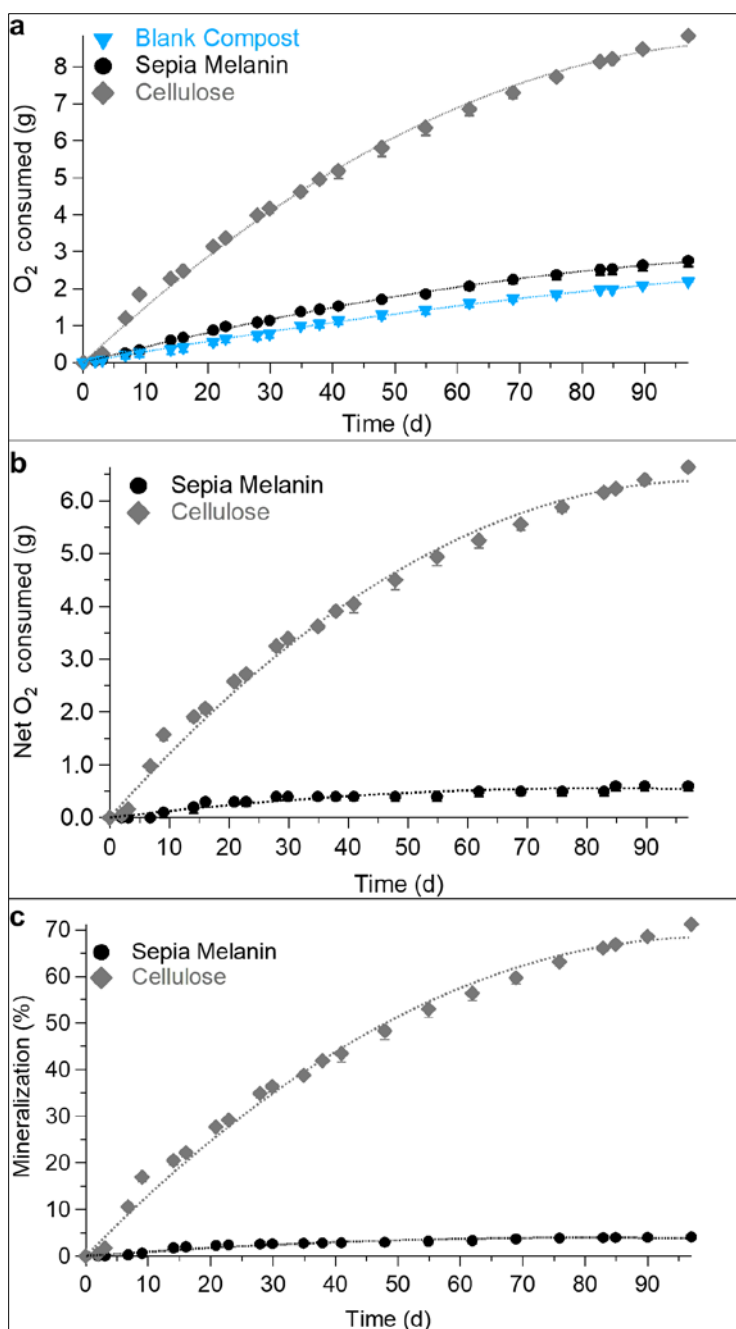
Figure 7.2 Biodegradation under mesophilic conditions. **a**, Cumulative O_2 consumed at 25°C: blank compost, Sepia Melanin and cellulose. **b**, Net O_2 consumed by Sepia Melanin and cellulose, with respect to the O_2 consumption of the blank compost. **c**, Mineralization of Sepia Melanin and cellulose.

7.5.2 Eumelanin: Biodegradability Test under Thermophilic Conditions (58°C)

The biodegradability test under thermophilic conditions (58°C, composting conditions) implied the monitoring of the respiration activity of the compost microbiota by the measurement of the CO_2 evolved, by means of wet CO_2 scrubbers (i.e. $Ba(OH)_2$ traps). The cumulative CO_2 evolved was measured for the blank compost (baseline), polyethylene (PE) pellets buried in compost (negative control), cellulose blended with compost (positive control) and Sepia Melanin blended with compost (Figure 7.3, a). The net cumulative CO_2 produced was computed by subtraction of the CO_2 evolved from the blank compost (Figure 7.3, b). From the net cumulative CO_2 evolved, by means of equations (2) and (3), the mineralization levels of cellulose, PE and Sepia Melanin were computed (Figure 7.3, c). The mineralization level of PE (negative control) was zero, whereas cellulose (positive control) almost completely biodegraded after 98 days (97%). Sepia Melanin attained a mineralization level of 37% at the end of the incubation period (Figure 7.3, c), which is almost 10x higher than under mesophilic conditions (Table 7.1). In particular, eumelanin showed a 12x lower mineralization rate with respect to cellulose in the first 21 days (Δt_{0-21}). In the following 77 d, the mineralization rate of cellulose leveled off (plummeting by a factor 20x), due to its depletion, while the biodegradation of eumelanin continued (Figure 7.3, c).
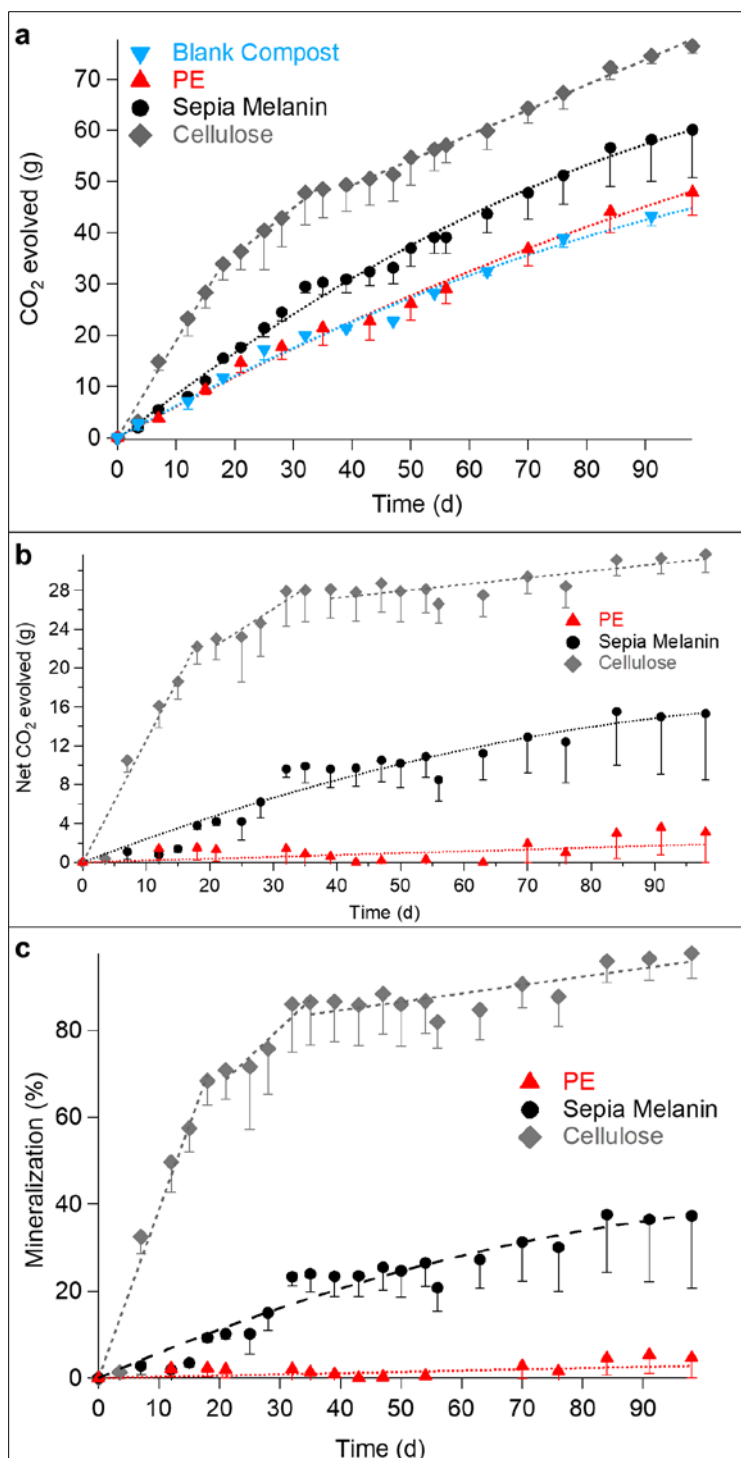
Figure 7.3 Biodegradation of Sepia Melanin in composting conditions. **a**, Cumulative CO_2 evolved at 58°C from blank compost, polyethylene (PE), Sepia Melanin and cellulose. For the first two, only half of the points are shown for the sake of clarity, as they overlapped (see

Supplementary Figure 3). **b**, Net CO_2 evolved from PE, Sepia Melanin and cellulose. **c**, Mineralization of PE, Sepia Melanin and cellulose.

According to ASTM D6400, to be labelled as aerobically biodegradable under composting conditions, test materials need to attain or surpass the 90% threshold value with respect to the positive control (cellulose), in a period ranging between 45 and 180 days. The projection (extrapolation) of cellulose mineralization at the upper time limit of ASTM D6400, i.e. 180 d, with the 0.19 %/d rate of the second part of the incubation time (($\Delta t_{35\text{-}98}$), Supplementary Figure 4 and related explanation), entails that cellulose mineralization would be complete. Consequently, the threshold value in 180 days becomes 90%. With the mineralization rate of the second half of the incubation time (0.26 %/d for $\Delta t_{35\text{-}98}$), Sepia Melanin would reach 58% mineralization projected over 180 days.

7.5.3 PPS and Cu-Pc: Biodegradability Test under Thermophilic Conditions (58°C)

The *apparent* respiration rate (the ratio of the total CO_2 produced to the final incubation time) of PPS blended with compost (478 ± 46 mg/d) falls within the range of the blank compost (457 ± 24 mg/d) (Figure 7.4, a) during the biodegradability test under thermophilic conditions. Regarding Cu-Pc, in the first 50 days, the respiration rate is similar to the blank compost. However, starting from day 50 onward, the cumulative CO_2 respired by Cu-Pc blended with compost is always lower with respect to the blank compost, with the difference ranging between 34% and 14% (Figure 7.4, a). The apparent final respiration rate is 400 ± 9 mg/d while the blank compost featured 457 ± 24 mg/d.
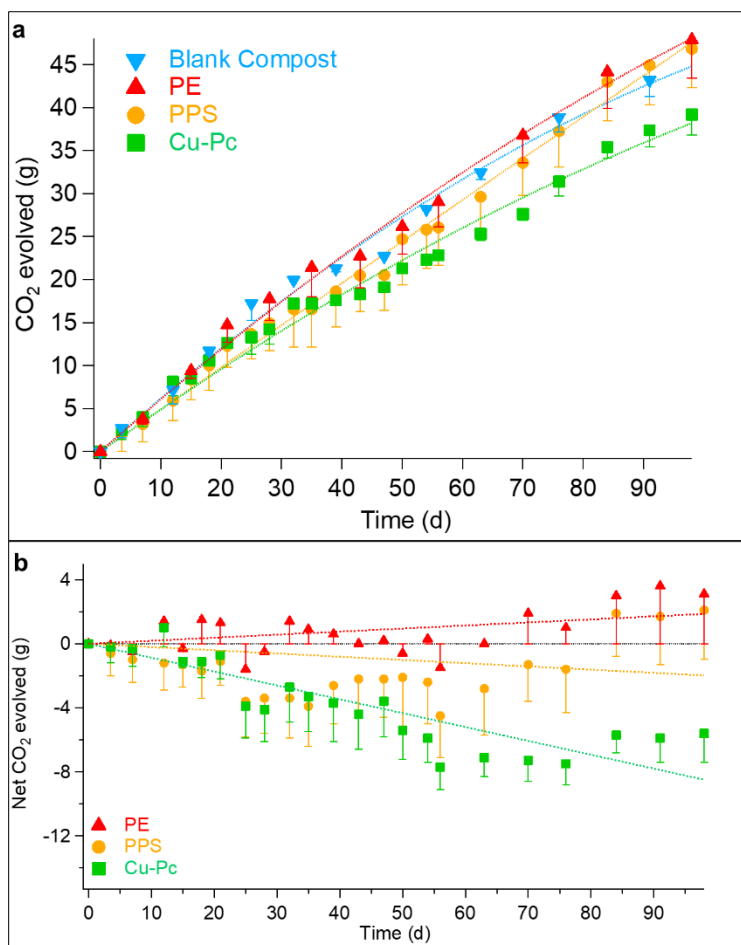
Figure 7.4 Biodegradation in composting conditions of synthetic materials. **a**, Cumulative CO_2 evolved from blank compost, PE, PPS and Cu-Pc. **b**, Net cumulative CO_2 evolved from PE, PPS and Cu-Pc, with respect to blank compost.

A summary of the cumulative O_2 consumed at 25°C, the cumulative CO_2 evolved at 58°C, the apparent respiration rates, and the mineralization levels at the end of the two biodegradation tests is provided in Table 7.1.

Table 7.1 Biodegradation summary. Respiration rates under mesophilic (25°C) and thermophilic (58°C) conditions for various combinations of compost and test material buried into 100 g and 250 g of compost, respectively.

Compost + Test Material	Biodegradability test (25°C), after 97 days			Biodegradability test (58°C), after 98 days		
	Cumulative O_2 consumed (mg)	O_2 consumption apparent rate (mg/d)	Mineralization level (%)	Cumulative CO_2 evolved (mg)	CO_2 evolution apparent rate (mg/d)	Mineralization level (%)
Blank compost (Baseline)	2,194 ± 3	22.62 ± 0.03	---	44,771 ± 2,387	457 ± 24	---
Polyethylene (Negative control)	n.d.	n.d.	n.d.	47,864 ± 4,455	488 ± 45	0
Cellulose (Positive control)	8,835 ± 23	91.08 ± 0.23	71.2 ± 0.2	76,454 ± 1,400	780 ± 14	98 ± 6
Sepia Melanin	2,759 ± 156	28.44 ± 1.61	4.1 ± 0.7	60,099 ± 9,385	613 ± 96	38 ± 17
Cu-Pc	n.d.	n.d.	n.d.	39,190 ± 885	400 ± 9	0
Poly(phenylene sulphide)	n.d.	n.d.	n.d.	46,833 ± 4,468	478 ± 46	0

7.5.4 Phytotoxicity Test

At the end of the test under thermophilic conditions (98 d), the samples were used for plant germination and growth tests. The seedling emergence (the number of plants that germinated from 20 seeds) and the plant biomass (the wet mass of such plants) were measured, for all the materials tested, after 19 days of incubation at 25°C (Table 7.2). According to ASTM D6400, in order to pass the phytotoxicity test, the seedling emergence and the plant biomass have to be at least 90% of the values obtained for blank compost [343].

Table 7.2 Phytotoxicity tests. Seedling emergence and plant biomass in wet sandy soil, used as a "pristine" or "clean" substratum, after 19 days; plants in wet sandy soil at day 19: 20 ± 0.

Sample	Seedling Emergence (%)	Plant Biomass (mg)	Apparent CO_2 Production Rate (g/d)
Blank Compost	78 ± 15	84 ± 28	0.46 ± 0.02
Threshold	70	76	---
Sepia Melanin	76 ± 12	77 ± 24	0.61 ± 0.01
Cellulose	89 ± 8	115 ± 30	0.78 ± 0.01
Polyethylene	66 ± 19	48 ± 26	0.49 ± 0.05
Poly(phenylene sulphide)	42 ± 15	14 ± 6	0.48 ± 0.05
Cu-Pc	57 ± 13	50 ± 33	0.40 ± 0.01

7.6 Discussion

The biodegradation phenomenon results from the combination of several abiotic and biotic factors. Such factors are partly intrinsic to the test material (its chemical composition, structure and surface area, C/N ratio [187]) and partly depend on the environment (e.g. temperature, pH) as well as on the microbial community of the compost [187]. Microbial degradation of an extracellular substrate is mediated by extracellular enzymes. Typically, in the case of a polymer, two steps take place. Firstly, the depolymerization step, corresponding to the cleavage of the chain, takes place. Once dimers or monomers are formed and brought inside the microorganism, the mineralization step occurs, with concomitant production of CO_2 [187].

Our results demonstrate that, at 25°C, and after an incubation period of 97 d, the mineralization level of Sepia Melanin is 18x lower than that of cellulose (positive control), i.e. 4% vs. 71%, respectively (Figure 7.2, c and Table 7.1). Under thermophilic conditions, Sepia Melanin attains a mineralization level of 37% in 98 days, 2.6x lower than the positive control (Figure 7.3, c and Table 7.1).

We suggest that the intrinsic features of eumelanin determining its biodegradation by the microbiota of the compost are its molecular and supramolecular structures [37] as well as the hygroscopicity of the biopigment [123].

It is well-established that eumelanin, rather than being composed of linear polymeric chains, is based on oligomeric planes of DHI and DHICA monomers (Figure 7.1) [37]. The oligomers differ one from the other by the number of units, types of units (DHI vs. DHICA) and polymerization sites [75]. In other words, eumelanin is a chemically disordered material [469]. Eumelanin's oligomers further organize in a complex supramolecular structure: the oligomeric sheets form protoparticles via π-π stacking [37]. The protoparticles arrange in an onion-like structure and densify into spherical particles (ca. 10 nm sized), and eventually undergo aggregation into larger spherical particles (ca. 100 nm sized) [37]. Eumelanin particles feature heterogeneity in size and supramolecular structure: the chemical disorder is paralleled by structural disorder [469].

The structural and chemical disorder are characteristics that may limit the biodegradability of eumelanin. Indeed, not all the oligomeric planes are exposed to the enzymes: the monomer-monomer bonds may be attacked only in the "external" oligomers (i.e. on the surface) of eumelanin particles. It has been suggested that the "opening" of the supramolecular structure, i.e. the de-stacking of the oligomers, is a necessary step for the biopigment degradation [212]. Furthermore, Sepia Melanin is a heterogenous substrate for the attack of extracellular enzymes. A type of enzyme able to act on one type of oligomer of eumelanin may have different affinity towards different oligomers [219]. In addition, a non-biodegraded oligomer will prevent the exposure to extracellular enzymes of all the oligomers stacking beneath it.

Once "freed" from the oligomers, after diffusion into the microorganism, the monomers are readily metabolized. Indoles are indeed known to be microbially degraded with the indole ring cleavage following a pathway that ends with the formation of fumarate and pyruvate [470].

Furthermore, eumelanin is known to be a hygroscopic material [123]. The Sepia Melanin extracted for this work absorbs 17% wt. of H_2O in 1 hour at 90% relative humidity (Supplementary Figure 2, Supplementary Table 1 and related explanation). We already reported that in 24 h Sepia Melanin can absorb a water quantity equal to its weight [123]. It is reasonable to assume water diffusion from the wet compost (containing 50% wt. of H_2O) towards Sepia Melanin in the bioreactors. Water is one of the means through which microorganisms bring inside their cells the monomers

that were cleaved from the extracellular substrate through the enzymatic attack [471]. Consequently, we suggest that the biopigment hygroscopicity favors its biodegradation.

The compost medium has an important effect on biodegradation. Indeed, the compost microbiota (community structure) in mesophilic and thermophilic conditions do not feature the same predominant bacterial and fungal species [472]. Furthermore, microbial decomposition of organic matter is a temperature-dependent phenomenon. Mesophilic microorganisms (optimal growth temperature range 10-42°C) show lower respiration rates as compared to thermophilic microorganisms (optimal growth temperature range 45-70°C) [473], [474]. This difference, well established in the literature, was confirmed by our tests on the blank compost in the two temperature ranges ("Blank Compost Characterization" in Supplementary Data).

The kinetics of growth of the mesophilic bacteria as well as the intrinsic biodegradation-hindering factors of eumelanin (structural and chemical disorder) could tentatively explain why eumelanin was recalcitrant to biodegradation in mesophilic conditions. Furthermore, in order to explain the difference with respect to cellulose (4% vs 71%), it has to be considered that the compost used was acclimated to cellulose biodegradation. This means that, in the microbiota of the compost used, cellulosic bacteria are already present as they adapted to the lignocellulosic biomass of vegetal compost added to compensate the C/N ratio in the composting facility.

On the other hand, in the thermophilic stage of composting, we suggest a synergy between the faster growth kinetics of thermophilic microorganisms and more abundant melanin degrading enzymes, whose rates of activity increase with temperature. It is worth noting that the fungus that biodegrades eumelanin at room temperature, *Aspergillus fumigatus*, can tolerate 50°C and above [475].

The proposed synergy can explain the final mineralization rate of Sepia Melanin in thermophilic conditions (37%) almost 10x higher than in mesophilic conditions (4%), after ca. 100 days. Taking into account both the compost acclimated to lignocellulosic biomass as well as the chemical and structural heterogeneity of eumelanin, eumelanin attains a significant mineralization level in thermophilic conditions. Although significant, such biodegradation level does not meet current industrial requirements for compostability (ASTM D6400, concerning plastics for food packaging and serving). Indeed, using the 0.26 %/d rate of the second period of incubation time (Δt_{35-98}), Sepia

Melanin would reach 58% if projected at the upper time limit suggested by ASTM D6400 (180 d), not fulfilling the threshold (90%) of biodegradability in composting conditions.

Both the thresholds of seedling emergence and plant biomass established for the phytotoxicity test were passed by Sepia Melanin (Table 7.2). The precursor of melanin, L-dopa, has been reported to have phytotoxic effects due to the formation of hydrogen peroxides during melanogenesis (the biosynthetic path that brings to melanin) [476]. Our results reveal that the biopigment may not be phytotoxic. Furthermore, fumarates, that result from the biodegradation of indoles [470], are not phytotoxic either [477].

The apparent respiration rate of Cu-Pc blended with compost initially falls within the range of the blank compost, but then, after 50 d, it becomes lower (Figure 7.4). This could be explained with a partial release of Cu ions by the molecule: such cations are able to inhibit the microbial activity [478]. This implies that there was no net CO_2 production with respect to the blank compost and, consequently, no biodegradation (Figure 7.4). The molecular structure of Cu-Pc presents a planar aromatic macrocycle with the metal cation at its center [479] (Figure 7.1). Such a plane is based, like eumelanin, on indoles. However, in Cu-Pc, the four indole units do not feature catecholic groups and are not directly chemically bound to each other [479] (Figure 7.1). The absence of biodegradation of Cu-Pc can be explained considering both the microbial metabolism inhibition by the released copper cations as well as the resistance of the nitrogen-including bonds between the indole units to enzyme-mediated scission [478]. The π-π stacking of the molecules of Cu-Pc and their insolubility in water may represent additional biodegradation-hindering factors [479]. Prior to our study, no phytotoxicity test has been conducted with Cu-Pc so far, although the phytotoxicity of several other phthalocyanines has been evaluated [480]. The presence of Cu-Pc in the compost in our study proved to have no detrimental effects on the seedling emergence nor on the growth (Table 7.2).

The apparent respiration rate of PPS blended with compost falls within the range of the blank compost over the entire incubation period (Table 7.1 and Figure 7.4). No mineralization, consequently, took place. We suggest that the chemical bond between a sulphur atom and a benzene ring is recalcitrant to the cleavage of extracellular enzymes in our compost under thermophilic conditions (Figure 7.1). PPS fails to pass both the phytotoxicity test thresholds, proving to limit

both the seedling emergence and the growth of plants. This points to a potential phytotoxicity of the polymer (Table 7.2).

7.7 Conclusion

The electronic industry is experiencing tremendous challenges. The waste electrical and electronic equipment is alarmingly increasing, the reserves of key chemical elements for device manufacturing are shrinking, the device embodied energy (energy consumed during manufacturing) is increasing, all causing an unsustainable environmental footprint. In the past decades, attention has been devoted to the performance of electronic devices, with limited consideration to their end of life (fate after service).

Recurring to abundant and biodegradable organic (carbon-based) electronic materials represents one of the viable solutions to alleviate the environmental footprint of the electronic industry. At present, no guideline to establish the biodegradability of organic electronic materials and devices is available.

We found that eumelanin, an organic electronic bio-sourced material, attained a mineralization level of 37% after 97 d under composting conditions (at 58°C), with no phytotoxic effects on the industrial compost.

We also tested the biodegradability in composting conditions of two non-bio-sourced (synthetic) organic electronic materials, namely copper (II) phthalocyanine, Cu-Pc, and poly(1-4 phenylene sulfide), PPS. Both materials featured negligible mineralization. In addition, Cu-Pc inhibited the metabolism of the microorganisms while PPS showed potential phytotoxicity.

The strikingly different results between bio-sourced and synthetic materials suggest that recurring to organic bio-sourced materials is a viable option to eco-design biodegradable organic electronic materials and devices. However, eumelanin did not pass the threshold of biodegradability in composting conditions, set by ASTM D6400. It is worthwhile to note that ASTM D6400 (and the corresponding international standards) addresses plastic polymers for food packaging and serving. No protocol dealing with the biodegradability in composting conditions of materials for organic electronics is available. Moreover, we found that, at room temperature, i.e. the biodegradability conditions of a natural ecosystem, eumelanin featured almost negligible biodegradation, confirming the need of streaming organic waste to industrial composting facilities. Further studies

in other types of compost featuring different microbial communities (e.g. in compost from manure or garden waste) are needed to identify the most suitable conditions for eumelanin's biodegradability. Work is in progress to evaluate the biodegradability of organic electronic devices, beyond the constituent materials.

7.8 Acknowledgments

7.9 Funding Sources

CHAPTER 8   ARTICLE 4: ON THE INTERFACES BETWEEN ORGANIC BIO-SOURCED MATERIALS AND METALS FOR SUSTAINABLE ELECTRONICS: THE EUMELANIN CASE

Article 4 has been published by the *Japanese Journal of Applied Physics* on April 26th, 2019. Supplementary Information is provided in <u>Appendix E</u>.

8.1 Authors

Eduardo Di Mauro[1], Emilie Hebrard[1], Yasmina Boulahia[1], Marco Rolandi[2] and Clara Santato[1]

[1] Department of Engineering Physics, Polytechnique Montreal, C.P. 6079, Succ. Centre-ville, Montreal, Quebec, H3C 3A7, Canada

[2] Department of Electrical and Computer Engineering, University of California Santa Cruz, Santa Cruz, California 95064, United States

8.2 Abstract

Organic bio-sourced materials featuring charge transfer and transport properties are of high interest in the field of sustainable (green) electronics, which aims at alleviating the environmental impact of conventional electronics. Such materials may contain, after extraction from biological media, traces of salts that can dramatically affect their electrical response, because of electrochemical processes at organic bio-sourced material/metal contact interfaces. Eumelanin, a bio-sourced pigment, is an attractive candidate for sustainable electronics. This work reports on chemical and structural changes occurring at interfaces between metal electrodes (Pd, Cu, Fe, Ni and Au) and hydrated films of eumelanin, under bias. The parameters affecting such changes, i.e. the chloride content in eumelanin, the relative humidity of the environment and the type of eumelanin (synthetic versus natural), were investigated. Our work contributes to establish criteria for selecting metal contacts suitable for the fruitful exploration and exploitation of organic bio-sourced materials in sustainable electronics.

8.3 Introduction

Sustainable electronics aims at responding to current environmental issues, such as the increase of waste electrical and electronic equipment (WEEE) [127]. Bio-sourced organic materials are investigated in sustainable electronics for their abundance, low cost and potential biocompatibility and biodegradability [127]. The study of interfaces between metal electrodes and bio-sourced organic materials is of the utmost importance for the design of sustainable (green) electronics devices [127], [128]. Bio-sourced organic materials typically feature a complex chemical composition, as they may contain traces of salts from the biological medium from which they are extracted [481], [482]. The presence of such salts may lead to electrochemical processes at the interface with metal contacts, which can dramatically affect the overall response of the materials during the characterization of their electrical properties.

The biopigment melanin is present in humans, animals, plants and microorganisms [344]. Eumelanin is the dark-brown subgroup of melanins [410], whose building blocks are 5,6-dihydroxyindole (DHI) and 5,6-dihydroxyindole-2-carboxylic acid (DHICA) (Figure 8.1) [2]. One of the most studied natural eumelanins is Sepia Melanin, extracted from the ink sac of the cephalopod *Sepia officinalis* (commonly known as cuttlefish) [9]. Eumelanin is an important candidate for organic electronics [132], as its molecular structure features conjugation (alternance of single and double bonds, typical of organic electronics materials) and the presence of quinone redox active groups [410], [411]. Since it is non-toxic and bio-sourced, eumelanin is also an interesting candidate for sustainable electronics [127].
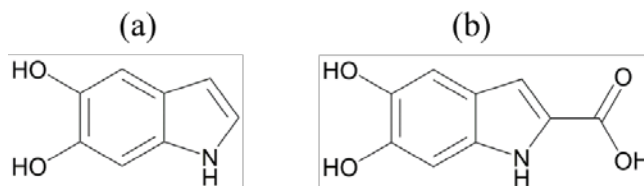
Figure 8.1 Building blocks of eumelanin: (a) DHI, (b) DHICA.

The hydration-dependent electrical conductivity of eumelanin was discovered in 1974 and explained with the amorphous semiconductor model [109]. Several studies on the electrical

conductivity of the biopigment ensued, entailing both eumelanin pellets and thin films [106], [115], [483]–[485]. Our groups recently reported on the proton transport properties of eumelanin thin films [108]. Besides the physicochemical properties of UV-visible broad absorption [27] and free radical scavenging [469], eumelanin features biocompatibility [125], [126] and binding affinity for metals, such as copper, iron and calcium [89]. The binding site can be the catechol, the amine or the carboxylic group (Figure 8.1) [70].

Eumelanin-based batteries [23], [201], flexible micro-supercapacitors [25], organic electrochemical transistors [132] and memristive devices [486], [487] have been demonstrated.

During the investigation of the electrical response of hydrated eumelanin films with supposedly inert contacts (Au), we reported on the electrochemical dissolution of gold electrodes, with formation of dendrites [210]. The dendrites led to a resistive switch, akin to the working mechanism of electrochemical metallization memories [135], [210]. The relative humidity of the environment influenced the extent of the current increase during the resistive switch [488]. These observations led us to conduct a more comprehensive study of interfaces between metals and melanin, considered as prototype organic bio-sourced material for sustainable electronics. As a matter of fact, the metal electrode dissolution during the electrical characterization of organic bio-sourced materials hinders the investigation of their electrical properties, overshadowing the *intrinsic* electrical response of the bio-sourced materials, and the assessment of their technological potential.

Here we report on possible structural and chemical changes taking place at the interface between hydrated eumelanin films and metal electrodes under electrical bias (Figure 8.2(a)). Various metals, types of eumelanin (e.g. natural vs. synthetic), relative humidity levels in the measurement atmosphere and chloride contents were considered. Such changes were studied using transient current measurements, scanning electron microscopy (SEM), energy-dispersive X-ray spectroscopy (EDX) and atomic force microscopy (AFM). Our aim was to discover the conditions under which electrode dissolution does/does not take place, for the selection of suitable metal contacts to characterize the electrical response of melanin and, more in general, organic bio-sourced materials. Such a selection is a required step for the exploitation of bio-sourced materials in green electronics technologies.

We interfaced eumelanin films to a number of metals, namely Pd, Cu, Fe, Ni and Au, selected on the basis of a number of considerations. Palladium metal contacts (in the form of PdH_x) are used

for the measurements of protonic currents in organic bio-sourced materials [108], [489], [490]. Eumelanin binds copper and iron in biological systems [70]. Nickel is investigated for biomedical [491] and biosensing applications [492], [493] as well as metal contact in organic single crystal transistors [494]–[496]. Gold, the metal of choice for the large majority of organic electronic devices, was included for comparative purposes [210].
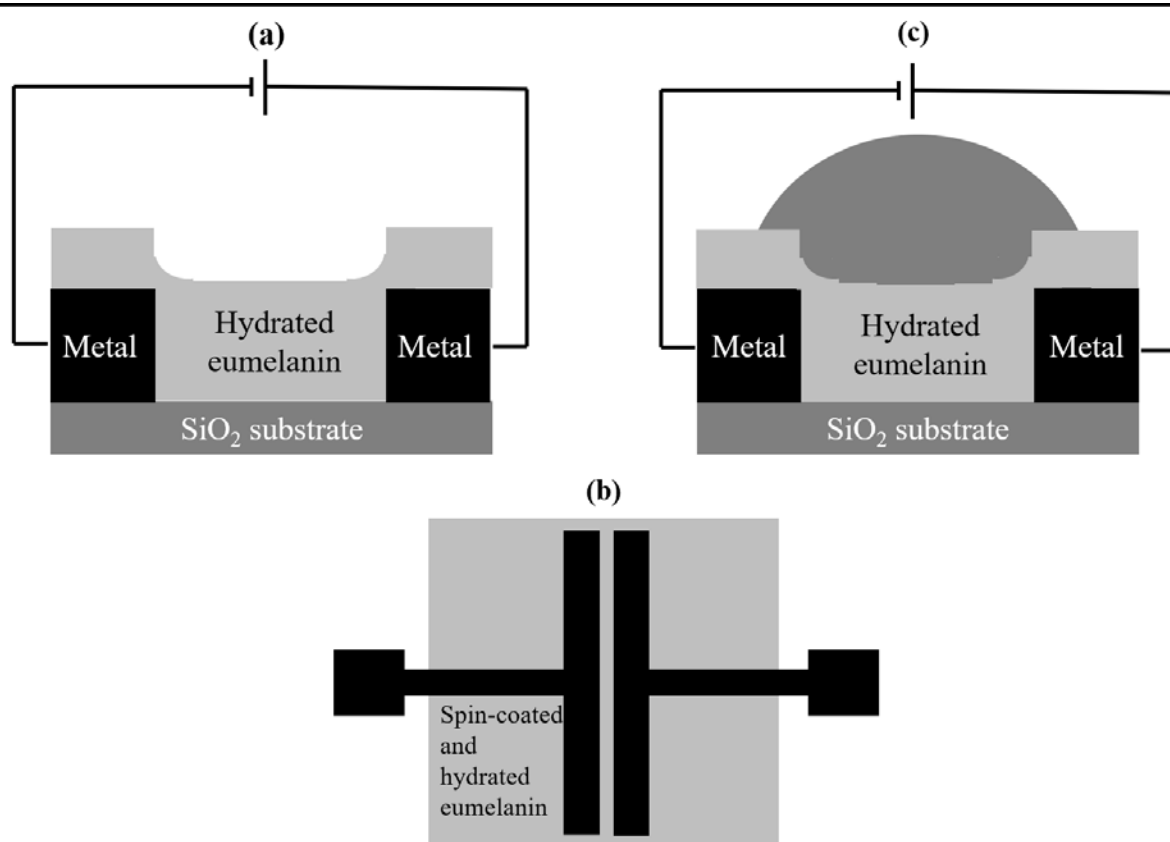
Figure 8.2 (a) Side view and (b) top view of the experimental configuration used to conduct electrical measurements in this work, (c) side view of the water drop that can stretch over the entire interelectrode distance during the measurements at high relative humidity. Images not in scale.

8.4 Experimental Methods

Synthetic (Sigma) eumelanin (Cl⁻ content ca 1% wt.), Sepia Melanin (natural eumelanin, Cl⁻ content ca 7% wt. [488]) and dimethyl sulfoxide (DMSO) were purchased from Sigma Aldrich (Canada). Synthetic eumelanin was used to ensure the absence of lipids and proteins that may still be present in Sepia Melanin after extraction from the natural source. Solutions of synthetic

eumelanin in DMSO containing a chloride content close to that of Sepia Melanin were obtained by addition of NaCl. DMSO-melanin (Cl$^-$ content 0.1 % wt.), a eumelanin-like material polymerized in DMSO, wherein the metal binding groups are partly absent, was synthesized by the group of Prof. C. Graeff (UNESP, Brazil) [310].

Metal electrodes were deposited by e-beam evaporation (Au, Pd, Cu and Ni) or radio frequency (RF) sputtering (Fe) and photolithographically patterned on Si wafers with 200 nm thermal SiO$_2$ (Silicon Quest International, San Jose, California, USA, thickness 525 ± 25 μm). The interelectrode area was 10 μm long and 4 mm wide. All electrodes were 30 nm thick and were deposited on a 5 nm Ti adhesion layer (except for Fe). Prior to spin coating of eumelanin, the patterned substrates were cleaned in an ultrasonic bath with acetone, isopropanol, acetone. Only for Pd and Au electrodes, a further sonication in de-ionized water and a 10-min UV-ozone treatment followed.

Copper, iron and nickel form a layer of native oxide in ambient atmosphere [497], [498]. We tested both untreated as well as treated Cu, Fe and Ni electrodes, where, prior to eumelanin spin coating, the native oxide had been etched (by 1-min sonication in acetic acid for Cu and Fe, in ammonium hydroxide for Ni).

The preparation of the 15 mg/ml solutions of eumelanin in DMSO, the solution processing and hydration steps at different relative humidity (RH) levels have been reported elsewhere [488].

Electrical measurements were carried out at room temperature and at controlled RH, as reported in [488], using a Source Measure Unit (SMU), Agilent 2900A, with Quick IV software for data recording.

The samples were characterized by scanning electron microscopy (SEM) at the end of the transient current measurements. A microscope JEOL JSM7600F was used. Energy-dispersive X-ray spectroscopy (EDX) was carried out using the same microscope with Aztec (Oxford) software, detector x-Max (80 mm^2) (Oxford), at 5 kV.

AFM images were acquired in air using FAST SCAN imaging with a Bruker Dimension FASTSCAN AFM, at a scan rate of 6-8 Hz using FastScan A cantilevers (Bruker, Santa Barbara, CA) with a resonance frequency around 1400 kHz, a spring constant of ≈ 18 N/m, and tip radius of < 10 nm.

8.5 Results and Discussion

8.5.1 Eumelanin and Palladium Electrodes

Palladium is a relevant material for studies of the proton conductivity of organic bio-sourced materials [108], [489], [490]. Transient current measurements carried out on hydrated films (1 hour at 90% RH) of synthetic eumelanin (8% wt. Cl⁻) and Sepia Melanin (Figure 8.3(a) and (b)), at 1 V, show an initial exponential decrease of the current, related to ion migration in the interelectrode area with formation of an electrical double layer, followed by a current increase of three orders of magnitude, due to the positive electrode dissolution and formation of metallic bridging structures. In particular, SEM images show that Pd interfaced with hydrated films of synthetic eumelanin dissolves during transient current measurements forming continuous bridging structures (inset of Figure 8.3(a)). The continuous morphology of the Pd structures points to a non-diffusion-limited growth [499]. EDX revealed that the structures are made of Pd (point 1 of the inset of Figure 8.3(a)). Conversely, Pd is absent in some parts of the positive electrode (point 2 in Figure 8.3 (a)). This absence indicates that the positive electrode dissolves during biasing, supplying metal cations for the nucleation and growth of the bridging structures at the negative electrode. The bridging structures grow protruding towards the positive electrode; when they connect one Pd electrode to the other, the resistive switch takes place and the current increases by three orders of magnitude within the first minute of bias.

Figure 8.3 Current vs time plot obtained with (a) a synthetic eumelanin film, 8% wt. Cl⁻, hydrated for 1 hour at 90% RH, spin coated on a substrate patterned with Pd electrodes, bias time of 30 min (current increase after ~ 46 s, compliance of 1 mA); (b) Sepia Melanin film, 7% wt. Cl⁻, hydrated for 1 hour at 90% RH, spin coated on a substrate patterned with Pd electrodes, bias time

of 3 hours (current increase after ~ 16 min); 1 V electrical bias. The interelectrode areas, delimited by the dotted blue lines, are shown in the two insets; SEM images taken in secondary electron mode, at 10 kV (a) and 5 kV (b).

In the case of Sepia Melanin (inset of Figure 8.3(b)), the Pd bridging structures show a morphology that is intermediate between continuous and dendritic. The difference in the shape of the bridging structures may result from a complex interplay of factors, including the binding affinity of the metal towards eumelanin [89], metal-Cl^- (ligand) interactions [500], metal cation reduction at surface catechols [501] and the coordinating action of DMSO [500], the solvent used to fabricate the films. The difference in morphology can also explain why the continuous bridging structures that form in the former can sustain a current after the resistive switch that is two orders of magnitude higher with respect to the bridging structures that form in Sepia Melanin. It is worth noting that the focus of this work was not providing a detailed growth mechanism of the metallic structures within the interelectrode distance. As opposed to that, the focus is on the occurrence of chemical and morphological changes at the interface between metal electrodes and organic bio-sourced materials, during the electrical characaterization of the latter (Table S1).

Palladium does not dissolve if the Cl^- content in eumelanin is decreased from 8% wt. to 1% wt. at 90% RH (Figure S1(a-b)) and if the RH level is decreased from 90% to 80% or 70% (Figure S1(c-d)) keeping 8% wt. Cl^-.

From the study of palladium-eumelanin interfaces we can conclude that Pd electrodes are more stable than Au electrodes, which dissolve at lower RH levels (80% and 70%) and chloride content (1% wt.) with formation of Au dendrites [488]. The two metals feature similar values of the standard free Gibbs energy ($\Delta G°$) for the formation of metal chloride complexes (equations S1-S5 of Table S2). On the other hand, the fact that Pd electrodes dissolve at high chloride contents (8% wt.) can be tentatively explained considering that, for Pd, a higher number of Cl^- anions is involved per electron released in the oxidation with respect to Au, as inferrable from equations S1-S5, Table S2, where the chemical equations of the metal complexes that form in the presence of chlorides are provided.

8.5.2 Eumelanin and Copper Electrodes

Copper is a metal with a well-established affinity for eumelanin [70]. SEM images of the interelectrode area reveal that Cu electrodes treated to remove Cu_xO dissolve when interfaced with hydrated films of synthetic eumelanin during transient current measurements, with formation of bridging structures (Figure 8.4(a-b)). EDX measurements show that copper is also present in regions of the interelectrode distance other than the bridging structures. The high current condition after bridging is temporary (approximately two hours), and its decrease can be ascribed to the oxidation of the copper structures. Differently from Cu, in the case of Au dendrites, the current of the post-resistive switch is kept if the bias is applied again after 10 months [488]. Untreated Cu electrodes interfaced with hydrated films of synthetic eumelanin can also dissolve forming dendrites, under electrical bias. In presence of chlorides, copper oxides feature limited stability; therefore, it is reasonable to assume that the native oxide layer leaves some areas of bare metallic copper, electrochemically active [502]. The current increases by only one order of magnitude and, after the resistive switch, it immediately starts to decrease (Figure 8.4(c-d)): such a decrease can be ascribed to the dendrite oxidation.

In summary, dendrites form at the interface between copper electrodes (both treated and untreated) and synthetic eumelanin (8% wt. Cl$^-$) under bias: the extent and duration of the current increase depend on whether the electrodes were treated or not, as the treatment drastically influences the availability of metallic copper.

No electrode dissolution of the treated Cu electrodes takes place if the Cl$^-$ content of synthetic eumelanin is decreased from 8% wt. to 1% wt. (Figure S2(a,b)), confirming that chlorides play a key role in its dissolution. Despite the lower value of $\Delta G°$ (about one order of magnitude lower) for the formation of copper chloride complexes with respect to Au and Pd (Table S2), Cu electrodes may require high chloride contents to dissolve, as the favorable formation of the oxide (equations S6-S7 of Table S2) reduces the availability of bare copper.
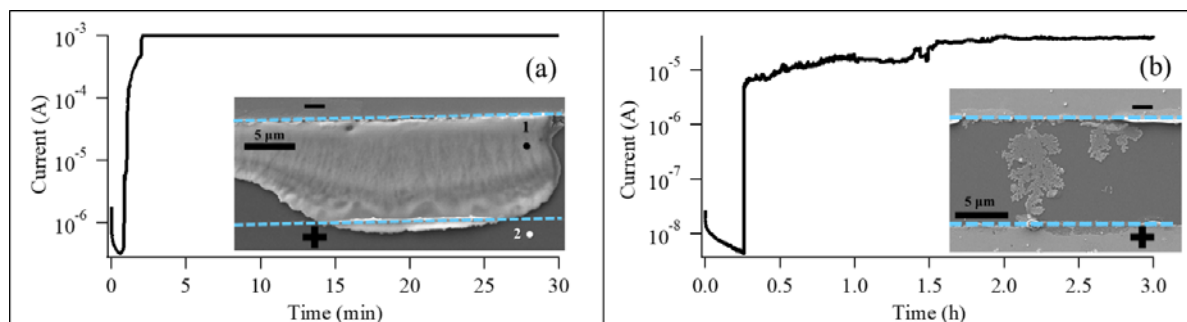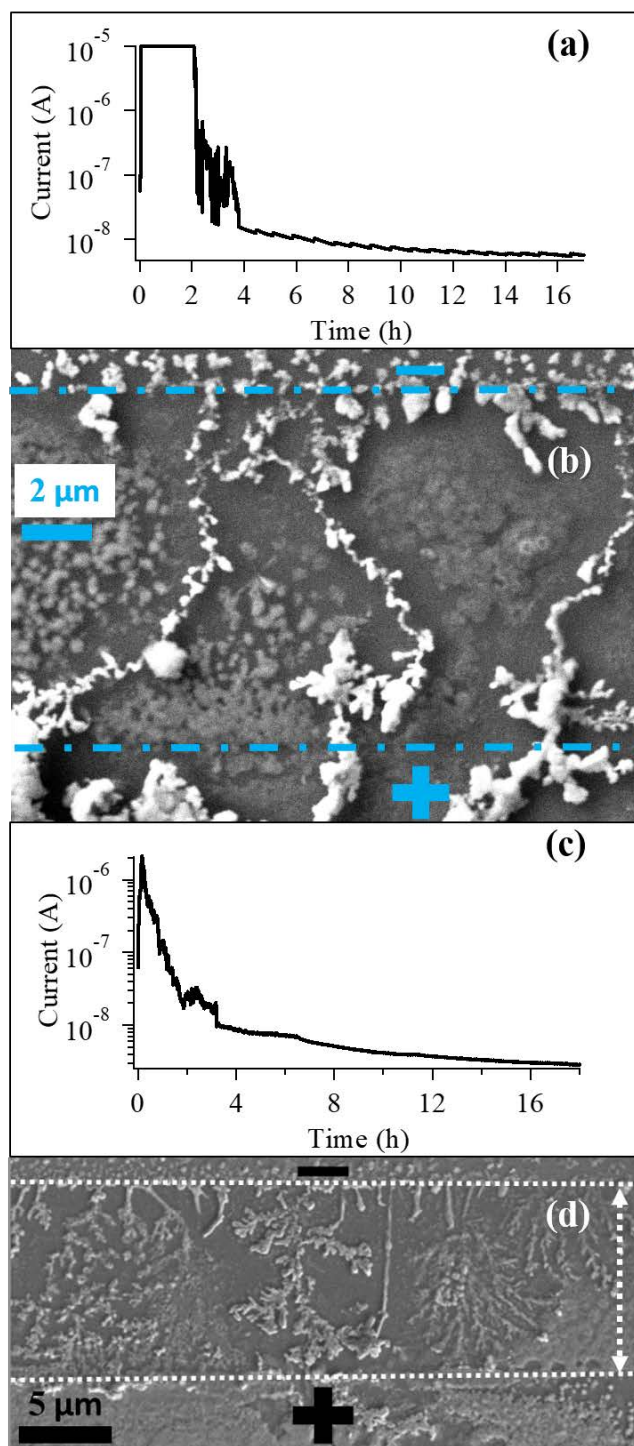
Figure 8.4 Current vs time plot obtained with synthetic eumelanin films, 8% wt. Cl⁻, hydrated for
1 hour at 90% RH, spin coated on a substrate patterned with Cu electrodes, and corresponding
SEM image of the interelectrode area (delimited by the dotted lines): (a-b) treated Cu electrodes,
bias of 17 hours (current increase after ~ 3 min); (c-d) non treated Cu electrodes, bias of 18 hours

(current increase after ~ 30 s); 1 V electrical bias; images taken in secondary electron mode, at 10 kV (b) and 5 kV (d) .

Surprisingly, no dissolution takes place with Sepia Melanin (7% wt. Cl⁻) in contact with treated Cu electrodes (Figure S2(c,d), where the characteristic spherical aggregates of Sepia Melanin are noticeable). The absence of dissolution is tentatively explained considering the hygroscopicity of Sepia Melanin [123] as well as the absence of UV-ozone treatment of the copper substrates. The former renders water, which plays a key role in the electrode dissolution, less available for the process [488]. The latter is expected to limit substrate's hydrophilicity with respect to ozone-treated substrates. Both factors point to an inefficient transport of ions in aqueous or hydrated media, in turn leading to a limited electrical continuity, required for metal dissolution, in the region included between the metal contacts.

8.5.3 Eumelanin and Iron Electrodes

Iron is another metal with a high binding affinity for eumelanin [70]. SEM images of hydrated eumelanin films on substrates patterned with Fe electrodes, after bias, show that micrometric platelets form, to a higher extent on the positive electrode. This observation is valid both for treated and untreated iron electrodes, interfaced both with Sepia and synthetic eumelanin films (Figures S3-S4 and Figure 8.5(a-b), where the typical aggregates of natural eumelanin are visible, too). These platelets are separated by iron-free areas, as shown by EDX (point 1 of Figure 8.5(b) is devoid of Fe). It is reasonable to assume that the platelets are formed of iron oxide (point 2 of Figure 8.5(b), at. %: 57% O, 29% Fe, 9% C, 4% Si), which proved to be stable enough not to provide cations to feed the growth of bridging structures, as opposed to what was observed with Au, Pd and Cu electrodes (Table S2). It can be inferred that Fe electrodes are of limited interest for fundamental studies on the electrical response of eumelanin, given their structural discontinuity (platelets surrounded by iron-free areas) induced by the application of the electrical bias (Figure S3).
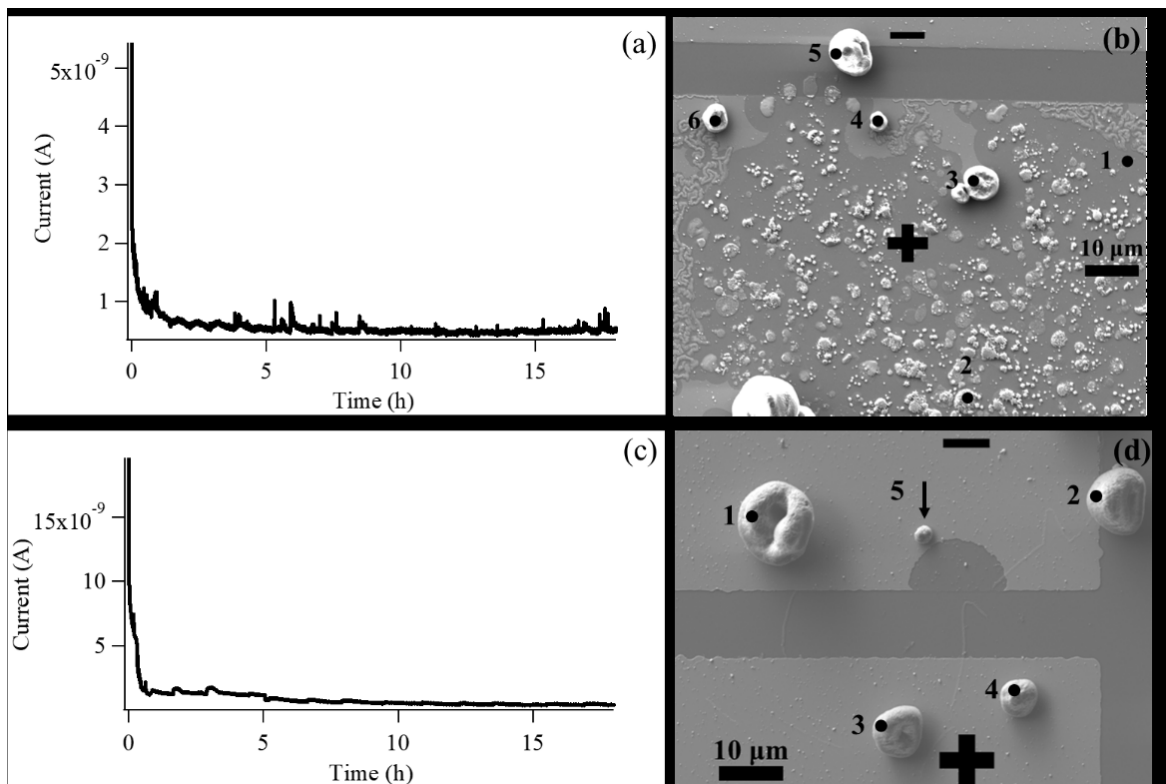
Figure 8.5 Current vs time plots and corresponding SEM images of the interelectrode area obtained with Sepia Melanin films, 7% wt. Cl⁻, hydrated for 1 hour at 90% RH and spin coated on (a-b) a substrate patterned with untreated Fe electrodes, bias time of 19 hours; (c-d) on a substrate patterned with untreated Ni electrodes, bias time of 18 hours; points 3-6 of (b) and 1-5 of (d) indicate aggregates of Sepia Melanin; 1 V electrical bias; images taken in secondary electron mode, at 5 kV.

8.5.4 Eumelanin and Nickel Electrodes

For Ni electrodes, both treated and untreated, interfaced with boh synthetic and Sepia Melanin, only partial dissolution was observed (Figure 8.5(c-d) and Figures S5-S6). This observation can be tentatively explained considering the good electrochemical stability of nickel oxide (e.g. widely employed in electrochromic windows) (equations S10-S11) [503]. We only observe local dissolutions (pits) at the electrodes, likely attributable to the chemical attack of the native oxide layer by chlorides [504]–[506] (Figure 8.5(d) and Figures S5-S6). The stability of Ni electrodes renders the use of such metal suitable for fundamental studies on the electrical conduction of eumelanin.

8.5.5 The Role of Chloride-containing Water Drops

By means of fast scan AFM and optical images, we observed that, besides being absorbed within the film (matrix water) [124], water can also condense in micrometric drops on the films (<u>Figures S7</u>-<u>S8</u>). Some of these drops cover the entire interelectrode distance (10 μm) (<u>Figure S7</u>), stretching from one electrode to the other. As a consequence, the interelectrode material may consist of hydrated eumelanin and overlying water drops (Figure 8.2(c)). As eumelanin contains chlorides [488], it is reasonable to assume the diffusion of chlorides to the water drops, due to a concentration gradient. In order to explore the possible effect on metal dissolution of the chloride-containing water drops forming on the surface of eumelanin, we investigated eumelanin films included between metal (Au) electrodes, that, after hydration, were buried under a micrometric layer of hydrated chitosan, to avoid the formation of water drops on eumelanin films. No resistive switch took place and bridging structures did not form after the application of the electrical bias (<u>Figure S9</u>). We therefore suggest that eumelanin can promote the formation of bridging structures by enabling the formation of chloride-including water drops on its surface. Despite the fact that eumelanin binds gold ions (as verified by time-of-flight secondary ion mass spectrometry, ToF-SIMS) [210], [488], our results suggest that chloride-containing drops play a key role in the process of Au dissolution (<u>Figure S9</u>).

8.6 Conclusions

We investigated phenomena at interfaces between hydrated films of the biopigment eumelanin and metal electrodes of Pd, Cu, Fe, Ni and Au, of interest in sustainable electronics. The stability of such interfaces under electrical bias is greatly affected by the presence of salts (chlorides) included in eumelanin, and, in general, intrinsically present in organic materials extracted from biological sources. Electrochemical processes can indeed take place. These processes can dramatically affect the interpretation of electrical measurements, overshadowing the *intrinsic* electrical response of bio-sourced materials, and the assessment of their technological potential. Our results show that the use of palladium electrodes at relative humidity below 90% and nickel electrodes is suitable for the characterization of the electrical properties of eumelanin. Iron and copper proved to be of limited interest, due to oxides formation and chlorides destabilization. Interestingly, preliminary results on copper electrodes suggest that if eumelanin is functionalized with non-binding groups replacing catechols (e.g. synthetic eumelanin synthetized in DMSO [310]), the dissolution

processes do not take place. Our work sheds light on complex phenomena taking place at the interface between metals and bio-sourced organic materials for their exploitation in sustainable electronics, with potential impact in a broad range of fields such as bioelectronics [195], electrochemical metallization memories [145] as well as bioresorbable [507] and transient electronics [508]. In perspective, after considering the caveats and the guidelines reported in this work, more conventional interfacial characterizations will have to follow, e.g. on charge carrier injection interfacial properties, to demonstrate reliable and high-performance sustainable devices based on bio-sourced materials.

8.7 Acknowledgments

CHAPTER 9   GENERAL DISCUSSION

The choice of eumelanin as the central material of this thesis stems from several considerations. First of all, its study implies an interdisciplinary approach. Eumelanin represents an intriguing biopigment as it features several different facets, that, in turn, make it a subject of investigation in several different fields: medicine (dermatology and oncology) [12], chemistry/physics, because of the large range of properties with several potential applications (organic electronics, additives for packaging, biotechnology, water purification and so on) [509], microbiology (fungal melanins in soils and as a factor of virulence) [6], art preservation (fungal melanins that affect the aesthetics of wooden works of art) [224], and even anthropology and sociology [510], because of the impact that skin complexation has had on society (e.g. colonization and racism) [511]. Its study thus implies that all the aforementioned fields are taken into consideration. Without such an approach, risks of neglecting or giving for granted certain properties of eumelanin is high (e.g. regarding the biodegradability of eumelanin, the material scientists community had taken it for granted in the last years [410], neglecting the work that many microbiologists had done in the previous decades [221]–[223]).

9.1   Interfaces between Eumelanin and Metal Electrodes under Bias

The use of eumelanin in organic electronics still faces many technological challenges. The affinity of eumelanin for free metal cations has been largely investigated [70]: Article 5 provides an extensive literature review on the topic [89]. On the contrary, little attention has been given to the interfaces between thin films of the pigment and metal electrodes, partly due to the limited solubility of eumelanin in common organic solvents that has hindered for decades the fabrication of homogeneous eumelanin thin films [469]. The stability of such interfaces can be studied from two points of view: in the case of ReRAMS, as explained above, electrochemical processes at the interface resulting in electrode dissolution and bridging structure formation are desirable, as they are at the core of ReRAMS working mechanism [133]. Conversely, the absence of electrode dissolution under bias is paramount for the proper characterization of the intrinsic electrical response of eumelanin films and for the functioning of eumelanin-based devices (except ReRAMS). Should the metal electrode dissolution be desirable or avoided, the study of the interfaces between eumelanin thin films and metal electrodes under electrical bias is of key interest.

The findings from Wuensche *et al.* regarding the dissolution of Au electrodes in contact with hydrated eumelanin thin films under bias [210] (see paragraph "Interfaces between Eumelanin and Metal Electrodes") paved the way for two investigation routes, complementary one to the other. From one side, the similarity between the formation of dendrites in hydrated eumelanin thin films included between Au electrodes and the working mechanism of ReRAMS pointed to the possibility of using eumelanin as a bio-sourced and environmentally benign material to be used as the ion conductor layer of Bio-ReRAMs. In addition, as the switching takes place in highly localized regions, filamentary-based systems can lead to nanoscale memory devices, thus rendering miniaturization easier [386]. From the other side, the instability of the metal electrode-eumelanin interface in the case of a supposedly inert metal, such as gold, confirmed the necessity of "mapping" the conditions under which the metal electrode dissolution does/does not take place, with different metals [210].

In Article 1 [488], transient electrical measurements were carried out in planar configuration on eumelanin thin films (Au/eumelanin/Au systems) under different experimental conditions. The parameters studied were the relative humidity (RH), the hydration times and the type of eumelanin (commercial synthetic melanin, i.e. Sigma Melanin, commercial natural melanin, i.e. Sepia Melanin from Sigma-Aldrich, and DMSO-melanin, a synthetic eumelanin partially lacking the chelating hydroxyl groups, see paragraph "Diverse Synthetic Melanins"). In the case of synthetic eumelanin, another parameter studied was the chloride content (low, intermediate and high, i.e. 1, 4 and 8% wt.). Suspensions of eumelanin in DMSO were prepared and the intermediate and high chloride contents for synthetic eumelanin were obtained by addition of NaCl to the suspensions. The high chloride content is close to the chloride level found in natural Sepia Melanin. The films were spin coated from suspensions in DMSO on SiO_2 substrates patterned with Au electrodes (interelectrode distance of 10 μm, electrode width of 4 mm). Planar systems allow for a detailed investigation of the filament growth, with the following step being the development of stacked (vertical) resistive switching devices [398]. Scanning electron microscopy (SEM), atomic force microscopy (AFM) and time of flight-secondary ion mass spectrometry (ToF-SIMS) were used to gain insights on the morphology and chemical composition of the dendrites that formed in the hydrated films after the application of the electrical bias.

We could thus infer that, decreasing the relative humidity (from 90 to 80 and 70% RH) and keeping the same hydration time (1 hour), the change in resistivity occurring when the first dendrite bridges

one electrode to the other becomes less pronounced (hybrid resistive switch, ON/OFF ratio ~10^2). In this case, the dendrites have a less continuous metallic backbone and contain less gold with respect to the dendrites that cause the "standard resistive switch", with ON/OFF ratio ~10^4-10^5 [488]. Furthermore, we found out that chlorides play a crucial role in the dendrite formation, as an increase of the chloride amount decreases the time of Au dendrite growth. DMSO-melanin, lacking chelating groups, did not feature resistive switch, even with the highest chloride content, suggesting that the chelating groups may play an important role in the migration of the nanoaggregates.

In Article 4 [512], the interfaces between eumelanin films and different types of metal electrodes were studied, namely Pd, Cu, Ni and Fe.

Palladium (in the form of PdH_x) is used for the measurements of protonic currents in organic bio-sourced materials [108], [489], [490]. In biological systems, eumelanin chelates iron and copper [70]. Nickel is studied as metal contact in organic single crystal transistors [494]–[496] as well as for biomedical [491] and biosensing applications [492], [493]. The other parameters varied were the chloride content (low and high, i.e. 1 and 8% wt.) and the type of eumelanin (commercial synthetic eumelanin, i.e. Sigma Melanin from Sigma-Aldrich, and commercial natural eumelanin, i.e. Sepia Melanin from Sigma-Aldrich). Cu, Fe and Ni form a layer of native oxide on their surface in ambient atmosphere [497], [498]. For such metals, both untreated and treated electrodes (after etching of the native oxide) were tested. After preparation of eumelanin suspensions in DMSO, the films were spin coated on electrode-patterned SiO_2 substrates and hydrated for 1 hour at 90% RH. Transient current measurements at 1 V were carried out and the metal electrode-eumelanin interface was studied by SEM.

Palladium electrodes proved to dissolve under bias, in contact with hydrated synthetic eumelanin films with high (8% wt.) chloride content, forming continuous bridging structures. Such a continuous morphology of the Pd structures indicates a non-diffusion-limited growth [499]. If the chloride content is decreased from 8 to 1% wt. or the relative humidity level is reduced from 90 to 80 or 70%, Pd electrode dissolution does not take place. In the case of Sepia Melanin (ca. 8% wt.), bridging structures with an intermediate morphology, between continuous and dendritic, are observable. A complex interplay of factors, including the binding affinity of the metal towards eumelanin [89], metal-Cl$^-$ (ligand) interactions [500], metal cation reduction at surface catechols [501], coordinating action of DMSO (the solvent used to spin coat the films) [500], may explain the difference in the shape of the bridging structures.

Copper electrodes, chemically treated to remove Cu_xO, dissolved in contact with synthetic eumelanin films (8% wt.): dendritic bridging structures formed. However, the resistive switch is temporary (approximately two hours), most likely due to the oxidation of the structures bridging one electrode to the other. Untreated copper electrodes dissolve in the same conditions, too, but the current increases of only one order of magnitude and immediately after the resistive switch starts to decrease. This may be explained with the oxidation of the bridging structures. In the case of untreated Cu electrodes, less bare metallic Cu is available: this feature can explain the different duration of the resistive switch in the two cases. If the chloride amount is reduced from 8 to 1% wt., no electrode dissolution takes place.

No dissolution occurs with Sepia Melanin (7% wt. Cl^-) interfaced with treated Cu electrodes. It is worth noting that, differently from Au and Pd, in the case of Cu electrodes the electrode-patterned substrates, after the chemical removal of Cu_xO, are not UV-ozone treated. The hygroscopicity of Sepia Melanin [123] as well as the absence of UV-ozone treatment of the copper substrates may explain the surprising absence of dissolution in such a case. Due to hygroscopicity, water, which plays a determinant role in the electrode dissolution, is less available for the process [488]. The absence of the UV-ozone treatment is expected to reduce substrate's hydrophilicity with respect to ozone-treated substrates. Both factors suggest an inefficient transport of ions in aqueous or hydrated media: this, in turn, brings about a limited electrical continuity, necessary for metal dissolution, in the region included between the metal electrodes.

In the case of both treated and untreated Fe electrodes, interfaced both with synthetic and natural eumelanin, after the application of the electrical bias, platelets form, to a larger extent on the positive electrode. EDX revealed that such platelets are composed of iron oxides and they are separated by iron-devoid areas. Although no bridging structure forms, the discontinuity of the iron electrodes after the application of the electrical bias suggests that they have to be considered as unstable metal contacts when interfaced with hydrated eumelanin films.

In the case of Ni electrodes, both treated and untreated, interfaced both with synthetic and natural eumelanin, only partial dissolution was observed, with formation of pits. The good electrochemical stability of nickel oxide can tentatively explain this observation [503]. The chemical attack of the native oxide by chlorides can explain the local dissolution (pits) at the electrodes [504]–[506]. Ni electrodes can be thus considered for the electrical characterization of eumelanin films: however, in perspective, more conventional interfacial characterizations will have to ensue, e.g. on charge

carrier injection interfacial properties, in order to compare the performance of Ni electrodes with other electrodes that proved to be stable (Pd).

9.2 Eumelanin as a Natural UV-absorption Enhancer of the Ethylene-Vinyl Acetate Copolymer (EVA)

UV-absorbers are added to polymers to enhance their absorption in the UV range (particularly important for plastics for packaging applications) and to stabilize them against UV-induced degradation (paramount for plastics used in outdoor environments) [192], [193]. Bio-sourced materials have been explored as replacements of commercial artificial additives in the endeavor towards sustainability (e.g. green tea extracts and α-tocopherol have been studied as anti-oxidants in polymers [413], [414]). Eumelanin can be explored as a UV-absorber for plastics due to several features: it is bio-sourced and non-toxic [125]. Thanks to such features, the use of eumelanin would be greener compared to many commercial additives [185]. Furthermore, as the biopigment is composed of protomolecules [37], leaching from the polymer matrix would be less likely to occur than for the case of small molecule additives [269], [415].

It is worth noting that commercial polymers usually contain several types of additives apart from UV-absorbers (e.g. anti-oxidants for thermal stabilization, slip agents to reduce the coefficient of friction) [420]. Consequently, while the simplest scenario to assess the performance of any potential natural UV-absorber is surely represented by using a pure polymer matrix, an investigation regarding a commercial grade polymer already including other additives is closer to the actual practical (market) scenario. Antagonistic or synergistic effects could indeed take place among different additives [420]–[422].

In Article 2 [513], eumelanin was evaluated as an additive for the UV-absorption enhancement of a commercial grade of the copolymer ethylene-vinyl acetate, EVA (ELVAX®3128-1 from DuPont[TM]). This polymer is used for packaging applications [417]. Two synthetic types of eumelanin based on only one of the two building blocks (DHI-melanin and DHICA-melanin) as well as their natural counterpart (Sepia Melanin, extracted from cuttlefish ink) were tested. The originality of our work stemmed from the fact that eumelanin was not merely added as-polymerized or as-extracted nor functionalized [194]: the Melanin Free Acid (MFA) treatment was used to improve eumelanin dispersion in the plastic matrix. Besides the improved dispersibility, the effect of such a treatment is that the biopigment supramolecular structure is opened and the size of the

oligomers is reduced [80], [418]. Consequently, the effect of the MFA is also the shift of eumelanin's absorption towards the UV [80], [419]. Indeed, the electronic delocalization is affected both by the π-π stacking of the supramolecular structure and the size of the oligomers [418]. An extended delocalization due both to an extended π-π stacking and/or a large oligomer size leads to a red shift of the optical absorption spectrum [80], [418].

Eumelanin was added to the polymers by melt-compounding, and the eumelanin-including pellets were compression-molded in a hot press. The so-obtained films were stabilized in a cold press. UV-visible spectra were obtained with a spectrophotometer equipped with an integrating sphere and the center-mount set-up; an equivalent absorption coefficient (cm^{-1}) was computed by normalizing by the thickness. Our results revealed that the three types of eumelanin (amounts of 0.2% wt.) worked as UV-absorption enhancers of the commercial grade EVA, with an increase of the equivalent absorption coefficient of a factor 6-8 in the UVA and UVB ranges with respect to the control film. Furthermore, the presence of eumelanin caused absorption peaks at ca. 320 nm (attributable to collections of oligomers [419], [428] and polypyrroles resulting from eumelanin's peroxidation [429], [430]) and 370 nm (attributable to collections of oligomers [419], [428]). As DHICA-melanin features lower visible absorption and higher absorption in the UV range with respect to synthetic DHI-melanin and natural Sepia Melanin, higher amounts of DHICA-melanin (0.6% and 0.8% wt.) were tested [77], [81]. The amount of 0.8% wt. brings about an increase of the equivalent absorption coefficient with respect to the control film as high as by a factor ~30 in the UVA. However, for all the types and concentrations of eumelanin, the absorption increase occurs not only in the UV range but also in the visible one, revealing the residual presence of some oligomers assembling via π-π stacking and/or with a size sufficiently extended to generate a high level of conjugation.

Thermogravimetric analyses, both in inert and oxidizing atmosphere, revealed no interference of eumelanin with the anti-oxidant already present in the commercial grade EVA (butylated hydroxytoluene). The onset degradation temperature was computed considering the temperature at which the DTG reaches 0.1 %/°C, following the ASTM E 2550-07 standard. As aforementioned, eumelanin's UV-absorption properties can have a double effect, either photoprotective or photodamaging [95], with the latter effect having being reported to prevail after prolonged exposure of eumelanin to UVA radiation (320 – 400 nm) [98]. Therefore, in this thesis, it was also evaluated if, upon prolonged UV irradiation, the photoprotective or the photodamaging role of the

biopigment prevails in the polymer matrix. The UV-aging test lasted 144 days, with a lamp of ~10 $W·m^{-2}$ in the 290 nm – 440 nm spectral range, with the samples held at 10 cm from the lamp, in air at 25 °C. IR spectra revealed that samples including eumelanin underwent photo-oxidation (presence of carbonyl groups of ketones [442]–[448], ɣ-lactone [447], [449], esters [450] and vinyl groups [450], [451] as well as UV-induced elimination of the vinyl acetate group [452]) to a larger extent with respect to the control films of commercial grade EVA. The higher extent of photo-oxidation was also confirmed by the decrease of the onset degradation temperature that was more remarkable for films including eumelanin than for control films. This result can be explained considering that the UV-visible spectra of the films containing eumelanin, at the end of the UV-aging test, featured a decrease of the absorption peak at ca. 370 nm, attributed to collections of oligomers of eumelanin [419], [428]. Eumelanin underwent UVA-induced photodegradation, that, as reported in the literature, is characterized not only by the formation of pyrrole-2,3,5-tricarboxylic acid and fission of indolequinone [441] but also by reactive oxygen species (ROS) generation [92], [93], [98]. As the radical scavenging properties of eumelanin were reduced by the MFA treatment [415], we suggest that such ROS could then contribute to the photo-oxidation process of the commercial grade EVA.

The commercial benzophenone BLS®531 provided to commercial EVA one order of magnitude enhancement of the absorption coefficient in the UV range with a sharp absorption cut-off between the UV and the visible. It managed also to reduce, but not completely hinder, the photo-oxidation of the commercial grade EVA. However, BLS®531 belongs to a category of compounds that gave evidence of carcinogenic effects [457]–[459], differently from eumelanin that is edible and biocompatible [125].

9.3 Biodegradability of Eumelanin and Synthetic Materials for Organic Electronics

The ubiquitous presence of electrical and electronic equipment in our everyday life has caused mounting pressure on the environment [128]. In particular, the two main concerns are represented by the depletion of chemical elements of key importance in the electronic industry (e.g. gallium and indium) [128] and by the increase of waste electrical and electronic equipment (WEEE, 44.6 Mt worldwide in 2016 [460]). However, the possible EEE end-of-life scenarios have received

limited attention, with the focus being on the device performance, as the technological advances of the last few decades confirm [128].

Economically and environmentally viable solutions to deal with WEEE have been identified in refurbishment and recycling of electronic devices, among others [461]. Apart from that, the use of abundant materials (e.g. biomolecules extracted from biomass feedstock), novel production schemes (e.g. involving non-toxic solvents) and eco-design of devices that includes biodegradation at the end-of-life stem as promising routes towards achieving sustainable (green) electronics [128]. Ideal candidates to explore such route are, in principle, organic (carbon-based) electronic materials [128]. It is thus evident that investigating the biodegradability of organic electronic materials is paramount to predict their end-of-life scenario with the lowest environmental footprint. In other words, a non-biodegradable material may be better suitable for end-of-life scenarios such as incineration or recycling rather than biodegradation in composting facilities.

In Article 3, we investigated the aerobic biodegradability of Sepia Melanin. The extracted biopigment was characterized by infrared spectroscopy, thermogravimetric analysis, nuclear activation analysis, as well as elemental analyses of total carbon and total inorganic carbon before the biodegradability studies. Sepia Melanin was blended with an industrial compost obtained from solid municipal waste (kindly provided by *Englobe Corporation*) and its biodegradability was tested under mesophilic conditions (25 °C) and under thermophilic conditions (58 °C, composting). As mentioned before, two synthetic organic electronic materials were included in the biodegradability test in composting conditions: Cu-Pc and PPS. After the 98-day incubation period under composting conditions, the potential transfer of toxicity from the test materials to the compost was also assessed, by means of plant germination and growth tests (phytotoxicity test).

Several abiotic and biotic factors determine biodegradation. Some of such factors depend on the environment (e.g. temperature, pH) and on the microbial community structure of the compost [187], whereas others are intrinsic to the test material (its structure and surface area, chemical composition, C/N ratio [187]). Extracellular enzymes mediate microbial degradation of an extracellular substrate. In the case of a polymer, two steps take place:

1. the depolymerization step, featuring chain cleavage,
2. once dimers or monomers are formed and brought inside the microorganism, the mineralization step, with production of CO_2 [187].

Our results show that the mineralization level of Sepia Melanin at 25 °C is 4% (18x lower than that of cellulose, positive control, 71%, in 97 days) while, under thermophilic conditions, it reaches a mineralization level of 37% (2.6x lower than the positive control, 100%, in 98 days).

The main intrinsic characteristics of eumelanin affecting its biodegradation by the microbiota of the compost may be its molecular and supramolecular structures [37] as well as its hygroscopicity [123].

Eumelanin is usually referred to as a chemically disordered material [469]: it does not consist of linear polymeric chains, but rather of oligomeric planes of DHI and DHICA monomers [37], that differ one from the other by types of units (DHI vs. DHICA), number of units, and polymerization sites [75]. Such oligomers organize in a complex supramolecular structure (see paragraph "Supramolecular structure"). Eumelanin particles in turn differ one from the other in size and supramolecular structure: the chemical disorder brings about structural disorder [469].

The biodegradability of eumelanin may be hindered by its structural and chemical disorder. For instance, not all the oligomeric planes are exposed to the extracellular enzymes: only in the oligomers on the surface of eumelanin particles the monomer-monomer bonds may be attacked. In addition, it has been suggested that the de-stacking of the oligomers, i.e. "opening" of the supramolecular structure, is an indispensable step for the biopigment degradation [212]. A chemical disordered material implies a heterogenous substrate for the extracellular enzymes. An enzyme capable of attacking the monomers' bonds of one type of oligomer may have different affinity towards other oligomers of eumelanin [219]. In addition to that, a non-biodegraded oligomeric plane will protect all the oligomers stacking beneath it from the attack of the extracellular enzymes.

Once a monomer is no longer part of an oligomeric plane, after diffusion into the microorganism, it is metabolized: indoles are known to be microbially degraded. The indole ring is cleaved and a series of reactions takes place ending with the formation of fumarate and pyruvate [470].

Furthermore, given the hygroscopicity of eumelanin [123], we can hypothesize water diffusion from the wet compost (50% wt. of H_2O) towards Sepia Melanin, in the bioreactors. The monomers that are cleaved from the extracellular substrate through the enzymatic attack are brought inside the microorganisms cells through water [471], so that it can be suggested that eumelanin's hygroscopicity favors its biodegradation.

Furthermore, mesophilic and thermophilic conditions differ by the community structure (bacterial and fungal species [472]) as well as by the rate of microbial decomposition activity, which is higher under thermophilic conditions [473], [474].

The recalcitrance of eumelanin to biodegradation in mesophilic conditions can be thus explained considering the kinetics of growth of the mesophilic bacteria as well as the intrinsic biodegradation-limiting factors of eumelanin (structural and chemical disorder). The difference with respect to cellulose (4% vs 71%) can be understood taking into consideration that the municipal waste compost used was acclimated to the biodegradation of lignocellulosic biomass.

Conversely, the final mineralization rate of eumelanin in thermophilic conditions (37%), almost 10x higher than in mesophilic conditions (4%), can be explained suggesting a synergy between the faster growth kinetics of thermophilic microorganisms and more abundant melanin degrading enzymes. In addition, temperatures of 50 °C and above can be tolerated by the fungus that biodegrades eumelanin at room temperature, *Aspergillus fumigatus* [475].

The final mineralization level in thermophilic conditions, 37%, is remarkable if we consider that the compost was acclimated to lignocellulosic biomass and that eumelanin is chemically and structurally heterogeneous.

However, if projected at the upper time limit suggested by ASTM D6400 (180 days), Sepia Melanin would attain 58% with the 0.26 %/d rate of the second period of incubation time (Δt_{35-98}). This means that it does not fulfill the threshold (90%) of biodegradability in composting conditions, established for plastics for food packaging and serving.

Regarding the phytotoxicity test, both the thresholds of seedling emergence (i.e. number of sown seeds that germinated into plants) and plant biomass were passed by Sepia Melanin. Our results reveal that the biopigment is not phytotoxic. Furthermore, the products of biodegradation of indoles, fumarates [470], are not phytotoxic either [477]. Our results are somehow surprising considering that, during melanogenesis (the biosynthetic path that brings to melanin), hydrogen peroxide forms, so that the precursor of melanin, L-dopa, has been reported to have phytotoxic effects [476].

The synthetic dye Cu-Pc showed no biodegradation over the 98-day incubation period. In addition to that, the production of CO_2 of the compost blended with Cu-Pc is lower than that of plain

compost starting from day 50 of incubation: the partial release of the Cu ion by the molecule may have inhibited the microbial activity [478].

The metal cation Cu is at the center of a planar aromatic macrocycle in Cu-Pc (Figure 3.1). The plane is composed of indoles, like in the case of eumelanin; however, such indoles do not feature catecholic hydroxyl groups and are not directly chemically bound to each other [479]. Both the microbial metabolism inhibition by the released copper cations as well as the resistance of the nitrogen-including bonds between the indole units to enzyme-mediated scission can explain the absence of biodegradation of Cu-Pc [478]. Additional biodegradation-hindering factors may be represented by Cu-Pc insolubility in water as well as by the π-π stacking of the molecules [479]. Regarding the phytotoxicity test, our results show that no detrimental effects on the seedling emergence nor on the growth was induced by the presence of Cu-Pc in the compost (Figure 9.1).
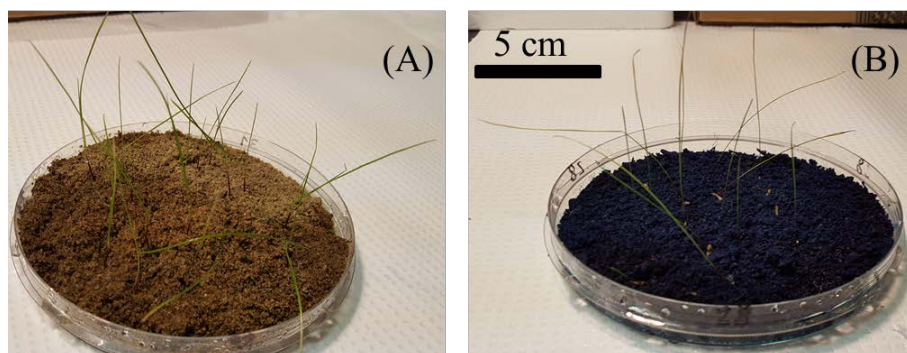
Figure 9.1 Plants growing after 19 days of incubation in (A) plain sandy soil and (B) sandy soil mixed with compost and Cu-Pc (compost blended with Cu-Pc had undergone the 98-day biodegradability in composting conditions test prior to the phytotoxicity test).

The polymer PPS showed no mineralization over the 98-day incubation period. Our results suggest a recalcitrance of the chemical bond between a sulphur atom and a benzene ring (Figure 3.1) to the cleavage of extracellular enzymes in our compost under thermophilic conditions. Both the phytotoxicity test thresholds were not passed by PPS. As PPS hinders both the seedling emergence and the plant growth, our results point to a potential phytotoxicity of the polymer.

CHAPTER 10   CONCLUSIONS AND PERSPECTIVES

In conclusion, the different endeavors of the present thesis aimed at providing further insights for the exploitation of eumelanin as a bio-sourced material in the context of green electronics and more sustainable additives for plastic polymers. The present work confirmed the challenges related to working with bio-sourced, chemically and structurally disordered materials, which can contain salts coming from the natural environment from which they were extracted.

The study of the interfaces between metal electrodes and hydrated eumelanin films under bias revealed the occurrence of electrochemical processes in certain experimental conditions, determined by the type of eumelanin, the chloride content, the relative humidity level and the type of metal. Such processes can dramatically affect the interpretation of electrical measurements, overshadowing the *intrinsic* electrical response of eumelanin, and the assessment of its technological potential.

For synthetic eumelanin films with a chloride content close to natural Sepia Melanin (8% wt.), hydrated for 1 hour at 90% RH, dissolution of the metal contact with formation of bridging structures takes place in the case of Au, Pd and Cu. Gold contacts dissolved and bridging structures formed even if the chloride content was reduced (from 8 to 1% wt.) and if the relative humidity was decreased (from 90 to 80 or 70% RH). Au is thus suggested if the use of eumelanin as the ion conductor layer of Bio-ReRAMS, in vertical configuration, is foreseen. Iron and copper proved to be of limited interest, due to formation of oxides and chlorides destabilization. Our results prove that the use of Pd electrodes at relative humidity below 90% and nickel electrodes is suitable for the characterization of the electrical properties of eumelanin. All in all, the works of Article 1 and Article 4 prove that measuring the amount of chlorides in the biopigment is essential before the characterization of the electrical properties of eumelanin or its exploitation in green electronic devices. From the technical point of view, many improvements of the design of the experiments can be envisaged. A first improvement can be represented by re-sizing the electrodes geometry. As a matter of fact, scanning the 4 mm width of the electrodes proved to be tedious at the SEM and very time-consuming at the AFM. A new mask design could be conceived, with lower electrode width, e.g. 100 µm. Such a size can be still sufficient to discover if electrochemical processes happen at the eumelanin-metal electrode interface. Furthermore, it is advisable that images at the SEM are taken before eumelanin spin coating (and not only after the transient current

measurement), in order to avoid any confusion between microfabrication defects and electrochemical processes at the interface. Other types of eumelanin, such as chemically controlled DHI-melanin, DHICA-melanin or DHI-DHICA-melanin with the same monomer ratio as natural Sepia Melanin can be used in alternative to commercial Sepia Melanin from Sigma-Aldrich, whose filmability proved to be challenging (inevitable presence of spherical particles even after the suspension sonication). Finally, the water amount taken up by the different types of the biopigment could be quantified with adsorption isotherms of the powders as well as of the spin coated films.

We also added eumelanin to a commercial grade polymer used for packaging application, the ethylene-vinyl acetate copolymer, EVA, aiming at increasing the polymer absorption in the UV range. The target of the work was not merely adding an as-polymerized biopigment powder and proving a UV-absorption enhancement to a pure additive-free polymer, but rather starting to fill the gap with respect to the real commercial world by (i) using a commercial polymer, already containing additives and (ii) improving the distribution of the biopigment in the polymer matrix (in other words, granting a uniform color rather than black dots surrounded by eumelanin-free areas). The same treatment used to improve the biopigment dispersion, Melanin Free Acid, was also expected to reduce its absorption in the visible range. Eumelanin proved to work as a UV-absorption enhancer for the commercial grade of EVA studied: the improvement of the equivalent absorption coefficient was as high as by a factor ~30 in the UVA with respect to the control film for an amount of eumelanin as low as 0.8% wt. (synthetic DHICA-melanin). Eumelanin did not interfere with the thermal stabilization provided by the commercial anti-oxidant already present in the commercial grade polymer (butylated hydroxytoluene). However, the Melanin Free Acid treatment used to improve the dispersion and reduce the absorption in the visible range proved to be double-edged, because the UV-aging treatment revealed that under prolonged UV irradiation eumelanin favors, rather than hindering, the photo-oxidation of the polymer, most likely due to ROS generation concomitant to reduced radical scavenging abilities of eumelanin after the treatment. Furthermore, the absorption increase took place not only in the UV range but also in the visible one.

In perspective, the optimization of the Melanin Free Acid treatment can be envisaged with the target of reducing eumelanin's peroxidation (i.e. the amount of polypyrroles generated after the MFA treatment [429], [430]), keeping the biopigment's radical scavenging properties while reducing the absorption in the visible range. Apart from synthetic DHICA-melanin and DHI-

melanin, DHI-DHICA melanin could be tested, with the ratio DHICA vs DHI equal to the one of the natural counterpart, Sepia Melanin. Different amounts of H_2O_2, times and temperatures of the MFA treatment and the use of ultra-sonication can be tested. The so-obtained different types of MFA-treated eumelanins can be characterized (quantification of polypyrroles amount and UV-visible spectrum). In parallel, a UV-aging test can be carried out on films featuring the same additive-free base polymer and the same amount of the biopigment, but with the different types of MFA-treated eumelanins. This would allow to identify the MFA treatment parameters that shift the balance between the photoprotective and photodamaging role towards photoprotection (anti-oxidation) of the embedding polymer matrix. An alternative to the Melanin-Free Acid approach, that implies reducing the oligomers size once the biopigment already polymerized [80], would be engineering the solid-state polymerization process. This could be obtained by controlling the O_2 concentration and relative humidity in the atmosphere during the polymerization as well as the polymerization time to synthesize eumelanin nanostructures of controlled size prior to their mixing with the polymer matrix. Another advantage would be the possibility to tailor the UV-visible absorption properties of eumelanin nanostructures.

The optimization of the polymer films processing can be a further point of improvement, to have polymer films with uniform thickness. Using a mechanical tool to cut the polymer melt-compounded with eumelanin could provide eumelanin-including pellets with a more regular shape. Keeping the same compression molding parameters, films with the same thickness can be obtained, so that the transmission spectra of different films can be directly compared, without the need of recurring to the equivalent absorption coefficient.

Furthermore, films could be thermally quenched after compression molding, to reduce their scattering properties. Once the eumelanin extraction process has been scaled up, other processes such as extrusion and film casting or film blowing can be envisaged, too. It is worth noting that scattering increases absorption [514]: in the present work, it was assumed that the level of scattering was the same for the control film and for the eumelanin-including films, being the base polymer the same. Adding eumelanin to non-scattering films can allow to evaluate absorption increases solely due to the biopigment, without effects related to polymer matrix scattering.

Regarding the characterization part, the UV-visible diffusive transmittance can be measured separately from diffusive reflectance, with the integrating sphere (set-up of Figure 4.4-B), in order

to elucidate more conclusively the color perceived through the plastic films, as the context is packaging applications.

Regarding the FT-IR characterization, the films tested featured thicknesses in the range of hundreds of microns and were consequently too thick to be probed in transmission mode. A possibility to improve the IR characterization would be represented by obtaining films with thickness in the order of tens of microns, which could be studied in transmission mode. This would render the ATR sampling technique, that may be influenced by the sample roughness, not necessary. Furthermore, other relevant issues would be: (a) shedding light on the morphology at the micro and nano scale of the eumelanin-including films, by SEM and AFM; (b) evaluating if chemical interactions (covalent bonds) are formed between eumelanin and the polymer chains; (c) extracting the amount of eumelanin effectively present and comparing it to the added (nominal) concentration to assess if a fraction of eumelanin is lost during melt-compounding, compression molding or simply by leaching out of the polymer matrix; (d) evaluating if the addition of eumelanin affects the mechanical properties, by measuring the yield stress of control samples and eumelanin-including samples. In addition, the UV-aging test can be improved by referring to the related ASTM standards, such as ASTM D2565-2016 (*Standard Practice for Xenon-Arc Exposure of Plastics Intended for Outdoor Applications*).

The biodegradability of eumelanin was tested in a compost medium under mesophilic conditions, at 25 °C, and under thermophilic conditions (composting, 58 °C). Shedding light on the conditions under which the biopigment biodegrades is paramount both in the in the field of additives for polymers and in the context of materials for green electronics, as biodegradability is one of its pillars. Natural eumelanin (Sepia Melanin) was extracted from cuttlefish ink and blended with compost from municipal waste. At 25 °C the biodegradation level of eumelanin after ca. 100 days was 4% while in composting conditions it attained 37%. The chemical disorder (oligomers differing one from the other by number of units, type of units DHI vs DHICA and polymerization site) as well as the complex supramolecular structure of the biopigment were identified as biodegradation-hindering factors. Conversely, the hygroscopicity of eumelanin could favor its biodegradation by the compost microbiota. The biodegradation level in composting conditions (37%), even if not attaining the threshold level for plastic compostability set by the standard ASTM D6400, is strikingly better than the two synthetic materials for organic electronics studied (Cu-Pc and PPS), which both had a biodegradation level equal to 0 after approximately 100 days of

incubation. This confirmed that recurring to bio-sourced materials is a viable option to eco-design biodegradable organic electronic materials and devices. On the other side, eumelanin's low biodegradation rate at room temperature, i.e. biodegradability conditions of a natural ecosystem, was a further confirmation of the need of streaming organic waste to industrial composting facilities and provide an advice for our daily life: do not expect compostable plastics to biodegrade in few months if abandoned in nature, but assure that they end up in the compost bin. Furthermore, in order to properly evaluate the biodegradability of materials and devices for organic electronics, an international protocol should be established. The biodegradability project also presents various points of improvement and opens several investigation routes. The biodegradability in different types of compost (compost from garden waste or manure) can be tested. Furthermore, the community structure of the compost microbiota (i.e. the bacterial and fungal species present) can be mapped before starting the test. Identifying the bacteria or fungi that can more easily metabolize eumelanin can open to the possibility of inoculating specific microorganisms in the end-of-life environment where a eumelanin-including device is disposed, in order to facilitate its biodegradation. Furthermore, ASTM D6400 suggests using two plant species for the phytotoxicity test, whereas only one was used in Article 3 due to limited availability of compost after the incubation period: the next biodegradability tests in composting conditions have to be designed in such a way that compost quantity can be sufficient for a more complete phytotoxicity test.

REFERENCES

[1] N. G. Jablonski and G. Chaplin, "Human skin pigmentation as an adaptation to UV radiation.," *Proc. Natl. Acad. Sci. U. S. A.*, vol. 107, pp. 8962–8968, 2010.

[2] M. d'Ischia *et al.*, "Melanins and melanogenesis: Methods, standards, protocols," *Pigment Cell Melanoma Res.*, vol. 26, no. 5, pp. 616–633, 2013.

[3] J. Feltwell, *Black and White in the Wild*. RedDoor Publishing, 2016.

[4] J. Berzelius, *Lehrbuch der Chemie*. 1840.

[5] R. A. Nicolaus, *Melanins*. Paris: Hermann, 1969.

[6] F. Solano, "Melanins: skin pigments and much more—types, structural models, biological functions, and formation routes," *New J. Sci.*, vol. 2014, 2014.

[7] S. Dubey and A. Roulin, "Evolutionary and biomedical consequences of internal melanins," *Pigment Cell Melanoma Res.*, vol. 27, no. 3, pp. 327–338, May 2014.

[8] R. L. Schroeder, K. L. Double, and J. P. Gerber, "Using Sepia melanin as a PD model to describe the binding characteristics of neuromelanin - A critical review.," *J. Chem. Neuroanat.*, vol. 64–65, pp. 20–32, 2015.

[9] C. D. Derby, "Cephalopod ink: Production, chemistry, functions and applications," *Mar. Drugs*, vol. 12, no. 5, pp. 2700–2730, 2014.

[10] J. P. Césarini, "Melanins and their possible roles through biological evolution," *Adv. Sp. Res.*, vol. 18, no. 12, pp. 35–40, 1996.

[11] A. Slominski, "Melanin Pigmentation in Mammalian Skin and Its Hormonal Regulation," *Physiol. Rev.*, vol. 84, no. 4, pp. 1155–1228, 2004.

[12] J. D'Orazio, S. Jarrett, A. Amaro-Ortiz, and T. Scott, "UV radiation and the skin," *Int. J. Mol. Sci.*, vol. 14, no. 6, pp. 12222–12248, 2013.

[13] N. G. Lindquist, "Accumulation of drugs on melanin," *Acta Radiol. Diagn. (Stockh).*, vol. 1., p. 325, 1973.

[14] S. Ito and K. Wakamatsu, "Chemistry of Mixed Melanogenesis—Pivotal Roles of

Dopaquinone," *Photochem. Photobiol.*, vol. 84, no. 3, pp. 582–592, May 2008.

[15] M. d'Ischia *et al.*, "Melanins and melanogenesis: from pigment cells to human health and technological applications," *Pigment Cell Melanoma Res.*, vol. 28, no. 5, pp. 520–544, Sep. 2015.

[16] L. Panzella, A. Napolitano, and M. D'Ischia, "Is DHICA the key to dopachrome tautomerase and melanocyte functions?," *Pigment Cell Melanoma Res.*, vol. 24, no. 1, pp. 248–9, Feb. 2011.

[17] A. Pezzella *et al.*, "Towards the development of a novel bioinspired functional material: Synthesis and characterization of hybrid TiO2/DHICA-melanin nanoparticles," *Mater. Sci. Eng. C*, vol. 33, no. 1, pp. 347–355, 2012.

[18] A. Pezzella, D. Vogna, and G. Prota, "Atropoisomeric melanin intermediates by oxidation of the melanogenic precursor 5,6-dihydroxyindole-2-carboxylic acid under biomimetic conditions," *Tetrahedron*, vol. 58, no. 19, pp. 3681–3687, May 2002.

[19] M. Arzillo *et al.*, "Eumelanin buildup on the nanoscale: Aggregate growth/assembly and visible absorption development in biomimetic 5,6-dihydroxyindole polymerization.," *Biomacromolecules*, vol. 13, no. 8, pp. 2379–2390, 2012.

[20] F. H. J. Figge, "Melanin: A Natural Reversible Oxidation-Reduction System and Indicator," *Exp. Biol. Med*, vol. 41, p. 127, 1939.

[21] E. V. Gan, H. F. Haberman, and I. A. Menon, "Electron transfer properties of melanin," *Arch. Biochem. Biophys.*, vol. 173, no. 2, pp. 666–672, Apr. 1976.

[22] C. C. Felix, J. S. Hyde, T. Sarna, and R. C. Sealy, "Interactions of melanin with metal ions. Electron spin resonance evidence for chelate complexes of metal ions with free radicals," *J. Am. Chem. Soc.*, vol. 100, no. 12, pp. 3922–3926, Jun. 1978.

[23] Y. J. Kim, W. Wu, S.-E. Chun, J. F. Whitacre, and C. J. Bettinger, "Catechol-Mediated Reversible Binding of Multivalent Cations in Eumelanin Half-Cells," *Adv. Mater.*, vol. 26, no. 38, pp. 6572–6579, 2014.

[24] S. Gidanian and P. J. Farmer, "Redox behavior of melanins: Direct electrochemistry of

dihydroxyindole-melanin and its Cu and Zn adducts," *J. Inorg. Biochem.*, vol. 89, no. 1–2, pp. 54–60, 2002.

[25] P. Kumar *et al.*, "Melanin-based flexible supercapacitors," *J. Mater. Chem. C*, vol. 4, no. 40, pp. 9516–9525, 2016.

[26] E. Kaxiras, A. Tsolakidis, G. Zonios, and S. Meng, "Structural Model of Eumelanin," *Phys. Rev. Lett.*, vol. 97, no. 21, p. 218102, 2006.

[27] A. A. R. Watt, J. P. Bothma, and P. Meredith, "The supramolecular structure of melanin," *Soft Matter*, vol. 5, no. 19, p. 3754, 2009.

[28] M. d'Ischia, A. Napolitano, A. Pezzella, P. Meredith, and T. Sarna, "Chemical and structural diversity in eumelanins: Unexplored bio-optoelectronic materials," *Angew. Chemie - Int. Ed.*, vol. 48, no. 22, pp. 3914–3921, 2009.

[29] C. T. Chen *et al.*, "Self-assembly of tetramers of 5,6-dihydroxyindole explains the primary physical properties of eumelanin: Experiment, simulation, and design," *ACS Nano*, vol. 7, no. 2, pp. 1524–1532, 2013.

[30] M. Xiao *et al.*, "Elucidation of the hierarchical structure of natural eumelanins," *J. R. Soc. Interface*, vol. 15, no. 140, p. 20180045, Mar. 2018.

[31] G. W. Zajac, J. M. Gallas, J. Cheng, M. Eisner, S. C. Moss, and A. E. Alvarado-Swaisgood, "The fundamental unit of synthetic melanin: a verification by tunneling microscopy of X-ray scattering results," *Biochim. Biophys. Acta - Gen. Subj.*, vol. 1199, no. 3, pp. 271–278, Apr. 1994.

[32] A. Büngeler, B. Hämisch, and O. Strube, "The Supramolecular Buildup of Eumelanin: Structures, Mechanisms, Controllability," *Int. J. Mol. Sci.*, vol. 18, no. 9, p. 1901, Sep. 2017.

[33] Y. Liu and J. D. Simon, "The Effect of Preparation Procedures on the Morphology of Melanin from the Ink Sac of Sepia officinalis," *Pigment Cell Res.*, vol. 16, no. 1, pp. 72–80, Feb. 2003.

[34] A. Antidormi, C. Melis, E. Canadell, and L. Colombo, "Understanding the Polymerization Process of Eumelanin by Computer Simulations," *J. Phys. Chem. C*, vol. 122, no. 49, pp.

28368–28374, 2018.

[35] F. De Marchi *et al.*, "Room-temperature surface-assisted reactivity of a melanin precursor: Silver metal-organic coordination: Versus covalent dimerization on gold," *Nanoscale*, vol. 10, no. 35, pp. 16721–16729, 2018.

[36] F. De Marchi *et al.*, "Self-assembly of 5,6-dihydroxyindole-2-carboxylic acid: polymorphism of a eumelanin building block on Au(111)," *Nanoscale*, 2019.

[37] A. Büngeler, B. Hämisch, K. Huber, W. Bremser, and O. I. Strube, "Insight into the Final Step of the Supramolecular Buildup of Eumelanin," *Langmuir*, vol. 33, no. 27, 2017.

[38] J. M. Belitsky, M. Z. Ellowitz, D. Lye, and A. L. Kilbo, "Small molecule modulators of aggregation in synthetic melanin polymerizations," *Bioorganic Med. Chem. Lett.*, vol. 22, no. 17, pp. 5503–5507, 2012.

[39] S. Ito *et al.*, "Acid hydrolysis reveals a low but constant level of pheomelanin in human black to brown hair," *Pigment Cell Melanoma Res.*, 2017.

[40] E. N. Chikvaidze, T. M. Partskhaladze, and T. V. Gogoladze, "Electron spin resonance (ESR/EPR) of free radicals observed in human red hair: A new, simple empirical method of determination of pheomelanin/eumelanin ratio in hair," *Magn. Reson. Chem.*, vol. 52, no. 7, pp. 377–382, 2014.

[41] A. El Nahhas, T. Pascher, L. Leone, L. Panzella, A. Napolitano, and V. Sundström, "Photochemistry of pheomelanin building blocks and model chromophores: Excited-state intra- and intermolecular proton transfer," *J. Phys. Chem. Lett.*, vol. 5, no. 12, pp. 2094–2100, 2014.

[42] F. Agapito and B. J. C. Cabral, "Energetics of Radical Formation in Eumelanin Building Blocks: Implications for Understanding Photoprotection Mechanisms in Eumelanin," *J. Phys. Chem. A*, vol. 120, no. 50, pp. 10018–10022, 2016.

[43] W. Collins *et al.*, "Functional Effects of a Neuromelanin Analogue on Dopaminergic Neurons in 3D Cell Culture," *ACS Biomater. Sci. Eng.*, vol. 5, no. 1, pp. 308–317, 2019.

[44] F. A. Zucca *et al.*, "Neuromelanin of the human substantia Nigra: An update," *Neurotox.*

Res., vol. 25, no. 1, pp. 13–23, 2014.

[45]   J. M. Fearnley and A. J. Lees, "Ageing and Parkinson'S Disease: Substantia Nigra Regional Selectivity," *Brain*, vol. 114, pp. 2283–2301, 1991.

[46]   O. Karlsson and N. G. Lindquist, "Melanin and neuromelanin binding of drugs and chemicals: toxicological implications," *Arch. Toxicol.*, vol. 90, no. 8, pp. 1883–1891, 2016.

[47]   H. Barek, M. Sugumaran, S. Ito, and K. Wakamatsu, "Insect cuticular melanins are distinctly different from those of mammalian epidermal melanins," *Pigment Cell Melanoma Res.*, 2017.

[48]   R. C. R. Gonçalves, H. C. F. Lisboa, and S. R. Pombeiro-Sponchiado, "Characterization of melanin pigment produced by Aspergillus nidulans," *World J. Microbiol. Biotechnol.*, vol. 28, no. 4, pp. 1467–1474, 2012.

[49]   A. K. Pal, D. U. Gajjar, and A. R. Vasavada, "DOPA and DHN pathway orchestrate melanin synthesis in Aspergillus species," *J. Music Ther.*, vol. 52, no. 1, pp. 10–18, 2015.

[50]   A. A. Bell and M. H. Wheeler, "Biosynthesis and Functions of Fungal Melanins," *Annu. Rev. Phytopathol.*, vol. 24, no. 1, pp. 411–451, 1986.

[51]   N. N. Gessler, A. S. Egorova, and T. A. Belozerskaya, "Melanin pigments of fungi under extreme environmental conditions (Review)," *Appl. Biochem. Microbiol.*, vol. 50, no. 2, pp. 105–113, 2014.

[52]   R. J. B. Cordero and A. Casadevall, "Functions of fungal melanin beyond virulence," *Fungal Biol. Rev.*, vol. 31, no. 2, pp. 99–112, 2017.

[53]   D. Kothamasi *et al.*, "Exposure to ionizing radiation affects the growth of ectomycorrhizal fungi and induces increased melanin production and increased capacities of reactive oxygen species scavenging enzymes," *J. Environ. Radioact.*, vol. 197, no. October 2018, pp. 16–22, 2019.

[54]   E. Dadachova and A. Casadevall, "Ionizing radiation: how fungi cope, adapt, and exploit with the help of melanin," *Curr. Opin. Microbiol.*, vol. 11, no. 6, pp. 525–531, 2008.

[55]   M. J. Beltrán-García *et al.*, "Singlet molecular oxygen generation by light-activated DHN-

melanin of the fungal pathogen Mycosphaerella fijiensis in black sigatoka disease of bananas," *PLoS One*, vol. 9, no. 3, 2014.

[56] O. V. Kovalchuk, "Nonmonotonic (in concentration) conductivity of aqueous solutions of fungal melanin," *Semicond. Phys. Quantum Electron. Optoelectron.*, vol. 21, no. 1, pp. 95–99, Mar. 2018.

[57] Y. Zou and M. Tian, "Fermentative Production of Melanin by Auricularia auricula," *J. Food Process. Preserv.*, vol. 41, no. 3, p. e12909, Jun. 2017.

[58] H. Saleh, A. Abdelrazak, A. E. Elsayed, and Y. Osman, "Exploring Antimicrobial Potentials of Melanin from A Black Yeast Strain," *J. Biol. Life Sci.*, vol. 9, no. 2, p. 24, Apr. 2018.

[59] R. Prados-Rosales *et al.*, "Structural Characterization of Melanin Pigments from Commercial Preparations of the Edible Mushroom Auricularia auricula," *J. Agric. Food Chem.*, vol. 63, no. 33, pp. 7326–7332, Aug. 2015.

[60] R. Hou *et al.*, "Characterization of the physicochemical properties and extraction optimization of natural melanin from Inonotus hispidus mushroom," *Food Chem.*, vol. 277, no. July 2018, pp. 533–542, 2019.

[61] J. Ribera *et al.*, "Scalable Biosynthesis of Melanin by the Basidiomycete Armillaria cepistipes," *J. Agric. Food Chem.*, vol. 67, pp. 132–139, 2018.

[62] V. Vijayan *et al.*, "Sponge-Associated Bacteria Produce Non-cytotoxic Melanin Which Protects Animal Cells from Photo-Toxicity," *Appl. Biochem. Biotechnol.*, 2017.

[63] S. Amin, R. P. Rastogi, R. R. Sonani, A. Ray, R. Sharma, and D. Madamwar, "Bioproduction and characterization of extracellular melanin-like pigment from industrially polluted metagenomic library equipped Escherichia coli," *Sci. Total Environ.*, vol. 635, pp. 323–332, Sep. 2018.

[64] X. Xiao, J. Zhang, L. Cheng, X. Liu, Y. Jiang, and T. Zhang, "Isolation and characterization of melanin from palm fiber," *J. Nat. Fibers*, vol. 00, no. 00, pp. 1–13, 2018.

[65] M. Varga, O. Berkesi, Z. Darula, N. V. May, and A. Palágyi, "Structural characterization of allomelanin from black oat," *Phytochemistry*, vol. 130, pp. 313–320, 2016.

[66] Y. N. Kartushina, E. E. Nefedieva, G. A. Sevriukova, N. V Gracheva, and V. F. Zheltobryukhov, "Technological Desition of Extraction of Melanin from the Waste of Production of Sunflower-Seed Oil," *IOP Conf. Ser. Earth Environ. Sci.*, vol. 66, p. 012014, May 2017.

[67] J. Montes-Avila *et al.*, "Physicochemical properties and biological activities of melanins from the black-edible fruits Vitex mollis and Randia echinocarpa," *J. Food Meas. Charact.*, vol. 0, no. 0, p. 0, Apr. 2018.

[68] H. Li, J. Li, and Z. Zhao, "Characterization of melanin extracted from apricot (Armeniaca sibirica) and its effect on hydrazine-induced rat hepatic injury," *ScienceAsia*, vol. 42, no. 6, p. 382, 2016.

[69] P. Meredith and T. Sarna, "The physical and chemical properties of eumelanin," *Pigment Cell Res.*, vol. 19, no. 6, pp. 572–594, 2006.

[70] L. Hong and J. D. Simon, "Current understanding of the binding sites, capacity, affinity, and biological significance of metals in melanin," *J. Phys. Chem. B*, vol. 111, no. 28, pp. 7938–7947, 2007.

[71] Y. Zhong and F. Shahidi, "Methods for the assessment of antioxidant activity in foods," in *Handbook of Antioxidants for Food Preservation*, Elsevier, 2015, pp. 287–333.

[72] P. K. J. P. D. Wanasundara and F. Shahidi, "Antioxidants: Science, Technology, and Applications," in *Bailey's Industrial Oil and Fat Products, Volumes 1-6 (6th Edition)*, F. Shahidi, Ed. John Wiley & Sons, 2005, pp. 431–432.

[73] B. Halliwell, M. A. Murcia, S. Chirico, and O. I. Aruoma, "Free Radicals and Antioxidants in Food and In Vivo: What They Do and How They Work," *Crit. Rev. Food Sci. Nutr.*, vol. 35, no. 1–2, pp. 7–20, 1995.

[74] Y. Liang, Q. Han, N. Byrne, L. Sun, and X. Wang, "Recyclable One-Step Extraction and Characterization of Intact Melanin from Alpaca Fibers," *Fibers Polym.*, vol. 19, no. 8, pp. 1640–1646, 2018.

[75] M. L. Tran, B. J. Powell, and P. Meredith, "Chemical and structural disorder in eumelanins:

a possible explanation for broadband absorbance.," *Biophys. J.*, vol. 90, no. 3, pp. 743–752, 2006.

[76] C.-T. Chen, C. Chuang, J. Cao, V. Ball, D. Ruch, and M. J. Buehler, "Excitonic effects from geometric order and disorder explain broadband optical absorption in eumelanin," *Nat. Commun.*, vol. 5, p. 3859, 2014.

[77] L. Panzella *et al.*, "Atypical structural and π-electron features of a melanin polymer that lead to superior free-radical-scavenging properties," *Angew. Chemie - Int. Ed.*, vol. 52, no. 48, pp. 12684–12687, 2013.

[78] S. E. Forest and J. D. Simon, "Wavelength-dependent Photoacoustic Calorimetry Study of Melanin," *Photochem. Photobiol.*, vol. 68, no. 3, pp. 296–298, 1998.

[79] A. Brunetti, M. Arciuli, L. Triggiani, F. Sallustio, A. Gallone, and R. Tommasi, "Do thermal treatments influence the ultrafast opto-thermal processes of eumelanin?," *Eur. Biophys. J.*, no. 0123456789, 2019.

[80] K. B. Stark *et al.*, "Effect of stacking and redox state on optical absorption spectra of melanins -- comparison of theoretical and experimental results.," *J. Phys. Chem. B*, vol. 109, pp. 1970–1977, 2005.

[81] R. Micillo, L. Panzella, K. Koike, G. Monfrecola, A. Napolitano, and M. D'Ischia, "'Fifty Shades' of Black and Red or How Carboxyl Groups Fine Tune Eumelanin and Pheomelanin Properties," *Int. J. Mol. Sci.*, vol. 17, no. 5, p. 746, May 2016.

[82] R. Micillo *et al.*, "Eumelanin broadband absorption develops from aggregation-modulated chromophore interactions under structural and redox control," *Sci. Rep.*, vol. 7, no. December 2016, p. 41532, 2017.

[83] P. Ghosh and D. Ghosh, "Elucidating the Photoprotection Mechanism of Eumelanin Monomers," *J. Phys. Chem. B*, vol. 121, no. 24, pp. 5988–5994, 2017.

[84] I. A. Menon and H. F. Haberman, "MECHANISMS OF ACTION OF MELANINS," *Br. J. Dermatol.*, vol. 97, no. 1, pp. 109–112, Jul. 1977.

[85] M. P. Marszałł, A. Buciński, K. Goryński, A. Proszowska, and R. Kaliszan, "Magnetic beads

method for determination of binding of drugs to melanin.," *J. Chromatogr. A*, vol. 1218, no. 2, pp. 229–36, 2011.

[86] B. K. Wiernek, B. Pilawa, M. Zdybel, E. Buszman, and D. Wrześniok, "Interaction of free radicals of DOPA-melanin-streptomycin complexes with paramagnetic oxygen O2," *J. Appl. Biomed.*, vol. 12, no. 3, pp. 161–169, 2014.

[87] Y. Omata *et al.*, "A disadvantageous effect of adsorption of barium by melanin on transforming activity," *Chemosphere*, vol. 210, pp. 384–391, 2018.

[88] Y. Liu, L. Hong, V. R. Kempf, K. Wakamatsu, S. Ito, and J. D. Simon, "Ion-exchange and adsorption of Fe(III) by Sepia melanin," *Pigment Cell Res.*, vol. 17, no. 3, pp. 262–269, 2004.

[89] E. Di Mauro, R. Xu, G. Soliveri, and C. Santato, "Natural melanin pigments and their interfaces with metal ions and oxides: emerging concepts and technologies," *MRS Commun.*, vol. 7, no. 02, pp. 141–151, Jun. 2017.

[90] E. Kim *et al.*, "Spectroelectrochemical Reverse Engineering DemonstratesThat Melanin's Redox and Radical Scavenging Activities Are Linked," *Biomacromolecules*, p. acs.biomac.7b01166, 2017.

[91] T. Herrling, K. Jung, and J. Fuchs, "The role of melanin as protector against free radicals in skin and its role as free radical indicator in hair," *Spectrochim. Acta - Part A Mol. Biomol. Spectrosc.*, vol. 69, no. 5, pp. 1429–1435, 2008.

[92] G. Szewczyk, A. Zadlo, M. Sarna, S. Ito, K. Wakamatsu, and T. Sarna, "Aerobic photoreactivity of synthetic eumelanins and pheomelanins: generation of singlet oxygen and superoxide anion," *Pigment Cell Melanoma Res.*, Aug. 2016.

[93] S. Ito *et al.*, "Roles of reactive oxygen species in UVA-induced oxidation of 5,6-dihydroxyindole-2-carboxylic acid-melanin as studied by differential spectrophotometric method," *Pigment Cell Melanoma Res.*, vol. 29, no. 3, pp. 340–351, 2016.

[94] S. Ito, L. Kolbe, G. Weets, and K. Wakamatsu, "Visible light accelerates the ultraviolet A-induced degradation of eumelanin and pheomelanin," *Pigment Cell Melanoma Res.*, p.

pcmr.12754, Dec. 2018.

[95] F. Solano, "Photoprotection versus photodamage: updating an old but still unsolved controversy about melanin," *Polym. Int.*, vol. 65, no. 11, pp. 1276–1287, Nov. 2016.

[96] J. M. Menter, I. Willis, M. E. Townsel, G. D. Williamson, and C. L. Moore, "Melanin is a Double-Edged Sword," in *Photobiology*, Boston, MA: Springer US, 1991, pp. 873–886.

[97] T. Sarna, "Properties and function of the ocular melanin - A photobiophysical view," *J. Photochem. Photobiol. B Biol.*, vol. 12, no. 3, pp. 215–258, Feb. 1992.

[98] S. Ito, K. Wakamatsu, and T. Sarna, "Photodegradation of Eumelanin and Pheomelanin and Its Pathophysiological Implications," *Photochem. Photobiol.*, vol. 94, no. 3, pp. 409–420, 2018.

[99] J. B. Nofsinger, Y. Liu, and J. D. Simon, "Aggregation of eumelanin mitigates photogeneration of ROS," *Free Rad. Biol. Med.*, vol. 32, no. 8, pp. 720–730, 2002.

[100] Y. Liu and J. D. Simon, "Isolation and Biophysical Studies of Natural Eumelanins: Applications of Imaging Technologies and Ultrafast Spectroscopy," *Pigment Cell Research*, vol. 16, no. 6. pp. 606–618, 2003.

[101] R. D. Glickman, J. M. Gallas, S. L. Jacques, B. A. Rockwell, and D. K. Sardar, "Physical and photochemical properties of ocular melanin," *Saratov Fall Meet. 2000 Opt. Technol. Biophys. Med. II*, vol. 4241, no. 2001, pp. 112–123, 2001.

[102] W. Korytowski and T. Sarna, "Bleaching of melanin pigments. Role of copper ions and hydrogen peroxide in autooxidation and photooxidation of synthetic dopa-melanin," *J. Biol. Chem.*, vol. 265, pp. 12410–12416, 1990.

[103] B. Rózanowski, J. M. Burke, M. E. Boulton, T. Sarna, and M. Rózanowska, "Human RPE melanosomes protect from photosensitized and iron-mediated oxidation but become pro-oxidant in the presence of iron upon photodegradation," *Investig. Ophthalmol. Vis. Sci.*, vol. 49, no. 7, pp. 2838–2847, 2008.

[104] J. B. Nofsinger, S. E. Forest, and J. D. Simon, "Explanation for the Disparity among Absorption and Action Spectra of Eumelanin," *J. Phys. Chem. B*, vol. 103, no. 51, pp.

11428–11432, 1999.

[105] T. Cecchi *et al.*, "On the antioxidant activity of eumelanin biopigments: a quantitative comparison between free radical scavenging and redox properties," *Nat. Prod. Res.*, pp. 1–9, Jan. 2019.

[106] M. R. Powell and B. Rosenberg, "The nature of the charge carriers in solvated biomacromolecules," *J. Bioenerg.*, vol. 1, no. 6, pp. 493–509, Nov. 1970.

[107] J. P. Bothma, J. De Boor, U. Divakar, P. E. Schwenn, and P. Meredith, "Device-quality electrically conducting melanin thin films," *Adv. Mater.*, vol. 20, no. 18, pp. 3539–3542, 2008.

[108] J. Wünsche *et al.*, "Protonic and Electronic Transport in Hydrated Thin Films of the Pigment Eumelanin," *Chem. Mater.*, vol. 27, no. 2, pp. 436–442, 2015.

[109] J. McGinness, P. Corry, and P. Proctor, "Amorphous semiconductor switching in melanins.," *Science*, vol. 183, no. 127, pp. 853–855, 1974.

[110] P. R. Crippa, V. Cristofoletti, and N. Romeo, "A band model for melanin deduced from optical absorption and photoconductivity experiments," *Biochim. Biophys. Acta - Gen. Subj.*, vol. 538, no. 1, pp. 164–170, Jan. 1978.

[111] M. Jastrzebska, a. Kocot, J. K. Vij, J. Zalewska-Rejdak, and T. Witecki, "Dielectric studies on charge hopping in melanin polymer," *J. Mol. Struct.*, vol. 606, no. 1–3, pp. 205–210, 2002.

[112] M. M. Jastrzebska and S. Jussila, "Dielectric response and a.c. conductivity of synthetic dopa-melanin polymer," *J. Mater. Sci.*, vol. 33, no. 16, pp. 4023–4028, 1998.

[113] B. Mostert *et al.*, "Role of semiconductivity and ion transport in the electrical conduction of melanin," *Proc. Natl. Acad. Sci.*, vol. 109, no. 23, pp. 8943–8947, 2012.

[114] S. B. Rienecker, A. B. Mostert, G. Schenk, G. R. Hanson, and P. Meredith, "Heavy Water as a Probe of the Free Radical Nature and Electrical Conductivity of Melanin," *J. Phys. Chem. B*, vol. 119, no. 48, pp. 14994–15000, 2015.

[115] M. Sheliakina, A. B. Mostert, and P. Meredith, "Decoupling Ionic and Electronic Currents

in Melanin," *Adv. Funct. Mater.*, vol. 28, no. 46, p. 1805514, Nov. 2018.

[116] M. Jastrzebska, A. Kocot, and L. Tajber, "Photoconductivity of synthetic dopa–melanin polymer," *J. Photochem. Photobiol. B Biol.*, vol. 66, no. 3, pp. 201–206, Apr. 2002.

[117] V. Capozzi, G. Perna, P. Carmone, A. Gallone, M. Lastella, and E. Mezzenga, "Optical and photoelectronic properties of melanin," *Thin Film Solids*, vol. 512, pp. 362–366, 2006.

[118] M. Abbas *et al.*, "Structural, electrical, electronic and optical properties of melanin films," *Eur. Phys. J. E*, vol. 28, no. 3, pp. 285–291, 2009.

[119] A. B. Mostert, G. R. Hanson, T. Sarna, I. R. Gentle, B. J. Powell, and P. Meredith, "Hydration-controlled X-band EPR spectroscopy: A tool for unravelling the complexities of the solid-state free radical in eumelanin," *J. Phys. Chem. B*, vol. 117, no. 17, pp. 4965–4972, 2013.

[120] A. B. Mostert, S. B. Rienecker, C. Noble, G. R. Hanson, and P. Meredith, "The photoreactive free radical in eumelanin," *Sci. Adv.*, vol. 4, no. 3, p. eaaq1293, Mar. 2018.

[121] L. Migliaccio, M. Gryszel, V. Đerek, A. Pezzella, and E. D. Głowacki, "Aqueous photo(electro)catalysis with eumelanin thin films," *Mater. Horizons*, pp. 17–19, 2018.

[122] A. B. Mostert, K. J. P. Davy, J. L. Ruggles, B. J. Powell, I. R. Gentle, and P. Meredith, "Gaseous adsorption in melanins: Hydrophilic biomacromolecules with high electrical conductivities," *Langmuir*, vol. 26, no. 1, pp. 412–416, 2010.

[123] L. G. Albano, E. Di Mauro, P. Kumar, F. Cicoira, C. F. Graeff, and C. Santato, "Novel insights on the physicochemical properties of eumelanins and their DMSO derivatives," *Polym. Int.*, vol. 26, no. 24, pp. 19007–19013, 2016.

[124] A. J. Clulow *et al.*, "The structural impact of water sorption on device-quality melanin thin films," *Soft Matter*, vol. 13, pp. 3954–3965, 2017.

[125] M. Araújo *et al.*, "Natural melanin: A potential pH-responsive drug release device," *Int. J. Pharm.*, vol. 469, no. 1, pp. 140–145, Jul. 2014.

[126] C. J. Bettinger, J. P. Bruggeman, A. Misra, J. T. Borenstein, and R. Langer, "Biocompatibility of biodegradable semiconducting melanin films for nerve tissue

engineering," *Biomaterials*, vol. 30, no. 17, pp. 3050–3057, 2009.

[127] M. Irimia-Vladu, "'Green' electronics: biodegradable and biocompatible materials and devices for sustainable future.," *Chem. Soc. Rev.*, vol. 43, no. 2, pp. 588–610, 2014.

[128] M. Baumgartner, M. E. Coppola, N. S. Sariciftci, E. D. Glowacki, S. Bauer, and M. Irimia-Vladu, "Emerging 'Green' Materials and Technologies for Electronics," in *Green Materials for Electronics*, M. Irimia-Vladu, E. D. Glowacki, N. S. Sariciftci, and S. Bauer, Eds. Weinheim, Germany: Wiley-VCH Verlag GmbH & Co. KGaA, 2017, pp. 1–53.

[129] U. United Nations, *Report of the World Commission on Environment and Development: Our Common Future*, Oxford Uni. Oxford, 1987.

[130] G. Malliaras and R. Friend, "An organic electronics primer," *Phys. Today*, vol. 58, no. 5, pp. 53–58, 2005.

[131] M. Berggren and A. Richter-Dahlfors, "Organic Bioelectronics," *Adv. Mater.*, vol. 19, no. 20, pp. 3201–3213, Sep. 2007.

[132] M. Sheliakina, A. B. Mostert, and P. Meredith, "An all-solid-state biocompatible ion-to-electron transducer for bioelectronics," *Mater. Horizons*, vol. 5, no. 2, pp. 256–263, 2018.

[133] W. Lu, D. S. Jeong, M. Kozicki, and R. Waser, "Electrochemical metallization cells—blending nanoionics into nanoelectronics?," *MRS Bull.*, vol. 37, no. 02, pp. 124–130, Feb. 2012.

[134] R. Waser, R. Dittmann, G. Staikov, and K. Szot, "Redox-Based Resistive Switching Memories - Nanoionic Mechanisms, Prospects, and Challenges," *Adv. Mater.*, vol. 21, no. 25–26, pp. 2632–2663, Jul. 2009.

[135] I. Valov, R. Waser, J. R. Jameson, and M. N. Kozicki, "Electrochemical metallization memories—fundamentals, applications, prospects," *Nanotechnology*, vol. 22, no. 28, p. 289502, 2011.

[136] S. Tappertzhofen, I. Valov, T. Tsuruoka, T. Hasegawa, R. Waser, and M. Aono, "Generic Relevance of Counter Charges for Cation-Based Nanoscale Resistive Switching Memories," *ACS Nano*, vol. 7, no. 7, pp. 6396–6402, Jul. 2013.

[137] N. Raghavan, "Performance and reliability trade-offs for high-κ RRAM," *Microelectron. Reliab.*, vol. 54, no. 9–10, pp. 2253–2257, Sep. 2014.

[138] F. Pan, C. Chen, Z. Wang, Y. Yang, J. Yang, and F. Zeng, "Nonvolatile resistive switching memories-characteristics, mechanisms and challenges," *Prog. Nat. Sci. Mater. Int.*, vol. 20, pp. 1–15, Nov. 2010.

[139] J. Qi, M. Olmedo, J.-G. Zheng, and J. Liu, "Multimode Resistive Switching in Single ZnO Nanoisland System," *Sci. Rep.*, vol. 3, p. 2405, Aug. 2013.

[140] S. Wu *et al.*, "A Polymer-Electrolyte-Based Atomic Switch," *Adv. Funct. Mater.*, vol. 21, no. 1, pp. 93–99, Jan. 2011.

[141] N. Raeis-Hosseini and J.-S. Lee, "Resistive switching memory using biomaterials," *J. Electroceramics*, no. September, 2017.

[142] Y. Ji *et al.*, "Stable Switching Characteristics of Organic Nonvolatile Memory on a Bent Flexible Substrate," *Adv. Mater.*, vol. 22, no. 28, pp. 3071–3075, Jun. 2010.

[143] L. Li *et al.*, "A flexible polymer memory device," *Org. Electron.*, vol. 8, no. 4, pp. 401–406, Aug. 2007.

[144] H.-D. Kim, M. J. Yun, J. H. Lee, K. H. Kim, and T. G. Kim, "Transparent Multi-level Resistive Switching Phenomena Observed in ITO/RGO/ITO Memory Cells by the Sol-Gel Dip-Coating Method," *Sci. Rep.*, vol. 4, p. 4614, Apr. 2014.

[145] N. R. Hosseini and J.-S. Lee, "Biocompatible and Flexible Chitosan-Based Resistive Switching Memory with Magnesium Electrodes," *Adv. Funct. Mater.*, vol. 25, no. 35, pp. 5586–5592, Sep. 2015.

[146] K. Nagashima *et al.*, "Cellulose Nanofiber Paper as an Ultra Flexible Nonvolatile Memory," *Sci. Rep.*, vol. 4, p. 5532, Jul. 2014.

[147] H. Wang *et al.*, "Sericin for Resistance Switching Device with Multilevel Nonvolatile Memory," *Adv. Mater.*, vol. 25, no. 38, pp. 5498–5503, Oct. 2013.

[148] N. Raeis Hosseini and J.-S. Lee, "Resistive Switching Memory Based on Bioinspired Natural Solid Polymer Electrolytes," *ACS Nano*, vol. 9, no. 1, pp. 419–426, Jan. 2015.

[149] J. J. Kim, B. Cho, K. S. Kim, T. Lee, and G. Y. Jung, "Electrical Characterization of Unipolar Organic Resistive Memory Devices Scaled Down by a Direct Metal-Transfer Method," *Adv. Mater.*, vol. 23, no. 18, pp. 2104–2107, May 2011.

[150] Y.-P. Hsiao *et al.*, "Improving retention properties by thermal imidization for polyimide-based nonvolatile resistive random access memories," *Microelectron. Reliab.*, vol. 55, no. 11, pp. 2188–2197, Nov. 2015.

[151] F. M. Raymo, "Digital Processing and Communication with Molecular Switches," *Adv. Mater.*, vol. 14, no. 6, pp. 401–414, 2002.

[152] L. P. Ma, J. Liu, and Y. Yang, "Organic electrical bistable devices and rewritable memory cells," *Appl. Phys. Lett.*, vol. 80, no. 16, p. 2997, 2002.

[153] B. Cho, J.-M. Yun, S. Song, Y. Ji, D.-Y. Kim, and T. Lee, "Direct Observation of Ag Filamentary Paths in Organic Resistive Memory Devices," *Adv. Funct. Mater.*, vol. 21, no. 20, pp. 3976–3981, Oct. 2011.

[154] V. C. Nguyen and P. S. Lee, "Optically readout write once read many memory with single active organic layer," *Appl. Phys. Lett.*, vol. 108, no. 3, p. 033301, Jan. 2016.

[155] W.-J. Joo, T.-L. Choi, K.-H. Lee, and Y. Chung, "Study on Threshold Behavior of Operation Voltage in Metal Filament-Based Polymer Memory," *J. Phys. Chem. B*, vol. 111, no. 27, pp. 7756–7760, Jul. 2007.

[156] S. Gao, C. Song, C. Chen, F. Zeng, and F. Pan, "Dynamic Processes of Resistive Switching in Metallic Filament-Based Organic Memory Devices," *J. Phys. Chem. C*, vol. 116, no. 33, pp. 17955–17959, Aug. 2012.

[157] Y. Busby *et al.*, "Direct observation of conductive filament formation in Alq3 based organic resistive memories," *J. Appl. Phys.*, vol. 118, no. 7, p. 075501, Aug. 2015.

[158] Z. Wang, K. Sierros, M. S. Seehra, and D. Korakakis, "Development of indigo-based nonvolatile write-once-read-many-times memory device," *Mater. Lett.*, vol. 206, pp. 128–131, 2017.

[159] D. A. Lapkin *et al.*, "Polyaniline-based memristive microdevice with high switching rate

and endurance," vol. 043302, pp. 1–9, 2018.

[160] S.-H. Lee, H.-L. Park, C.-M. Keum, I.-H. Lee, M.-H. Kim, and S.-D. Lee, "Organic Flexible Memristor with Reduced Operating Voltage and High Stability by Interfacial Control of Conductive Filament Growth," *Phys. status solidi - Rapid Res. Lett.*, vol. 1900044, p. 1900044, Feb. 2019.

[161] B. Sun *et al.*, "From dead leaves to sustainable organic resistive switching memory," *J. Colloid Interface Sci.*, vol. 513, pp. 774–778, 2018.

[162] W. Wu *et al.*, "Biodegradable skin-inspired nonvolatile resistive switching memory based on gold nanoparticles embedded alkali lignin," *Org. Electron. physics, Mater. Appl.*, vol. 59, no. January, pp. 382–388, 2018.

[163] G. Zhou, B. Sun, A. Zhou, B. Wu, and H. Huang, "A larger nonvolatile bipolar resistive switching memory behaviour fabricated using eggshells," *Curr. Appl. Phys.*, vol. 17, no. 2, pp. 235–239, Feb. 2017.

[164] J. Xu *et al.*, "Biodegradable Natural Pectin-Based Flexible Multilevel Resistive Switching Memory for Transient Electronics," *Small*, vol. 1803970. p. 1803970, 2018.

[165] H.-Y. Jeng, T.-C. Yang, L. Yang, J. G. Grote, H.-L. Chen, and Y.-C. Hung, "Non-volatile resistive memory devices based on solution-processed natural DNA biomaterial," *Org. Electron.*, vol. 54, no. November 2017, pp. 216–221, 2018.

[166] H.-Y. Jeng, T.-C. Yang, C.-Y. Hung, and Y.-C. Hung, "Characterizations of DNA biopolymer-based rewritable memory devices," in *2017 Conference on Lasers and Electro-Optics Pacific Rim (CLEO-PR)*, 2017, pp. 1–2.

[167] A. P. Rananavare, S. J. Kadam, S. V. Prabhu, S. S. Chavan, P. V. Anbhule, and T. D. Dongale, "Organic non-volatile memory device based on cellulose fibers," *Materials Letters*, vol. 232. pp. 99–102, 2018.

[168] U. Celano *et al.*, "All-nanocellulose nonvolatile resistive memory," *NPG Asia Mater.*, vol. 8, no. 9, p. e310, 2016.

[169] L. Ge *et al.*, "Biomaterial gelatin film based crossbar structure resistive switching devices,"

IEEE Trans. Nanotechnol., vol. 17, no. 1, pp. 1–1, 2017.

[170] Y.-C. Chang, C.-J. Lee, L.-W. Wang, and Y.-H. Wang, "Air-stable gelatin composite memory devices on a paper substrate," *Org. Electron.*, vol. 65, no. April 2018, pp. 77–81, 2019.

[171] Z. X. Lim, S. Sreenivasan, Y. H. Wong, F. Zhao, and K. Y. Cheong, "Filamentary Conduction in Aloe Vera Film for Memory Application," *Procedia Eng.*, vol. 184, pp. 655–662, 2017.

[172] Z. X. Lim and K. Y. Cheong, "Nonvolatile Memory Device Based on Bipolar and Unipolar Resistive Switching in Bio-Organic Aloe Polysaccharides Thin Film," *Adv. Mater. Technol.*, vol. 3, no. 5, pp. 1–14, 2018.

[173] J. X. Zhu *et al.*, "Flexible, transferable and conformal egg albumen based resistive switching memory devices," *RSC Adv.*, vol. 7, no. 51, pp. 32114–32119, 2017.

[174] C.-C. Lin, C.-C. Chung, K.-J. Hou, and T.-L. Tseng, "Improved properties in albumen of duck egg based resistive switching memory by doping with Fe Ions," in *2016 5th International Symposium on Next-Generation Electronics (ISNE)*, 2016, pp. 1–2.

[175] G. Kook *et al.*, "Wafer-scale fabrication of biodegradable silk-fibroin-based memristors," *Proc. IEEE Int. Conf. Micro Electro Mech. Syst.*, vol. 2018–Janua, no. January, pp. 86–89, 2018.

[176] J. Yong *et al.*, "A Silk Fibroin Bio-Transient Solution Processable Memristor," *Sci. Rep.*, vol. 7, no. 1, p. 14731, 2017.

[177] F. Song *et al.*, "ZnO based Physically Transient and Bioresorbable Memory on Silk Protein," *IEEE Electron Device Lett.*, vol. 3106, no. c, pp. 1–1, 2017.

[178] H. Wang, B. Zhu, H. Wang, X. Ma, Y. Hao, and X. Chen, "Ultra-Lightweight Resistive Switching Memory Devices Based on Silk Fibroin," *Small*, vol. 12, no. 25, pp. 3360–3365, Jul. 2016.

[179] X. Ji *et al.*, "Biodegradable and Flexible Resistive Memory for Transient Electronics," *J. Phys. Chem. C*, vol. 122, no. 29, pp. 16909–16915, 2018.

[180] S. P. Park, Y. J. Tak, H. J. Kim, J. H. Lee, H. Yoo, and H. J. Kim, "Analysis of the Bipolar Resistive Switching Behavior of a Biocompatible Glucose Film for Resistive Random Access Memory," *Adv. Mater.*, vol. 30, no. 26, pp. 1–8, 2018.

[181] M.-K. Kim and J.-S. Lee, "Ultralow Power Consumption Flexible Biomemristors," *ACS Appl. Mater. Interfaces*, vol. 10, no. 12, pp. 10280–10286, 2018.

[182] X. He *et al.*, "Transient Resistive Switching Devices Made from Egg Albumen Dielectrics and Dissolvable Electrodes," *ACS Appl. Mater. Interfaces*, vol. 8, no. 17, pp. 10954–10960, May 2016.

[183] L. Ge, X. Wang, S. Dong, H. Jin, and J. Luo, "Green memristors array based on gelatin film dielectrics," in *2016 IEEE International Nanoelectronics Conference (INEC)*, 2016, pp. 1–2.

[184] J. Ko, L. T. H. Nguyen, A. Surendran, B. Y. Tan, K. W. Ng, and W. L. Leong, "Human Hair Keratin for Biocompatible Flexible and Transient Electronic Devices," *ACS Appl. Mater. Interfaces*, vol. 9, no. 49, pp. 43004–43012, 2017.

[185] P. Anastas and N. Eghbali, "Green Chemistry: Principles and Practice," *Chem. Soc. Rev.*, vol. 39, no. 1, pp. 301–312, 2010.

[186] M. Falkiewicz-Dulik, K. Janda, and G. Wypych, "Introduction," in *Handbook of Material Biodegradation, Biodeterioration, and Biostablization*, Elsevier, 2015, pp. 1–6.

[187] M. van der Zee, "Methods for Evaluating the Biodegradability of Environmentally Degradable Polymers," in *Handbook of Biodegradable Polymers*, 2nd ed., Smithers Rapra Technology Ltd, 2014, pp. 1–28.

[188] A. Ghasemi Ghodrat, M. Tabatabaei, M. Aghbashlo, and S. I. Mussatto, "Waste Management Strategies; the State of the Art," in *Biogas: Fundamentals, Process, and Operation*, M. Tabatabaei and H. Ghanavati, Eds. Cham: Springer International Publishing, 2018, pp. 1–33.

[189] J. W. C. Wong, A. Selvam, and M. K. Awasthi, "Composting for Organic Waste Management," in *Sustainable Solid Waste Management*, Reston, VA: American Society of

Civil Engineers, 2016, pp. 233–272.

[190] E. Castro-Aguirre, R. Auras, S. Selke, M. Rubino, and T. Marsh, "Insights on the aerobic biodegradation of polymers by analysis of evolved carbon dioxide in simulated composting conditions," *Polym. Degrad. Stab.*, vol. 137, pp. 251–271, 2017.

[191] L. Martino *et al.*, "Bio-based polyamide 11: Synthesis, rheology and solid-state properties of star structures," *Eur. Polym. J.*, vol. 59, pp. 69–77, 2014.

[192] S. E. M. Selke and J. D. Culter, *Plastics Packaging: Properties, Processing, Applications, and Regulations*, 3rd ed. Hanser Publications, Cincinnati, 2016.

[193] L. K. Krehula, A. Papić, S. Krehula, V. Gilja, L. Foglar, and Z. Hrnjak-Murgić, "Properties of UV protective films of poly(vinyl-chloride)/TiO2 nanocomposites for food packaging," *Polym. Bull.*, Aug. 2016.

[194] Q. Li, G. Liao, J. Tian, and Z. Xu, "Preparation of Novel Fluorinated Copolyimide/Amine-Functionalized Sepia Eumelanin Nanocomposites with Enhanced Mechanical, Thermal, and UV-Shielding Properties," *Macromol. Mater. Eng.*, vol. 1700407, p. 1700407, 2017.

[195] R. Kautz, D. D. Ordinario, V. Tyagi, P. Patel, T. N. Nguyen, and A. A. Gorodetsky, "Cephalopod-Derived Biopolymers for Ionic and Protonic Transistors," *Adv. Mater.*, vol. 30, no. 19, p. 1704917, May 2018.

[196] J. Wünsche, F. Cicoira, C. F. O. Graeff, and C. Santato, "Eumelanin thin films: solution-processing, growth, and charge transport properties," *J. Mater. Chem. B*, vol. 1, pp. 3836–3842, 2013.

[197] I. Bonadies, F. Cimino, C. Carfagna, and A. Pezzella, "Eumelanin 3D architectures: Electrospun PLA fiber templating for mammalian pigment microtube fabrication," *Biomacromolecules*, vol. 16, no. 5, pp. 1667–1670, 2015.

[198] L. Migliaccio *et al.*, "Eumelanin-PEDOT:PSS Complementing En Route to Mammalian-Pigment-Based Electrodes: Design and Fabrication of an ITO-Free Organic Light-Emitting Device," *Adv. Electron. Mater.*, vol. 1600342, p. 1600342, 2017.

[199] L. Migliaccio *et al.*, "Impact of Eumelanin-PEDOT Blending: Increased PEDOT Crystalline

Order and Packing-Conductivity Relationship in Ternary PEDOT:PSS:Eumelanin Thin Films," *Adv. Electron. Mater.*, vol. 1800585, p. 1800585, 2019.

[200] G. Tarabella *et al.*, "Irreversible evolution of eumelanin redox states detected by an organic electrochemical transistor: en route to bioelectronics and biosensing," *J. Mater. Chem. B*, vol. 1, no. 31, p. 3843, 2013.

[201] Y. J. Kim, W. Wu, S.-E. Chun, J. F. Whitacre, and C. J. Bettinger, "Biologically derived melanin electrodes in aqueous sodium-ion energy storage devices.," *Proc. Natl. Acad. Sci. U. S. A.*, vol. 110, no. 52, pp. 20912–7, 2013.

[202] M. Piacenti Da Silva, J. C. Fernandes, N. B. De Figueiredo, M. Congiu, M. Mulato, and C. F. De Oliveira Graeff, "Melanin as an active layer in biosensors," *AIP Adv.*, vol. 4, no. 3, pp. 0–8, 2014.

[203] A. Antidormi, C. Melis, E. Canadell, and L. Colombo, "Assessing the Performance of Eumelanin/Si Interface for Photovoltaic Applications," *J. Phys. Chem. C*, p. acs.jpcc.7b02970, 2017.

[204] E. Pinna *et al.*, "Deciphering Molecular Mechanisms of Interface Buildup and Stability in Porous Si/Eumelanin Hybrids," *Int. J. Mol. Sci.*, vol. 18, no. 7, p. 1567, 2017.

[205] J.-W. Lee *et al.*, "Dye-sensitized solar cells using purified squid ink nanoparticles coated on TiO2 nanotubes/nanoparticles," *Nippon Seramikkusu Kyokai Gakujutsu Ronbunshi/Journal Ceram. Soc. Japan*, vol. 121, no. 1409, pp. 123–127, 2013.

[206] C. Silva *et al.*, "Evaluation of dye sensitized solar cells based on a pigment obtained from Antarctic Streptomyces fildesensis," *Sol. Energy*, vol. 181, no. July 2018, pp. 379–385, 2019.

[207] C.-P. Yen, P.-F. Yu, J. Wang, J.-Y. Lin, Y.-M. Chen, and S. Chen, "Deposition of organic dyes for dye-sensitized solar cell by using matrix-assisted pulsed laser evaporation," *AIP Adv.*, vol. 6, no. 8, p. 085011, Aug. 2016.

[208] J. Ihssen, A. Braun, G. Faccio, K. Gajda-Schrantz, and L. Thöny-Meyer, "Light Harvesting Proteins for Solar Fuel Generation in Bioengineered Photoelectrochemical Cells," *Curr.*

Protein Pept. Sci., vol. 15, no. 4, pp. 374–384, 2014.

[209] S. Selvaraju *et al.*, "Eumelanin-inspired core derived from vanillin: a new building block for organic semiconductors.," *Chem. Commun. (Camb).*, vol. 51, no. Scheme 2, pp. 7–9, 2015.

[210] J. Wünsche *et al.*, "In situ formation of dendrites in eumelanin thin films between gold electrodes," *Adv. Funct. Mater.*, vol. 23, no. 45, pp. 5591–5598, 2013.

[211] N. Ohtaki and M. Seiji, "Degradation of Melanosomes by Lysosomes," *J. Invest. Dermatol.*, vol. 57, no. 1, pp. 1–5, 1971.

[212] J. Borovanský and M. Elleder, "Melanosome degradation: Fact or fiction," *Pigment Cell Res.*, vol. 16, no. 3, pp. 280–286, 2003.

[213] N. Otaki, "Melanosome and lysosome. II. Digestion of melanosome with mouse liver lysosome.," *Bull. Tokyo Med. Dent. Univ.*, vol. 17, no. 3, pp. 179–86, Sep. 1970.

[214] J. Lindgren *et al.*, "Molecular preservation of the pigment melanin in fossil melanosomes," *Nat. Commun.*, vol. 3, no. May, p. 824, 2012.

[215] K. Glass *et al.*, "Direct chemical evidence for eumelanin pigment from the Jurassic period," *Proc. Natl. Acad. Sci.*, vol. 109, no. 26, pp. 10218–10223, 2012.

[216] F. Zhang *et al.*, "Fossilized melanosomes and the colour of Cretaceous dinosaurs and birds," *Nature*, vol. 463, no. 7284, pp. 1075–1078, 2010.

[217] R. A. Wogelius *et al.*, "Trace metals as biomarkers for eumelanin pigment in the fossil record," *Science (80-.).*, vol. 333, no. 6049, pp. 1622–1626, 2011.

[218] A. S. Wilson, H. I. Dodson, R. C. Janaway, A. M. Pollard, and D. J. Tobin, "Selective biodegradation in hair shafts derived from archaeological, forensic and experimental contexts," *Br. J. Dermatol.*, vol. 157, no. 3, pp. 450–457, Sep. 2007.

[219] M. S. Blois, "Random polymers as a matrix for chemical evolution - example of melanin," in *The origins of prebiological systems and of their molecular matrices*, S. W. Fox, Ed. New York: Academic Press, Inc., 1965, pp. 19–33.

[220] M. Kuo and M. Alexander, "Inhibition of the Lysis of Fungi by Melanins," *J. Bacteriol.*, vol. 94, no. 3, pp. 624–629, 1967.

[221] B. S. Kim, M. Blaghen, H. Hong, and K. Lee, "Purification and characterization of a melanin biodegradation enzyme from Geotrichum sp .," pp. 622–626, 2016.

[222] M. Mohorčič, J. Friedrich, I. Renimel, P. André, D. Mandin, and J.-P. Chaumont, "Production of melanin bleaching enzyme of fungal origin and its application in cosmetics," *Biotechnol. Bioprocess Eng.*, vol. 12, no. 3, pp. 200–206, Jun. 2007.

[223] J. P. Luther and H. Lipke, "Degradation of melanin by Aspergillus fumigatus," *Appl. Environ. Microbiol.*, vol. 40, no. 1, pp. 145–155, 1980.

[224] F. Pohleven, C. Tavzes, and I. Vidic, "Degradation of Melanin and Biocides by Ligninolytic Fungi," in *Wood science for conservation of cultural heritage-Braga 2008 : proceedings of the international conference held by Cost action IE0601 in Braga (Portugal) 5-7 November 2008*, 2010.

[225] Č. Tavzes *et al.*, "Enzymatic degradation of mould stains on paper analysed by colorimetry and DRIFT-IR spectroscopy," *Int. Biodeterior. Biodegrad.*, vol. 63, no. 7, pp. 873–879, 2009.

[226] Y.-T. Liu, S. Lee, and Y. Liao, "Isolation of a Melanolytic Fungus and Its Hydrolytic Activity on Melanin," *Mycologia*, vol. 87, no. 5, p. 651, Sep. 1995.

[227] P. P. Martin and K. Haider, "Biodegradation of 14C-Labeled Model and Cornstalk Lignins , Phenols , Model Phenolase Humic Polymers , and Fungal Melanins as Influenced by a Readily Available Carbon Source and Soil," *Appl. Environ. Microbiol.*, vol. 38, no. 2, pp. 283–289, 1979.

[228] L. F. Linhares and J. P. Martin, "Decomposition in Soil of the Humic Acid-type Polymers (Melanins) of Eurotium echinulatum, Aspergillus glaucus Sp. and Other Fungi," *Soil Sci. Soc. Am. J.*, vol. 42, no. 5, p. 738, 1978.

[229] J. P. Martin, H. Zunino, P. Peirano, M. Caiozzi, and K. Haider, "Decomposition of14C-labeled lignins, model humic acid polymers, and fungal melanins in allophanic soils," *Soil Biol. Biochem.*, vol. 14, no. 3, pp. 289–293, 1982.

[230] G. Kassim, J. P. Martin, and K. Haider, "Incorporation of a wide variety of organic substrate

carbons into soil biomass as estimated by the fumigation procedure," *Soil Sci. Soc. Am. J.*, vol. 45, no. 6, pp. 1106–1112, 1981.

[231] D. W. Nelson, J. P. Martin, and J. O. Ervin, "Decomposition of Microbial Cells and Components in Soil and Their Stabilization Through Complexing with Model Humic Acid-Type Phenolic Polymers1," *Soil Sci. Soc. Am. J.*, vol. 43, no. 1, p. 84, 1979.

[232] B. J. Bloomfield and M. Alexander, "Melanins and Resistance of Fungi to Lysis," *J. Bacteriol.*, vol. 93, no. 4, pp. 1276–1280, 1967.

[233] K. M. Old and W. M. Robertson, "Effects of lytic enzymes and natural soil on the fine structure of conidia of Cochliobolus sativus," *Trans. Br. Mycol. Soc.*, vol. 54, no. 3, pp. 343-IN4, 1970.

[234] A. T. Bull, "Inhibition of polysaccharases by melanin: Enzyme inhibition in relation to mycolysis," *Arch. Biochem. Biophys.*, vol. 137, no. 2, pp. 345–356, 1970.

[235] M. KOHNO, H. ISHIZAKI, P.-H. LIN, K. YAMAMORI, and H. KUNOH, "Effect of polyoxin on fungi. Ultrastructural and cytochemical analyses of polyoxin-treated hyphae of Alternaria kikuchiana Tanaka.," *Japanese J. Phytopathol.*, vol. 49, no. 1, pp. 38–46, 1983.

[236] A. L. Rehnstrom and S. J. Free, "The isolation and characterization of melanin-deficient mutants of Monilinia fructicola," *Physiol. Mol. Plant Pathol.*, vol. 49, no. 5, pp. 321–330, 1996.

[237] R. M. Ray and J. D. Desai, "Effect of melanin on enzymatic hydrolysis of cellulosic waste," *Biotechnol. Bioeng.*, vol. 26, no. 7, pp. 699–701, 1984.

[238] A. De Cal and P. Melgarejo, "Effects of Penicillium frequentans and its antibiotics on unmelanized hyphae of Monilinia laxa," *Phytopathology*, vol. 84, no. 10, pp. 1010–1014, 1994.

[239] W. F. Paolo, E. Dadachova, P. Mandal, A. Casadevall, P. J. Szaniszlo, and J. D. Nosanchuk, "Effects of disrupting the polyketide synthase gene WdPKS1 in Wangiella [Exophiala] dermatitidis on melanin production and resistance to killing by antifungal compounds, enzymatic degradation, and extremes in temperature," *BMC Microbiol.*, vol. 6, pp. 1–16,

2006.

[240] I. Chet, Y. Henis, and R. Mitchell, "Chemical Composition of Hyphal and Sclerotial Walls of Sclerotium Rolfsii Sacc.," *Can. J. Microbiol.*, vol. 13, no. 2, pp. 137–141, 1967.

[241] H. C. Huang and E. G. Kokko, "Ultrastructure of Hyperparasitism of Coniothyrium-Minitans on Sclerotia of Sclerotinia-Sclerotiorum," *Can. J. Bot. Can. Bot.*, vol. 65, no. 12, pp. 2483–2489, 1987.

[242] Y. Kubo and I. Furusawa, "Localization of melanin in appressoria of Colletotrichum lagenarium," *Can. J. Microbiol.*, vol. 32, no. 3, pp. 280–282, 1986.

[243] Á. L. Rosas and A. Casadevall, "Melanization decreases the susceptibility of Cryptococcus neoformans to enzymatic degradation," *Mycopathologia*, vol. 151, no. 2, pp. 53–56, 2001.

[244] H. M. Hurst and G. H. Wagner, "Decomposition of 14C-Labeled Cell Wall and Cytoplasmic Fractions from Hyaline and Melanic Fungi1," *Soil Sci. Soc. Am. J.*, vol. 33, no. 5, p. 707, 1969.

[245] H. J. Potgieter and M. Alexander, "Susceptibility and resistance of several fungi to microbial lysis.," *J. Bacteriol.*, vol. 91, no. 4, pp. 1526–1532, 1966.

[246] M. J. Butler and A. W. Day, "Destruction of Fungal Melanins by Ligninases of Phanerochaete chrysosporium and Other White Rot Fungi," *Int. J. Plant Sci.*, vol. 159, no. 6, pp. 989–995, Nov. 1998.

[247] D. E. Stott, J. P. Martin, D. D. Focht, and K. Haider, "Biodegradation, Stabilization in Humus, and Incorporation into Soil Biomass of 2,4-D and Chlorocatechol Carbons," *Soil Sci. Soc. Am. J.*, vol. 47, no. 1, p. 66, 1983.

[248] Y. A. Zavgorodnyaya, V. V. Demin, and A. V. Kurakov, "Biochemical degradation of soil humic acids and fungal melanins," *Org. Geochem.*, vol. 33, no. 3, pp. 347–355, 2002.

[249] S. H. Woo, J. S. Cho, B. S. Lee, and E. K. Kim, "Decolorization of melanin by lignin peroxidase from Phanerochaete chrysosporium," *Biotechnol. Bioprocess Eng.*, vol. 9, no. 4, pp. 256–260, Aug. 2004.

[250] M. J. Tan, C. Owh, P. L. Chee, A. K. K. Kyaw, D. Kai, and X. J. Loh, "Biodegradable

electronics: cornerstone for sustainable electronics and transient applications," *J. Mater. Chem. C*, 2016.

[251] V. R. Feig, H. Tran, and Z. Bao, "Biodegradable Polymeric Materials in Degradable Electronic Devices," *ACS Cent. Sci.*, vol. 4, no. 3, pp. 337–348, Mar. 2018.

[252] V. Edupuganti and R. Solanki, "Fabrication, characterization, and modeling of a biodegradable battery for transient electronics," *J. Power Sources*, vol. 336, pp. 447–454, 2016.

[253] Y. Du, J. Ge, Y. Li, P. X. Ma, and B. Lei, "Biomimetic elastomeric, conductive and biodegradable polycitrate-based nanocomposites for guiding myogenic differentiation and skeletal muscle regeneration," *Biomaterials*, vol. 157, pp. 40–50, 2018.

[254] J.-K. Chang, H.-P. Chang, Q. Guo, J. Koo, C.-I. Wu, and J. A. Rogers, "Biodegradable Electronic Systems in 3D, Heterogeneously Integrated Formats," *Adv. Mater.*, vol. 1704955, p. 1704955, 2018.

[255] R. K. Pal, S. C. Kundu, and V. K. Yadavalli, "Fabrication of Flexible, Fully Organic, Degradable Energy Storage Devices Using Silk Proteins," *ACS Appl. Mater. Interfaces*, p. acsami.7b19309, 2018.

[256] T. Lei *et al.*, "Biocompatible and totally disintegrable semiconducting polymer for ultrathin and ultralightweight transient electronics," *Proc. Natl. Acad. Sci.*, p. 201701478, 2017.

[257] R. Pan *et al.*, "Fully biodegradable triboelectric nanogenerators based on electrospun polylactic acid and nanostructured gelatin films," *Nano Energy*, vol. 45, no. December 2017, pp. 193–202, 2018.

[258] Y. Zhang, F. Zheng, Z. Zhou, Y. Zhang, F. Wang, and H. Tao, "A transient triboelectric nanogenerator with optical feedback," in *2018 IEEE Micro Electro Mechanical Systems (MEMS)*, 2018, no. January, pp. 632–634.

[259] G. A. Salvatore *et al.*, "Biodegradable and Highly Deformable Temperature Sensors for the Internet of Things," *Adv. Funct. Mater.*, vol. 1702390, pp. 1–10, 2017.

[260] J. P. Esquivel, P. Alday, O. A. Ibrahim, B. Fernández, E. Kjeang, and N. Sabaté, "A Metal-

Free and Biotically Degradable Battery for Portable Single-Use Applications," *Adv. Energy Mater.*, vol. 1700275, 2017.

[261] H. Jeong, S. Baek, S. Han, H. Jang, S. H. Kim, and H. S. Lee, "Novel Eco-Friendly Starch Paper for Use in Flexible, Transparent, and Disposable Organic Electronics," *Adv. Funct. Mater.*, vol. 1704433, pp. 1–9, 2017.

[262] F. Deng *et al.*, "The effect of dopamine modified titanium dioxide nanoparticles on the performance of Poly (vinyl alcohol)/titanium dioxide composites," *Compos. Sci. Technol.*, 2017.

[263] Y. Wang *et al.*, "Simultaneous Enhancements of UV-Shielding Properties and Photostability of Poly(vinyl alcohol) via Incorporation of Sepia Eumelanin," *ACS Sustain. Chem. Eng.*, vol. 4, no. 4, pp. 2252–2258, Apr. 2016.

[264] Y. Wang *et al.*, "A Novel UV-Shielding and Transparent Polymer Film: When Bioinspired Dopamine–Melanin Hollow Nanoparticles Join Polymers," *ACS Appl. Mater. Interfaces*, vol. 9, no. 41, pp. 36281–36289, Oct. 2017.

[265] Y. Wang *et al.*, "Effects of Melanin on Optical Behavior of Polymer: From Natural Pigment to Materials Applications," *ACS Appl. Mater. Interfaces*, vol. 10, no. 15, 2018.

[266] J. Y. Cheon and W. H. Park, "Enhanced thermal stabilization of polymer nanofibrous web using self-polymerized 3,4-dihydroxy-L-phenylalanine," *Polymer (Guildf).*, vol. 125, pp. 126–133, Sep. 2017.

[267] W. Dong *et al.*, "Enhanced thermal stability of poly(vinyl alcohol) in presence of melanin," *J. Therm. Anal. Calorim.*, vol. 115, no. 2, pp. 1661–1668, Feb. 2014.

[268] Ł. Łopusiewicz, F. Jedra, and M. Mizieińska, "New poly(lactic acid) active packaging composite films incorporated with fungal melanin," *Polymers (Basel).*, vol. 10, no. 4, pp. 5–8, 2018.

[269] K. Shanmuganathan, J. H. Cho, P. Iyer, S. Baranowitz, and C. J. Ellison, "Thermooxidative Stabilization of Polymers Using Natural and Synthetic Melanins," *Macromolecules*, vol. 44, no. 24, pp. 9499–9507, Dec. 2011.

[270] G. S. Kiran, S. A. Jackson, S. Priyadharsini, A. D. W. Dobson, and J. Selvin, "Synthesis of Nm-PHB (nanomelanin-polyhydroxy butyrate) nanocomposite film and its protective effect against biofilm-forming multi drug resistant Staphylococcus aureus," *Sci. Rep.*, vol. 7, no. 1, p. 9167, Dec. 2017.

[271] S. Roy and J.-W. Rhim, "Preparation of carrageenan-based functional nanocomposite films incorporated with melanin nanoparticles," *Colloids Surfaces B Biointerfaces*, vol. 176, no. September 2018, pp. 317–324, 2019.

[272] S. Roy and J.-W. Rhim, "Carrageenan-based antimicrobial bionanocomposite films incorporated with ZnO nanoparticles stabilized by melanin," *Food Hydrocoll.*, vol. 90, no. December 2018, pp. 500–507, 2019.

[273] S. Liu *et al.*, "Polydopamine particles as a β-nucleating agent and antioxidant for isotactic polypropylene," *Chemical Engineering Journal*, vol. 363. pp. 1–12, 2019.

[274] C. Ninh, M. Cramer, and C. J. Bettinger, "Photoresponsive hydrogel networks using melanin nanoparticle photothermal sensitizers," *Biomater. Sci.*, vol. 2, no. 5, p. 766, 2014.

[275] Q. Fan *et al.*, "Transferring biomarker into molecular probe: Melanin nanoparticle as a naturally active platform for multimodality imaging," *J. Am. Chem. Soc.*, vol. 136, no. 43, pp. 15185–15194, 2014.

[276] L. P. da Silva *et al.*, "Eumelanin-releasing spongy-like hydrogels for skin re-epithelialization purposes," *Biomed. Mater.*, vol. 12, no. 2, p. 025010, Mar. 2017.

[277] M. Kim, H. S. Kim, M. A. Kim, H. Ryu, H. J. Jeong, and C. M. Lee, "Thermohydrogel Containing Melanin for Photothermal Cancer Therapy," *Macromol. Biosci.*, vol. 17, no. 5, pp. 1–6, 2017.

[278] M. A. Kim, S. Do Yoon, E. Kim, H. Jeong, and C.-M. Lee, "Natural melanin-loaded nanovesicles for near-infrared mediated tumor ablation by photothermal conversion," *Nanotechnology*, vol. 29, no. 41, p. 415101, Oct. 2018.

[279] Qin Jiang a *et al.*, "Red blood cell membrane-camouflaged melanin nanoparticles for enhanced photothermal therapy," *Biomaterials*, vol. 143, pp. 29–45, 2017.

[280] Q. Jiang *et al.*, "Erythrocyte-cancer hybrid membrane-camouflaged melanin nanoparticles for enhancing photothermal therapy efficacy in tumors," *Biomaterials*, vol. 192, no. October 2018, pp. 292–308, 2019.

[281] K. Jimbow *et al.*, "Characterization of Melanogenesis and Morphogenesis of Melanosomes by Physicochemical Properties of Melanin and Melanosomes in Malignant Melanoma," *Cancer Res.*, vol. 44, pp. 1128–1134, 1984.

[282] R. Zhang *et al.*, "Engineering Melanin Nanoparticles as an Efficient Drug-Delivery System for Imaging-Guided Chemotherapy," *Adv. Mater.*, vol. 27, no. 34, pp. 5063–5069, 2015.

[283] J. Wang *et al.*, "Eumelanin–Fe $_3$ O $_4$ hybrid nanoparticles for enhanced MR/PA imaging-assisted local photothermolysis," *Biomater. Sci.*, pp. 586–595, 2018.

[284] Z. Wang *et al.*, "*In situ* growth of Au nanoparticles on natural melanin as biocompatible and multifunctional nanoagent for efficient tumor theranostics," *J. Mater. Chem. B*, pp. 133–142, 2019.

[285] J. Reinen, P. Van Sas, T. Van Huygevoort, L. Rubio, K. Scase, and M. Wenker, "Development of a Phototoxicity Testing Strategy for Accurate Photosafety Evaluation of Pharmaceuticals Based on the Assessment of Possible Melanin-Binding Effects," 2018.

[286] A. De Trizio *et al.*, "Natural based eumelanin nanoparticles functionalization and preliminary evaluation as carrier for gentamicin," *React. Funct. Polym.*, 2017.

[287] M. Araújo *et al.*, "Bioactivity, mechanical properties and drug delivery ability of bioactive glass-ceramic scaffolds coated with a natural-derived polymer," *Mater. Sci. Eng. C*, vol. 77, pp. 342–351, 2017.

[288] T. Eom *et al.*, "Nanoarchitecturing of Natural Melanin Nanospheres by Layer-by-Layer Assembly: Macroscale Anti-inflammatory Conductive Coatings with Optoelectronic Tunability," *Biomacromolecules*, vol. 18, no. 6, pp. 1908–1917, Jun. 2017.

[289] A. Pezzella *et al.*, "Stem cell-compatible eumelanin biointerface fabricated by chemically controlled solid state polymerization," *Mater. Horiz.*, vol. 2, no. 2, pp. 212–220, 2015.

[290] M. Nune, S. Manchineella, T. Govindaraju, and K. S. Narayan, "Melanin incorporated

electroactive and antioxidant silk fibroin nanofibrous scaffolds for nerve tissue engineering," *Mater. Sci. Eng. C*, vol. 94, no. October 2017, pp. 17–25, 2019.

[291] G. Vitiello *et al.*, "Antimicrobial activity of eumelanin-based hybrids: The role of TiO 2 in modulating the structure and biological performance," *Mater. Sci. Eng. C*, vol. 75, pp. 454–462, 2017.

[292] G. Vitiello *et al.*, "Bioinspired hybrid eumelanin–TiO2 antimicrobial nanostructures: the key role of organo–inorganic frameworks in tuning eumelanin's biocide action mechanism through membrane interaction," *RSC Adv.*, pp. 28275–28283, 2018.

[293] B. Silvestri *et al.*, "Probing the Eumelanin-Silica Interface in Chemically Engineered Bulk Hybrid Nanoparticles for Targeted Subcellular Antioxidant Protection.," *ACS Appl. Mater. Interfaces*, vol. 9, no. 43, pp. 37615–37622, 2017.

[294] S. Song, S. Li, N. Su, J. Li, F. Shi, and M. Ye, "Structural characterization, molecular modification and hepatoprotective effect of melanin from Lachnum YM226 on acute alcohol-induced liver injury in mice," *Food Funct.*, vol. 7, no. 8, pp. 3617–3627, 2016.

[295] F. Shi, J. Li, L. Yang, G. Hou, and M. Ye, "Hypolipidemic effect and protection ability of liver-kidney functions of melanin from *Lachnum* YM226 in high-fat diet fed mice," *Food Funct.*, pp. 880–889, 2018.

[296] Z. Temoçin *et al.*, "The Analgesic Acetaminophen and the Antipsychotic Clozapine Can Each Redox-Cycle with Melanin," *ACS Chem. Neurosci.*, vol. 8, no. 12, pp. 2766–2777, 2017.

[297] E. Kim *et al.*, "Paraquat-Melanin Redox-Cycling: Evidence from Electrochemical Reverse Engineering," *ACS Chem. Neurosci.*, vol. 7, no. 8, pp. 1057–1067, 2016.

[298] F. Solano, "Melanin and melanin-related polymers as materials with biomedical and biotechnological applications— Cuttlefish ink and mussel foot proteins as inspired biomolecules," *Int. J. Mol. Sci.*, vol. 18, no. 7, 2017.

[299] G. Panzarasa *et al.*, "Preparation of a Sepia Melanin and Poly(ethylene-alt-maleic Anhydride) Hybrid Material as an Adsorbent for Water Purification," *Nanomaterials*, vol.

8, no. 2, p. 54, Jan. 2018.

[300] A. Tripathi and J. S. Melo, "Synthesis of a low-density biopolymeric chitosan–agarose cryomatrix and its surface functionalization with bio-transformed melanin for the enhanced recovery of uranium(<scp>vi</scp>) from aqueous subsurfaces," *RSC Adv.*, vol. 6, no. 43, pp. 37067–37078, 2016.

[301] A. Tripathi and J. S. Melo, "Self-assembled biogenic melanin modulated surface chemistry of biopolymers-colloidal silica composite porous matrix for the recovery of uranium," *J. Appl. Polym. Sci.*, vol. 46937, p. 46937, 2018.

[302] M. Lindroos, D. Hörnström, G. Larsson, M. Gustavsson, and A. J. A. van Maris, "Continuous removal of the model pharmaceutical chloroquine from water using melanin-covered Escherichia coli in a membrane bioreactor," *J. Hazard. Mater.*, vol. 365, no. July 2018, pp. 74–80, 2019.

[303] Y. O. Kim *et al.*, "Eumelanin as a support for efficient palladium nanoparticle catalyst for Suzuki coupling reaction of aryl chlorides in water," *Tetrahedron Lett.*, vol. 58, no. 22, pp. 2149–2152, 2017.

[304] M. Zhao, S. Ou, and C.-D. Wu, "Improvement of the CO2 Capture Capability of a Metal-Organic Framework by Encapsulating Dye Molecules inside the Mesopore Space," *Cryst. Growth Des.*, p. acs.cgd.7b00188, 2017.

[305] H. Kalil, S. Maher, T. Bose, O. Al-Mahmoud, C. Kay, and M. Bayachou, "Synthetic Melanin Films as Potential Interfaces for Peroxynitrite Detection and Quantification," *ECS Trans.*, vol. 80, no. 10, pp. 1447–1458, Oct. 2017.

[306] Y. Zhang, B. Dong, A. Chen, X. Liu, L. Shi, and J. Zi, "Using Cuttlefish Ink as an Additive to Produce Non-iridescent Structural Colors of High Color Visibility," *Adv. Mater.*, vol. 27, no. 32, pp. 4719–4724, 2015.

[307] Y. Liang, E. Pakdel, M. Zhang, L. Sun, and X. Wang, "Photoprotective properties of alpaca fiber melanin reinforced by rutile TiO2 nanoparticles: A study on wool fabric," *Polym. Degrad. Stab.*, vol. 160, pp. 80–88, 2019.

[308] S. N. Dezidério, C. a. Brunello, M. I. N. Da Silva, M. a. Cotta, and C. F. O. Graeff, "Thin films of synthetic melanin," *J. Non. Cryst. Solids*, vol. 338–340, no. 1 SPEC. ISS., pp. 634–638, 2004.

[309] M. I. N. Da Silva, S. N. Dezidério, J. C. Gonzalez, C. F. O. Graeff, and M. a. Cotta, "Synthetic melanin thin films: Structural and electrical properties," *J. Appl. Phys.*, vol. 96, no. 10, pp. 5803–5807, 2004.

[310] E. S. Bronze-Uhle, A. Batagin-Neto, P. H. P. Xavier, N. I. Fernandes, E. R. De Azevedo, and C. F. O. Graeff, "Synthesis and characterization of melanin in DMSO," *J. Mol. Struct.*, vol. 1047, pp. 102–108, 2013.

[311] J. V. Paulin, A. G. Veiga, Y. Garcia-Basabe, M. L. M. Rocco, and C. F. Graeff, "Structural and optical properties of soluble melanin analogues with enhanced photoluminescence quantum efficiency," *Polym. Int.*, vol. 67, no. 5, pp. 550–556, May 2018.

[312] M. P. da Silva, A. A. Matos, J. V. Paulin, R. A. da Silva Alavarce, R. C. de Oliveira, and C. F. O. Graeff, "Biocompatibility investigations of Synthetic Melanin and Melanin analogue for application in bioelectronics," *Polym. Int.*, Jun. 2016.

[313] R. Micillo *et al.*, "Unexpected impact of esterification on the antioxidant activity and (photo)stability of a eumelanin from 5,6-dihydroxyindole-2-carboxylic acid," *Pigment Cell Melanoma Res.*, 2018.

[314] R. R. Chance *et al.*, "Highly conducting charge-transfer complexes of a processible polymer: poly(p-phenylene sulphide)," *J. Chem. Soc. Chem. Commun.*, no. 8, p. 348, 1980.

[315] A. S. Rahate, K. R. Nemade, and S. A. Waghuley, "Polyphenylene sulfide (PPS): State of the art and applications," *Rev. Chem. Eng.*, vol. 29, no. 6, pp. 471–489, 2013.

[316] D. D. ELEY, "Phthalocyanines as Semiconductors," *Nature*, vol. 162, no. 4125, pp. 819–819, Nov. 1948.

[317] Z. Bao, A. J. Lovinger, and A. Dodabalapur, "Organic field-effect transistors with high mobility based on copper phthalocyanine," *Appl. Phys. Lett.*, vol. 69, no. 20, pp. 3066–3068, 1996.

[318] Y. Kinoshita, T. Hasobe, and H. Murata, "Control of open-circuit voltage in organic photovoltaic cells by inserting an ultrathin metal-phthalocyanine layer," *Appl. Phys. Lett.*, vol. 91, no. 8, 2007.

[319] D. Johnson, N. Hilal, and W. R. Bowen, "Basic Principles of Atomic Force Microscopy," in *Atomic Force Microscopy in Process Engineering*, Elsevier, 2009, pp. 1–30.

[320] A. Yacoot and L. Koenders, "Aspects of scanning force microscope probes and their effects on dimensional measurement," *J. Phys. D. Appl. Phys.*, vol. 41, no. 10, 2008.

[321] G. Binnig, C. F. Quate, and C. Gerber, "Atomic Force Microscope," *Phys. Rev. Lett.*, vol. 56, no. 9, pp. 930–933, Mar. 1986.

[322] J. I. Goldstein *et al.*, *Scanning Electron Microscopy and X-ray Microanalysis*. Boston, MA: Springer US, 2003.

[323] "Scanning Electron Microscope A to Z. Basic knowledge for using the SEM, JEOL Ltd." 2012.

[324] D. A. Cole, S. Attavar, and L. Zhang, "Surface Analysis Methods for Contaminant Identification," in *Developments in Surface Contamination and Cleaning: Second Edition*, vol. 1, 2015, pp. 333–394.

[325] T. A. Germer, J. C. Zwinkels, and B. K. Tsai, "Introduction," in *Experimental Methods in the Physical Sciences*, F. Fernandez-Alonso and D. L. Price, Eds. Elsevier, 2014, pp. 1–9.

[326] A. Höpe, "Diffuse Reflectance and Transmittance," in *Experimental Methods in the Physical Sciences*, F. Fernandez-Alonso and D. L. Price, Eds. Elsevier, 2014, pp. 179–219.

[327] A. A. Ismail, F. R. van de Voort, and J. Sedman, "Fourier transform infrared spectroscopy: Principles and applications," in *Instrumental Methods in Food Analysis*, vol. 18, no. C, J. R. J. Paré and J. M. R. Bélanger, Eds. Elsevier, 1997, pp. 93–139.

[328] P. R. Griffiths and J. A. de Haseth, "Introduction to Vibrational Spectroscopy," in *Fourier transform infrared spectrometry*, 2nd ed., vol. 391, no. 7, Wiley, Ed. 2008, pp. 2379–2380.

[329] M. Baker, "Infrared spectroscopy," in *Biophotonics: Vibrational Spectroscopic Diagnostics*, IOP Publishing, 2016.

[330] N. K. Aras and O. Y. Ataman, "Nuclear Activation Analysis," in *Trace Element Analysis of Food and Diet*, Cambridge: Royal Society of Chemistry, 2007, pp. 172–191.

[331] R. Zeisler, N. Vajda, G. Kennedy, G. Lamaze, and G. L. Molnár, "Activation Analysis," in *Handbook of Nuclear Chemistry*, Boston, MA: Springer US, 2011, pp. 1553–1617.

[332] F. Farina Arboccò, "Experimental determination and re-evaluation of nuclear data for the parametric and k0-standardization of Neutron Activation Analysis," Ghent University, 2017.

[333] C. M. Earnest, *Compositional Analysis by Thermogravimetry, ASTM STP 997*. Philadelphia: ASM International, 1988.

[334] R. Bruce Prime, H. E. Bair, S. Vyazovkin, P. K. Gallagher, and A. Riga, "Thermogravimetric Analysis (TGA)," in *Thermal Analysis of Polymers: Fundamentals and Applications*, J. D. Menczel and R. Bruce Prime, Eds. John Wiley & Sons, Incorporated, 2009, pp. 241–318.

[335] R. Bottom, "Thermogravimetric Analysis," in *Principles and Applications of Thermal Analysis*, G. Paul, Ed. 2008, pp. 88–118.

[336] *ASTM E2550 - 07, Standard Test Method for Thermal Stability by Thermogravimetry*. 2007.

[337] *Specifications for compostable plastics CAN / BNQ 0017-088 / 2010 (ISO 17088 : 2008 , MOD)*. 2010.

[338] D. Rho and G. André, "Growth and stoichiometry of a Catharanthus roseus cell suspension culture grown under nitrogen-limiting conditions," *Biotechnol. Bioeng.*, vol. 38, no. 6, pp. 579–587, Sep. 1991.

[339] "ASTM D5338- 2015, Standard Test Method for Determining Aerobic Biodegradation of Plastic Materials Under Controlled Composting Conditions." 2015.

[340] Galbraith Laboratories, "Carbon, Hydrogen, and Nitrogen Determination using PerkinElmer 2400 Series II CHNS/O Analyszer." 2018.

[341] E. W. D. Huffman, "Performance of a new automatic carbon dioxide coulometer," *Microchem. J.*, vol. 22, no. 4, pp. 567–573, 1977.

[342] H. J. Boniface and R. H. Jenkins, "The determination of carbon in steel by coulometric titration in partially aqueous medium," *Analyst*, vol. 96, no. 1138, p. 37, 1971.

[343] "ASTM D6400-12, Standard Specification for Labeling of Plastics Designed to be Aerobically Composted in Municipal or Industrial Facilities," *ASTM International*, vol. 1. pp. 1–3, 2012.

[344] G. Prota, *Melanins and Melanogenesis*. San Diego: Academic Press, 1992.

[345] G. W. Zajac, J. M. Gallas, and A. E. Alvarado-Swaisgood, "Tunneling microscopy verification of an x-ray scattering-derived molecular model of tyrosine-based melanin," *Journal of Vacuum Science & Technology B: Microelectronics and Nanometer Structures*, vol. 12, no. 3. p. 1512, 1994.

[346] K. B. Stark, J. M. Gallas, G. W. Zajac, M. Eisner, and J. T. Golab, "Spectroscopic Study and Simulation from Recent Structural Models for Eumelanin: II. Oligomers," *J. Phys. Chem. B*, vol. 107, no. 41, pp. 11558–11562, Oct. 2003.

[347] C. M. R. Clancy and J. D. Simon, "Ultrastructural organization of eumelanin from Sepia officinalis measured by atomic force microscopy," *Biochemistry*, vol. 40, no. 44, pp. 13353–13360, 2001.

[348] A. Kunwar *et al.*, "Melanin, a promising radioprotector: Mechanisms of actions in a mice model," *Toxicol. Appl. Pharmacol.*, vol. 264, no. 2, pp. 202–211, Oct. 2012.

[349] V. M. Sava, B. N. Galkin, M.-Y. Hong, P.-C. Yang, and G. S. Huang, "A novel melanin-like pigment derived from black tea leaves with immuno-stimulating activity," *Food Res. Int.*, vol. 34, no. 4, pp. 337–343, Jan. 2001.

[350] R. Crippa, V. Horak, G. Prota, P. Svoronos, and L. Wolfram, "Chapter 6 Chemistry of Melanins," *Alkaloids Chem. Pharmacol.*, vol. 36, pp. 253–323, 1990.

[351] S. Colombo, I. Berlin, V. Delmas, and L. Larue, "Classical and Nonclassical Melanocytes in Vertebrates," in *Melanins and Melanosomes*, Weinheim, Germany: Wiley-VCH Verlag GmbH & Co. KGaA, 2011, pp. 21–61.

[352] J. M. Bowness and R. A. Morton, "The association of zinc and other metals with melanin

and a melanin-protein complex," *Biochem J.*, vol. 53, no. 4, pp. 620–626, 1953.

[353] B. J. Panessa and J. A. Zadunaisky, "Pigment granules: A calcium reservoir in the vertebrate eye," *Exp. Eye Res.*, vol. 32, no. 5, pp. 593–604, 1981.

[354] J. Borovanský, "Zinc in pigmented cells and structures, interactions and possible roles," *Sb. lékasky J.*, vol. 95, no. 4, pp. 309–320, 1994.

[355] W. D. Bush and J. D. Simon, "Quantification of Ca 2+ binding to melanin supports the hypothesis that melanosomes serve a functional role in regulating calcium homeostasis," *Pigment Cell Res.*, vol. 20, no. 2, pp. 134–139, 2007.

[356] J. M. Bowness and R. a Morton, "Distribution of copper and zinc in the eyes of fresh-water fishes and frogs. Occurrence of metals in melanin fractions from eye tissues.," *Biochem. J.*, vol. 51, no. 4, pp. 530–535, 1952.

[357] J. Horcicko, J. Borovansky, J. Ducholi, and B. Prochazkova, "Distribution of Zinc and Copper in Pigmented Tissues," *Hoppe-Seyler´s Zeitschrift für Physiol. Chemie*, vol. 354, no. 1, pp. 203–204, 1973.

[358] M. Chatelain, J. Gasparini, L. Jacquin, and A. Frantz, "The adaptive function of melanin-based plumage coloration to trace metals," *Biol. Lett.*, vol. 10, no. 3, pp. 20140164–20140164, 2014.

[359] W. D. Stein, "Chemical Composition of the Melanin Granule and its Relation to the Mitochondrion," *Nature*, vol. 175, no. 4449, pp. 256–257, 1955.

[360] J. Andrzejczak; and E. Buszman, "Interaction of Fe3, Cu2 and Zn2 with melanin and melanoproteins from bovine eyes," *Acta Biochim. Pol.*, vol. 39, no. 1, pp. 85–88, 1992.

[361] L. Hong and J. D. Simon, "Physical and Chemical Characterization of Iris and Choroid Melanosomes Isolated from Newborn and Mature Cows¶," *Photochem. Photobiol.*, vol. 81, no. 3, pp. 517–523, Apr. 2007.

[362] H. M. Swartz, T. Sarna, and L. Zecca, "Modulation by neuromelanin of the availability and reactivity of metal ions," *Ann. Neurol.*, vol. 32, no. S1, pp. S69–S75, 1992.

[363] P. Flesch, "The Role of Copper in Mammalian Pigmentation.," *Exp. Biol. Med.*, vol. 70, no.

1, pp. 79–80, 1949.

[364] W. S. Enochs, M. J. Nilges, and H. M. Swartz, "Purified Human Neuromelanin, Synthetic Dopamine Melanin as a Potential Model Pigment, and the Normal Human Substantia Nigra: Characterization by Electron Paramagnetic Resonance Spectroscopy," *J. Neurochem.*, vol. 61, no. 1, pp. 68–79, 1993.

[365] R. Salceda and G. Sánchez-Chávez, "Calcium uptake, release and ryanodine binding in melanosomes from retinal pigment epithelium," *Cell Calcium*, vol. 27, no. 4, pp. 223–229, 2000.

[366] A. Lydén, B. S. Larsson, and N. G. Lindquist, "Melanin Affinity of Manganese," *Acta Pharmacol. Toxicol. (Copenh).*, vol. 55, no. 2, pp. 133–138, 1984.

[367] G. C. Cotzias, P. S. Papavasiliou, and S. T. Miller, "Manganese in Melanin," *Nature*, vol. 201, no. 4925, pp. 1228–1229, 1964.

[368] B. S. Larsson, "Interaction Between Chemicals and Melanin," *Pigment Cell Res.*, vol. 6, no. 3, pp. 127–133, 1993.

[369] R. A. Nicolaus, "Biogenesis of melanins," *Rass. Med. Sper*, vol. 9.Suppl 1, no. 1, 1962.

[370] B. Larsson and H. Tjälve, "Studies on the melanin-affinity of metal ions," *Acta Physiol. Scand.*, vol. 104, no. 4, pp. 479–484, 1978.

[371] L. P. White, "Melanin: A Naturally Occurring Cation Exchange Material," *Nature*, vol. 182, no. 4647, pp. 1427–1428, 1958.

[372] M. Okazaki, K. Kuwata, Y. Miki, S. Shiga, and T. Shiga, "Electron spin relaxation of synthetic melanin and melanin-containing human tissues as studied by electron spin echo and electron spin resonance," *Arch. Biochem. Biophys.*, vol. 242, no. 1, pp. 197–205, 1985.

[373] L. Hong and J. D. Simon, "Insight into the binding of divalent cations to Sepia eumelanin from IR absorption spectroscopy.," *Photochem. Photobiol.*, vol. 82, no. 5, pp. 1265–1269, 2006.

[374] T. Shima, T. Sarna, H. M. Swartz, A. Stroppolo, R. Gerbasi, and L. Zecca, "Binding of Iron to Neuromelanin of Human Substantia Nigra and Synthetic Melanin: An Electron

Paramagnetic Resonance Spectroscopy Study," *Free Radic. Biol. Med.*, vol. 23, no. 1, pp. 110–119, 1997.

[375] B. Larsson and H. Tjälve, "Studies on the mechanism of drug-binding to melanin," *Biochem. Pharmacol.*, vol. 28, no. 7, pp. 1181–1187, 1979.

[376] K. Jellinger *et al.*, "Iron-Melanin Complex in Substantia Nigra of Parkinsonian Brains: An X-Ray Microanalysis," *J. Neurochem.*, vol. 59, no. 3, pp. 1168–1171, 1992.

[377] D. Ben-Shachar, P. Riederer, and M. B. H. Youdim, "Iron-Melanin Interaction and Lipid Peroxidation: Implications for Parkinson's Disease," *J. Neurochem.*, vol. 57, no. 5, pp. 1609–1614, 1991.

[378] M. B. H. Youdim, D. Ben-Shachar, and P. Riederer, "Is Parkinson's disease a progressive siderosis of substantia nigra resulting in iron and melanin induced neurodegeneration?," *Acta Neurol. Scand.*, vol. 80, pp. 47–54, 1989.

[379] S. Bohic *et al.*, "Intracellular Chemical Imaging of the Developmental Phases of Human Neuromelanin Using Synchrotron X-ray Microspectroscopy," *Anal. Chem.*, vol. 80, no. 24, pp. 9557–9566, 2008.

[380] L. Zecca *et al.*, "The neuromelanin of human substantia nigra and its interaction with metals," *J. Neural Transm.*, vol. 109, no. 5–6, pp. 663–672, 2002.

[381] L. Zecca *et al.*, "Iron, neuromelanin and ferritin content in the substantia nigra of normal subjects at different ages: consequences for iron storage and neurodegenerative processes," *J. Neurochem.*, vol. 76, no. 6, pp. 1766–1773, 2001.

[382] D. T. Dexter *et al.*, "Increased Nigral Iron Content and Alterations in Other Metal Ions Occurring in Brain in Parkinson's Disease," *J. Neurochem.*, vol. 52, no. 6, pp. 1830–1836, 1989.

[383] E. C. Hirsch, J.-P. Brandel, P. Galle, F. Javoy-Agid, and Y. Agid, "Iron and Aluminum Increase in the Substantia Nigra of Patients with Parkinson's Disease: An X-Ray Microanalysis," *J. Neurochem.*, vol. 56, no. 2, pp. 446–451, 1991.

[384] M. d'Ischia, A. Napolitano, V. Ball, C. Chen, and M. J. Buehler, "Polydopamine and

Eumelanin: From Structure–Property Relationships to a Unified Tailoring Strategy," *Acc. Chem. Res.*, vol. 47, no. 12, pp. 3541–3550, Dec. 2014.

[385] D. Ben-Shachar and M. B. H. Youdim, "Iron, melanin and dopamine interaction: relevance to Parkinson's disease," *Prog. Neuro-Psychopharmacology Biol. Psychiatry*, vol. 17, no. 1, pp. 139–150, Jan. 1993.

[386] B. Cho, S. Song, Y. Ji, T.-W. Kim, and T. Lee, "Organic Resistive Memory Devices: Performance Enhancement, Integration, and Advanced Architectures," *Adv. Funct. Mater.*, vol. 21, no. 15, pp. 2806–2829, Aug. 2011.

[387] J. C. Scott and L. D. Bozano, "Nonvolatile Memory Elements Based on Organic Materials," *Adv. Mater.*, vol. 19, no. 11, pp. 1452–1463, Jun. 2007.

[388] W.-P. Lin, S.-J. Liu, T. Gong, Q. Zhao, and W. Huang, "Polymer-Based Resistive Memory Materials and Devices," *Adv. Mater.*, vol. 26, no. 4, pp. 570–606, Jan. 2014.

[389] Q.-D. Ling, D.-J. Liaw, C. Zhu, D. S.-H. Chan, E.-T. Kang, and K.-G. Neoh, "Polymer electronic memories: Materials, devices and mechanisms," *Prog. Polym. Sci.*, vol. 33, no. 10, pp. 917–978, Oct. 2008.

[390] Q.-D. Ling *et al.*, "Polymer memories: Bistable electrical switching and device performance," *Polymer (Guildf).*, vol. 48, no. 18, pp. 5182–5201, Aug. 2007.

[391] S. Song *et al.*, "Three-Dimensional Integration of Organic Resistive Memory Devices," *Adv. Mater.*, vol. 22, no. 44, pp. 5048–5052, Nov. 2010.

[392] S. R. Mohapatra, T. Tsuruoka, T. Hasegawa, K. Terabe, and M. Aono, "Flexible resistive switching memory using inkjet printing of a solid polymer electrolyte," *AIP Adv.*, vol. 2, no. 2, p. 022144, 2012.

[393] K. Krishnan, T. Tsuruoka, and M. Aono, "Direct observation of anodic dissolution and filament growth behavior in polyethylene-oxide-based atomic switch structures," *Jpn. J. Appl. Phys.*, vol. 55, no. 6S1, p. 06GK02, Jun. 2016.

[394] F. Santoni *et al.*, "Modeling of Filamentary Conduction in Organic Thin Film Memories and Comparison With Experimental Data," *IEEE Trans. Nanotechnol.*, vol. 15, no. 1, pp. 60–

69, Jan. 2016.

[395] N. Knorr *et al.*, "Evidence of electrochemical resistive switching in the hydrated alumina layers of Cu/CuTCNQ/(native AlOx)/Al junctions," *J. Appl. Phys.*, vol. 114, no. 12, p. 124510, 2013.

[396] T. Graves-Abe and J. C. Stunn, "Dynamics of Write and Erase Mechanisms in a Novel Organic Memory With Extremely Low ON Resistance," *IEEE*, vol. 0-7803–904, no. 7, 2005.

[397] Y. Busby, N. Crespo-Monteiro, M. Girleanu, M. Brinkmann, O. Ersen, and J.-J. Pireaux, "3D imaging of filaments in organic resistive memory devices," *Org. Electron.*, vol. 16, pp. 40–45, Jan. 2015.

[398] K. Krishnan, T. Tsuruoka, C. Mannequin, and M. Aono, "Mechanism for Conducting Filament Growth in Self-Assembled Polymer Thin Films for Redox-Based Atomic Switches," *Adv. Mater.*, vol. 28, no. 4, pp. 640–648, Jan. 2016.

[399] S. R. Mohapatra, T. Tsuruoka, K. Krishnan, T. Hasegawa, and M. Aono, "Effects of temperature and ambient pressure on the resistive switching behaviour of polymer-based atomic switches," *J. Mater. Chem. C*, vol. 3, no. 22, pp. 5715–5720, 2015.

[400] H. Wang *et al.*, "Configurable Resistive Switching between Memory and Threshold Characteristics for Protein-Based Devices," *Adv. Funct. Mater.*, vol. 25, no. 25, pp. 3825–3831, Jul. 2015.

[401] C. Mukherjee, M. K. Hota, D. Naskar, S. C. Kundu, and C. K. Maiti, "Resistive switching in natural silk fibroin protein-based bio-memristors," *Phys. status solidi*, pp. 1797–1805, May 2013.

[402] M. K. Hota, M. K. Bera, B. Kundu, S. C. Kundu, and C. K. Maiti, "A Natural Silk Fibroin Protein-Based Transparent Bio-Memristor," *Adv. Funct. Mater.*, vol. 22, no. 21, pp. 4493–4499, Nov. 2012.

[403] B. Sun, D. Liang, X. Li, and P. Chen, "Nonvolatile bio-memristor fabricated with natural bio-materials from spider silk," *J. Mater. Sci. Mater. Electron.*, vol. 27, no. 4, pp. 3957–

3962, Apr. 2016.

[404] Y.-C. Chen, H.-C. Yu, C.-Y. Huang, W.-L. Chung, S.-L. Wu, and Y.-K. Su, "Nonvolatile Bio-Memristor Fabricated with Egg Albumen Film," *Sci. Rep.*, vol. 5, p. 10022, May 2015.

[405] S. Yue, G. C. Berry, and R. D. McCullough, "Intermolecular association and supramolecular organization in dilute solution .1. Regioregular poly(3-dodecylthiophene)," *Macromolecules*, vol. 29, no. 3, pp. 933–939, 1996.

[406] A. Mbonyiryivuze *et al.*, "Multi-scale Assembly in Nano-scaled Sepia Melanin Natural Dye," *Mater. Today Proc.*, vol. 2, no. 7, pp. 3988–3997, 2015.

[407] A. Mbonyiryivuze *et al.*, "Morphological and Chemical Composition Characterization of Commercial Sepia Melanin," *Am. J. Nanomater.*, vol. 3, no. 1, pp. 22–27, Jun. 2015.

[408] Y. Liu and J. D. Simon, "Metal-ion interactions and the structural organization of Sepia eumelanin," *Pigment Cell Res.*, vol. 18, no. 1, pp. 42–48, 2005.

[409] P. Meredith, B. J. Powell, J. Riesz, S. P. Nighswander-Rempel, M. R. Pederson, and E. G. Moore, "Towards structure–property–function relationships for eumelanin," *Soft Matter*, vol. 2, no. 1, pp. 37–44, Dec. 2006.

[410] E. Vahidzadeh, A. P. Kalra, and K. Shankar, "Melanin-based electronics: From proton conductors to photovoltaics and beyond," *Biosens. Bioelectron.*, vol. 122, pp. 127–139, Dec. 2018.

[411] R. Xu, C. T. Prontera, E. Di Mauro, A. Pezzella, F. Soavi, and C. Santato, "An electrochemical study of natural and chemically controlled eumelanin," *APL Mater.*, vol. 5, no. 12, p. 126108, Dec. 2017.

[412] S. Honda, Y. Takekoshi, and Y. Arai, "Cosmetics based on naturally derived melanin-coated pigments," 1995.

[413] M. D. M. Castro López, C. L. De Dicastillo, J. M. L. Vilariño, and M. V. G. Rodríguez, "Improving the capacity of polypropylene to be used in antioxidant active films: Incorporation of plasticizer and natural antioxidants," *J. Agric. Food Chem.*, vol. 61, no. 35, pp. 8462–8470, 2013.

[414] J. L. Koontz, J. E. Marcy, S. F. O'Keefe, S. E. Duncan, T. E. Long, and R. D. Moffitt, "Polymer processing and characterization of LLDPE films loaded with α-tocopherol, quercetin, and their cyclodextrin inclusion complexes," *J. Appl. Polym. Sci.*, vol. 117, no. 4, pp. 2299–2309, Aug. 2010.

[415] J. W. Nicholson, "Polymer Degradation," in *Chemistry of Polymers*, 3rd ed., Royal Society of Chemistry, 2006.

[416] K. Tarangini and S. Mishra, "Production of melanin by soil microbial isolate on fruit waste extract: two step optimization of key parameters," *Biotechnol. Reports*, vol. 4, pp. 139–146, Dec. 2014.

[417] S. Y. Sung *et al.*, "Antimicrobial agents for food packaging applications," *Trends Food Sci. Technol.*, vol. 33, no. 2, pp. 110–123, 2013.

[418] H. Eckhardt, L. W. Shacklette, K. Y. Jen, and R. L. Elsenbaumer, "The electronic and electrochemical properties of poly(phenylene vinylenes) and poly(thienylene vinylenes): An experimental and theoretical study," *J. Chem. Phys.*, vol. 91, no. 2, pp. 1303–1315, 1989.

[419] A. Pezzella *et al.*, "Lack of visible chromophore development in the pulse radiolysis oxidation of 5,6-dihydroxyindole-2-carboxylic acid oligomers: DFT investigation and implications for eumelanin absorption properties," *J. Org. Chem.*, vol. 74, no. 10, pp. 3727–3734, 2009.

[420] P. Gijsman, "Polymer Stabilization," in *Applied Plastics Engineering Handbook*, Elsevier, 2017, pp. 395–421.

[421] J. R. White and A. Turnbull, "Weathering of polymers: mechanisms of degradation and stabilization, testing strategies and modelling," *J. Mater. Sci.*, vol. 29, no. 3, pp. 584–613, 1994.

[422] J. M. Peña, N. S. Allen, M. Edge, C. M. Liauw, and B. Valange, "Studies of synergism between carbon black and stabilisers in LDPE photodegradation," *Polym. Degrad. Stab.*, vol. 72, no. 2, pp. 259–270, 2001.

[423] M. Magarelli, P. Passamonti, and C. Renieri, "Purification , characterization and analysis of

sepia melanin from commercial sepia ink (Sepia Officinalis) Purificación , caracterización y análisis de la melanina de sepia a partir de la tinta de sepia (Sepia Officinalis) Resumen," *Rev. CES Med. Vet. y Zootec.*, vol. 5, no. 2, pp. 18–28, 2010.

[424] M. Araujo, J. R. Xavier, C. D. Nunes, P. D. Vaz, and M. Humanes, "Marine sponge melanin: A new source of an old biopolymer," *Struct. Chem.*, vol. 23, no. 1, pp. 115–122, 2012.

[425] K. C. Littrell, J. M. Gallas, G. W. Zajac, and P. Thiyagarajan, "Structural Studies of Bleached Melanin by Synchrotron Small-angle X-ray Scattering," *Photochem. Photobiol.*, vol. 77, pp. 115–120, 2003.

[426] L. J. Wolfram, K. Hall, and I. Hui, "The Mechanism of Hair Bleaching," *J. Soc. Cosmet. Chem.*, vol. 900, pp. 875–900, 1970.

[427] Q. Liu, Z. Chen, D. Wei, and Y. Du, "Acute toxicity formation potential of benzophenone-type UV filters in chlorination disinfection process," *J. Environ. Sci. (China)*, vol. 26, no. 2, pp. 440–447, 2014.

[428] M. D'Ischia *et al.*, "Structural effects on the electronic absorption properties of 5,6-dihydroxyindole oligomers: The potential of an integrated experimental and DFT approach to model eumelanin optical properties," *Photochem. Photobiol.*, vol. 84, no. 3, pp. 600–607, 2008.

[429] A. Napolitano, A. Pezzella, M. D'Ischia, and G. Prota, "New pyrrole acids by oxidative degradation of eumelanins with hydrogen peroxide. Further hints to the mechanism of pigment breakdown," *Tetrahedron*, vol. 52, no. 26, pp. 8775–8780, 1996.

[430] R. A. W. Smith *et al.*, "Mechanistic insights into the bleaching of melanin by alkaline hydrogen peroxide," *Free Radic. Biol. Med.*, vol. 108, no. November 2016, pp. 110–117, 2017.

[431] M. Arroyo, M. A. López-Manchado, and B. Herrero, "Organo-montmorillonite as substitute of carbon black in natural rubber compounds," *Polymer (Guildf).*, vol. 44, no. 8, pp. 2447–2453, 2003.

[432] Y. Soudais, L. Moga, and J. Blazek, "Coupled DTA – TGA – FT-IR investigation of

pyrolytic decomposition of EVA , PVC and cellulose," vol. 78, pp. 46–57, 2007.

[433] F. Pern and A. Czanderna, "Characterization of ethylene vinyl acetate (EVA) encapsulant: Effects of thermal processing and weathering degradation on its discoloration," *Sol. Energy Mater. Sol. Cells*, vol. 25, no. 1–2, pp. 3–23, Jan. 1992.

[434] V. Ambrogi *et al.*, "An antioxidant bioinspired phenolic polymer for efficient stabilization of polyethylene," *Biomacromolecules*, vol. 15, no. 1, pp. 302–310, 2014.

[435] P. Persico, V. Ambrogi, C. Carfagna, P. Cerruti, I. Ferrocino, and G. Mauriello, "Nanocomposite polymer films containing carvacrol for antimicrobial active packaging," *Polym. Eng. Sci.*, vol. 49, no. 7, pp. 1447–1455, Jul. 2009.

[436] S. A. Kyriakou, M. Statherpoulos, G. K. Parissakis, C. D. Papaspyrides, and C. N. Kartalis, "Oxidative induction time method based on thermogravimetry for monitoring the restabilization of post-use LDPE," *Polym. Degrad. Stab.*, vol. 66, no. 1, pp. 49–53, 1999.

[437] N. S. Allen, M. Edge, M. Rodriguez, C. M. Liauw, and E. Fontan, "Aspects of the thermal oxidation of ethylene vinyl acetate copolymer," *Polym. Degrad. Stab.*, vol. 68, no. 3, pp. 363–371, 2000.

[438] J. A. Burke, W. Korytowski, and T. Sarna, "In vitro photooxidation of RPE melanin: role of hydrogen peroxide and hydroxyhadicals," *Photochem. Photobiol.*, vol. 53, p. 15S, 1991.

[439] J. M. Gallas, G. W. Zajac, T. Sarna, and P. L. Stotter, "Structural differences in unbleached and mildly-bleached synthetic tyrosine-derived melanins identified by scanning probe microscopies.," *Pigment Cell Res.*, vol. 13, no. 2, pp. 99–108, 2000.

[440] J. McGinness and P. Proctor, "The importance of the fact that melanin is black," *J. Theor. Biol.*, vol. 39, no. 3, pp. 677–678, 1973.

[441] K. Wakamatsu, Y. Nakanishi, N. Miyazaki, L. Kolbe, and S. Ito, "UVA-induced oxidative degradation of melanins: Fission of indole moiety in eumelanin and conversion to benzothiazole moiety in pheomelanin," *Pigment Cell Melanoma Res.*, vol. 25, no. 4, pp. 434–445, 2012.

[442] T. Corrales, F. Catalina, C. Peinado, N. S. Allen, and E. Fontan, "Photooxidative and thermal

degradation of polyethylenes: interrelationship by chemiluminescence, thermal gravimetric analysis and FTIR data," *J. Photochem. Photobiol. A Chem.*, vol. 147, no. 3, pp. 213–224, Apr. 2002.

[443] R. Yang, Y. Li, and J. Yu, "Photo-stabilization of linear low density polyethylene by inorganic nano-particles," *Polym. Degrad. Stab.*, vol. 88, no. 2, pp. 168–174, May 2005.

[444] L. Costa, M. P. Luda, and L. Trossarelli, "Ultra high molecular weight polyethylene - II. Thermal- and photo-oxidation," *Polym. Degrad. Stab.*, vol. 58, no. 1–2, pp. 41–54, 1997.

[445] J. Lacoste and D. J. Carlsson, "Gamma-, photo-, and thermally-initiated oxidation of linear low density polyethylene: A quantitative comparison of oxidation products," *J. Polym. Sci. Part A Polym. Chem.*, vol. 30, no. 3, pp. 493–500, Mar. 1992.

[446] F. Severini, R. Gallo, S. Ipsale, and N. Del Fanti, "Environmental degradation of stabilized LDPE. Later stages," *Polym. Degrad. Stab.*, vol. 17, no. 1, pp. 57–64, 1987.

[447] J. V Gulmine, P. R. Janissek, H. M. Heise, and L. Akcelrud, "Degradation profile of polyethylene after artificial accelerated weathering," *Polym. Degrad. Stab.*, vol. 79, pp. 385–397, 2003.

[448] A. N. Shebani, A. J. Van Reenen, and M. Meincken, "The Effect of Wood Species on the Mechanical and Thermal Properties of Wood—LLDPE Composites," *J. Compos. Mater.*, vol. 43, no. 11, pp. 1305–1318, Jun. 2009.

[449] O. Chiantore, L. Trossarelli, and M. Lazzari, "Photooxidative degradation of acrylic and methacrylic polymers," *Polymer (Guildf).*, vol. 41, no. 5, pp. 1657–1668, Mar. 2000.

[450] L. Guadagno, C. Naddeo, V. Vittoria, G. Camino, and C. Cagnani, "Chemical and morphologial modifications of irradiated linear low density polyethylene (LLDPE)," *Polym. Degrad. Stab.*, vol. 72, pp. 175–186, 2001.

[451] M. Çopuroğlu and M. Şen, "A comparative study of thermal ageing characteristics of poly(ethylene-co-vinyl acetate) and poly(ethylene-co-vinyl acetate)/carbon black mixture," *Polym. Adv. Technol.*, vol. 15, no. 7, pp. 393–399, 2004.

[452] J. Jin, S. Chen, and J. Zhang, "UV aging behaviour of ethylene-vinyl acetate copolymers

(EVA) with different vinyl acetate contents," *Polym. Degrad. Stab.*, vol. 95, no. 5, pp. 725–732, 2010.

[453] T. A. Skowronski, J. F. Rabek, and B. Rånby, "Photo-oxidation of ethylene-vinyl acetate copolymers," *Polym. Photochem.*, vol. 3, no. 5, pp. 341–355, 1983.

[454] P. Klemchuk, M. Ezrin, G. Lavigne, W. Holley, J. Galica, and S. Agro, "Investigation of the degradation and stabilization of EVA-based encapsulant in field-aged solar energy modules," *Polym. Degrad. Stab.*, vol. 55, no. 3, pp. 347–365, Mar. 1997.

[455] O. Inganäs, T. Skotheim, and I. Lundström, "Polypyrrole-semiconductor Schottky barriers," *J. Appl. Phys.*, vol. 54, no. 6, pp. 3636–3639, 1983.

[456] S. Jiang, K. Wang, H. Zhang, Y. Ding, and Q. Yu, "Encapsulation of PV Modules Using Ethylene Vinyl Acetate Copolymer as the Encapsulant," *Macromol. React. Eng.*, vol. 9, no. 5, pp. 522–529, 1995.

[457] R. S. Chhabra, "NTP Technical Report on the Toxicity Studies of Benzophenone," 2000.

[458] M. C. Rhodes, J. R. Bucher, J. C. Peckham, G. E. Kissling, M. R. Hejtmancik, and R. S. Chhabra, "Carcinogenesis studies of benzophenone in rats and mice," *Food Chem. Toxicol.*, vol. 45, no. 5, pp. 843–851, May 2007.

[459] H. Zhao, D. Wei, M. Li, and Y. Du, "Substituent contribution to the genotoxicity of benzophenone-type UV filters," *Ecotoxicol. Environ. Saf.*, vol. 95, pp. 241–246, Sep. 2013.

[460] C. P. Balde, V. Forti, V. Gray, R. Kuehr, and P. Stegmann, "The Global E-waste Monitor 2017: Quantities, Flows and Resources," 2017.

[461] V. Goodship, A. Stevels, and J. Huisman, Eds., "Waste Electrical and Electronic Equipment (WEEE) Handbook," in *Waste Electrical and Electronic Equipment (WEEE) Handbook*, 2nd ed., Woodhead Publishing, 2019.

[462] A. J. Heeger, "Semiconducting and Metallic Polymers: The Fourth Generation of Polymeric Materials (Nobel Lecture)," *Angew. Chemie Int. Ed.*, vol. 40, no. 14, pp. 2591–2611, Jul. 2001.

[463] M. L. Tietze *et al.*, "Elementary steps in electrical doping of organic semiconductors," *Nat.*

Commun., vol. 9, no. 1, p. 1182, Dec. 2018.

[464] S. Park *et al.*, "Self-powered ultra-flexible electronics via nano-grating-patterned organic photovoltaics," *Nature*, vol. 561, no. 7724, pp. 516–521, 2018.

[465] S. E. Root, S. Savagatrup, A. D. Printz, D. Rodriquez, and D. J. Lipomi, "Mechanical Properties of Organic Semiconductors for Stretchable, Highly Flexible, and Mechanically Robust Electronics," *Chem. Rev.*, vol. 117, no. 9, pp. 6467–6499, 2017.

[466] G. Prota, "The chemistry of melanins and melanogenesis.," *Fortschritte der Chemie Org. Naturstoffe. Prog. Chem. Org. Nat. Prod. Prog. dans la Chim. des Subst. Org. Nat.*, vol. 64, pp. 93–148, 1995.

[467] D. F. Williams, "B," in *The Williams Dictionary of Biomaterials*, Liverpool: Liverpool University Press, 2012, pp. 33–54.

[468] *Test No. 208: Terrestrial Plant Test: Seedling Emergence and Seedling Growth Test*. OECD, 2006.

[469] P. Meredith and T. Sarna, "The physical and chemical properties of eumelanin," *Pigment Cell Res.*, vol. 19, no. 6, pp. 572–594, Dec. 2006.

[470] G. Claus and H. J. Kutzner, "Degradation of indole by Alcaligenes spec.," *Syst. Appl. Microbiol.*, vol. 4, no. 2, pp. 169–180, 1983.

[471] S. Grima, V. Bellon-Maurel, P. Feuilloley, and F. Silvestre, "Aerobic biodegradation of polymers in solid-state conditions: A review of environmental and physicochemical parameter settings in laboratory simulations," *J. Polym. Environ.*, vol. 8, no. 4, pp. 183–196, 2000.

[472] P. Partanen, J. Hultman, L. Paulin, P. Auvinen, and M. Romantschuk, "Bacterial diversity at different stages of the composting process," *BMC Microbiol.*, vol. 10, p. 94, 2010.

[473] J. Pietikäinen, M. Pettersson, and E. Bååth, "Comparison of temperature effects on soil respiration and bacterial and fungal growth rates," *FEMS Microbiol. Ecol.*, vol. 52, no. 1, pp. 49–58, 2005.

[474] Z. Tang, X. Sun, Z. Luo, N. He, and O. J. Sun, "Effects of temperature, soil substrate, and

microbial community on carbon mineralization across three climatically contrasting forest sites," *Ecol. Evol.*, vol. 8, no. 2, pp. 879–891, 2018.

[475] R. Bhabhra and D. S. Askew, "Thermotolerance and virulence of Aspergillus fumigatus: Role of the fungal nucleolus," *Med. Mycol.*, vol. 43, no. SUPPL.1, pp. 87–93, 2005.

[476] M. Hachinohe and H. Matsumoto, "Mechanism of selective phytotoxicity of L-3,4-dihydroxyphenylalanine (L-dopa) in barnyardglass and lettuce," *J. Chem. Ecol.*, vol. 33, no. 10, pp. 1919–1926, 2007.

[477] P. Jha, R. Jobby, S. Kudale, N. Modi, A. Dhaneshwar, and N. Desai, "Biodegradation of phenol using hairy roots of Helianthus annuus L.," *Int. Biodeterior. Biodegrad.*, vol. 77, pp. 106–113, 2013.

[478] W. A. Said, D. L. Lewis, and F. Ecology, "Quantitative Assessment of the Effects of Metals on Microbial Degradation of Organic Chemicals," vol. 57, no. 5, pp. 1498–1503, 1991.

[479] C. G. Claessens, U. Hahn, and T. Torres, "Phthalocyanines: From outstanding electronic properties to emerging applications," *Chem. Rec.*, vol. 8, no. 2, pp. 75–97, 2008.

[480] D. Jančula and B. Maršálek, "The toxicity of phthalocyanines to the aquatic plant Lemna minor (duckweed) - Testing of 31 compounds," *Chemosphere*, vol. 88, no. 8, pp. 962–965, 2012.

[481] S. Shiva Shakthi, S. P. Archana, C. Arulvasu, and N. Neethiselvan, "Biochemical Composition of Cuttlefish Sepia Prabahari Ink and Its Bioactive Properties In-Vitro," *J. Pharm. Sci. Res.*, vol. 7, no. 7, pp. 2966–2975, 2016.

[482] A. Neifar, F. Ben Rebah, A. Gargouri, and A. Abdelmouleh, "Physicochemical characterization of Sepia officinalis ink and the effects of storage conditions on the coagulation process," *J. Mar. Biol. Assoc. United Kingdom*, vol. 89, no. 4, pp. 803–807, 2009.

[483] M. Bridelli, R. Capelletti, and P. R. Crippa, "Electret state and hydrated structure of melanin," *J. Electroanal. Chem.*, vol. 128, no. C, pp. 555–567, 1981.

[484] P. J. Gonçalves, O. B. Filho, and C. F. O. Graeff, "Effects of hydrogen on the electronic

properties of synthetic melanin," *J. Appl. Phys.*, vol. 99, no. 10, p. 104701, 2006.

[485] M. Ambrico *et al.*, "Melanin layer on silicon: an attractive structure for a possible exploitation in bio-polymer based metal-insulator-silicon devices.," *Adv. Mater.*, vol. 23, no. 29, pp. 3332–6, Aug. 2011.

[486] S. T. Gurme *et al.*, "An Organic Bipolar Resistive Switching Memory Device Based on Natural Melanin Synthesized From Aeromonas sp. SNS," *Phys. status solidi*, vol. 215, no. 24, p. 1800550, Dec. 2018.

[487] M. Ambrico *et al.*, "Memory-like behavior as a feature of electrical signal transmission in melanin-like bio-polymers," *Appl. Phys. Lett.*, vol. 100, no. 25, p. 253702, 2012.

[488] E. Di Mauro *et al.*, "Resistive switching controlled by the hydration level in thin films of the biopigment eumelanin," *J. Mater. Chem. C*, vol. 4, no. 40, pp. 9544–9553, 2016.

[489] H. Morgan, R. P. A, and G. T. Stevens, "A proton-injecting technique for the measurement of hydration-dependent protonic conductivity," *J. Phys. E.*, vol. 19, p. 80, 1986.

[490] C. Zhong, Y. Deng, A. F. Roudsari, A. Kapetanovic, M. P. Anantram, and M. Rolandi, "A polysaccharide bioprotonic field-effect transistor," *Nat. Commun.*, vol. 2, p. 476, 2011.

[491] P. Brunswick, H. Mayaudon, V. Albin, V. Lair, A. Ringuede, and M. Cassir, "Use of Ni electrodes chronoamperometry for improved diagnostics of diabetes and cardiac diseases," *Annu. Int. Conf. IEEE Eng. Med. Biol. - Proc.*, vol. 33, no. 1, pp. 4544–4547, 2007.

[492] X. X. Han *et al.*, "Nickel electrodes as a cheap and versatile platform for studying structure and function of immobilized redox proteins," *Anal. Chim. Acta*, vol. 941, pp. 35–40, 2016.

[493] M. M. Mardanpour and S. Yaghmaei, "Characterization of a microfluidic microbial fuel cell as a power generator based on a nickel electrode," *Biosens. Bioelectron.*, vol. 79, pp. 327–333, 2016.

[494] I. N. Hulea, S. Russo, A. Molinari, and A. F. Morpurgo, "Reproducible low contact resistance in rubrene single-crystal field-effect transistors with nickel electrodes," *Appl. Phys. Lett.*, vol. 88, no. 11, p. 113512, Mar. 2006.

[495] A. Molinari, I. Gutiérrez, I. N. Hulea, S. Russo, and A. F. Morpurgo, "Bias-dependent

contact resistance in rubrene single-crystal field-effect transistors," *Appl. Phys. Lett.*, vol. 90, no. 21, p. 212103, May 2007.

[496] A. S. Molinari, I. Gutiérrez Lezama, P. Parisse, T. Takenobu, Y. Iwasa, and A. F. Morpurgo, "Quantitative analysis of electronic transport through weakly coupled metal/organic interfaces," *Appl. Phys. Lett.*, vol. 92, no. 13, p. 133303, Mar. 2008.

[497] K. L. Chavez and D. W. Hess, "A Novel Method of Etching Copper Oxide Using Acetic Acid," *J. Electrochem. Soc.*, vol. 148, no. 11, p. G640, 2001.

[498] P. Walker and W. H. Tarn, *Handbook of Metal Etchants*. CRC Press LLC, 1991.

[499] I. Valov *et al.*, "Nanobatteries in redox-based resistive switches require extension of memristor theory," *Nat. Commun.*, vol. 4, pp. 1771–1779, 2013.

[500] D. W. Meek, D. K. Straub, and R. S. Drago, "Transition Metal Ion Complexes of Dimethyl Sulfoxide," *J. Am. Chem. Soc.*, vol. 82, no. 23, pp. 6013–6016, 1960.

[501] S. Ma, L. Liu, V. Bromberg, and T. J. Singler, "Electroless copper plating of inkjet-printed polydopamine nanoparticles: A facile method to fabricate highly conductive patterns at near room temperature," *ACS Appl. Mater. Interfaces*, vol. 6, no. 22, pp. 19494–19498, 2014.

[502] J. K. Burdett and S. Sevov, "Stability of the Oxidation States of Copper," *J. Am. Chem. Soc.*, vol. 117, no. 51, pp. 12788–12792, 1995.

[503] R. Paulose, R. Mohan, and V. Parihar, "Nanostructured nickel oxide and its electrochemical behaviour—A brief review," *Nano-Structures and Nano-Objects*, vol. 11, pp. 102–111, 2017.

[504] J. Postlethwaite, "Breakdown of passivity of nickel in alkaline chloride solutions at 25-275°C," *Electrochim. Acta*, vol. 12, no. 3, pp. 333–346, 1967.

[505] M. R. Barbosa, J. A. Bastos, J. J. García-Jareño, and F. Vicente, "Chloride role in the surface of nickel electrode," *Electrochimica Acta*, vol. 44, no. 6–7. pp. 957–965, 1998.

[506] J. R. Vilche, D. C. Exactas, and L. Plata, "Kinetics and Mechanism of the Nickel Concentration of Chloride and Nickel Ions," *Corros. Sci.*, vol. 15, no. January, 1975.

[507] S. W. Hwang *et al.*, "Materials and fabrication processes for transient and bioresorbable

high-performance electronics," *Adv. Funct. Mater.*, vol. 23, no. 33, pp. 4087–4093, 2013.

[508] H. Cheng and V. Vepachedu, "Recent development of transient electronics," *Theor. Appl. Mech. Lett.*, vol. 6, no. 1, pp. 21–31, 2016.

[509] M. Barra *et al.*, "Eumelanin-Based Organic Bioelectronics: Myth or Reality?," *MRS Adv.*, vol. 1, no. 57, pp. 3801–3810, 2016.

[510] T. J. Guess, "The Social Construction of Whiteness: Racism by Intent, Racism by Consequence," *Crit. Sociol.*, vol. 32, no. 4, pp. 649–673, Jul. 2006.

[511] R. E. Hall, *The Melanin Millennium: Skin Color as 21st Century International Discourse*, Illustrate. Springer Science & Business Media, 2012.

[512] E. Di Mauro, E. Hebrard, Y. Boulahia, M. Rolandi, and C. Santato, "On the interfaces between organic bio-sourced materials and metals for sustainable electronics: the eumelanin case," *Jpn. J. Appl. Phys.*, vol. 58, no. 5, p. 051014, May 2019.

[513] E. Di Mauro *et al.*, "Eumelanin for Nature-Inspired UV-Absorption Enhancement of Plastics," *Polym. Int.*, p. pi.5790, Feb. 2019.

[514] B. Herzog and F. Sengün, "Scattering particles increase absorbance of dyes – a model study with relevance for sunscreens," *Photochem. Photobiol. Sci.*, vol. 14, pp. 2054–2063, 2015.

[515] P. Atkins and J. de Paula, *Physical Chemistry*, 10th ed. Oxford: Oxford University Press, 2014.

[516] S. Krimm, C. Y. Liang, and G. B. B. M. Sutherland, "Infrared Spectra of High Polymers. II. Polyethylene," *J. Chem. Phys.*, vol. 25, no. 3, pp. 549–562, Sep. 1956.

[517] R. Chércoles Asensio, M. San Andrés Moya, J. M. de la Roja, and M. Gómez, "Analytical characterization of polymers used in conservation and restoration by ATR-FTIR spectroscopy," *Anal. Bioanal. Chem.*, vol. 395, no. 7, pp. 2081–2096, Dec. 2009.

[518] S. T. Sam, H. Ismail, and Z. Ahmad, "Linear low-density polyethylene/(soya powder) blends containing polyethylene- g -(maleic anhydride) as a compatibilizer," *J. Vinyl Addit. Technol.*, vol. 15, no. 4, pp. 252–259, Dec. 2009.

[519] A. Strålin and T. Hjertberg, "FTIR Study on interfacial interactions between hydrated

aluminium and polar groups in ethylene copolymers," *Surf. Interface Anal.*, vol. 20, no. 5, pp. 337–340, 1993.

[520] G. Masetti, F. Cabassi, G. Morelli, and G. Zerbi, "Conformational Order and Disorder in Poly(tetrafluoroethylene) from the Infrared Spectrum," *Macromolecules*, vol. 6, no. 5, pp. 700–707, 1973.

[521] S. A. Centeno and J. Shamir, "Surface enhanced Raman scattering (SERS) and FTIR characterization of the sepia melanin pigment used in works of art," *J. Mol. Struct.*, vol. 873, no. 1–3, pp. 149–159, Feb. 2008.

[522] J. C. Young, W. Garner, and J. W. Clark, "An Improved Apparatus for Biochemical Oxygen Demand," *Anal. Chem.*, vol. 20, no. 20, p. 1964, 1964.

[523] J. C. Young and R. M. Cowan, *Respirometry for Environmental Science and Engineering*. SJ Enterprises, 2004.

[524] A. M. T. Magalhães, P. J. Shea, M. D. Jawson, E. A. Wicklund, and D. W. Nelson, "Practical Simulation of Composting in the Laboratory," *Waste Manag. Res.*, vol. 11, no. 2, pp. 143–154, Mar. 1993.

[525] S. G. Dodard *et al.*, "Ecotoxicological assessment of a high energetic and insensitive munitions compound: 2,4-Dinitroanisole (DNAN)," *J. Hazard. Mater.*, vol. 262, pp. 143–150, 2013.

[526] S. Rocheleau *et al.*, "Phytotoxicity and uptake of nitroglycerin in a natural sandy loam soil," *Sci. Total Environ.*, vol. 409, no. 24, pp. 5284–5291, 2011.

[527] S. G. Bratsch, "Standard Electrode Potentials and Temperature Coefficients in Water at 298.15 K," *J. Phys. Chem. Ref. Data*, vol. 1, 1989.

[528] R. C. Weast, *Handbook of Chemistry and Physics*, 1st Studen. CRC Press LLC.

[529] K. M. Heather Bateman, Howard Sargeant, "Dictionary of Food Science and Nutrition," International Food Information Service, Ed. International Food Information Service (IFIS Publishing), 2006, p. 181.

[530] IUPAC, *IUPAC Compendium of Chemical Terminology*, 2nd ed. Research Triangle Park,

NC: IUPAC, 2009.

APPENDIX A – SUPPORTING INFORMATION OF ARTICLE 1

Resistive Switching Controlled by the Hydration Level in Thin Films of the Biopigment Eumelanin

Eduardo Di Mauro, Olivier Carpentier, Sergio Iván Yáñez Sánchez, Ndembi Ignoumba Ignoumba, Myriam Lalancette-Jean, Josianne Lefebvre, Shiming Zhang, Carlos F. O. Graeff, Fabio Cicoira, Clara Santato

Table S1**.** Chloride concentrations for different suspensions of eumelanin in dimethyl sulfoxide (DMSO) used in this work.

Type of eumelanin	Intrinsic Cl^- amount (% wt. over eumelanin)	NaCl added (mg/ml)	Cl^- added (% wt. over eumelanin)	Final Cl^- amount (%wt. over eumelanin)	Referred to as
Sigma	0.83±0.04	0.8	3.2	≈4	Intermediate chloride amount
		1.8	7.3	≈8	High chloride amount
DMSO-melanin	0.10±0.01	0.8	3.2	≈3	Intermediate chloride amount
		1.8	7.3	≈7	High chloride amount

Table S2. ON/OFF ratios for the *standard* and *hybrid* resistive switch.

Resistive switch	ON/OFF ratio			Number of samples
	Minimum	Maximum	Average	
Standard	$9 \cdot 10^2$	$5 \cdot 10^4$	$2 \cdot 10^4$	16
Hybrid	$2 \cdot 10^1$	$7 \cdot 10^2$	$3 \cdot 10^2$	5
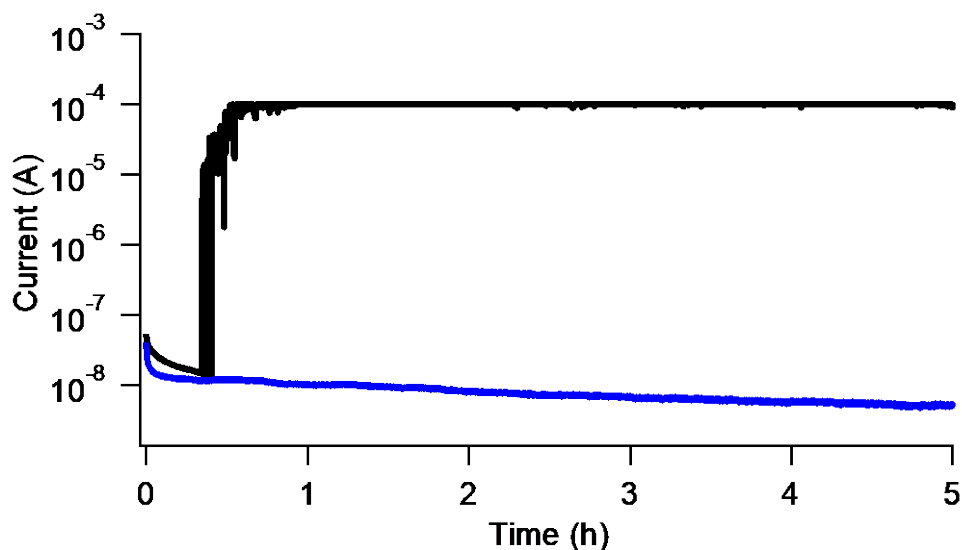
Figure S1. Current vs time plots for the first 5 hours of transient current measurements performed on (i) a thin film of Sigma eumelanin, hydrated for 1 hour at 90% RH and biased for ≈28 hours at 1 V, wherein a resistive switch took place after 23 minutes (current compliance set at 10^{-4} A, black curve) and (ii) a thin film of Sigma eumelanin, hydrated for 1 hour at 90% RH and biased for 15 hours at 1 V, wherein a resistive switch did not take place (blue curve).
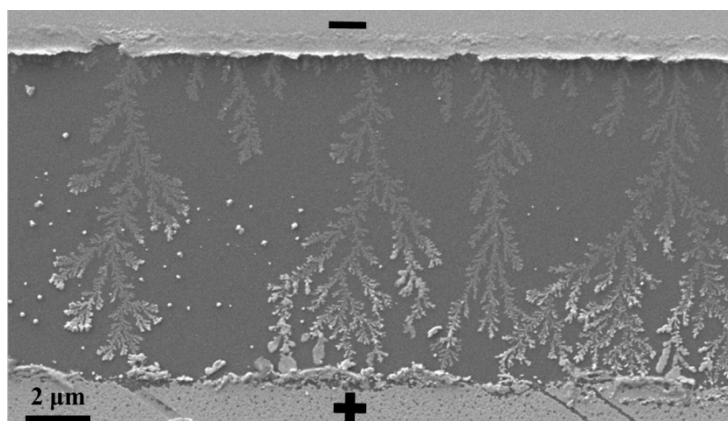
Figure S2. SEM image of dendrites bridging the two electrodes and of nanoclusters migrating, in a thin film of Sigma eumelanin, hydrated for 1 hour at 90% RH and biased at 1 V for 19 hours. The resistive switch took place after 28 minutes. SEM voltage = 5kV.
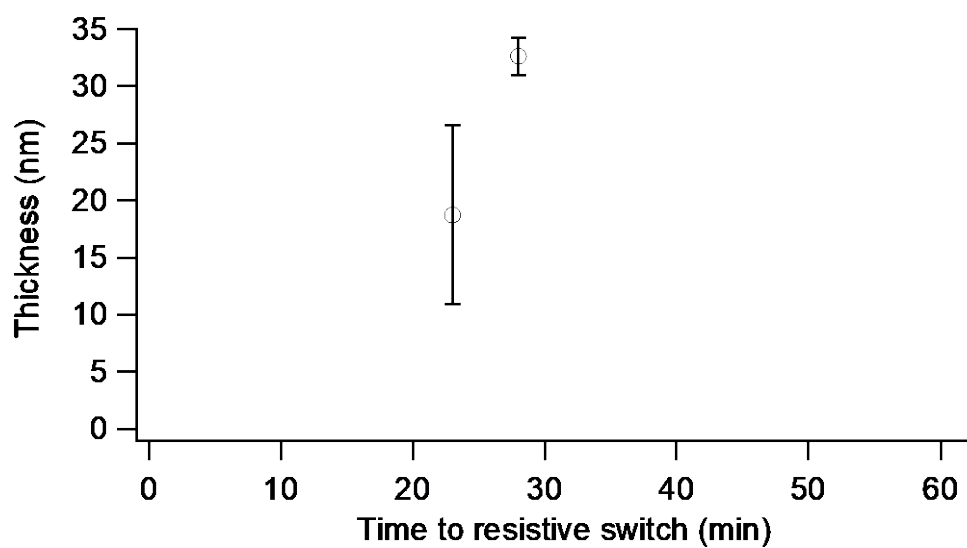
Figure S3. Average thickness versus time to resistive switch for Sigma eumelanin thin films (1 hour-hydration, 1 V electrical bias) that showed a *standard* resistive switch within the first hour of the measurement (each point refers to a sample).
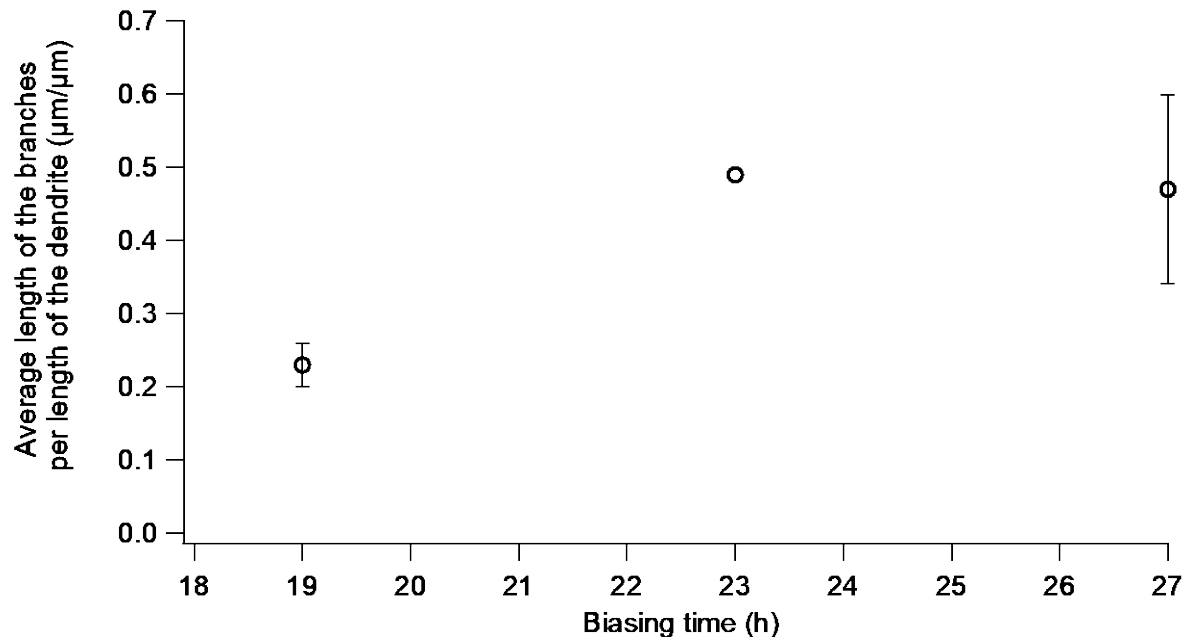
Figure S4. Average length of the branches of the dendrites, normalized by the length of the dendrite from which the branches were developing (*L*), versus biasing time (protruding dendrites shorter than 3 microns were not considered). The farther *L* is from 0, the more the dendrite growth is lateral rather than straight. As the electrical measurements were not stopped when the resistive switch took place, only a correlation with the biasing time, rather than with the time to resistive switch, could be found, as expected, as once the dendrite has produced the bridge, the rest of the biasing time can likely only promote an increase of its lateral extent.
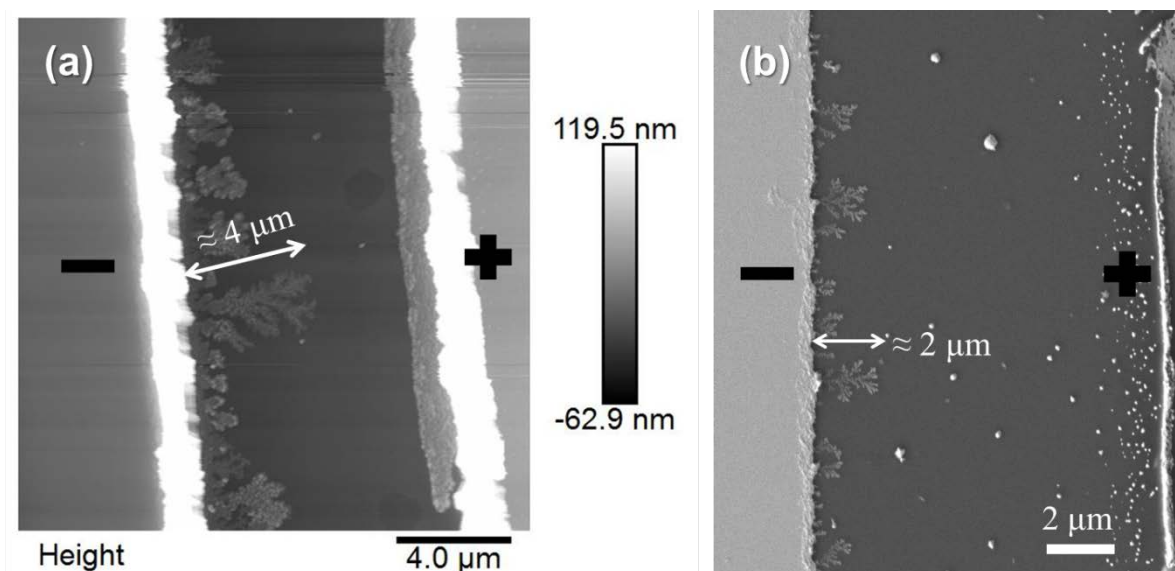
Figure S5. Effects of the hydration time: AFM and SEM images comparing the length of the dendrites in two Sigma eumelanin thin films that differ for the hydration time (spin coated from the same suspension, hydrated at 90% RH, and biased at 1 V) (a) AFM image, 18 μm × 18 μm, film hydrated for 1 hour (biasing time of approximately 28 hours), (b) SEM image, film hydrated for 4 ½ days (biasing time of 24 hours). SEM voltage=5kV.
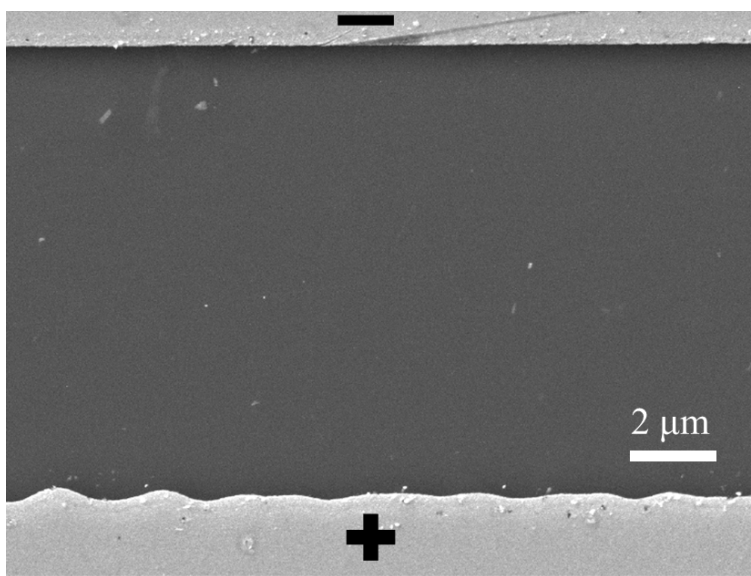
Figure S6. SEM image of a thin film of Sigma eumelanin hydrated for 14 days at 90% RH and biased for 3 hours at 1 V. No dissolution of the positive electrode was observed. SEM voltage=10kV.

Late resistive switch for thin films with high chloride content

For thin films with 8% wt. Cl⁻ content, hydrated for one hour at 90% RH, in one case the resistive switch took place after 52 minutes of biasing at 1 V: SEM images reveal that several dendrites grew one next to the other in the channel (Figures S7 and S8). Consequently, the late resistive switch may be due to the fact that the preferential pathways for nanoclusters were very close one to the other, and came to competition, causing the opening of several lateral branches, thus promoting a lateral (rather than straight) dendrite growth. The effect was a delay of the whole process. This is confirmed by a study of the shape of the dendrites: the lateral extension of the dendrites for this sample was 9.7±2.4 μm, more than twice the average for other samples with a resistive switch within 7 minutes (3.5±0.5 μm).
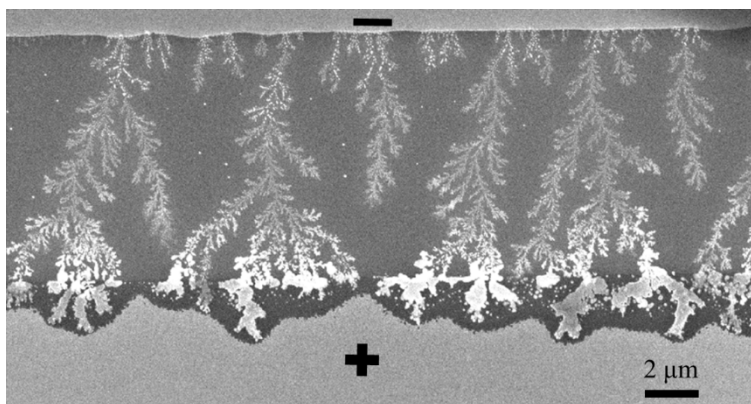
Figure S7. SEM image of dendrites bridging the two electrodes in a Sigma eumelanin thin film (8% wt. Cl⁻), hydrated for 1 hour at 90% RH and biased for 12 hours at 1 V, where the resistive switch took place after 52 minutes. SEM voltage=10kV.
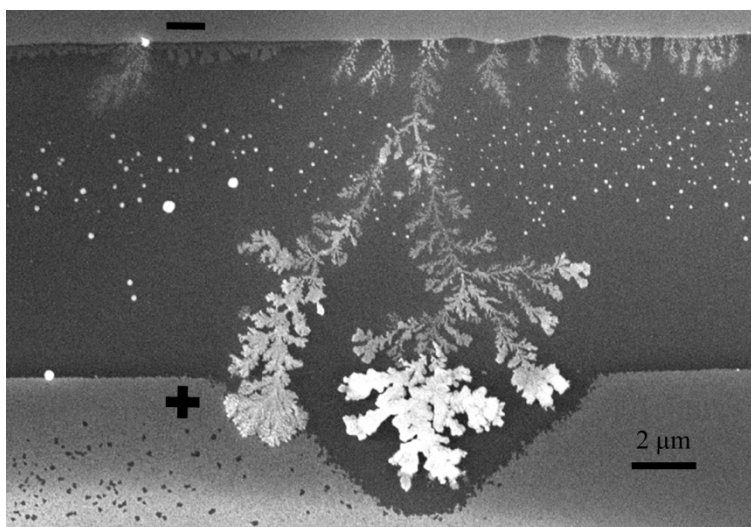
Figure S8. SEM image of dendrites bridging the two electrodes in a eumelanin thin film, same sample of <u>Fig. S7</u>. It is worth noting that, once the dendrite reached the cove that had generated the material for its growth, the dendrite started receiving nanoclusters also from its sides. This is the reason why the thickness at its end, in the cove, appears higher (corresponding to the brighter region in the image) than that of the body of the dendrite. SEM voltage=10kV.
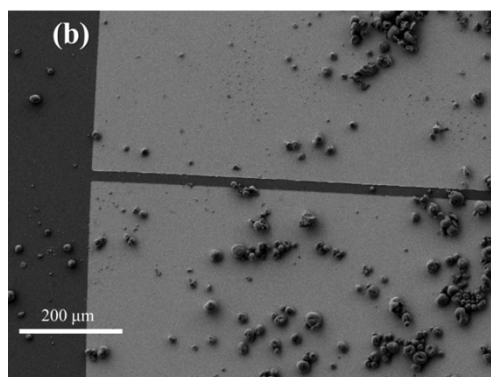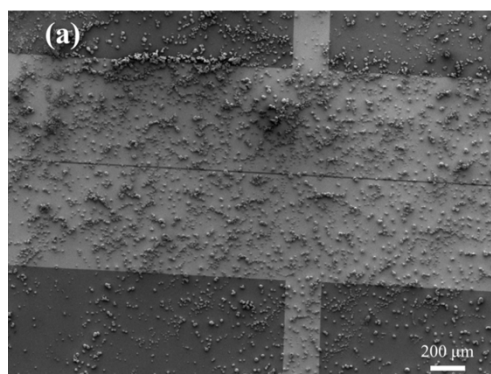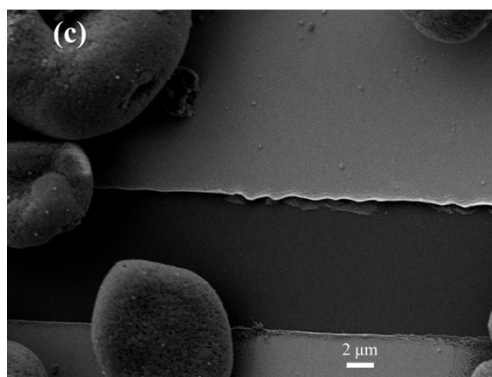
Figure S9. SEM images of gold electrodes after the spin coating of a suspension of Sepia eumelanin in DMSO at different magnifications: (a) 40X, (b) 250X and (c) 3330 X. Several granules can be observed. SEM voltage=5 kV.
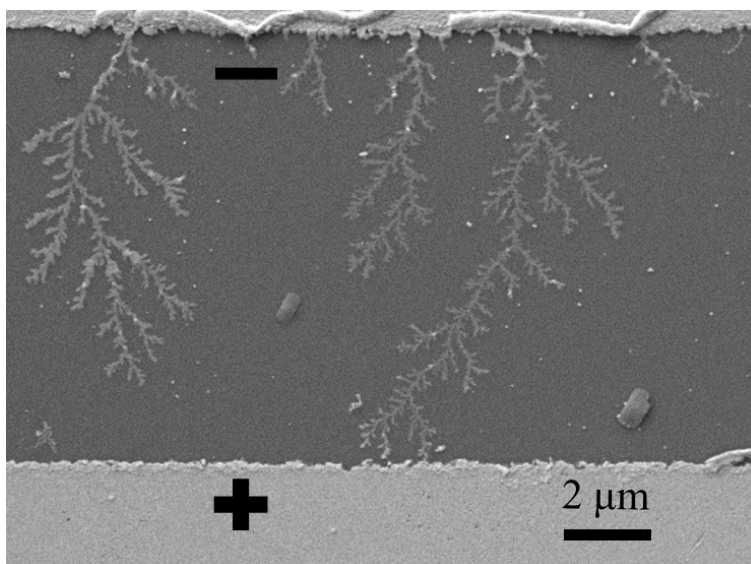
Figure S10. SEM image of dendrites bridging one electrode to the other after 3 hours of electrical bias at 1 V in a thin film of Sepia eumelanin (7% wt. Cl⁻), hydrated for 1 hour at 90% RH. The resistive switch took place after 34 minutes. It is worth noting that dendrites grew where there were no granules, revealing the presence of a thin film of Sepia eumelanin. SEM voltage=5kV.

Table S3. Summary of the occurrence of the resistive switch within certain time frames for thin films of eumelanin with different chloride contents, hydrated for 1 hour at 90% RH and biased at 1 V.

Chloride amount	Number of suspensions tested	Absence of resistive switch within 3 hours (% of samples)	Resistive switches (%) within		
			7 min	30 min	63 min
Low (1% wt., intrinsic in Sigma eumelanin)	4	57	0	29	43
High (7% wt., Sepia eumelanin)	2	25	25	50	75
High (8% wt., Sigma eumelanin)	4	11	78	78	89
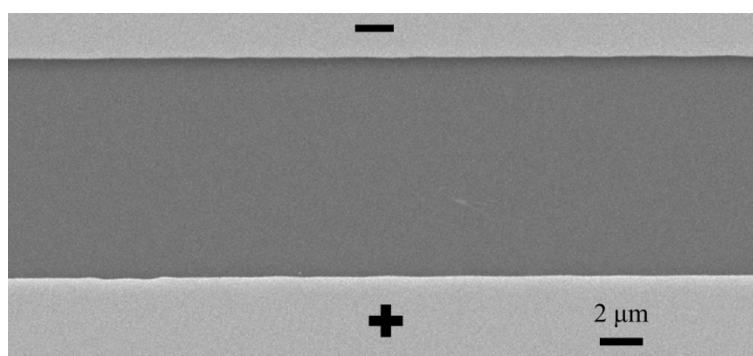
Figure S11. SEM image of Au electrodes in contact with a DMSO-melanin thin film, 7.4% wt. Cl⁻, hydrated for 1 hour at 90% RH and biased at 1 V for 3 hours. The positive electrode did not dissolve. The absence of dissolution and material migration in the channel could be observed also for samples biased for 12 hours, with the same hydration treatment and at the same electrical bias. SEM voltage=10kV.
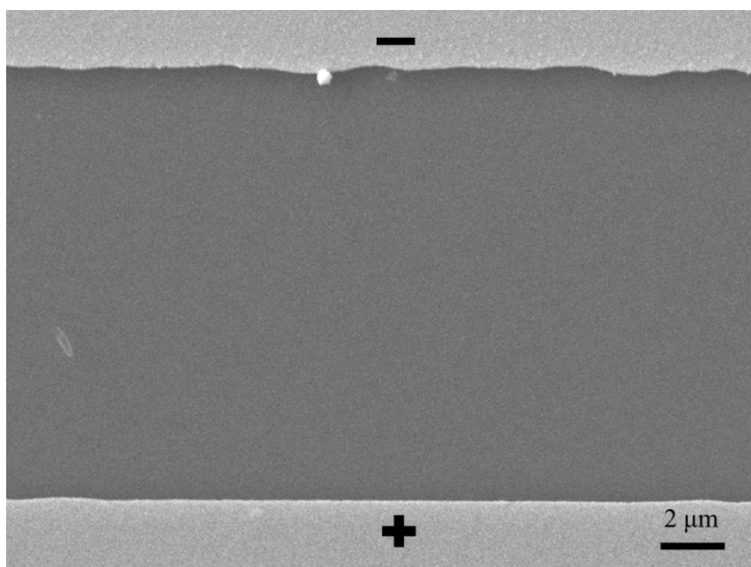
Figure S12. SEM image of the interelectrode area after 19h½ of biasing at 1 V after a DMSO drop had been confined between the electrodes. SEM voltage=10kV

DMSO drops on Au electrodes at different electrical biases and chloride contents

The results observed with the DMSO drop confined in the channel depend on the electrical bias and on the chloride amount:

Table S4**.** Summary of the phenomena occurring when a DMSO drop, with and without NaCl added, is confined between gold electrodes under electrical bias.

Biasing voltage (V)	Effect of		
	DMSO drop	DMSO drop 0.8mg/ml NaCl	DMSO drop 1.8mg/ml NaCl
1	No dissolution of the positive electrode	Growth of nanostructures	Growth of nanostructures
2.1	Fine dendrites	Interelectrode region filled by the material originated by the massive dissolution of the positive electrode	Interelectrode region filled by the material originated by the massive dissolution of the positive electrode

At 2.1V, when a drop of pure DMSO is confined in the channel, fine dendrites grow from the negative electrode after 3 hours of electrical bias (Figure S14). At 2.1V in the presence of chlorides, conversely, the positive electrode was severely damaged: it was massively consumed, so that a resistive switch was caused by the interelectrode distance filled with material originating from the dissolution of the positive electrode, after less than 1 minute (approximately 40 seconds).
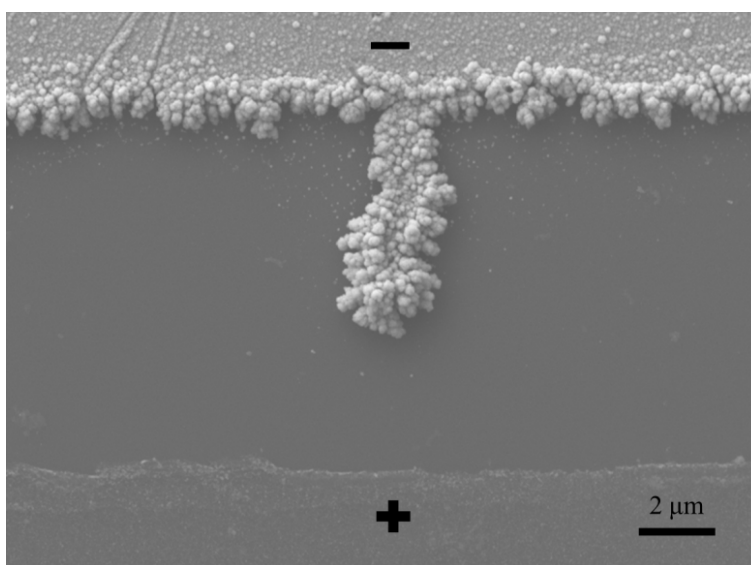
Figure S13. SEM image of gold electrodes after 3 hour-biasing at 1 V while a DMSO drop with 1.8mg/ml of NaCl was confined between the electrodes. SEM voltage=10kV.
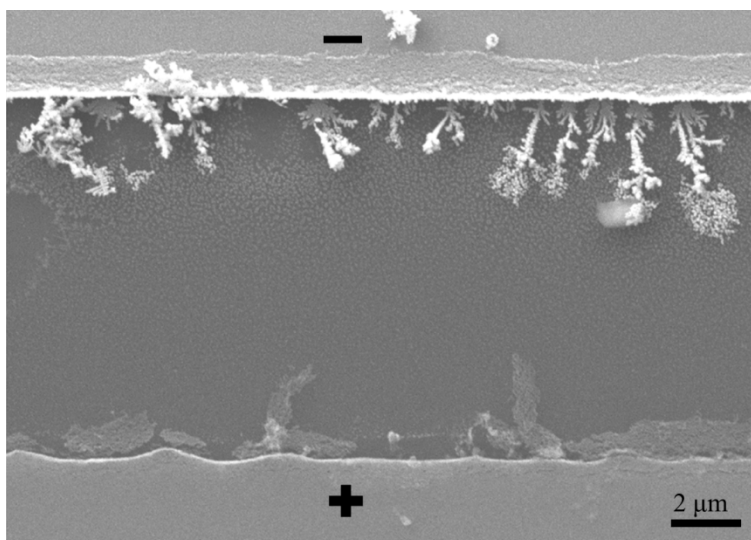
Figure S14. SEM image of gold electrodes after 3 hour-electrical biasing at 2.1 V while a DMSO drop was confined between the electrodes. The positive electrode dissolved and fine dendrites grew from the negative electrode. SEM voltage=10kV.
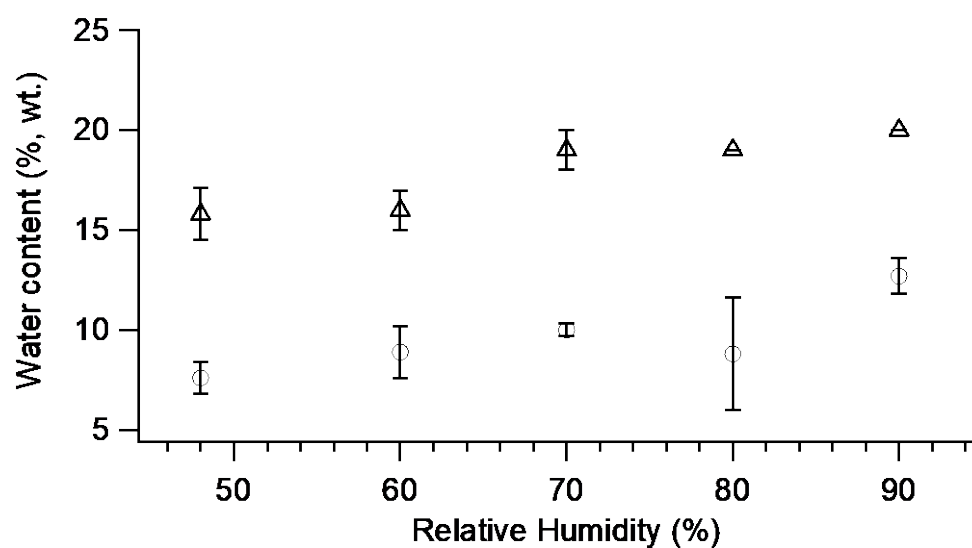
Figure S15. Water content of Sigma (circles) and Sepia (triangles) eumelanin powders hydrated for 1 hour at different relative humidity levels as deduced from Thermogravimetric Analyses [123].

Hydration at 48% and 60% RH

For synthetic eumelanin 8% wt. Cl⁻, at 48% RH (water content of approximately 7.6±0.7% wt.) [123] and 60% RH (water content of approximately 8.9±0.2% wt.) [123], the process of conductive bridge formation proved to be ongoing after 1 hour of electrical bias (respectively, little nanocluster migration in the channel -Figure S16- and dendrites protruding from the negative electrode, Figure S17).

This result indicates that at RH levels up to 60%, that is, when the amount of water in the thin films is lower than approximately 9% wt. [123], the phenomenon takes place but at a slower pace and the consumption of the positive electrode is very uniform.
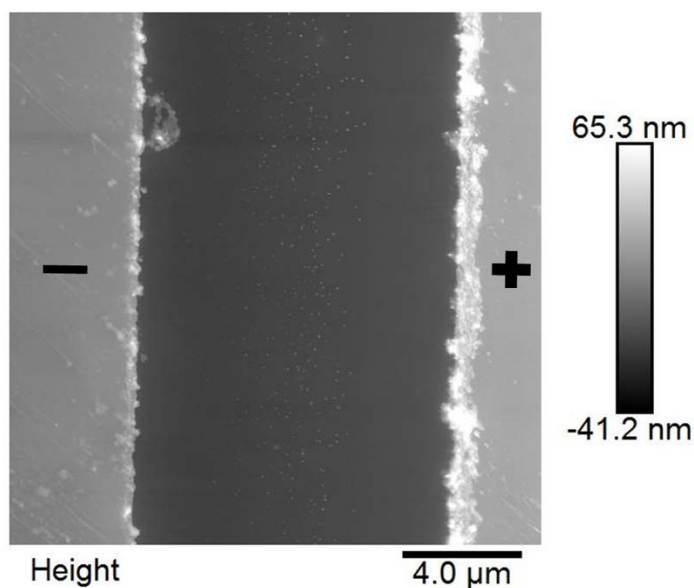
Figure S16. AFM image, 17.5 μm x 17.5 μm of the interelectrode area of a Sigma eumelanin thin film (8% wt. Cl⁻ content) hydrated for 1 hour at 48% RH and biased for 1 hour at 1 V. The migration of nanoclusters can be observed.
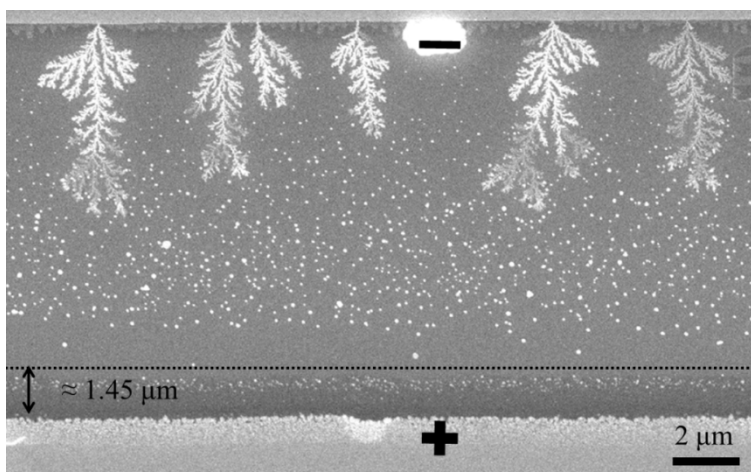
Figure S17. SEM image of a Sigma eumelanin thin film hydrated for 1 hour at 60% RH and biased for 1 hour at 1 V. The dotted line represents the initial position of the positive electrode before biasing: in spite of the high Cl⁻ content (8% wt.), the positive electrode is uniformly consumed. Image taken at 10 kV.

Table S5. Water content of Sigma eumelanin powders hydrated for different times and at different Relative Humidity levels as deduced from Thermogravimetric Analyses [123].

Relative Humidity (%)	Hydration time (min)	Water content (% wt.)	Standard deviation (%)
70	60	10.3	0.1
80	60	10.8	0.3
90	45	11.2	0.8
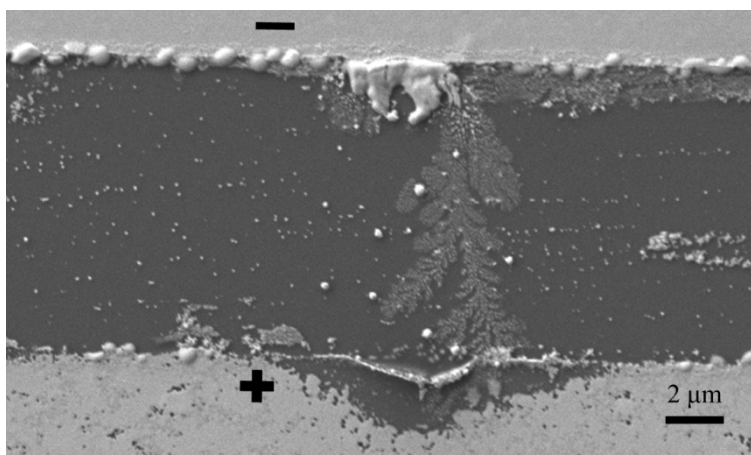
Figure S18. SEM image of a dendrite bridging the two electrodes in a thin film of Sigma eumelanin (8% wt. Cl⁻), hydrated for 30 minutes at 90% RH and biased for 3 hours at 1 V. The hybrid resistive switch took place after 11 minutes. SEM voltage=5kV.
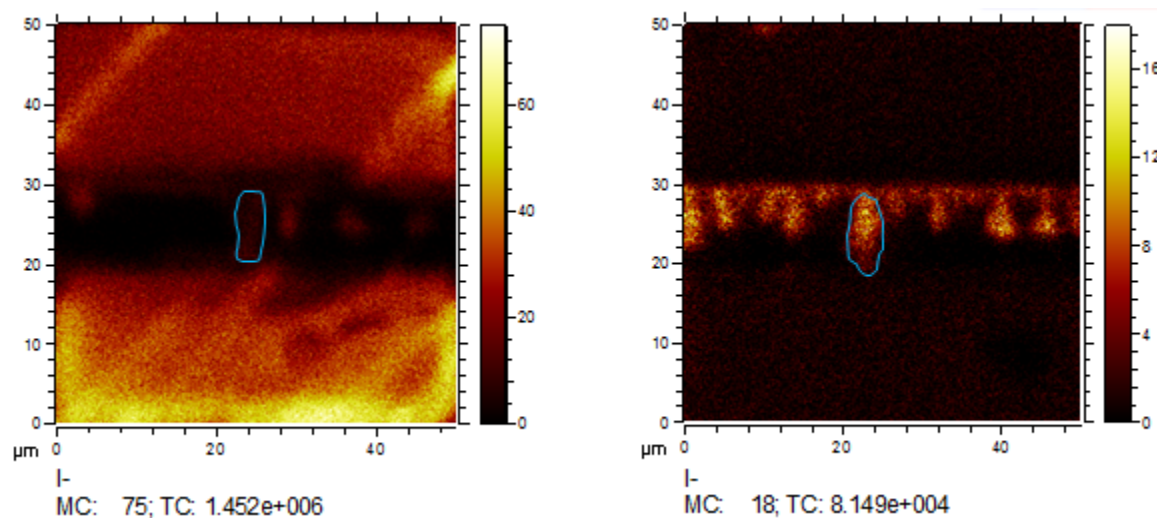
Figure S19. Reconstructed ToF-SIMS images (I⁻ ion) of dendrites formed between two Au electrodes in (a) Sigma eumelanin thin film, 8% wt. Cl⁻, hydrated for 1 hour at 90% RH, biased for 1 hour at 1 V (*standard* resistive switch after ≈5 minutes) (b) Sigma eumelanin thin film, 8% wt. Cl⁻, hydrated for 1 hour at 80% RH, biased for 1 hour at 1 V (hybrid resistive switch after ≈12 minutes). The blue lines enclose the regions from which the spectra were selected to extract the ion intensities of Table S6 and Table S7.

Table S6. Peak intensity of selected ToF-SIMS negative ions normalized to Au⁻ intensity of the dendrites of Figure S19. In italic the peaks with unit mass resolution. ToF-SIMS data was acquired in burst alignment mode so only unit mass resolution is achieved. For this reason, ions other than the one assigned could contribute to the peak intensities (spectra from the selected regions only).

Center Mass (u)	Assignment	Area		Normalized to Au⁻ intensity	
		Dendrite of the *standard* RS	Dendrite of the *hybrid* RS	*Standard* dendrite	*Hybrid* dendrite
38.01963	C_2N^-	83	113	9.01E-02	1.69E-01
42.00102	CNO^-	968	745	1.05E+00	1.11E+00
50.02183	C_3N^-	1017	1493	1.10E+00	2.23E+00
51.00242	C_3NH^-	94	92	1.02E-01	1.38E-01
61.97614	*C_4N^-*	*674*	*89*	*7.31E-01*	*1.33E-01*
66.03133	*C_3NO^-*	*357*	*234*	*3.87E-01*	*3.51E-01*
71.95398	C_6^-	114	143	1.24E-01	2.14E-01
74.0123	C_5N^-	503	655	5.46E-01	9.79E-01
83.98354	*C_7^-*	*162*	*68*	*1.76E-01*	*1.02E-01*
86.00078	*C_6N^-*	*108*	*70*	*1.17E-01*	*1.05E-01*
86.98935	*C_6HN^-*	*94*	*46*	*1.02E-01*	*6.88E-02*
96.98573	$C_4H_3NO_2^-$	388	305	4.21E-01	4.56E-01
98.00895	C_7N^-	308	275	3.34E-01	4.11E-01
120.9917	$C_6H_3NO_2^-$	148	155	1.61E-01	2.32E-01
144.9473	$C_8H_3NO_2^-$	133	106	1.45E-01	1.59E-01
196.9794	Au^-	922	669	1.00E+00	1.00E+00

Table S7. Normalized peak intensity of selected ToF-SIMS negative ions corresponding to MAu_x ($x \geq 2$)/MAu (where M is a eumelanin-Au complex, that is $CNAu_x$, $CNOAu_x$, C_3NAu_x, with $x \geq 2$) for the two samples of Figure S19. Cells highlighted in red indicate ions for which the peak intensity was less than 10 counts which is roughly the noise level and no peak could be seen (spectra from the selected regions only).

CNAu$_x$ fragments		
Ion	**Normalized to CNAu$^-$ intensity**	
	Dendrite of the *standard* RS	**Dendrite of the *hybrid* RS**
CNAu$^-$	1	1
CNAu$_2^-$	1.17E+00	1.26E+00
CNAu$_3^-$	4.29E-02	1.37E-01
CNAu$_4^-$	1.47E-01	1.16E-01
CNAu$_6^-$	3.07E-02	6.32E-02
CNAu$_8^-$	3.07E-02	6.32E-02
CNOAu$_x$ fragments		
Ion	**Normalized to CNOAu$^-$ intensity**	
	Dendrite of the *standard* RS	**Dendrite of the *hybrid* RS**
CNOAu$^-$	1	1
CNOAu$_2^-$	4.84E-01	8.53E-01
CNOAu$_4^-$	1.25E-01	4.41E-01
C$_3$NAu$_x$ fragments		
Ion	**Normalized to C$_3$NAu$^-$ intensity**	
	Dendrite of the *standard* RS	**Dendrite of the *hybrid* RS**
C$_3$NAu$^-$	1	1
C$_3$NAu$_2^-$	4.33E-01	1.38E+00
CNAu$_x$I fragments		
Ion	**Normalized to CNAuI$^-$ intensity**	
	Dendrite of the *standard* RS	**Dendrite of the *hybrid* RS**

CNAuI⁻	1	1
$CNAu_3I^-$	7.83E-02	1.35E-01
$CNAu_5I^-$	3.48E-02	2.03E-02

$C_6NOAu_xI_2$ fragments

Ion	Normalized to $C_6NOAuI_2^-$ intensity	
	Dendrite of the *standard* RS	Dendrite of the *hybrid* RS
$C_6NOAuI_2^-$	1	1
$C_6NOAu_3I_2^-$	4.49E-01	3.54E-01

C_6NOAu_xI fragments

Ion	Normalized to C_6NOAuI^- intensity	
	Dendrite of the *standard* RS	Dendrite of the *hybrid* RS
$C_6NOAu_2I^-$	1	1
$C_6NOAu_4I^-$	6.27E-01	5.74E-01

Au_xI fragments

Ion	Normalized to C_6NOAuI^- intensity	
	Dendrite of the *standard* RS	Dendrite of the *hybrid* RS
AuI⁻	1	1
Au_2I^-	2.00E+00	2.90E+00
Au_3I^-	1.33E-01	2.31E-01
Au_4I^-	3.94E-01	3.83E-01
Au_5I^-	3.19E-02	4.62E-02
Au_6I^-	3.72E-02	1.58E-01
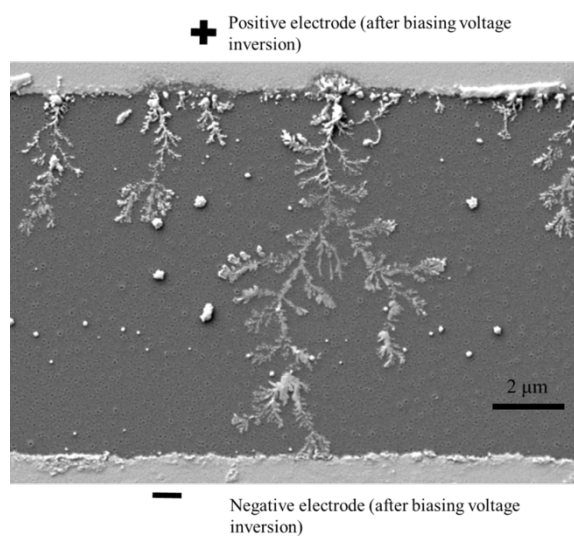
Figure S20. SEM image of the interelectrode region of a thin film of Sigma eumelanin (Cl⁻ 8% wt.) biased for 12 minutes at 1 V and, immediately after, for 12 hours at -1 V. The dendrites that grew in the first 12 minutes (resistive switch after 6 minutes) were not erased by the inversion of the bias that lasted 12 hours. SEM voltage=5 kV.
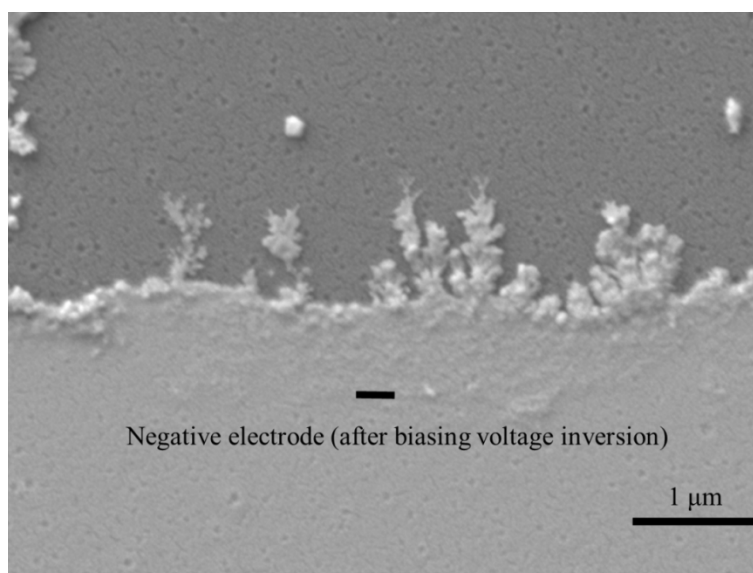
Figure S21. SEM image showing new dendrites starting to nucleate on the negative electrode after the inversion of the polarity of the applied electrical bias, same sample of Figure S20. SEM voltage=5 kV.
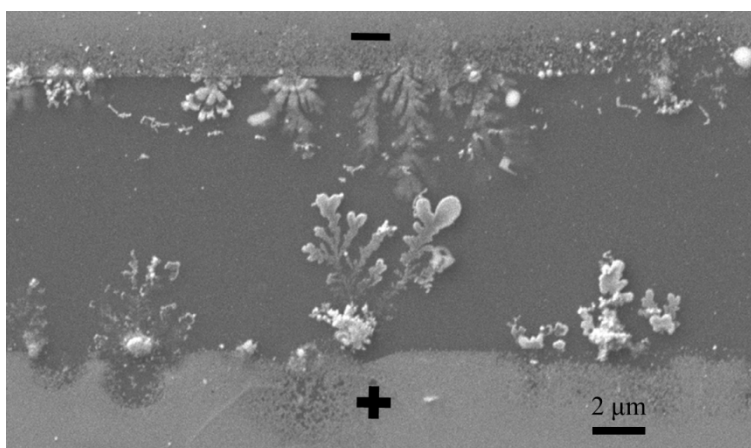
Figure S22. SEM image of dendrites protruding from both Au electrodes. Thin film of Sigma eumelanin (8% wt. Cl⁻), hydrated for 1 hour at 90% RH, biased for ≈21 hours, sweeping voltage 2 mV/s. For each cycle, initial and final bias = 0 V, max bias applied |2.5| V, for 15 cycles. The first switch took place after ≈9 minutes at 1.13 V. SEM voltage=10kV.

APPENDIX B – ARTICLE 5: NATURAL MELANIN PIGMENTS AND THEIR INTERFACES WITH METAL IONS AND OXIDES: EMERGING CONCEPTS AND TECHNOLOGIES

Article 5 is an invited Prospective Article. It has been published in *MRS Communications* in June 2017 (*Eduardo Di Mauro, Ri Xu, Guido Soliveri, and Clara Santato*, "Natural Melanin Pigments and Their Interfaces with Metal Ions and Oxides: Emerging Concepts and Technologies." *MRS Communications* 7, no. 02 (June 11, 2017): 141–51. Doi:10.1557/mrc.2017.33).

204

MRS Communications

Prospective Article

Natural melanin pigments and their interfaces with metal ions and oxides: emerging concepts and technologies

Eduardo Di Mauro, Ri Xu, Guido Soliveri, and **Clara Santato,** Department of Engineering Physics, Polytechnique Montréal, C.P. 6079, Succ. Centre-ville, Montréal, Québec, H3C 3A7, Canada

Address all correspondence to Clara Santato at **clara.santato@polymtl.ca**

Abstract

Melanin (from the Greek μέλας, mélas, black) is a biopigment ubiquitous in flora and fauna, featuring broadband optical absorption, hydration-dependent electrical response, ion-binding affinity as well as antioxidative and radical-scavenging properties. In the human body, photoprotection in the skin and ion flux regulation in the brain are some biofunctional roles played by melanin. Here we discuss the progress in melanin research that underpins emerging technologies in energy storage/conversion, ion separation/water treatment, sunscreens, and bioelectronics. The melanin research aims at developing approaches to explore natural materials, well beyond melanin, which might serve as a prototype benign material for sustainable technologies.

Introduction

The migration of human beings from the tropics to the rest of the globe has been marked by variation in the production of the brown–black melanin pigment of the skin. While hominins near the equator developed dark photoprotective melanin-rich pigmentation due to high ultraviolet (UV) radiation exposure, those settling in low-UVB ($\lambda = 280$–315 nm) environments developed depigmented skin with facultative pigmentation (tanning) to sustain the photosynthesis of vitamin D_3. Melanin is thus a key factor in one of the most noticeable human polymorphisms: skin color.[1]

Humans lacking melanocytes (melanin-producing cells) in the ear and animals with albinism (a deficit or absence of melanin) display hearing conditions as in domestic cats with white fur and blue eyes, thus suggesting a biofunctional role of melanin beyond photoprotection.[2, 3]

In the melanin biopigments family, eumelanin is a brown–black type found in the human body, other mammals, reptiles, amphibians, and fishes as well as in invertebrates, such as cuttlefish and insects; Sepia melanin is a type of natural eumelanin extracted from the ink sac of cuttlefish. Pheomelanin is a yellowish-red melanin.[4, 5]

Eumelanin has been intensively studied in recent decades for functional properties, such as UV–vis absorption, metal chelation, and free radical scavenging. It also features an antioxidant behavior. The limited solubility of eumelanin in most organic solvents has rendered challenging the understanding of its physicochemical properties.[4, 6]

Here, after a brief introduction of molecular structural aspects of eumelanin biopigments and their effect on the properties of the pigment, we critically review the binding

properties of eumelanin toward metal cations and eumelanin–metal oxide interfaces. Eumelanin is involved in the accumulation and release of metal cations in the human body.[7] It is also worthy of note that the interactions between iron and neuromelanin, a pigment made of eumelanin and pheomelanin present in the brain of humans and primates, have been related to Parkinson's disease.[8] The remarkable adhesion properties of melanin-like materials on surfaces, including metal oxides is the underpinning for emerging applications in the biomedical, water treatment, and energy fields.[9, 10]

Molecular aspects of eumelanin: building blocks, free radicals, hierarchical development

Eumelanin consists of building blocks of 5,6-dihydroxyindole (DHI) and 5,6-dihydroxyindole-2-carboxylic acid (DHICA) (Fig. 1).[6] The building blocks can polymerize into eumelanin oligomers and polymers at different molecular sites of the monomers (indicated as 2, 3, 4, 7 in Fig. 1). The presence of two building blocks, different polymerization sites, and redox states [the reduced form is the hydroquinone (H2Q), the intermediate form is the semiquinone (SQ), and the oxidized form is the quinone Q and its tautomer (QI)] co-existing in the pigment result in the well-established chemical heterogeneity of eumelanin.[11]

Hierarchical development characterizes the formation of eumelanin-based materials, generated by supramolecular aggregation. Eumelanin planar oligomers can form from four or more DHI monomers (protomolecules),[11] possibly stacking via π–π interactions (Fig. 2). Tetramers have been proposed as molecular units to explain a number of functional properties of

MRS Communications
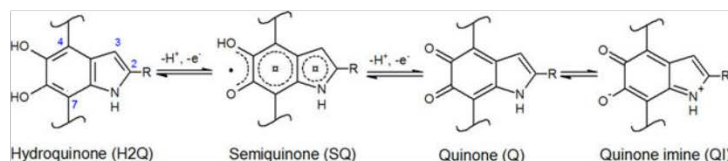
Figure 1. The 5,6-dihydroxyindole (DHI) and 5,6-dihydroxyindole-2-carboxylic acid (DHICA): R is –H in DHI, whereas it is the –COOH group in DHICA. The scheme also illustrates the redox forms of DHI and DHICA: hydroquinone (H2Q), semiquinone (SQ), and quinone (Q). The quinone imine form (QI) is the tautomer of Q.

eumelanin.[13–17] The π–π-stacked eumelanin protomolecules with different sizes, randomly oriented, leading to peculiar excitonic interactions among them, have been proposed to explain the broadband optical absorption of eumelanin (see "Photophysical behavior of eumelanin: absorption spectrum, chromophoric species" section and Fig. 3).[18]

The steric hindrance of the carboxyl groups on the DHICA building blocks causes DHICA to polymerize into non-planar structures, differently from the DHI case. The negative charge, possibly present in the deprotonated carboxyl groups, can induce a further twist in the polymer chain. This leads to rod-shaped assemblies in DHICA polymers (usually referred to as DHICA-melanin, Fig. 2). DHICA-melanin exhibits an absorption peak below 400 nm, which DHI-melanin (solely composed of DHI monomers) does not. In addition, DHICA-melanin has a lower optical absorption in the visible.[12]

Melanin contains intrinsic stationary-free radicals (observed predominantly in the solid state and likely carbon-centered species associated with defects in the polymer backbone),[19–21] with additional extrinsic free radicals generated under UV or visible irradiation or in high hydration conditions.[22–25] The presence of intrinsic radicals is independent of the pH value.[11, 26, 27] DHICA-melanin exhibits hydroxyl radical-scavenging properties in the Fenton reaction, differently from DHI-melanin.[12, 28] DHICA-melanin features relatively homogeneous free-radical species, i.e., spatially confined within restricted segments of the polymer, in contrast to the broader variety of free-radical species generated within the delocalized π-electron systems of the DHI-melanin.

Photophysical behavior of eumelanin: absorption spectrum, chromophoric species

Chemical disorder and geometric disorder models have been proposed to explain the broad optical absorption spectrum of eumelanin. The chemical disorder model posits that eumelanin is made of many chemically distinct species such that its broadband absorption spectrum results from the convolution over the spectra of these species.[29] However, it has been reported that the spectrum is affected by interactions among eumelanin protomolecules.[30] Recently, Buehler and co-workers, considering excitonic couplings between eumelanin oligomers (tetramers, pentamers, and octamers), found that the computational spectra with geometric (packing) disorder of a single species of DHI oligomers (Fig. 3) agree with experiments, and that excitonic couplings among eumelanin protomolecules have a considerable role in the increase of the probability of absorption toward the higher energy end of the spectrum.[18]
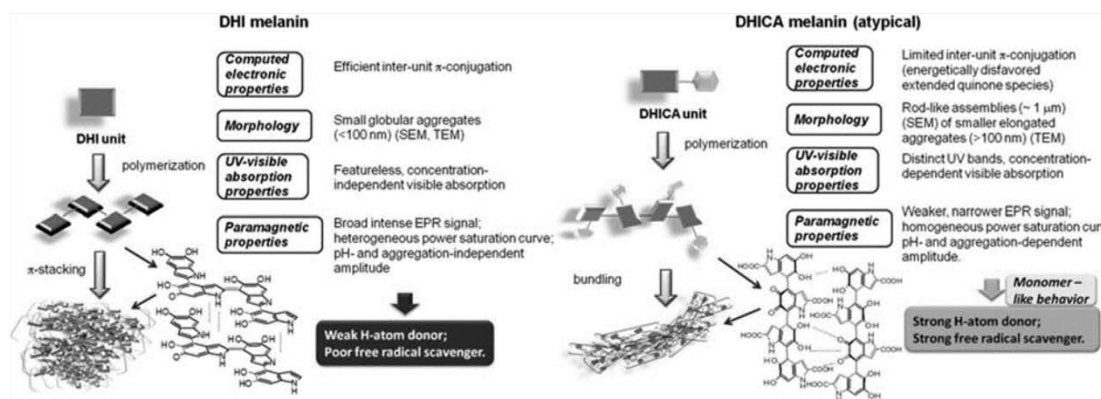
Figure 2. Formation of 5,6-dihydroxyindole (DHI)-melanin [solely composed of DHI monomers, (a)] and 5,6-dihydroxyindole-2-carboxylic acid (DHICA)-melanin [solely composed of DHICA monomers, (b)]. Adapted with permission from Ref. 12. Wiley–VCH, 2013.
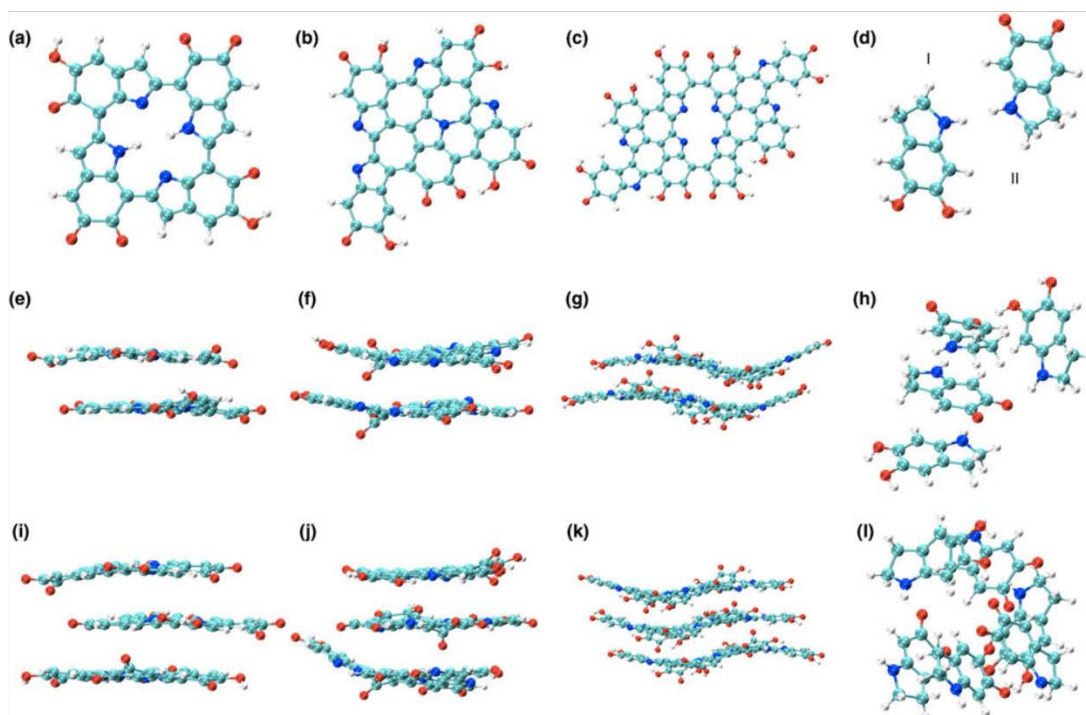
Figure 3. Molecular models and equilibrium structures of small-scale systems in eumelanin. (a) Tetrameric model proposed by Kaxiras et al.;[14] (b) pentameric model, and (c) octameric models proposed by Chen et al. in Refs. 21 and 22 in Ref. 18 (d) monomeric model proposed by Dreyer et al. in Ref. 33 in Ref. 18. Reduced (I) and oxidized (II) forms of the 5,6-dihydroxyindole (DHI) monomer. Two-layer stacked structure of the (e) tetrameric model, (f) pentameric model, and (g) octameric model, respectively. (h) Two-set (two I monomers and two II monomers) stacked structure of the monomeric model. Three-layer stacked structure of the: (i) tetrameric model, (j) pentameric model, and (k) octameric model, respectively. (l) Three-set (three I monomers and three II monomers) stacked structure of the monomeric model. Reprinted with permission from Ref. 18. Nature Publishing Group, 2014.

Electrical response of eumelanin: amorphous semiconductor model, mixed ionic–electronic conduction, electrochemical interfacial processes, and energy storage

Biologic materials, such as proteins, peptides, and melanin, occur naturally in hydrated environments, such that their electrical response includes an important contribution from water-assisted proton transport.[31–34] The electrical properties of eumelanin have fascinated scientists since the late 1960s. After the observation of a reversible resistive switching in eumelanin pellets reported in 1974 by McGinness et al.,[35] the amorphous semiconductor model was adopted to explain the strong hydration dependence of the conductivity. This model considered the increase of the dielectric constant of eumelanin pellets with the increase of the humidity level to explain the decreased activation energy for charge-carrier hopping. Recently, Mostert and co-workers demonstrated that the amorphous semiconductor model does not properly describe the hydration-dependent conductivity of eumelanin pellets. The presence of a comproportionation equilibrium between the reduced (hydroquinone) and oxidized (quinone) forms of

eumelanin to give two semiquinones (intermediate redox species) (Fig. 1) would make eumelanin a mixed ionic–electronic material.[21, 23, 36] Wünsche et al. proposed an explanation of the charge-carrier transport properties of hydrated eumelanin thin films included between metal electrodes with an interplay between proton migration, interfacial metal electrode/eumelanin charge transfer (redox) processes, and electronic transport[37, 38] (Fig. 4). The favorable proton conduction properties of eumelanin have been recently used to demonstrate melanin-based supercapacitors, working in slightly acidic aqueous media, in the absence of metal cations with a well-established affinity for melanin.[39]

Eumelanin and metals: ion chelation in biologic systems, eumelanin/metal electrode interfaces for memory devices, self-assembly on metallic surfaces

The affinity of melanin with pharmaceutical organic compounds has been intensively studied in the past 60 years.[40] Its role in the accumulation and release of metal cations in vivo, such as

MRS Communications
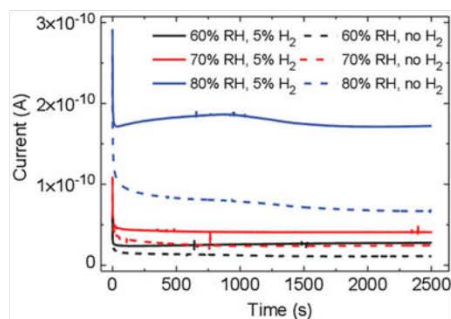
Figure 4. Transient current measurements of a eumelanin film ($d = 50$ nm) with Pd electrodes (electron injecting) and PdHx (proton and electron injecting) contacts ($L = 9$ μm, $W = 20$ μm) at 60, 70, and 80% relative humidity (RH). The applied bias is 0.5 V. Reprinted with permission from Ref. 37. American Chemical Society, 2015.

calcium,[7, 41] copper,[42] zinc,[42, 43] manganese,[44] iron, and other metals,[42, 45, 46] has received great attention, too. The uranyl oxycation has been used to reveal, by scanning electron microscopy (SEM), the presence of eumelanin deposited on carbon-based electrodes in supercapacitors.[39]

The primary binding site for a specific cation with respect to a building block is its most favorable group for binding; if a primary binding site is already occupied, binding will then take place at a secondary binding site.[47] Ion binding includes coulombic electrostatic interactions as well as coordination, possibly through chelation (multidentate binding, from Greek χηλή, chelè, meaning "claw"). The amine and catechol hydroxyl groups of DHI and DHICA as well as the carboxylic group of DHICA can work as primary or secondary binding sites for metal cations[11, 48]; factors determining the binding site for each cation are mainly the type of eumelanin (natural or synthetic) and the pH (Table I). Crucial features of melanogenesis, such as the rate of formation of eumelanin[49] and the relative percentage of the two indolic building blocks present (DHI versus DHICA),[50, 51] are influenced by the presence of metal ions. Whether their influence on self-assembly and structure is significant[52, 53] or not[54] is still a matter of debate.

Neuromelanin, another class of melanins, is a black insoluble pigment found in some (but not all) dopaminergic neurons of three regions of the brain: the "substantia nigra" of the midbrain (where it derives from dopamine), the "locus coeruleus" in the pons and small regions of the "medulla oblongata" (where it derives from noradrenaline) (Fig. 5).[84] Neuromelanin has been reported to have a dichotomous role (adverse or protective): beneficial when it reduces the oxidative stress in the brain due to its ability to bind cations; detrimental when it exacerbates the oxidative stress releasing H_2O_2 or by reducing redox-active metals to a more reactive state.[85–87] Particular efforts have been made in understanding the binding of iron to neuromelanin,[76, 88 95] as iron was reported in dopaminergic neurons of Parkinsonian brains.[8] Recently, Sepia melanin has

been identified as a suitable model to describe the binding characteristics of neuromelanin.[84]

Lately, some studies addressed the interactions between melanin and metal electrodes,[96, 97] after decades of focus on the melanin–metal cation affinity.[47] Hydrated eumelanin thin films proved able to promote the formation of tree-shaped electrically conductive bridges, dendrites, when in contact with gold electrodes, under electrical bias, in a planar configuration.[96] Once the dendrites connected one electrode to the other, the resistivity plummeted: a resistive switch took place. The factors playing a determining role are: the chelating groups of indolic building blocks, the electrical bias, the amount of water, and chlorides, whose presence is highly likely in biomaterials. The amount of water in the thin films was proven to determine two types of switches, standard and hybrid, differing by the orders of magnitude of the current increase at the resistive switch as well as by the dendrite composition (pure gold versus gold–eumelanin complexes)[97] (Fig. 6).

The mechanism of formation of the electrically conductive bridges in hydrated eumelanin thin films is strikingly similar to the working mechanism of resistive switching devices based on electrochemical metallization (electrochemical metallization memory cells).[98] Here, melanin could be considered as biodegradable ion conductor,[99] for the development of "green" non-volatile resistive switching memories.

The binding of the biopigment to monovalent and multivalent cations has been recently exploited in melanin-based electrochemical storage devices.[58, 79]

Polydopamine, a synthetic melanin analog, has been used to selectively extract and separate metal cations from aqueous solutions, leveraging on the different binding affinities of the pigments toward different cations.[67, 100, 101] Films of polydopamine can reduce Ag^+ cations into Ag nanoparticles, which impart antibacterial properties to the same films.[83]

Self-assembled molecular networks of indole-2-carboxylic acid (I2CA, i.e., melanin's monomer DHICA lacking the two hydroxyl phenolic groups) have been investigated on Au (111) surfaces: I2CA showed, both in ultrahigh vacuum and at liquid/solid interfaces, hydrogen-bonded assemblies from molecular dimers,[102] the next step being the same study with DHI and DHICA. This study represents an important contribution in understanding, at the nanoscale, the process of formation of melanin, from the building blocks to the polymers.

Melanin/metal oxides interfaces: adhesion, biocompatibility, and photosensitization technologies

The underpinning of emerging technologies making use of interfaces between melanin and metal oxides is melanin biocompatibility together with its optical absorption and charge-carrier transport properties. Such interfaces are largely undiscovered since the poor processability of melanin thwarts contact between the pigment and the surface of the oxides. Nevertheless, promising results have been obtained with synthetic melanin-like polymers, e.g., polydopamine.[10, 103]

Table I. Molecular sites used by the indicated metal cations to bind to the melanin biopigments (synthetic and natural); dopa, 3,4-dihydroxyphenyl-alanine; 5,6-dimethoxyindole-2-carboxylic acid (DMICA)-melanin, synthetic melanin-like material from the oxidative polymerization of DMICA.

Metal cation	Binding site		
	Hydroxyl group	Carboxylic group	Amine
Zn^{2+}	L-dopa[43, 55]	Natural (Sepia,[48, 56] bovine eye[41])	5,6-Dihydroxyindole (DHI)-melanin (QI)[57]
Mg^{2+}	Natural (Sepia[58])	Natural (bovine eye,[41, 45] Sepia,[48, 56, 59] squid[60]), dopa-melanin[45]	
Ca^{2+}		Natural (bovine eye,[41, 45] Sepia,[48, 56, 59, 61] squid[60]), dopa-melanin[45]	
Fe^{3+}	Natural (Sepia,[56, 59, 62] human hair,[63] black rabbit hair[64]), neuromelanin,[65–67] dopa,[68–70] catechols,[71] polydopamine,[72–74] DHI-melanin,[63] melanin from cys-dopamine,[75] diethylamine–dopamine–melanin[74]	Neuromelanin,[76] dopa-melanin,[74] natural (Sepia),[74] diethylamine–dopamine–melanin[74]	Natural (Sepia),[56] neuromelanin,[76] melanin from cys-dopamine,[75] polydopamine,[74] diethylamine–dopamine–melanin[74]
Cu^{2+}	L-dopa,[55] natural (Sepia,[48, 56] bovine eye,[77] black rabbit hair[64]), catechol melanin,[25] dopa-melanin[25]	Natural [bovine eye,[45, 77] Sepia (secondary)],[48] dopa-melanin,[25, 45, 65, 66] catechol melanin[25]	Natural [bovine eye,[77] Sepia (secondary)],[48] DHI-melanin (QI),[57] L-dopa,[55] dopa-melanin[25, 66]
Ni^{2+}	Natural [bovine eye (secondary)][76]	Natural (bovine eye),[45, 76] dopa-melanin[45]	L-dopa[55]
Co^{2+}	L-dopa,[55] natural (black rabbit hair)[64]	Dopa-melanin,[45] natural (bovine eye)[45]	
Pb^{2+}	Natural (squid[60])	Dopa-melanin,[78] natural (mouse melanoma)[78]	Natural (squid)[60]
Cs^+		Natural (bovine eye),[45] dopa-melanin[45]	
Rb^+		Natural (bovine eye),[45] dopa-melanin[45]	
K^+		Natural (bovine eye),[45] dopa-melanin[45]	Tyrosine-melanin (Sigma)[52]
Na^+		Natural (bovine eye,[45] squid,[60] Sepia[79]), dopa-melanin,[45] tyrosine–melanin (Sigma),[79] DMICA-melanin[79, 80]	Tyrosine–melanin (Sigma),[79] sepia,[79] DMICA-melanin[79, 80]
Li^+		Natural (bovine eye),[45] dopa-melanin[45]	
Ba^{2+}		Natural (bovine eye),[45] dopa-melanin[45]	
Sr^{2+}		Natural (bovine eye),[45] dopa-melanin[45]	
Tl^+		Natural (bovine eye),[45] dopa-melanin[45]	
Mn^{2+}	Dopa-melanin[81]	Natural (bovine eye),[45] dopa-melanin[45, 81]	Dopa-melanin[81]
La^{3+}		Natural (bovine eye),[45] dopa-melanin[45]	
Gd^{3+}		Natural (bovine eye),[45] dopa-melanin[45]	
Cd^{2+}		Natural (squid[60])	
Al^{3+}	Dopa-melanin[81]	Dopa-melanin[81]	Dopa-melanin[81]
Uranium (uranyl oxycation)		Dopa-melanin[46]	
Vanadium (vanadyl oxycation)	Dopa-melanin[66]		

Continued

MRS Communications

Table I. Continued

Metal cation	Binding site		
	Hydroxyl group	Carboxylic group	Amine
Au^+	Catechol (binding as organometallic complex)[82]		
Ag^+	Polydopamine[83]		

Adhesive proteins (rich in dopa and lysine amino acids) present in *Mytilus edulis* (mussels) inspired a method of making polydopamine coatings, featuring catechol (ortho-hydroquinone of dopa) and amine (lysine) functions, through simple dip coating in aqueous solutions of dopamine on a wide range of materials, including metal oxides.[9, 104]

Based on its ion-chelating properties, polydopamine has been used as a template to assemble nanoarchitectures[105, 106] and core (inorganic)-shell (polydopamine) nanoparticles.[10, 107] Fe_3O_4-polydopamine core–shell nanoparticles have been used for a wide range of technologic applications,[108, 109] including peroxidase-like catalysis for treatment of industrial waste and environmental monitoring.[110] Superhydrophobic and supero-leophilic particles, obtained by modification with low surface energy materials of Fe_3O_4 on polydopamine particles have been used for oil/water separation.[111] Iminodiacetic acid-Cu functionalized core–satellite Fe_3O_4/polydopamine/Au magnetic nanocomposites have been used for protein detection.[112]

Multifunctional nanocomposites can integrate sensing, diagnostic, and therapeutic functions into a single nanostructure. Fe_3O_4–polydopamine core–shell nanocomposites have been fabricated through in situ polymerization. Their ability to act as theranostic agents for intracellular mRNA detection and multimodal imaging-guided photothermal therapy has been reported.[113, 114] This work exploited polydopamine near-infrared absorption, high fluorescence quenching efficiency and the availability of a surface for further functionalization with biomolecules.

Graeff and co-workers prepared melanin-like/V_2O_5-layered hybrids for application in optoelectronics and electrochemistry, starting from dopa.[115] The presence of melanin-like units induced the reduction of V^{5+} ions to V^{4+} ions. The melanin insertion was observed to increase the stability and reproducibility of Li^+ electrochemical insertion/de-insertion.

Well-investigated metal oxide semiconductors, such as TiO_2, have been coupled to melanin or melanin-like polymers
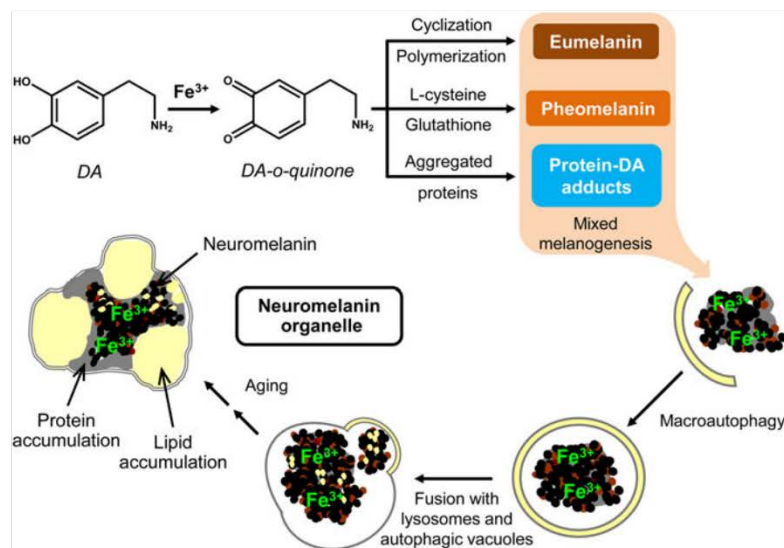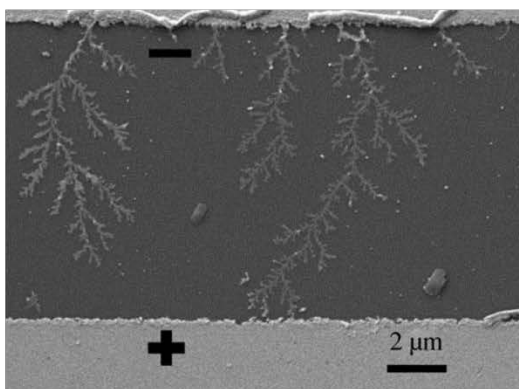

Figure 5. Possible neuromelanin formation mechanism. Reprinted with permission from Ref. 85. Elsevier, 2015.

Figure 6. Scanning electron microscopy (SEM) image of dendrites bridging one electrode to the other after 3 h of electrical bias at 1 V in a thin film of Sepia eumelanin (7 wt.% Cl⁻), hydrated for 1 h at 90% relative humidity (RH), deposited between Au electrodes (10 μm interelectrode distance). The resistive switch took place after 34 min. SEM voltage 5 kV. Reprinted with permission from Ref. 97. Royal Society of Chemistry, 2016.

for applications in solar energy conversion/storage. Purified natural melanin from squid ink and mussel-inspired synthetic polydopamine have been used as dyes in dye-sensitized solar cells.[103, 116] Polydopamine/TiO_2 nanocomposites and plasmonic structures fabricated exploiting the reducing properties of polydopamine have been used for photocatalytic applications.[117–119]

The biocompatibility and optical properties featured by TiO_2 have been used for self-cleaning, self-sterilization, and photolithography purposes[120, 121] and also in fields such as cosmetics, where TiO_2 has been used as filler and

UV-filter.[122] To ensure transparency to cosmetic formulations, the average dimension of TiO_2 particles has been typically of the order of 10–20 nm. Safety concerns about nano-TiO_2-based products have been raised.[123–125] Reports suggest that TiO_2 nanoparticles do not penetrate the intact epidermal barrier,[126, 127] with no evidence of significant penetration beyond the stratum corneum.[128] Melanin is used in cosmetic products, sometimes in combination with photoactive oxides. Melanin (both synthetic and natural)–TiO_2 interactions have been investigated,[129–131] in particular the photocatalytic activity of TiO_2 on the process of DHICA polymerization (Fig. 7).[132]

To conclude this Prospective article highlighting the exciting achievements reported in the field of melanin-based materials in recent years, we would like to emphasize the importance of an interdisciplinary approach for melanin research, where materials chemistry, physical chemistry, and materials physics all must be considered to effectively advance both the understanding of fundamental process in electrochemistry, photophysics, and transport physics, and the development of sustainable technologies. We believe this holistic approach will contribute to the advancement of knowledge about the functional properties of melanin-based materials in biologic systems.

At the fundamental level, exciting challenges loom for the melanin research community, such as (i) understanding the electron transfer processes in different electrolytes for sensing (and biosensing) as well as energy conversion/storage; (ii) advancing the knowledge of electron transport and proton transport in quasi-solid state for applications in (bio)electronics, e.g., protonic devices, edible devices, and transient electronics; (iii) gaining further insights into the nature of chromophoric units of melanin for photoprotection and solar energy conversion; (iv) establishing biocompatibility and biodegradability
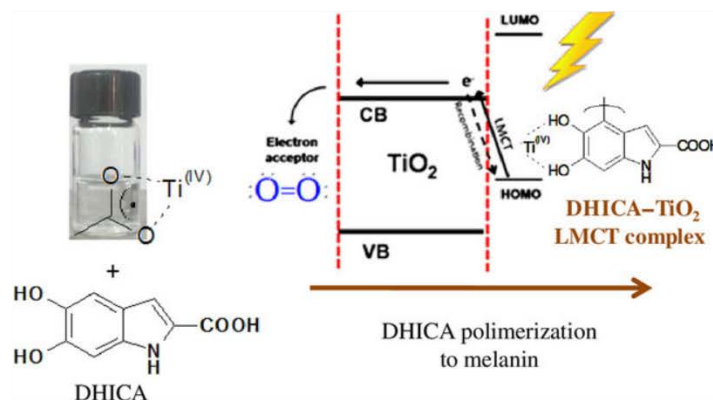
Figure 7. Photocatalytic activity of TiO_2 for 5,6-dihydroxyindole-2-carboxylic acid (DHICA) polymerization and formation of melanin–TiO_2 hybrid nanostructures with biocide behavior. Adapted with permission from Ref. 132. American Chemical Society, 2016.

MRS Communications

according to international standards; and (v) quantifying the physicochemical parameters defining ion binding for ion separation and water treatment.

Acknowledgments

References

1. N.G. Jablonski and G. Chaplin: Human skin pigmentation as an adaptation to UV radiation. *Proc. Natl. Acad. Sci. USA* **107**, 8962 (2010).
2. S. Murillo-cuesta, J. Contreras, E. Zurita, R. Cediel, and M. Cantero: Melanin precursors prevent premature age-related and noise-induced hearing loss in albino mice. *Pigment Cell Melanoma Res.* **23**, 72 (2009).
3. J. Borovansky: *Melanins and Melanosomes: Biosynthesis, Structure, Physiological and Pathological Functions* (Wiley–Blackwell, Weinheim, Germany, 2011).
4. M. d'Ischia, K. Wakamatsu, F. Cicoira, E. Di Mauro, J.C. Garcia-Borron, S. Commo, I. Galván, G. Ghanem, K. Kenzo, P. Meredith, A. Pezzella, C. Santato, T. Sarna, J.D. Simon, L. Zecca, F.A. Zucca, A. Napolitano, and S. Ito: Melanins and melanogenesis: from pigment cells to human health and technological applications. *Pigment Cell Melanoma Res.* **28**, 520 (2015).
5. H. Lamb: *Hydrodynamics*, 6th ed. (Cambridge University Press: Cambridge, England, 1940), pp. 573, 645.
6. G. Prota: *Melanins and Melanogenesis* (Academic Press, San Diego, USA, 1992).
7. B.J. Panessa and J.A. Zadunaisky: Pigment granules: a calcium reservoir in the vertebrate eye. *Exp. Eye Res.* **32**, 593 (1981).
8. D. Ben-Shachar and M.B.H. Youdim: Iron, melanin and dopamine interaction: relevance to Parkinson's disease. *Prog. Neuropsychopharmacol. Biol. Psychiatry* **17**, 139 (1993).
9. H. Lee, S.M. Dellatore, W.M. Miller, and P.B. Messersmith: Mussel-inspired surface chemistry for multifunctional coatings. *Science* **318**, 426 (2007).
10. Y. Liu, K. Ai, and L. Lu: Polydopamine and its derivative materials: synthesis and promising applications in energy, environmental, and biomedical fields. *Chem. Rev.* **114**, 5057 (2014).
11. M. d'Ischia, A. Napolitano, A. Pezzella, P. Meredith, and T. Sarna: Chemical and structural diversity in eumelanins: unexplored bio-optoelectronic materials. *Angew. Chem. – Int. Ed.* **48**, 3914 (2009).
12. L. Panzella, G. Gentile, G. D'Errico, N.F. Della Vecchia, M.E. Errico, A. Napolitano, C. Carfagna, and M. D'Ischia: Atypical structural and π-electron features of a melanin polymer that lead to superior free-radical-scavenging properties. *Angew. Chem. – Int. Ed.* **52**, 12684 (2013).
13. S. Meng, E. Kaxiras, A. Pezzella, L. Panzella, A. Natangelo, M. Arzillo, A. Napolitano, and M. D'Ischia: Theoretical models of eumelanin protomolecules and their optical properties. *J. Org. Chem.* **72**, 9225 (2007).
14. E. Kaxiras, A. Tsolakidis, G. Zonios, and S. Meng: Structural model of eumelanin. *Phys. Rev. Lett.* **97**, 218102 (2006).
15. Y.J. Kim, A. Khetan, W. Wu, S.-E. Chun, V. Viswanathan, J.F. Whitacre, and C.J. Bettinger: Evidence of porphyrin-like structures in natural melanin pigments using electrochemical fingerprinting. *Adv. Mater.* **28**, 3173 (2016).
16. A. Pezzella, L. Panzella, A. Natangelo, M. Arzillo, A. Napolitano, and M. D'Ischia: 5,6-Dihydroxyindole tetramers with 'anomalous' interunit bonding patterns by oxidative coupling of 5,5',6,6'-tetrahydroxy-2,7'-biindolyl: emerging complexities on the way toward an improved model of eumelanin buildup. *J. Org. Chem.* **72**, 9225 (2007).
17. C.T. Chen, V. Ball, J.J. De Almeida Gracio, M.K. Singh, V. Toniazzo, D. Ruch, and M.J. Buehler: Self-assembly of tetramers of 5,6-dihydroxyindole explains the primary physical properties of eumelanin: experiment, simulation, and design. *ACS Nano* **7**, 1524 (2013).
18. C-T. Chen, C. Chuang, J. Cao, V. Ball, D. Ruch, and M.J. Buehler: Excitonic effects from geometric order and disorder explain broadband optical absorption in eumelanin. *Nat. Commun.* **5**, 3859 (2014).
19. B-L.L. Seagle, E.M. Gasyna, W.F. Mieler, and J.R. Norris: Photoprotection of human retinal pigment epithelium cells against blue light-induced apoptosis by melanin free radicals from *Sepia officinalis. Proc. Natl. Acad. Sci. USA* **103**, 16644 (2006).
20. T. Sarna: Properties and function of the ocular melanin – a photobiophysical view. *J. Photochem. Photobiol. B Biol.* **12**, 215 (1992).
21. R. Sealy, C. Felix, J. Hyde, and H. Swartz: Structure and reactivity of melanins: influence of free radicals and metal ions. In *Free Radicals in Biology*, edited by W. Pryor (Academic Press, New York, NY, 1980), vol. **4**, pp. 209–259.
22. P. Meredith and T. Sarna: The physical and chemical properties of eumelanin. *Pigment Cell Res.* **19**, 572 (2006).
23. B. Mostert, B.J. Powell, F.L. Pratt, G.R. Hanson, T. Sarna, I.R. Gentle, and P. Meredith: Role of semiconductivity and ion transport in the electrical conduction of melanin. *Proc. Natl. Acad. Sci. USA* **109**, 8943 (2012).
24. M.S. Blois, A.B. Zahlan, and J.E. Maling: Electron spin resonance studies on melanin. *Biophys. J.* **4**, 471 (1964).
25. W. Froncisz, T. Sarna, and J.S. Hyde: Cu^{2+} probe of metal-ion binding sites in melanin using electron paramagnetic resonance spectroscopy, synthetic melanins. *Arch. Biochem. Biophys.* **202**, 289 (1980).
26. M. Pasenkiewicz-Gierula and R.C. Sealy: Analysis of the ESR spectrum of synthetic dopa melanin. *Biochim. Biophys. Acta – Gen. Subj.* **884**, 510 (1986).
27. J.M. Nilges: *The Pigmentary System, Physiology and Pathophysiology* (Oxford University Press, New York, USA, 1998).
28. S. Jiang, X-M. Liu, X. Dai, Q. Zhou, T-C. Lei, F. Beermann, K. Wakamatsu, and S.-Z. Xu: Regulation of DHICA-mediated antioxidation by dopachrome tautomerase: implication for skin photoprotection against UVA radiation. *Free Radic. Biol. Med.* **48**, 1144 (2010).
29. M.L. Tran, B.J. Powell, and P. Meredith: Chemical and structural disorder in eumelanins: a possible explanation for broadband absorbance. *Biophys. J.* **90**, 743 (2006).
30. K.B. Stark, J.M. Gallas, G.W. Zajac, M. Eisner, and J.T. Golab: Spectroscopic study and simulation from recent structural models for eumelanin: I. Monomer, dimers. *J. Phys. Chem. B* **107**, 3061 (2003).
31. M.R. Powell and B. Rosenberg: The nature of the charge carriers in solvated biomacromolecules, *J. Bioenerg.* **1**, 493 (1970).
32. P. Meredith, C.J. Bettinger, M. Irimia-Vladu, A.B. Mostert, and P.E. Schwenn: Electronic and optoelectronic materials and devices inspired by nature. *Rep. Prog. Phys.* **76**, 34501 (2013).
33. M. Amit, S. Appel, R. Cohen, G. Cheng, I.W. Hamley, and N. Ashkenasy: Hybrid proton and electron transport in peptide fibrils. *Adv. Funct. Mater.* **24**, 5873 (2014).
34. Z. Hemmatian, S. Keene, E. Josberger, T. Miyake, C. Arboleda, J. Soto-Rodríguez, F. Baneyx, and M. Rolandi: Electronic control of H^+ current in a bioprotonic device with Gramicidin A and Alamethicin. *Nat. Commun.* **7**, 12981 (2016).
35. J. McGinness, P. Corry, and P. Proctor: Amorphous semiconductor switching in melanins. *Science* **183**, 853 (1974).
36. S.B. Rienecker, A.B. Mostert, G. Schenk, G.R. Hanson, and P. Meredith: Heavy water as a probe of the free radical nature and electrical conductivity of melanin. *J. Phys. Chem. B* **119**, 14994 (2015).
37. J. Wünsche, Y. Deng, P. Kumar, E. Di Mauro, E. Josberger, J. Sayago, A. Pezzella, F. Soavi, F. Cicoira, M. Rolandi, and C. Santato: Protonic and electronic transport in hydrated thin films of the pigment eumelanin. *Chem. Mater.* **27**, 436 (2015).
38. J. Wünsche, F. Cicoira, C.F.O. Graeff, and C. Santato: Eumelanin thin films: solution-processing, growth, and charge transport properties. *J. Mater. Chem. B* **1**, 3836 (2013).
39. P. Kumar, E. Di Mauro, S. Zhang, A. Pezzella, F. Soavi, C. Santato, and F. Cicoira: Melanin-based flexible supercapacitors. *J. Mater. Chem. C* **4**, 9516 (2016).

40. C.R. Borges, J.C. Roberts, D.G. Wilkins, and D.E. Rollins: Cocaine, benzoylecgonine, amphetamine, and N-acetylamphetamine binding to melanin subtypes. *J. Anal. Toxicol.* **27**, 125 (2003).

41. L. Hong and J.D. Simon: Physical and chemical characterization of iris and choroid melanosomes isolated from newborn and mature cows. *Photochem. Photobiol.* **81**, 517 (2007).

42. J. Andrzejczak and E. Buszman: Interaction of Fe^{3+}, Cu^{2+} and Zn^{2+} with melanin and melanoproteins from bovine eyes. *Acta Biochim. Pol.* **39**, 85 (1992).

43. J. Borovanský: Zinc in pigmented cells and structures, interactions and possible roles. *Sb. Lékasky J.* **95**, 309 (1994).

44. A. Lydén, B.S. Larsson, and N.G. Lindquist: Melanin affinity of manganese. *Acta Pharmacol. Toxicol. (Copenh).* **55**, 133 (1984).

45. B. Larsson and H. Tjälve: Studies on the melanin-affinity of metal ions. *Acta Physiol. Scand.* **104**, 479 (1978).

46. A.S. Saini and J.S. Melo: Biosorption of uranium by melanin: kinetic, equilibrium and thermodynamic studies. *Bioresour. Technol.* **149**, 155 (2013).

47. L. Hong and J.D. Simon: Current understanding of the binding sites, capacity, affinity, and biological significance of metals in melanin. *J. Phys. Chem. B* **111**, 7938 (2007).

48. L. Hong and J.D. Simon: Insight into the binding of divalent cations to Sepia eumelanin from IR absorption spectroscopy. *Photochem. Photobiol.* **82**, 1265 (2006).

49. J-U. Sutter and D.J.S. Birch: Metal ion influence on eumelanin fluorescence and structure. *Meth. Appl. Fluoresc.* **2**, 24005 (2014).

50. A. Palumbo, F. Solano, G. Misuraca, P. Aroca, J.C. Garcia Borron, J. A. Lozano, and G. Prota: Comparative action of dopachrome tautomerase and metal ions on the rearrangement of dopachrome. *Biochim. Biophys. Acta – Gen. Subj.* **1115**, 1 (1991).

51. A. Palumbo, M. D'Ischia, G. Misuraca, G. Prota, and T.M. Schultz: Structural modifications in biosynthetic melanins induced by metal ions. *Biochim. Biophys. Acta – Gen. Subj.* **964**, 193 (1988).

52. L.G. Albano, E. Di Mauro, P. Kumar, F. Cicoira, C.F. Graeff, and C. Santato: Novel insights on the physicochemical properties of eumelanins and their DMSO derivatives. *Polym. Int.* **26**, 19007 (2016).

53. J.M. Gallas, K.C. Littrell, S. Seifert, G.W. Zajac, and P. Thiyagarajan: Solution structure of copper ion-induced molecular aggregates of tyrosine melanin. *Biophys. J.* **77**, 1135 (1999).

54. Y. Liu and J.D. Simon: Metal-ion interactions and the structural organization of Sepia eumelanin. *Pigment Cell Res.* **18**, 42 (2005).

55. T. Kiss and A. Gergely: Complexes of 3,4-dihydroxyphenyl derivatives. VI. Microprocesses of formation of proton and metal complexes of L-dopa. *Inorg. Chim. Acta* **78**, 247 (1983).

56. L. Hong, Y. Liu, and J.D. Simon: Binding of metal ions to melanin and their effects on the aerobic reactivity. *Photochem. Photobiol.* **80**, 477 (2004).

57. B. Szpoganicz, S. Gidanian, P. Kong, and P. Farmer: Metal binding by melanins: studies of colloidal dihydroxyindole-melanin, and its complexation by Cu(II) and Zn(II) ions. *J. Inorg. Biochem.* **89**, 45 (2002).

58. Y.J. Kim, W. Wu, S-E. Chun, J.F. Whitacre, and C.J. Bettinger: Catechol-mediated reversible binding of multivalent cations in eumelanin half-cells. *Adv. Mater.* **26**, 6572 (2014).

59. Y. Liu, L. Hong, V.R. Kempf, K. Wakamatsu, S. Ito, and J.D. Simon: Ion-exchange and adsorption of Fe(III) by Sepia melanin. *Pigment Cell Res.* **17**, 262 (2004).

60. S. Chen, C. Xue, J. Wang, H. Feng, Y. Wang, Q. Ma, and D. Wang: Adsorption of Pb(II) and Cd(II) by squid *Ommastrephes bartramii* melanin. *Bioinorg. Chem. Appl.* **2009**, 1 (2009).

61. W.D. Bush and J.D. Simon: Quantification of Ca^{2+} binding to melanin supports the hypothesis that melanosomes serve a functional role in regulating calcium homeostasis. *Pigment Cell Res.* **20**, 134 (2007).

62. A. Samokhvalov, Y. Liu, and J.D. Simon: Characterization of the Fe (III)-binding site in Sepia eumelanin by resonance Raman confocal microspectroscopy. *Photochem. Photobiol.* **80**, 84 (2007).

63. T.G. Costa, R. Younger, C. Poe, P.J. Farmer, and B. Szpoganicz: Studies on synthetic and natural melanin and its affinity for Fe(III) ion. *Bioinorg. Chem. Appl.* **2012**, 1 (2012).

64. H. Kikkawa, Z. Ogita, and S. Fujito: Nature of pigments derived from tyrosine and tryptophan in animals. *Science* **121**, 43 (1955).

65. L. Najder-Kozdrowska, B. Pilawa, A.B. Wieckowski, E. Buszman, and D. Wrześniok: Influence of copper(II) ions on radicals in DOPA-melanin. *Appl. Magn. Reson.* **36**, 81 (2009).

66. J. Stainsack, A.S. Mangrich, C.M.B.F. Maia, V.G. Machado, J.C.P. dos Santos, and S. Nakagaki: Spectroscopic investigation of hard and soft metal binding sites in synthetic melanin. *Inorg. Chim. Acta* **356**, 243 (2003).

67. H-A. Park, Y.J. Kim, I.S. Kwon, L. Klosterman, and C.J. Bettinger: Lithium purification from aqueous solutions using bioinspired redox-active melanin membranes. *Polym. Int.* **65**, 1331 (2016).

68. P.K. Grzyska, T.A. Müller, M.G. Campbell, and R.P. Hausinger: Metal ligand substitution and evidence for quinone formation in taurine/α-ketoglutarate dioxygenase. *J. Inorg. Biochem.* **101**, 797 (2007).

69. M.J. Harrington, A. Masic, N. Holten-Andersen, J.H. Waite, and P. Fratzl: Iron-clad fibers: a metal-based biological strategy for hard flexible coatings. *Science* **328**, 216 (2010).

70. B.P. Lee, P.B. Messersmith, J.N. Israelachvili, and J.H. Waite: Mussel-inspired adhesives and coatings. *Annu. Rev. Mater. Res.* **41**, 99 (2011).

71. N. Holten-Andersen, M.J. Harrington, H. Birkedal, B.P. Lee, P. B. Messersmith, K.Y.C. Lee, and J.H. Waite: pH-induced metal-ligand cross-links inspired by mussel yield self-healing polymer networks with near-covalent elastic moduli. *Proc. Natl. Acad. Sci. USA* **108**, 2651 (2011).

72. L. Klosterman and C. Bettinger: Calcium-mediated control of polydopamine film oxidation and iron chelation. *Int. J. Mol. Sci.* **18**, 14 (2016).

73. A.J. Kropf, B.A. Bunker, M. Eisner, S.C. Moss, L. Zecca, A. Stroppolo, and P.R. Crippa: X-ray absorption fine-structure spectroscopy studies of Fe sites in natural human neuromelanin and synthetic analogues. *Biophys. J.* **75**, 3135 (1998).

74. L. Bardani, M. Bridelli, M. Carbucicchio, and P. Crippa: Comparative Mössbauer and infrared analysis of iron-containing melanins. *Biochim. Biophys. Acta – Gen. Subj.* **716**, 8 (1982).

75. M.G. Bridelli, D. Tampellini, and L. Zecca: The structure of neuromelanin and its iron binding site studied by infrared spectroscopy. *FEBS Lett.* **457**, 18 (1999).

76. B. Larsson and H. Tjälve: Studies on the mechanism of drug-binding to melanin. *Biochem. Pharmacol.* **28**, 1181 (1979).

77. T. Sarna, W. Froncisz, and J.S. Hyde: Cu^{2+} probe of metal-ion binding sites in melanin using electron paramagnetic resonance spectroscopy. *Nat. Melanin Arch. Biochem. Biophys.* **202**, 304 (1980).

78. F.W. Bruenger, B.J. Stover, and D.R. Atherton: The incorporation of various metal ions into *in vivo*- and *in vitro*-produced melanin. *Radiat. Res.* **32**, 1 (1967).

79. Y.J. Kim, W. Wu, S.-E. Chun, J.F. Whitacre, and C.J. Bettinger: Biologically derived melanin electrodes in aqueous sodium-ion energy storage devices. *Proc. Natl. Acad. Sci. USA* **110**, 20912 (2013).

80. L.K. Povlich, J. Le, J. Kim, and D.C. Martin: Poly(5,6-dimethoxyindole-2-carboxylic acid) (PDMICA): a melanin-like polymer with unique electrochromic and structural properties. *Macromolecules* **43**, 3770 (2010).

81. S. Aime, M. Botta, and I. Camurati: NMR studies of L-dopa melanin-manganese(II) complex in water solution. *J. Inorg. Biochem.* **36**, 1 (1989).

82. C.G. Pierpont and C.W. Lange: *The Chemistry of Transition Metal Complexes Containing Catechol and Semiquinone Ligands* (John Wiley & Sons, Inc, New York, USA, 2007).

83. V. Ball, I. Nguyen, M. Haupt, C. Oehr, C. Arnoult, V. Toniazzo, and D. Ruch: The reduction of Ag+ in metallic silver on pseudomelanin films allows for antibacterial activity but does not imply unpaired electrons. *J. Colloid Interface Sci.* **364**, 359 (2011).

84. R.L. Schroeder, K.L. Double, and J.P. Gerber: Using Sepia melanin as a PD model to describe the binding characteristics of neuromelanin – a critical review. *J. Chem. Neuroanat.* **64–65**, 20 (2015).

85. F.A. Zucca, J. Segura-Aguilar, E. Ferrari, P. Muñoz, I. Paris, D. Sulzer, T. Sarna, L. Casella, and L. Zecca: Interactions of iron, dopamine and neuromelanin pathways in brain aging and Parkinson's disease. *Prog. Neurobiol.* (2015). In press.

86. W.S. Enochs, T. Sarna, L. Zecca, P.A. Riley, and H.M. Swartz: The roles of neuromelanin, binding of metal ions, and oxidative cytotoxicity in the

pathogenesis of Parkinson's disease: a hypothesis. *J. Neural Transm. – Park. Dis. Dement. Sect.* **7**, 83 (1994).

87. T. Sarna and H.M. Swartz: *The Pigmentary System: Physiology and Pathophysiology* (Wiley-Blac, Oxford, UK, 2006).

88. T. Shima, T. Sarna, H.M. Swartz, A. Stroppolo, R. Gerbasi, and L. Zecca: Binding of iron to neuromelanin of human substantia nigra and synthetic melanin: an electron paramagnetic resonance spectroscopy study. *Free Radic. Biol. Med.* **23**, 110 (1997).

89. K. Jellinger, E. Kienzl, G. Rumpelmair, P. Riederer, H. Stachelberger, D. Ben-Shachar, and M.B.H. Youdim: Iron-melanin complex in substantia nigra of parkinsonian brains: an X-ray microanalysis. *J. Neurochem.* **59**, 1168 (1992).

90. D. Ben-Shachar, P. Riederer, and M.B.H. Youdim: Iron-melanin interaction and lipid peroxidation: implications for Parkinson's disease. *J. Neurochem.* **57**, 1609 (1991).

91. M.B.H. Youdim, D. Ben-Shachar, and P. Riederer: Is Parkinson's disease a progressive siderosis of substantia nigra resulting in iron and melanin induced neurodegeneration?. *Acta Neurol. Scand.* **80**, 47 (1989).

92. L. Zecca, D. Tampellini, A. Gatti, R. Crippa, M. Eisner, D. Sulzer, S. Ito, R. Fariello, and M. Gallorini: The neuromelanin of human substantia nigra and its interaction with metals. *J. Neural Transm.* **109**, 663 (2002).

93. D.T. Dexter, F.R. Wells, A.J. Lee, F. Agid, Y. Agid, P. Jenner, and C.D. Marsden: Increased nigral iron content and alterations in other metal ions occurring in brain in Parkinson's disease. *J. Neurochem.* **52**, 1830 (1989).

94. E.C. Hirsch, J-P. Brandel, P. Galle, F. Javoy-Agid, and Y. Agid: Iron and aluminum increase in the substantia nigra of patients with Parkinson's disease: an X-ray microanalysis. *J. Neurochem.* **56**, 446 (1991).

95. L. Zecca, M. Gallorini, V. Schünemann, A.X. Trautwein, M. Gerlach, P. Riederer, P. Vezzoni, and D. Tampellini: Iron, neuromelanin and ferritin content in the substantia nigra of normal subjects at different ages: consequences for iron storage and neurodegenerative processes. *J. Neurochem.* **76**, 1766 (2001).

96. J. Wünsche, L. Cardenas, F. Rosei, F. Cicoira, R. Gauvin, C.F.O. Graeff, S. Poulin, A. Pezzella, and C. Santato: *In situ* formation of dendrites in eumelanin thin films between gold electrodes. *Adv. Funct. Mater.* **23**, 5591 (2013).

97. E. Di Mauro, O. Carpentier, S.I. Yáñez Sánchez, N. Ignoumba Ignoumba, M. Lalancette-Jean, J. Lefebvre, S. Zhang, C.F.O. Graeff, F. Cicoira, and C. Santato: Resistive switching controlled by the hydration level in thin films of the biopigment eumelanin. *J. Mater. Chem. C* **4**, 9544 (2016).

98. I. Valov, R. Waser, J.R. Jameson, and M.N. Kozicki: Electrochemical metallization memories – fundamentals, applications, prospects. *Nanotechnology* **22**, 289502 (2011).

99. C.J. Bettinger, J.P. Bruggeman, A. Misra, J.T. Borenstein, and R. Langer: Biocompatibility of biodegradable semiconducting melanin films for nerve tissue engineering. *Biomaterials* **30**, 3050 (2009).

100. B. Yu, J. Liu, S. Liu, and F. Zhou: Pdop layer exhibiting zwitterionicity: a simple electrochemical interface for governing ion permeability. *Chem. Commun.* **46**, 5900 (2010).

101. N. Farnad, K. Farhadi, and N.H. Voelcker: Polydopamine nanoparticles as a new and highly selective biosorbent for the removal of copper(II) ions from aqueous solutions. *Water Air Soil Pollut.* **223**, 3535 (2012).

102. F. De Marchi, D. Cui, J. Lipton-Duffin, C. Santato, J.M. MacLeod, and F. Rosei: Self-assembly of indole-2-carboxylic acid at graphite and gold surfaces. *J. Chem. Phys.* **142**, 101923 (2015).

103. H.J. Nam, B. Kim, M.J. Ko, M. Jin, J.M. Kim, and D.-Y. Jung: A new mussel-inspired polydopamine sensitizer for dye-sensitized solar cells: controlled synthesis and charge transfer. *Chem. – Eur. J.* **18**, 14000 (2012).

104. H. Lee, N.F. Scherer, and P.B. Messersmith: Single-molecule mechanics of mussel adhesion. *Proc. Natl. Acad. Sci. USA* **103**, 12999 (2006).

105. J. Yan, L. Yang, M-F. Lin, J. Ma, X. Lu, and P.S. Lee: Polydopamine spheres as active templates for convenient synthesis of various nanostructures. *Small* **9**, 596 (2013).

106. X. Yao, C. Zhao, J. Kong, H. Wu, D. Zhou, and X. Lu: Dopamine-assisted one-pot synthesis of zinc ferrite-embedded porous carbon nanospheres for ultrafast and stable lithium ion batteries. *Chem. Commun.* **50**, 14597 (2014).

107. Q. Yue, M. Wang, Z. Sun, C. Wang, C. Wang, Y. Deng, and D. Zhao: A versatile ethanol-mediated polymerization of dopamine for efficient surface modification and the construction of functional core–shell nanostructures. *J. Mater. Chem. B* **1**, 6085 (2013).

108. J. Si and H. Yang: Preparation and characterization of bio-compatible Fe_3O_4@polydopamine spheres with core/shell nanostructure. *Mater. Chem. Phys.* **128**, 519 (2011).

109. X. Gu, Y. Zhang, H. Sun, X. Song, C. Fu, and P. Dong: Mussel-inspired polydopamine coated iron oxide nanoparticles for biomedical application. *J. Nanomater.* **2015**, 1 (2015).

110. S. Liu, J. Fu, M. Wang, Y. Yan, Q. Xin, L. Cai, and Q. Xu: Magnetically separable and recyclable Fe_3O_4-polydopamine hybrid hollow microsphere for highly efficient peroxidase mimetic catalysts. *J. Colloid Interface Sci.* **469**, 69 (2016).

111. L. Zhang, L. Li, and Z.M. Dang: Bio-inspired durable, superhydrophobic magnetic particles for oil/water separation. *J. Colloid Interface Sci.* **463**, 266 (2016).

112. M. Zhang, X. He, L. Chen, and Y. Zhang: Preparation of IDA-Cu functionalized core-satellite Fe_3O_4/polydopamine/Au magnetic nanocomposites and their application for depletion of abundant protein in bovine blood. *J. Mater. Chem.* **20**, 10696 (2010).

113. L-S. Lin, Z-X. Cong, J-B. Cao, K-M. Ke, Q-L. Peng, J. Gao, H-H. Yang, G. Liu, and X. Chen: Multifunctional Fe_3O_4@polydopamine core–shell nanocomposites for intracellular mRNA detection and imaging-guided photothermal therapy. *ACS Nano* **8**, 3876 (2014).

114. X. Ma, C. Ding, X. Yao, and L. Jia: Ethylene glycol assisted preparation of Ti^{4+}-modified polydopamine coated magnetic particles with rough surface for capture of phosphorylated proteins. *Anal. Chim. Acta* **929**, 23 (2016).

115. H.P. Oliveira, C.F. Graeff, C.A. Brunello, and E.M. Guerra: Electrochromic and conductivity properties: a comparative study between melanin-like/$V_2O_5 \cdot nH_2O$ and polyaniline/$V_2O_5 \cdot nH_2O$ hybrid materials. *J. Non Cryst. Solids* **273**, 193 (2000).

116. J-W. Lee, H-B. Cho, T. Nakayama, T. Sekino, S-I. Tanaka, K. Minato, T. Ueno, T. Suzuki, H. Suematsu, Y. Tokoi, and K. Niihara: Dye-sensitized solar cells using purified squid ink nanoparticles coated on TiO_2 nanotubes/nanoparticles. *Nippon Seramikkusu Kyokai Gakujutsu Ronbunshi/J. Ceram. Soc. Japan.* **121**, 123 (2013).

117. J-J. Feng, P-P. Zhang, A-J. Wang, Q-C. Liao, J-L. Xi, and J-R. Chen: One-step synthesis of monodisperse polydopamine-coated silver core–shell nanostructures for enhanced photocatalysis. *New J. Chem.* **36**, 148 (2012).

118. W-X. Mao, X-J. Lin, W. Zhang, Z-X. Chi, R-W. Lyu, A-M. Cao, and L-J. Wan: Core–shell structured TiO_2@polydopamine for highly active visible-light photocatalysis. *Chem. Commun.* **52**, 7122 (2016).

119. G. Loget, J.E. Yoo, A. Mazare, L. Wang, and P. Schmuki: Highly controlled coating of biomimetic polydopamine in TiO_2 nanotubes. *Electrochem. Commun.* **52**, 41 (2015).

120. G. Soliveri, V. Pifferi, G. Panzarasa, S. Ardizzone, G. Cappelletti, D. Meroni, K. Sparnacci, and L. Falciola: Self-cleaning properties in engineered sensors for dopamine electroanalytical detection. *Analyst* **140**, 1486 (2015).

121. G. Panzarasa, G. Soliveri, K. Sparnacci, and S. Ardizzone: Patterning of polymer brushes made easy using titanium dioxide: direct and remote photocatalytic lithography. *Chem. Commun.* **51**, 7313 (2015).

122. M. Auffan, M. Pedeutour, J. Rose, A. Masion, F. Ziarelli, D. Borschneck, C. Chaneac, C. Botta, P. Chaurand, J. Labille, and J.Y. Bottero: Structural degradation at the surface of a TiO_2-based nanomaterial used in cosmetics. *Environ. Sci. Technol.* **44**, 2689 (2010).

123. N. Serpone, D. Dondi, and A. Albini: Inorganic and organic UV filters: their role and efficacy in sunscreens and suncare products. *Inorganica Chim. Acta.* **360**, 794 (2007).

124. M.I. Setyawati, C.Y. Tay, S.L. Chia, S.L. Goh, W. Fang, M.J. Neo, H.C. Chong, S.M. Tan, S.C.J. Loo, K.W. Ng, J.P. Xie, C.N. Ong, N.S. Tan, and D.T. Leong: Titanium dioxide nanomaterials cause endothelial cell leakiness by disrupting the homophilic interaction of VE-cadherin. *Nat. Commun.* **4**, 1673 (2013).

125. M.E. Carlotti, E. Ugazio, S. Sapino, I. Fenoglio, G. Greco, and B. Fubini: Role of particle coating in controlling skin damage photoinduced by titania nanoparticles. *Free Radic. Res.* **43**, 312 (2009).

126. B. Kiss, T. Bíró, G. Czifra, B.I. Tóth, Z. Kertész, Z. Szikszai, Á.Z. Kiss, I. Juhász, C.C. Zouboulis, and J. Hunyadi: Investigation of micronized titanium dioxide penetration in human skin xenografts and its effect on cellular functions of human skin-derived cells. *Exp. Dermatol.* **17**, 659 (2008).

127. M. Senzui, T. Tamura, K. Miura, Y. Ikarashi, Y. Watanabe, and M. Fujii: Study on penetration of titanium dioxide (TiO(2)) nanoparticles into intact and damaged skin in vitro. *J. Toxicol. Sci.* **35**, 107 (2010).

128. M.D. Newman, M. Stotland, and J.I. Ellis: The safety of nanosized particles in titanium dioxide- and zinc oxide-based sunscreens. *J. Am. Acad. Dermatol.* **61**, 685 (2009).

129. G. Vitiello, A. Pezzella, A. Zanfardino, M. Varcamonti, B. Silvestri, A. Costantini, F. Branda, and G. Luciani: Titania as a driving agent for DHICA polymerization: a novel strategy for the design of bioinspired antimicrobial nanomaterials. *J. Mater. Chem. B* **3**, 2808 (2015).

130. A. Pezzella, L. Capelli, A. Costantini, G. Luciani, F. Tescione, B. Silvestri, G. Vitiello, and F. Branda: Towards the development of a novel bioinspired functional material: synthesis and characterization of hybrid TiO_2/DHICA-melanin nanoparticles. *Mater. Sci. Eng. C* **33**, 347 (2012).

131. C.B. Lee, B.S. Kang, A. Benayad, M.J. Lee, S-E. Ahn, K.H. Kim, G. Stefanovich, Y. Park, and I.K. Yoo: Effects of metal electrodes on the resistive memory switching property of NiO thin films. *Appl. Phys. Lett.* **93**, 42115 (2008).

132. G. Vitiello, A. Pezzella, V. Calcagno, B. Silvestri, L. Raiola, G. D'Errico, A. Costantini, F. Branda, and G. Luciani: 5,6-Dihydroxyindole-2-carboxylic acid-TiO_2 charge transfer complexes in the radical polymerization of melanogenic precursor(s). *J. Phys. Chem. C* **120**, 6262 (2016).

APPENDIX C – SUPPORTING INFORMATION OF ARTICLE 2

Eumelanin for Nature-Inspired UV-Absorption Enhancement of Plastics

Eduardo Di Mauro, Matteo Camaggi, Nils Vandooren, Caleb Bayard, Jordan De Angelis,

Alessandro Pezzella, Bill Baloukas, Richard Silverwood, Abdellah Ajji, Christian Pellerin, Clara

Santato

Details of the Processing

Table S1. Processing parameters. Pellets were dried at 60 °C overnight prior to processing. A 10-minute pre-heating at 0.29 Mpa and at the same temperature of the hot press preceded the compression molding.

Melt compounding in the batch mixer			Compression molding			Cooling (25°C)	
Rotation speed (rpm)	Duration (min)	T (°C)	Duration (min)	T (°C)	P (Mpa)	Time (min)	P (Mpa)
50	20	135	15	115	1.58	3	0.43
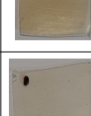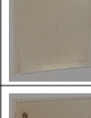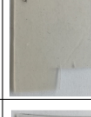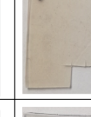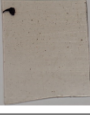
Table S2 Optical images of pellets of the commercial ELVAX®3128-1 as received as well as ELVAX®3128-1 melt compounded with the three types of eumelanin and the additive BLS®531.

Pellet + Additive	Optical Image
Control	
DHICA-melanin 0.2% wt.	
DHI-melanin 0.2% wt.	
Sepia Melanin 0.2% wt.	
BLS®531 0.3% wt.	

5 cm

Table S3. Optical Images of the films with the different additives at different times of UV-aging (day 0, 48, 96 and 144). The top left mark was drawn to clarify which of the two surfaces was exposed to the prolonged UV irradiation. For the thickness averages values, 5 samples were considered. *The compression molding parameters of the control film were adjusted to obtain a thicker film: no pre-heating, 115 °C for 2 minutes and cooling for 1 minute at room temperature, both at 0.22 Mpa (see paragraph "Equivalent absorption coefficient of the plastic films").

Film + Additive	No UV-Aging	48 days UV-Aging	96 days UV-Aging	144 days UV-Aging
Control film Size: 1.6 x 2.5 cm Thickness: 845 ± 83 μm *				
DHICA-melanin 0.2%wt. Size: 2.1 x 3.0 cm Thickness: 294 ± 76 μm				
DHICA-melanin 0.3% wt. Size: 2.3 x 3.0 cm Thickness: 162 ± 59 μm				
DHICA-melanin 0.6% wt. Size: 1.8 x 2.9 cm Thickness: 413 ± 24 μm				
DHICA-melanin 0.8% wt. Size: 1.8 x 2.6 cm Thickness: 195 ± 13 μm				
DHI-melanin 0.2% wt. Size: 1.8 x 2.7 cm Thickness: 688 ± 118 μm				
Sepia Melanin 0.2% wt. Size: 2.1 x 2.9 cm Thickness: 571 ± 106 μm				
BLS®531 0.3% wt. Size: 1.9 x 2.5 cm Thickness: 413 ± 53 μm				

Sepia Melanin Extraction

Sepia Melanin was extracted following established procedures [423], [424]. The cuttlefish ink (Seafoods Boston, Product of Spain) was bought at a local fish market. Eleven centrifugations and wash-suspensions were carried out on the cuttlefish ink with different solvents (hydrochloric acid, ethanol, ethyl acetate to remove carbohydrates, proteins and lipids, as well as deionized water). In particular, the commercial cuttlefish ink was vigorously shaken and added to HCl 2 M in a dark recipient (ratio ink/HCl= 50 g / 100 ml). The slurry was mixed by magnetic stirring for 30 minutes and kept for 24 hours at 10 °C. Subsequently, the solid was separated from the supernatant fluid by centrifugation (10000 rpm at 5 °C for 15 minutes) and then washed-suspended following the order: 0.5 M HCl (3 times), DI water, buffer solution (in 1 L, 95 ml monobasic sodium phosphate 200 mM, 405 ml dibasic sodium phosphate 200 mM, 500 ml DI water), DI Water (2 times), ethanol, ethyl acetate, DI water. The final step entailed a 24-hour lyophilization to remove all solvents. A black powder was obtained.

Melanin Free Acid Treatment

The Melanin Free Acid (MFA) treatment was carried out following existing protocols [426]. It entailed adding 100 mg of the melanin particles to 164 ml NH_3 0.5 M with 0.82 ml (for DHICA-melanin and DHI-melanin) or 2.46 ml (for Sepia Melanin) of H_2O_2 1%. The solution was mixed by magnetic stirring at 300 rpm for 60 minutes (for DHICA-melanin and DHI-melanin) or 1 day (Sepia Melanin) until complete dissolution. The higher amount of H_2O_2 and the longer stirring time for Sepia Melanin were deemed necessary as it proved to be much less soluble in the basic solution than the synthetic counterparts. At this point, 8.15 mg of sodium borohydride were added, and water was removed by evaporation on a steam bath. The solution was then acidified with HCl 12.4 M to reach a pH of 2 and left at 5°C for 4 days to allow the precipitation of the MFA. The precipitate was then isolated by centrifugation for 30 minutes at 5°C and 5000 rpm. The supernatant was removed, and the obtained paste left to dry under a chemical hood for 5 days. The MFA treatment transformed the powder into a paste. Such pastes showed light transmission decreasing with decreasing wavelength (Figure S1-A). With respect to films of DHI-melanin and DHICA-melanin (non-MFA-treated), the transmission in the UV range decreases after the MFA treatment (Figure S1-B). The films of DHICA-melanin and DHI-melanin were produced by dissolving the monomer

(DHI or DHICA) in methanol (10 mg/ml) in an oxygen free environment (nitrogen glovebox). The so-obtained solutions were spin coated (40 μl, 2000 rpm, 30 s) on fused silica substrates. The spin coated films were brought out of the nitrogen glovebox and polymerized by a solid-state polymerization method, following existing protocols [289].
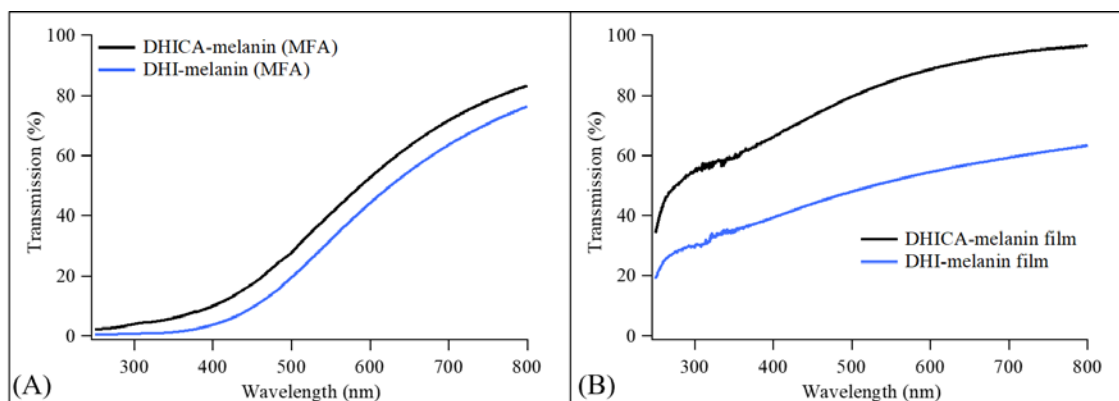
Figure S1. Transmission spectra of (A) DHI-melanin (MFA) and DHICA-melanin (MFA) drop-cast on fused silica and (B) of a DHI-melanin film as well as a DHICA-melanin film (Sepia Melanin (MFA) is reported in [430]).

Equivalent absorption coefficient of the plastic films

The absorption spectra of polymer films with different thicknesses cannot be directly compared as a higher thickness implies a higher absorption. Consequently, the addition of eumelanin would not be the only factor affecting the absorption spectra. According to Beer-Lambert's law in the case of a thin non-scattering film, $I = I_0 e^{-\alpha x}$ (where I_0 is the initial light intensity, α is the absorption coefficient and x the thickness of the material). I/I_0 thus gives the resulting transmitted light intensity following the absorption through the material. In first approximation, neglecting losses due to reflection, $1 - \frac{I}{I_0} = 1 - e^{-\alpha x} \approx A$, where A is the fraction of absorbed light. The center-mount technique allowed us to measure the total (specular and diffusive) reflected and transmitted light ($R+T$). Posing the total absorption of the films as $A = 1 - (R + T)$, we can obtain the value of α from (1) $1 - A \approx e^{-\alpha x}$, (2) $\ln(1 - A) \approx -\alpha x$, (3) $\alpha \approx \frac{-\ln(1-A)}{x} \approx \frac{-\ln(R+T)}{x}$.

As the obtained value of α is more valid in regions where the reflectivity is low and is the result of an approximation, we have termed it an "equivalent absorption coefficient". As a proof of concept of the hypothesis of a Beer-Lambert-like attenuation [515], α is shown to possess a linear dependence as a function of the concentration of DHICA-melanin (Figure S2). As a further proof of concept, for the control films, thicker samples were produced (approximately 0.65 mm – 1 mm) and their absorption coefficient compared to the control films produced with the "standard" processing parameters of this work (Table S1). The results were statistically equivalent (the averages of the thinner and thicker control films at different wavelength are the points at concentration 0% wt. of Figure S2).
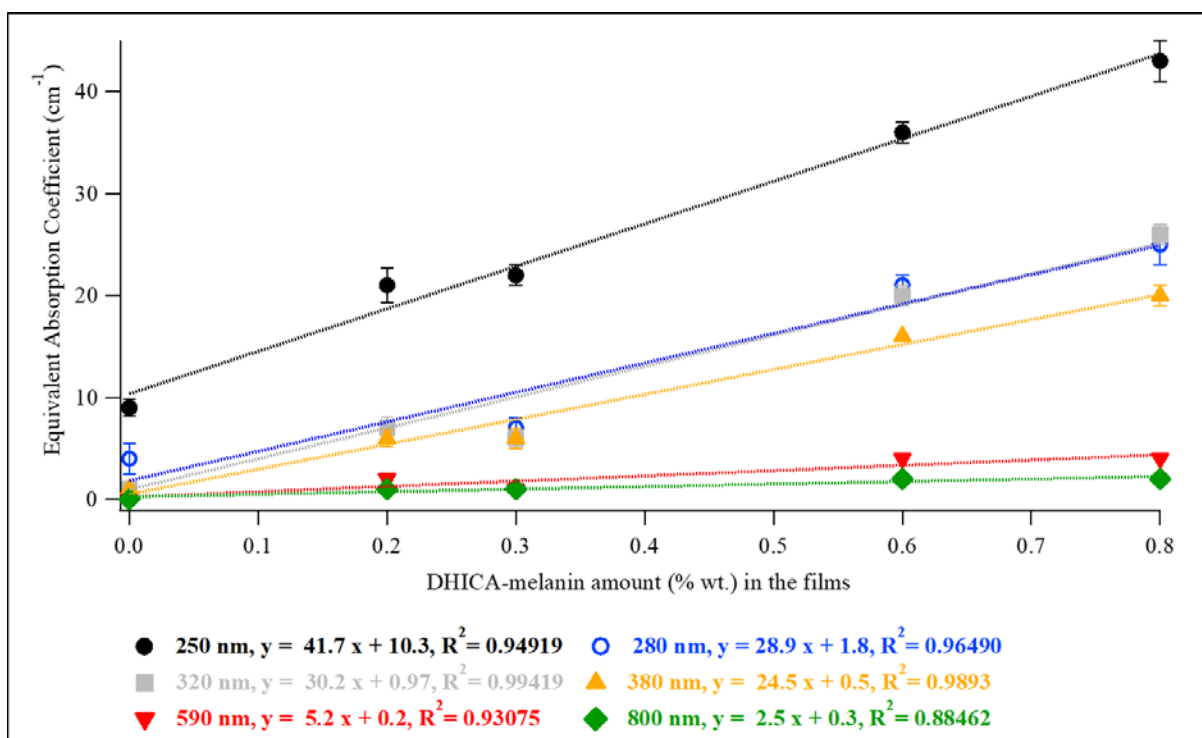
Figure S2. Equivalent absorption coefficient vs. concentration of DHICA-melanin.

Thermogravimetric Analyses before UV-Aging

(A)

Film + Additive (% wt.)	Inert Atmosphere			Air		
	Onset Degradation Temperature (°C)	Peak 1 (°C)	Main Degradation Peak (°C)	Onset Degradation Temperature (°C)	Peak 1 (°C)	Main Degradation Peak (°C)
Control	335 ± 4	354 ± 1	472 ± 3	297 ± 5	356 ± 7	446 ± 9
DHICA-melanin 0.2%	338 ± 7	355 ± 1	476 ± 1	304 ± 2	354 ± 1	442 ± 6
DHICA-melanin 0.3%	337 ± 6	357 ± 1	471 ± 2	297 ± 9	355 ± 11	446 ± 1
DHICA-melanin 0.6%	329 ± 4	350 ± 1	471 ± 1	287 ± 14	366 ± 9	456 ± 3
DHICA-melanin 0.8%	333 ± 1	351 ± 2	471 ± 2	295 ± 16	347 ± 5	450 ± 7
DHI-melanin 0.2%	331 ± 4	353 ± 3	471 ± 3	292 ± 4	349 ± 3	449 ± 3
Sepia-Melanin 0.2%	335 ± 1	355 ± 2	473 ± 2	279 ± 11	347 ± 1	448 ± 7
BLS5®531, 0.3%	334 ± 2	353 ± 2	472 ± 1	283 ± 1	351 ± 3	433 ± 9

Figure S3. (A) Collection of onset degradation temperatures, peak 1 and main degradation peaks, in inert atmosphere (argon) and air, of the control film and of films with the different additives; TGAs and DTGs of the control film and of the film including 0.8% wt. DHICA-melanin in argon (B) and air (C), with the inset of (C) showing the initial mass gain due to the reaction with O_2.

Infrared Spectra of Control Film before and after UV-Aging

The IR spectrum peaks identified for the control film before UV-aging are showed and listed in Figure S4: 719 and 730 cm^{-1} (CH$_2$ out-of-plane rocking [516]), 1020 cm^{-1} (C-O ester stretching [517]), 1240 cm^{-1} (O-C=O ester stretching [517]), 1368 cm^{-1} (CH$_2$ wagging in amorphous regions [516]), 1463 and 1472 cm^{-1} (CH$_2$ bend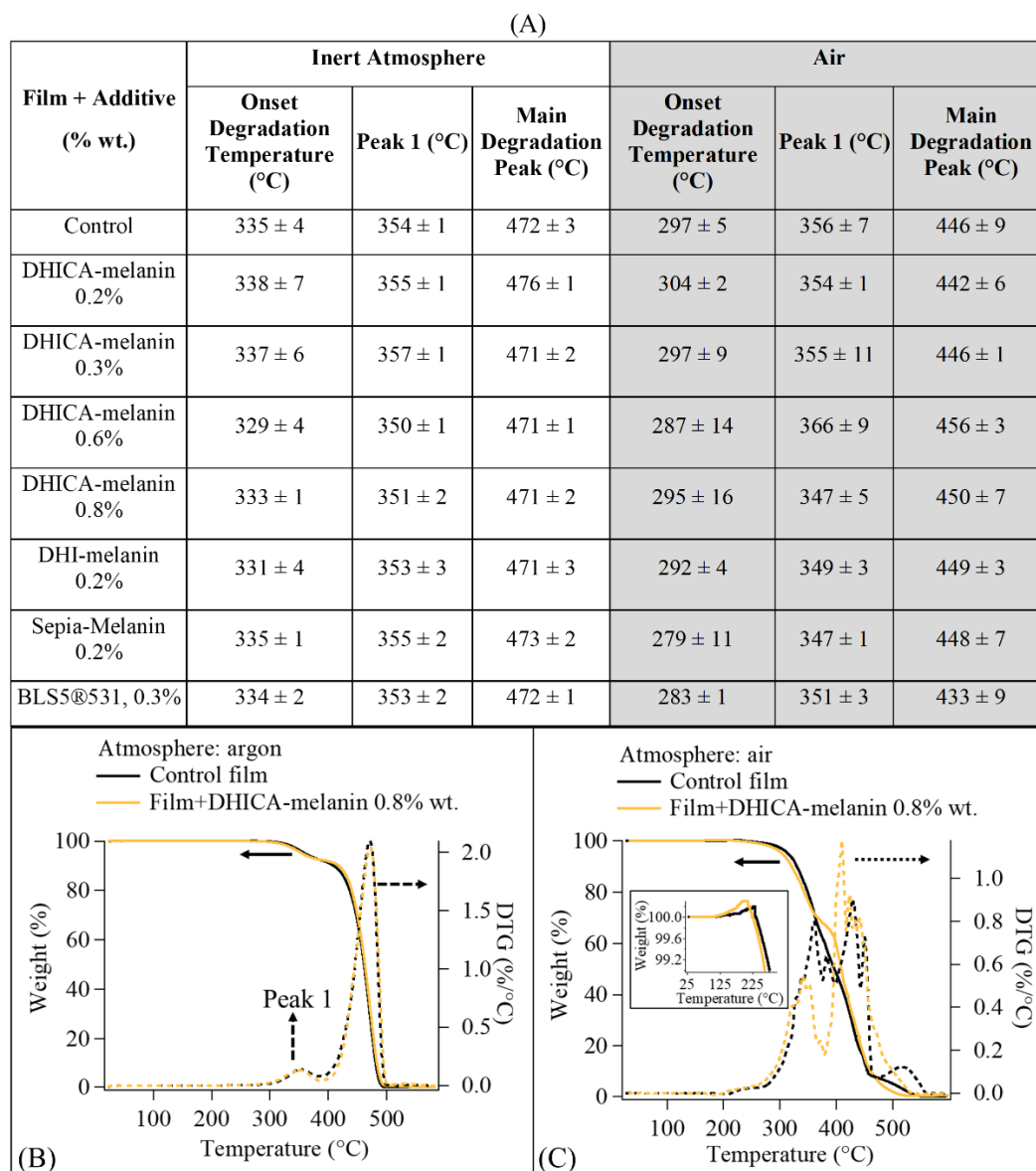ing [518]), 1740 cm^{-1} (ester carbonyl stretching [519]), 2848 and 2917 cm^{-1} (CH$_2$ symmetric and antisymmetric stretchings [518]).
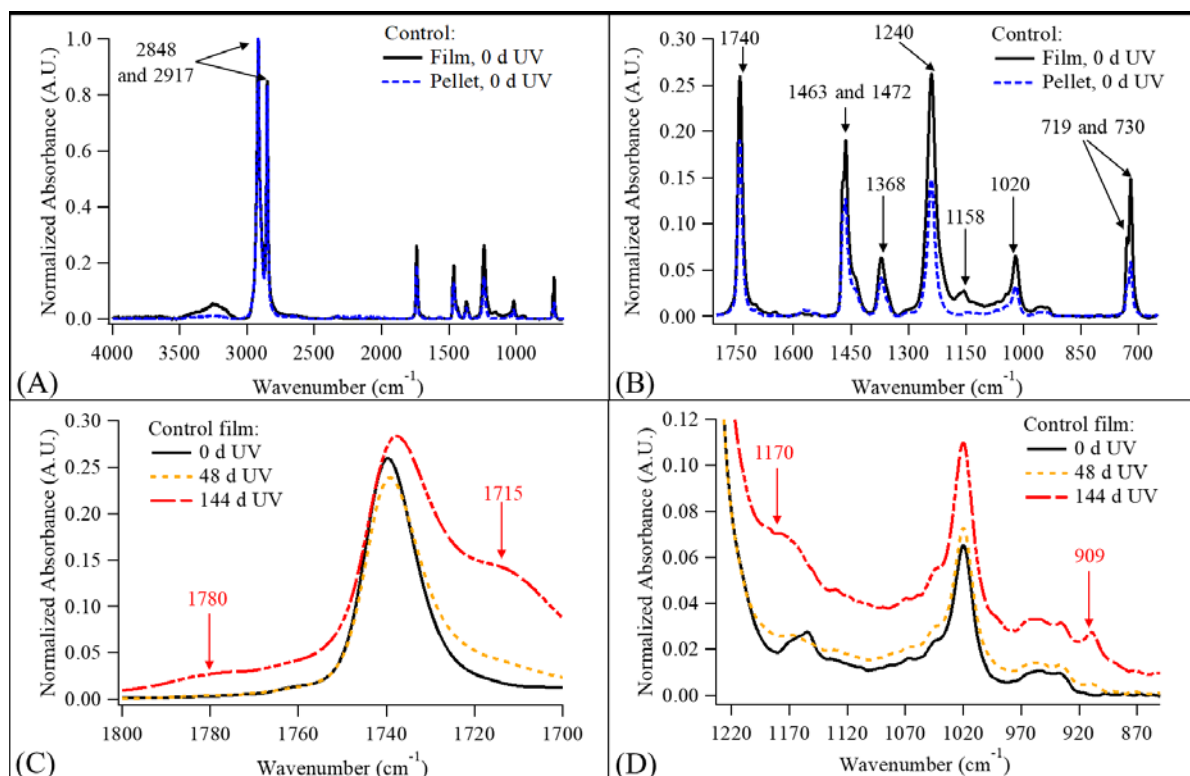
Figure S4. IR spectra of (A) pellet and control film of the commercial grade EVA before UV-Aging ((B) is a zoom in the range 1800 cm^{-1} – 650 cm^{-1}); the control film at different times of UV-aging (0, 48 and 144 days) in the range 1800 cm^{-1} – 1700 cm^{-1} (C) and 1230 cm^{-1} – 850 cm^{-1} (D). The broad band around 3250 cm^{-1} is due to ice buildup in the MCT detector and should be disregarded.

The small peak at 1158 cm^{-1}, present in the film but not in the pellets, is characteristics of poly(tetrafluoroethylene) (PTFE): as PTFE sheets were used to avoid direct contact between the

metal plates and the polymer films during compression molding, such a peak can be tentatively attributed to a surface contamination due to PTFE [520].

Infrared Spectra after UV-Aging of the films including eumelanin

Table S4. Ratio between the absorbance at the wavenumber of photo-oxidation products (909 cm^{-1}, 1170 cm^{-1}, 1715 cm^{-1} and 1780 cm^{-1}) and the absorbance of the vinyl acetate group at 1740 cm^{-1} for the control film and the films including different additives at different times of UV-aging.

Film + Additive (% wt.)	Absorbance at 909 cm^{-1} / Absorbance at 1740 cm^{-1} (A.U.)			Absorbance at 1170 cm^{-1} / Absorbance at 1740 cm^{-1} (A.U.)			Absorbance at 1715 cm^{-1} / Absorbance at 1740 cm^{-1} (A.U.)			Absorbance at 1780 cm^{-1} / Absorbance at 1740 cm^{-1} (A.U.)		
	0 d UV-Aging	48 d UV-Aging	144 d UV-Aging	0 d UV-Aging	48 d UV-Aging	144 d UV-Aging	0 d UV-Aging	48 d UV-Aging	144 d UV-Aging	0 d UV-Aging	48 d UV-Aging	144 d UV-Aging
Control	$1.7*10^{-4}$	$2.1*10^{-2}$	$1.0*10^{-1}$	0.09	0.11	0.25	0.08	0.19	0.54	0.01	0.02	0.10
DHICA-melanin 0.2%	N.D.	$2.9*10^{-2}$	$1.3*10^{-1}$	N.D.	0.24	0.55	N.D.	0.23	0.86	N.D.	0.03	0.20
DHICA-melanin 0.3%	N.D.	$2.6*10^{-2}$	$8.8*10^{-2}$	N.D.	0.10	0.28	N.D.	0.22	0.64	N.D.	0.03	0.16
DHICA-melanin 0.6%	N.D.	$3.7*10^{-2}$	$1.1*10^{-1}$	N.D.	0.19	0.49	N.D.	0.38	0.97	N.D.	0.05	0.25
DHICA-melanin 0.8%	$6.0*10^{-4}$	$4.4*10^{-2}$	$1.3*10^{-1}$	0.06	0.19	0.48	0.08	0.40	0.99	0.01	0.06	0.23
DHI-melanin 0.2%	N.D.	$2.7*10^{-2}$	$1.1*10^{-1}$	N.D.	0.13	0.38	N.D.	0.24	0.78	N.D.	0.03	0.17
Sepia-Melanin 0.2%	N.D.	$2.1*10^{-2}$	$8.1*10^{-2}$	N.D.	0.12	0.33	N.D.	0.19	0.59	N.D.	0.02	0.12
BLS5®531, 0.3%	$5.1*10^{-3}$	$6.9*10^{-3}$	$2.0*10^{-2}$	0.07	0.08	0.14	0.08	0.11	0.25	$3*10^{-3}$	0.01	0.03
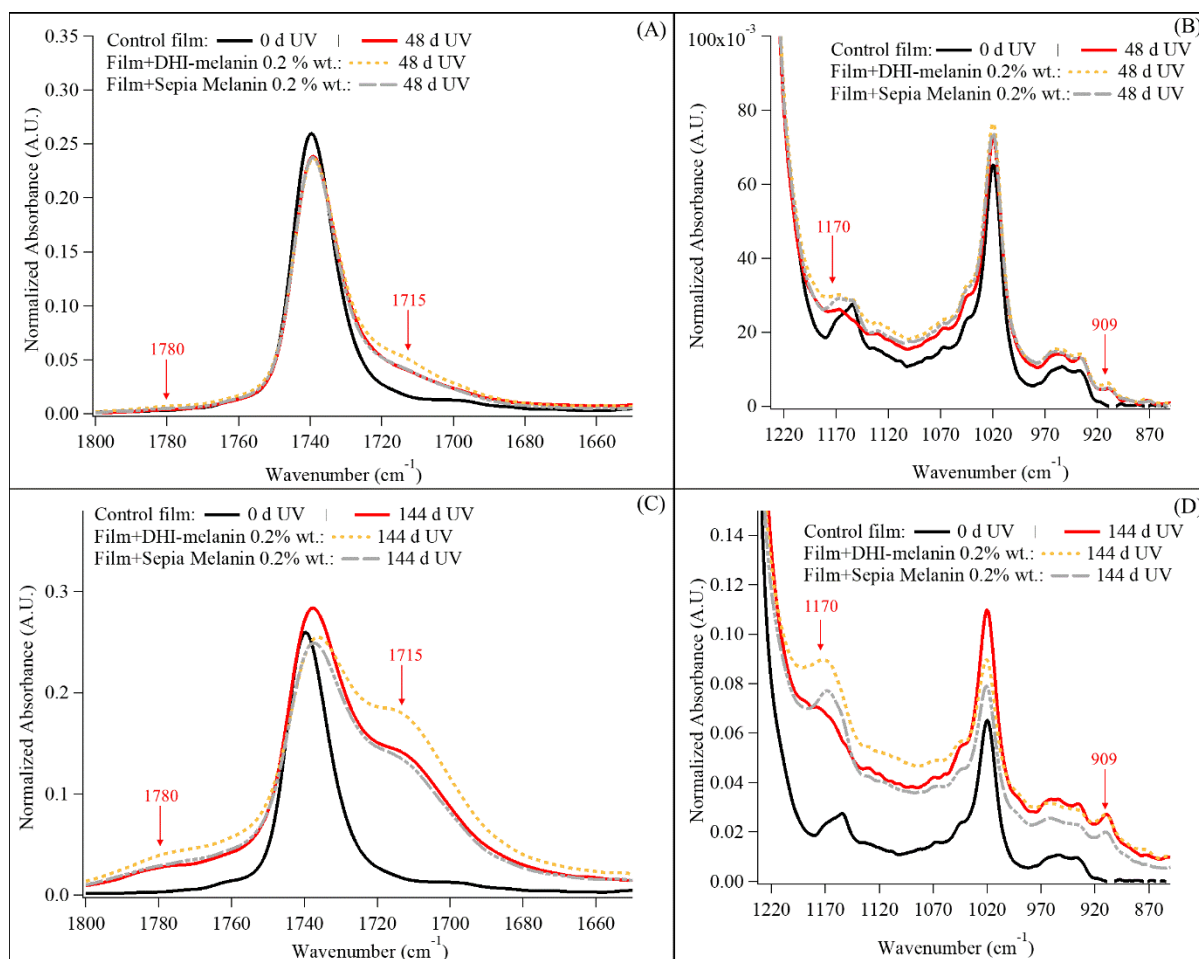
Figure S5. IR spectra of the control film and of films including DHI-melanin and Sepia Melanin 0.2% wt., after 48 days-UV-aging in the ranges: (A) 1800 cm^{-1} – 1650 cm^{-1} and (B) 1230 cm^{-1} – 850 cm^{-1}; after 144 days of UV-aging, in the ranges: (A) 1800 cm^{-1} – 1650 cm^{-1} and (B) 1230 cm^{-1} – 850 cm^{-1}. Arrows point to the most important photo-oxidation products. IR spectra of the control film at day 0 is reported for the sake of comparison.

Figure S5 reports only the wavenumber ranges where peaks related to photo-oxidation products are reported. At day 0 of UV-aging the IR spectra of the control film and of films containing the three types of eumelanin show no substantial difference, so that only the IR spectrum of the control film at day 0 is reported.

UV-Visible Absorption after UV-Aging

Table S5. Ratio $\alpha_{AFTER\ UV-AGING}/\alpha_{BEFORE\ UV-AGING}$ for the control film and films including different types and concentrations of eumelanin at different times of UV-aging.

| Film + Additive (% wt.)	Ratio alpha after UV-aging/alpha at day 0 of UV-aging							
	48 days				144 days			
	UVC	UVB		UVA	UVC	UVB		UVA
	250 nm	280 nm	320 nm	380 nm	250 nm	280 nm	320 nm	380 nm
Control	1.7	1.7	1.6	0.8	3.0	3.8	3.7	1.1
DHICA-melanin 0.2%	1.2	1.6	0.7	0.5	2.9	4.7	1.3	0.5
DHICA-melanin 0.3%	1.2	1.7	0.9	0.7	3.6	5.5	1.9	0.7
DHICA-melanin 0.5%	1.5	2.1	0.9	0.6	1.6	3.0	1.5	0.7
DHICA-melanin 0.8%	1.8	1.9	0.7	0.5	2.5	3.5	1.0	0.5
DHI-melanin 0.2%	1.3	1.8	0.8	0.6	1.9	5.1	2.3	0.9
Sepia-Melanin 0.2%	1.1	1.5	0.9	0.7	2.0	3.9	1.6	0.7
BLS5®531, 0.3%	0.9	0.9	0.9	0.8	0.8	0.8	0.6	0.5

Table S5 shows the absorption increase of the films that took place in the UVB and UVC ranges following prolonged UV-radiation: such increase was due to the formation of photo-oxidation products of the commercial EVA matrix [453]. The reduction of the absorption in the UVA is due to the photo-induced oxidative degradation of eumelanin, with formation of pyrrole-2,3,5-tricarboxylic acid and fission of indolequinone [441].

Thermogravimetric Analyses after UV-aging

(A)

Film + Additive (% wt.)	Onset Degradation Temperature (°C)			Main Degradation Peak (°C)		
	Before UV-Aging	48 days UV-Aging	144 days UV-Aging	Before UV-Aging	48 days UV-Aging	144 days UV-Aging
Control	335 ± 4	331 ± 1	335 ± 1	472 ± 3	467 ± 1	470 ± 2
DHICA-melanin 0.2%	338 ± 7	331 ± 1	325 ± 1	476 ± 1	463 ± 1	467 ± 2
DHICA-melanin 0.3%	337 ± 6	330 ± 1	324 ± 3	471 ± 2	456 ± 4	458 ± 5
DHICA-melanin 0.6%	329 ± 4	329 ± 1	322 ± 1	471 ± 1	469 ± 1	470 ± 1
DHICA-melanin 0.8%	333 ± 1	326 ± 2	316 ± 1	471 ± 2	468 ± 3	464 ± 2
DHI-melanin 0.2%	331 ± 4	334 ± 2	329 ± 1	471 ± 3	469 ± 4	471 ± 1
Sepia-Melanin 0.2%	335 ± 1	331 ± 1	331 ± 1	473 ± 2	464 ± 1	469 ± 2
BLS5®531, 0.3%	334 ± 2	332 ± 1	333 ± 1	472 ± 1	465 ± 1	466 ± 3
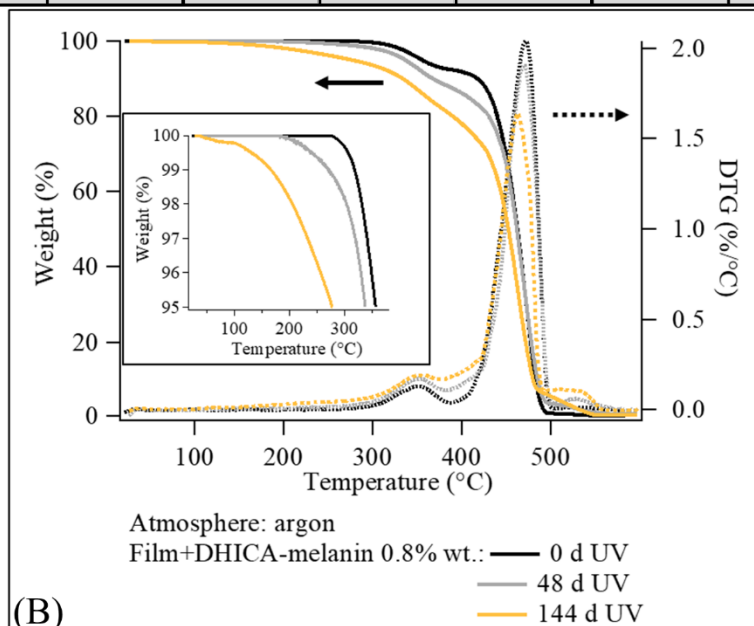
(B)

Figure S6. At different times of the UV-Aging treatment (0, 48 and 144 days): (A) collection of onset degradation temperatures and degradation peaks in inert atmosphere (argon) of the control

film and the films including the additives; (B) TGAs and DTGs of the film including DHICA-melanin 0.8% wt., with the inset pointing out the effect of UV-aging on the onset degradation temperature.

(A)

Film + Additive (% wt.)	Onset Degradation Temperature (°C)		Main Degradation Peak (°C)	
	Before UV-Aging	144 days UV-Aging*	Before UV-Aging	144 days UV-Aging
Control	297 ± 5	272 ± 10	446 ± 9	446 ± 4
DHICA-melanin 0.2%	304 ± 2	278 ± 8	442 ± 6	444 ± 1
DHICA-melanin 0.3%	297 ± 9	243 ± 2	446 ± 1	438 ± 1
DHICA-melanin 0.6%	287 ± 14	242 ± 8	456 ± 3	453 ± 4
DHICA-melanin 0.8%	295 ± 16	212 ± 1	450 ± 7	452 ± 1
DHI-melanin 0.2%	292 ± 4	275 ± 3	449 ± 3	443 ± 5
Sepia-Melanin 0.2%	279 ± 11	270 ± 1	448 ± 7	441 ± 7
BLS5®531, 0.3%	283 ± 1	304 ± 3	433 ± 9	437 ± 2

Atmosphere: air
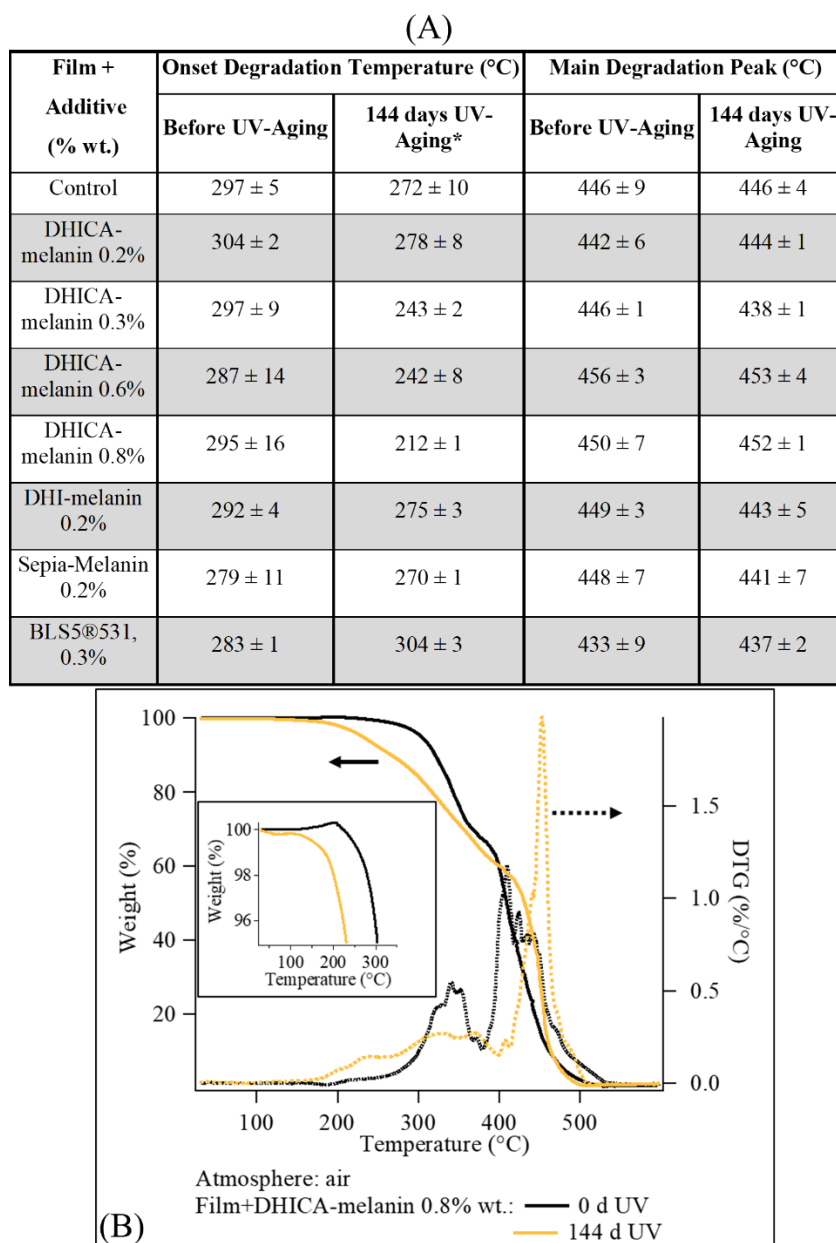Film+DHICA-melanin 0.8% wt.: —— 0 d UV
—— 144 d UV

(B)

Figure S7. At different times of the UV-Aging treatment (0 and 144 days): (A) collection of onset degradation temperatures and degradation peaks in air of the control film and of the films

including the additives; (B) TGAs and DTGs of the film including DHICA-melanin 0.8% wt., with inset pointing out the effect of UV-aging on the onset temperature.

*Two phenomena take place at the same time at the beginning of the thermo-oxidative degradation of photo-oxidized EVA: one entailing a mass gain (due to the uptake of O_2) [434]–[436], which would cause a decrease of the DTG, and one entailing a mass loss (degradation of the photo-oxidation products), which would cause an increase of the DTG. These opposite influences on the DTG rendered the temperature at which the DTG attains the value 0.1 %/°C not representative of the beginning of the degradation and, consequently, not suitable to be chosen as the onset degradation temperature in air after UV-aging, T_{on}(UV-air). Defining $\Delta m(T_{on}$(no-UV-air)) the mass loss (in %) at the onset degradation temperature of the non-UV-aged sample in air, the T_{on}(UV-air) was then computed as the temperature at which the UV-aged sample in air loses a mass percentage equal to $\Delta m(T_{on}$(no-UV-air)).

Film including the Commercial Benzophenone

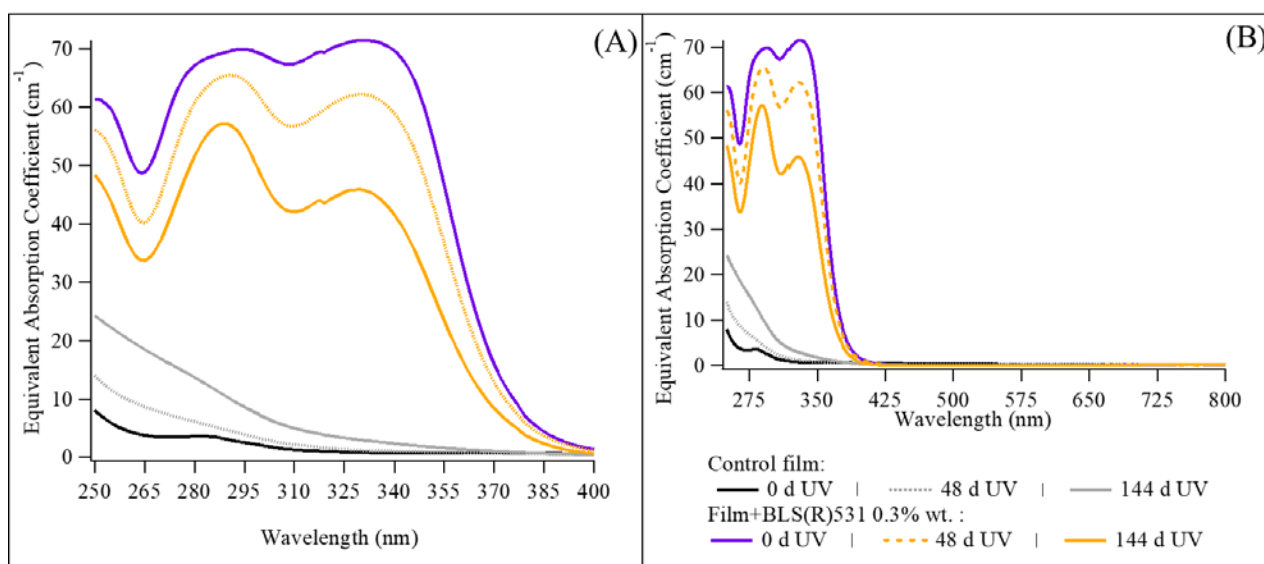

Figure S8. Equivalent absorption coefficient (A) in the UV range and (B) in the UV and visible ranges for the control film and the film including BLS®531 0.3% wt. at different times of UV-aging (0, 48 and 144 days).
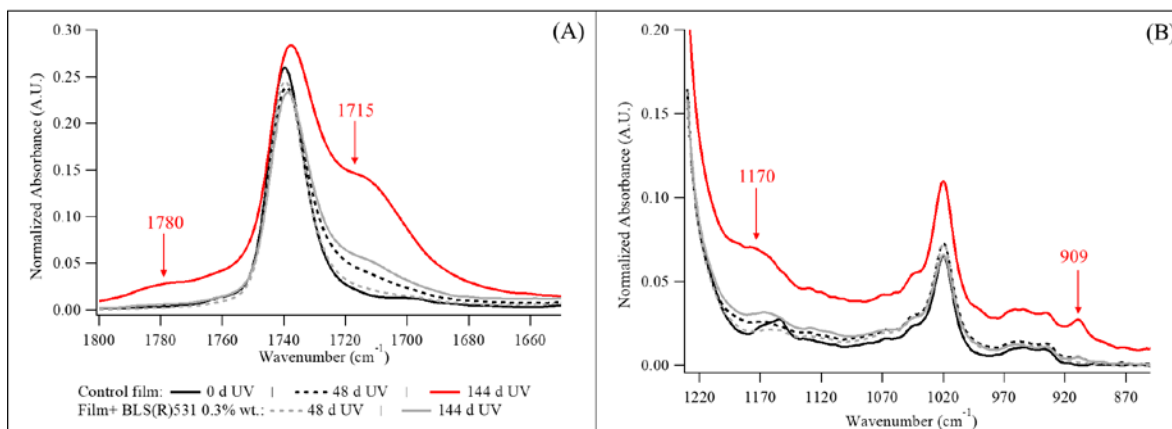
Figure S9. IR spectra of the control film as well as the film including the commercial benzophenone 0.3% wt. at different times of UV-Aging (0, 48 and 144 days): (A) range 1800 cm^{-1} – 1650 cm^{-1} and (B) 1220 cm^{-1} – 850 cm^{-1}.

The increase of the T_{on} for the sample incorporating BLS®531 (Figure S7) may point to the occurrence of cross-linking in presence of the commercial additive. The cross-linking as a result of prolonged UV-irradiation has already been reported for this combination polymer – UV-absorber [456].

APPENDIX D – SUPPORTING INFORMATION OF ARTICLE 3

Biodegradation of Bio-Sourced and Synthetic Organic Electronic Materials: Towards Green Organic Electronics

Eduardo Di Mauro, Denis Rho, Clara Santato

Submitted to *Nature Sustainability* on December 20th, 2018.

Extraction of Sepia Melanin

Sepia Melanin was extracted from cuttlefish ink (Seafoods Boston, Product of Spain), bought in a Montréal fish market, according to a procedure that was adapted from existing protocols [423], [424]. Eleven centrifugations and wash-suspensions were carried out, sequentially, on the cuttlefish ink with different solvents: hydrochloric acid, ethanol, ethyl acetate (to remove carbohydrates, proteins and lipids), and deionized water (DI). In particular, first, the commercial cuttlefish ink (2 kg) was vigorously shaken, then poured in a HCl solution (2 M) into a dark recipient (cuttlefish ink/acid ratio 50 g/100 ml). The slurry was mixed by magnetic stirring for 30 min and kept for 24 h at 10°C. Subsequently, the solids were separated from the supernatant by centrifugation (10000 rpm at 5°C for 15 min.) and then washed-suspended with: HCl solution (0.5 M) (3 x); deionized water; phosphate buffer (monobasic sodium phosphate (200mM, 95 ml) and dibasic sodium phosphate (200 mM, 405 ml) per 500 ml of DI water); DI water (2 x); ethanol; ethyl acetate; and DI water. Prior to each centrifugation, the suspensions were vigorously shaken (Vortex mixer). The last step entailed a 24-h lyophilization step to obtain a solvent-free melanin powder. A black powder (approximately 200 g) was obtained, and the extraction yield was approximately 10% wt.

Ethyl acetate (99.8%) and ethanol (95%) were purchased from Sigma-Aldrich (Canada). Hydrochloric acid solution (12 M) was purchased from EMD Millipore (Canada). Commercial Sepia Melanin (SM-C) was purchased from Sigma Aldrich and used as a reference material.

Sepia Melanin Characterization

The extracted Sepia Melanin (SM-E) was characterized by means of infrared spectroscopy (IR), thermogravimetric analysis (TGA), nuclear activation analysis (NAA), as well as elemental analyses of total carbon (CHN analysis) and total inorganic carbon (TIC).
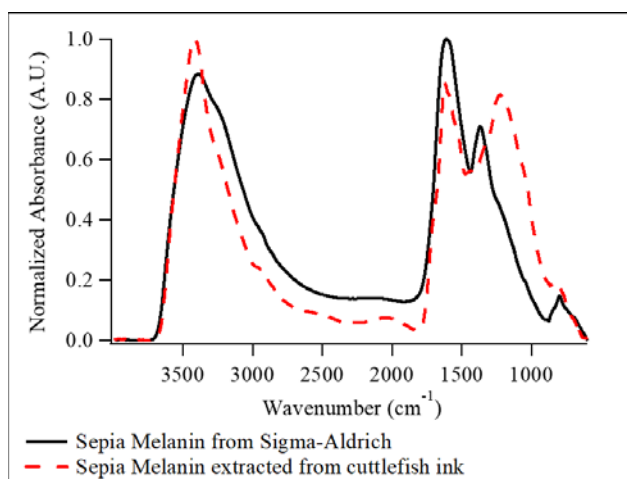
Supplementary Figure 1: IR spectra of commercial Sepia Melanin (----) and extracted Sepia Melanin (-- --).

The IR spectrum of the SM-E (Supplementary Figure 1) presents peaks at 3400 cm^{-1} (N-H stretching of the pyrrole ring), 2924 cm^{-1} (C-H stretching), 1600 cm^{-1} (C=C aromatic ring vibration/[NH$_2$] deformation), 1370 cm^{-1} (indole ring vibration/CNC stretching) and a broad band around 1220 cm^{-1} (C-H in-plane deformation, C-O stretching and O-H in-plane deformation in the carboxylic group COOH) [521].

Both weakly and strongly bound water can be present in Sepia Melanin after extraction [70], [123]. Consequently, the dry solids (residual mass after heating the material at 105°C until constant mass is reached) were quantified by means of a TGA. Such measurement entailed a ramp of 10 °C/min until 105°C and then an isotherm at 105°C until the derivative, DTG, was lower than 0.01 %/min in Ar atmosphere. The test was run for 5 times for SM-E and 2 times for SM-C. The dry solids of SM-E represented 83.1 ± 0.3% wt. of the initial weight, differing by 1% wt. from the dry solids of SM-C, 81.9 ± 0.4% wt.

Furthermore, TGA helps gaining insights into the thermal decomposition of a material. In particular, the minima of the DTG represent the completion of a thermogravimetric phenomenon and its maxima represent the maximum rate at which a thermogravimetric phenomenon takes place [123]. The TGAs of the two powders were carried out in inert atmosphere, ramp of 10 °C/min between 25°C – 500°C. The thermal decomposition of SM-E and SM-C featured the same trend (Supplementary Figure 2, a). The DTG has in both cases a first maximum (approximately 45°C)

followed by a minimum (approximately 140 °C), attributable to the maximum rate and to the end of the loss of weakly bound water, respectively. A step involving the decarboxylation of the DHICA units and opening of the supramolecular structure (Supplementary Figure 2 and Supplementary Table 1) [123] follows. At 500°C, the mass loss is 60% wt. in both cases. The hygroscopicity was studied comparing the TGAs at two relative humidity (RH) levels, 25% and 90%. The mass loss at the first DTG minimum gives an approximate but comparable estimation of the difference in the amount of weekly bound water absorbed at a certain RH level [123]. SM-C accommodates more weakly bound water in its supramolecular structure than SM-E as it features a water loss 5%-6% wt. higher (Supplementary Table 1).
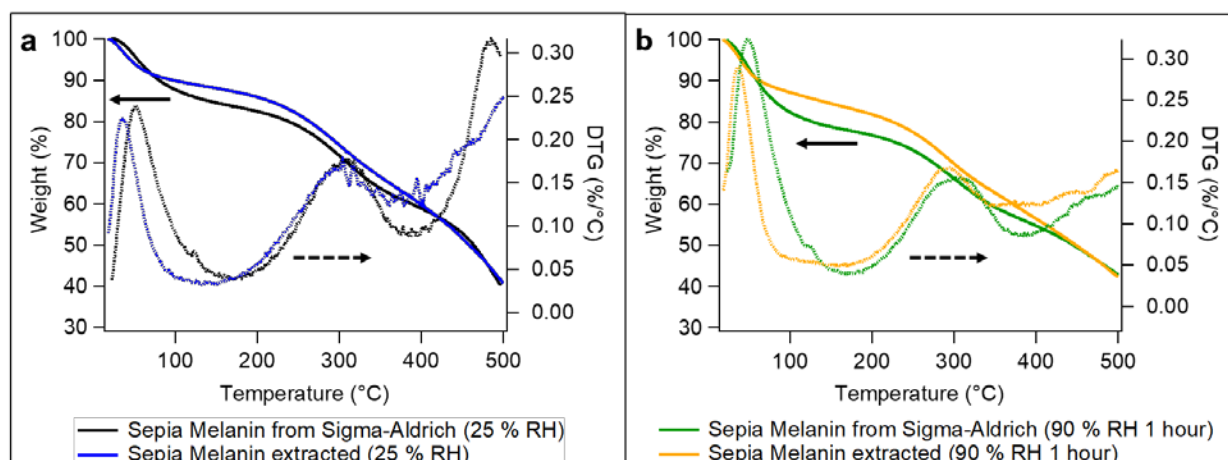
Supplementary Figure 2. **a**, Thermogravimetric analysis (TGA) of SM-E and SM-C without any hydration treatment and **b** after a 1-hour treatment at 90% RH, in inert atmosphere (N_2 and Ar atmosphere, respectively).

Supplementary Table 1. First minimum of the derivative of the TGA (DTG), attributable to the end of water loss, and the amount of weakly-bound water lost for Sepia Melanin from Sigma-Aldrich and Sepia Melanin extracted at 25% RH and 90% RH.

Eumelanin type	Relative Humidity (%)	First DTG minimum (°C)	Weight loss at first DTG minimum (%)
Sepia Melanin Extracted (SM-E)	25	138 ± 7	11.6 ± 0.4
	90	154 ± 12	16.6 ± 0.6
Commercial Sepia Melanin (SM-C)	25	169 ± 5	16.1 ± 0.3
	90	170 ± 1	22.2 ± 0.5

The composition of the inorganic matter was evaluated by means of nuclear activation analysis (NAA), to assess what are the cations and anions present after extraction (Supplementary Table 2).

Supplementary Table 2. Analytical composition of Sepia Melanin (SM-E) by means of NAA.

Element	Value (ppm)	Element	Value (ppm)
F	< 80	Fe	479 ± 90
Na	2685 ± 108	Co	7.36 ± 0.40
Mg	388 ± 80	Ni	< 30
Mn	6.99 ± 1.42	Cu	< 30
Cl	919 ± 70	Zn	< 20
K	< 170	Ag	< 7
Ca	926 ± 201	I	5.94 ± 0.95
Cr	15 ± 1	Au	< 0.002

Electrolytic Respirometers: Monitoring the O_2 Consumption

Electrolytic respirometers (designed by Young *et al.* [522]) were used to follow the O_2 consumption (Model BI-2000, Bioscience, Inc.) under mesophilic conditions. In this experimental set-up, the compost is exposed to a closed environment (1.2 L bioreactor), wherein respired CO_2 is trapped by a KOH solution (5 ml, 50% wt.), suspended within the headspace volume. As a consequence, consumption of O_2 inside the bioreactor causes a ΔP with respect to the external pressure. The cap of each bioreactor is occupied by a two-chamber electrolytic cell containing a H_2SO_4 solution (1 N). One chamber (containing the anode) is exposed to the internal pressure of the bioreactor. The other chamber (containing the cathode) is exposed to the external pressure. The ΔP causes a difference in the level of the acid in the two chambers. Such ΔP, by means of a switch electrode, activates the electrolytic cell. O_2 is consequently produced at the anode (and provided to the closed environment of the bioreactor) while H_2 is produced at the cathode (and vented to the atmosphere). From the power provided to the electrolytic cell, the moles of O_2 produced can be computed. Further details of the working principle of the electrolytic respirometers can be found in reference [523]. The software BI2000 (modified *ad hoc* for the National Research Council Canada) was used to collect the data.

Wet Scrubbers: Monitoring the CO_2 Evolution

The CO_2 evolved under thermophilic conditions was monitored using an indirect measurement method (Cumulative Measurement Respirometry). Three traps filled with $Ba(OH)_2$ were put in series after each bioreactor. Such solutions are able to capture CO_2 as the reaction (S1) takes place:

$$Ba(OH)_2 + CO_2(g) \rightarrow BaCO_3 + H_2O \qquad (S1)$$
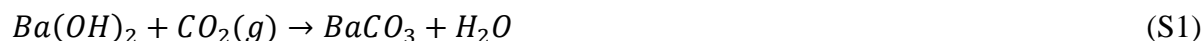
During the titration, the remaining $Ba(OH)_2$ that has not reacted with CO_2 is neutralized with HCl 0.1 M:

$$Ba(OH)_2 + 2HCl \rightarrow BaCl_2 + 2H_2O \qquad (S2)$$

From the molar ratios of equation (S2), at a certain incubation time t, it can be inferred that:

$$\text{moles } of\ CO_2\ trapped\ (t) = \text{moles of } Ba(OH)_2\ (t_0) - moles\ HCl\ (t)/2 \qquad (S3)$$

Blank Compost Characterization

The compost, organic fraction of municipal solid waste, was kindly provided by the company *GSI Environnement*, subsidiary of Englobe (Québec, Canada). Its characteristics satisfied the requirements of ASTM D5338 (sieved with a 10-mm mesh, ash content 51.4%, pH 7.3, dry solids 46 ± 4 % wt., C/N ratio 24.3 with %C = 50% organic matter).

The figure of merit that indicates if the respiration activity of the compost falls within the acceptable range (i.e. fresh compost) is represented by the specific respiration rate, i.e. CO_2 evolved per g of volatile solids per day, mg CO_2/(g volatile solids d)[339]. Consequently, the specific respiration rate of the compost was measured both under mesophilic (25°C) and thermophilic conditions (58°C) with *ad hoc* tests, before the main tests that involved the materials of interest.

Under thermophilic conditions, the specific respiration rate was assessed deploying 6 bioreactors filled with 1 kg of blank wet compost for 11 days. The CO_2 evolved was followed using wet scrubbers (working mechanism in "Wet Scrubbers"). The result was 10.5 ± 0.1 mg CO_2/(g d), and, consequently, fell within the acceptable range set by ASTM D5338, i.e. 5 – 15 mg CO_2 evolved per g volatile solids per day, in the first 10 days.

Under mesophilic conditions, the specific respiration rate was measured deploying 7 bioreactors of 1.2 L filled with 100 g of blank wet compost for 7 days, resulting to be 1.4 ± 0.1 mg CO_2/(g d). The O_2 consumed was monitored by means of electrolytic respirometers. The CO_2 evolved was

computed assuming the respiratory quotient CO_2 respired / O_2 consumed to be 1.0 mol/mol [338] (working mechanism in "Electrolytic Respirometers"). The specific respiration rate measured with this test, 8x lower than under thermophilic conditions, is in agreement with the difference in the respiration rate between the two temperature ranges already reported in the literature [524].

Biodegradability Test under Mesophilic Conditions

For the biodegradability test under mesophilic conditions (25°C), bioreactors of 1.2 L volume were filled with 100 g of wet compost. A total of 7 bioreactors were used: two of plain compost (blank), two with cellulose blended with compost (positive control) and three with Sepia Melanin blended with compost. The weight ratio material to dry compost was 1:6, as for the biodegradability test in composting conditions (ASTM D5338). Electrolytic respirometers (designed by Young *et al.*[522], model BI-2000, Bioscience, Inc.) were used to follow the O_2 consumption (working mechanism in "Electrolytic Respirometers"). The CO_2 evolved was computed assuming the respiratory quotient CO_2 respired / O_2 consumed to be 1.0 mol/mol [338].

Biodegradability Test, in Composting Conditions (ASTM D5338 2015)

The standards ASTM D6400 and ASTM D5338 define the terminology and the procedure to assess the aerobic biodegradability of a plastic material in composting conditions [339], [343].

Following ASTM D5338, the CO_2 evolving from two duplicates and four triplicates (16 bioreactors in total) was monitored for 98 days. The two duplicates contained Sepia Melanin blended with compost and blank compost, respectively. The four triplicates contained Cu-Pc, PPS and microcrystalline cellulose (the positive control) blended with compost as well as polyethylene (PE, the negative control) buried in compost. In each bioreactor, 250 g of wet compost were present, and materials were added following the ASTM D5338 1:6 weight ratio material/dry compost. The bioreactors were kept at a constant temperature of 58°C in a chamber with controlled temperature (Caron Stability Chamber) and fed with air (flow of 32 ± 5 ml/min). The air passed through a water column to be humidified before reaching the bioreactors.

Starting from day 47, the bioreactors were opened once a week, weighed, and the difference with respect to the initial weight was added as DI water to keep the dry weight below 50% wt. The DI

water added weekly was approximately 30 ml. Together with the water addition, the compost was carefully mixed by hand and the bioreactors shaken before being connected to the air line.

The CO_2 evolved was measured using an indirect measurement method (Cumulative Measurement Respirometry) (working mechanism in the paragraph "Wet Scrubbers"). Three $Ba(OH)_2$ traps (1.8 L, 0.12 M) were installed in series after each bioreactor. The air flow through the bioreactors and the three traps in series was checked at least once per day. Sampling was carried out by removing 30 ml from the traps that were titrated using HCl 0.1 M with an automatic titrator (Metrohm, Switzerland, model 855, interfaced with a Tiamo® Software version 2.5 with a pump model 772 to empty measured samples). The automatic titrator was equipped with a 34-sample holder. For each sampling, the average of two titrations was considered. Titrations were carried out also on the $Ba(OH)_2$ pristine solutions (approximately 0.12 M) that filled up the $Ba(OH)_2$ traps to measure their exact initial molarity, to compute the moles of $Ba(OH)_2$ $(t = 0)$ of equation (S3).

The cumulative CO_2 evolved from the blank compost and from PE buried in compost are shown in Supplementary Figure 3.
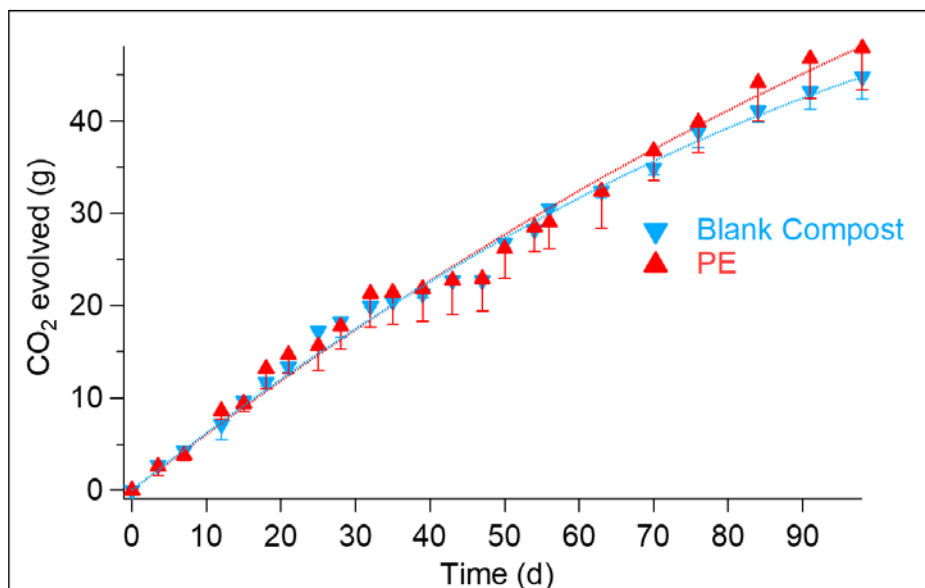
Supplementary Figure 3 Cumulative CO_2 production from the blank compost and PE buried in compost.

The samples with the blank compost and PE buried in compost had statistically equivalent apparent respiration rates (457 ± 24 mg/d and 488 ± 45 mg/d, respectively).
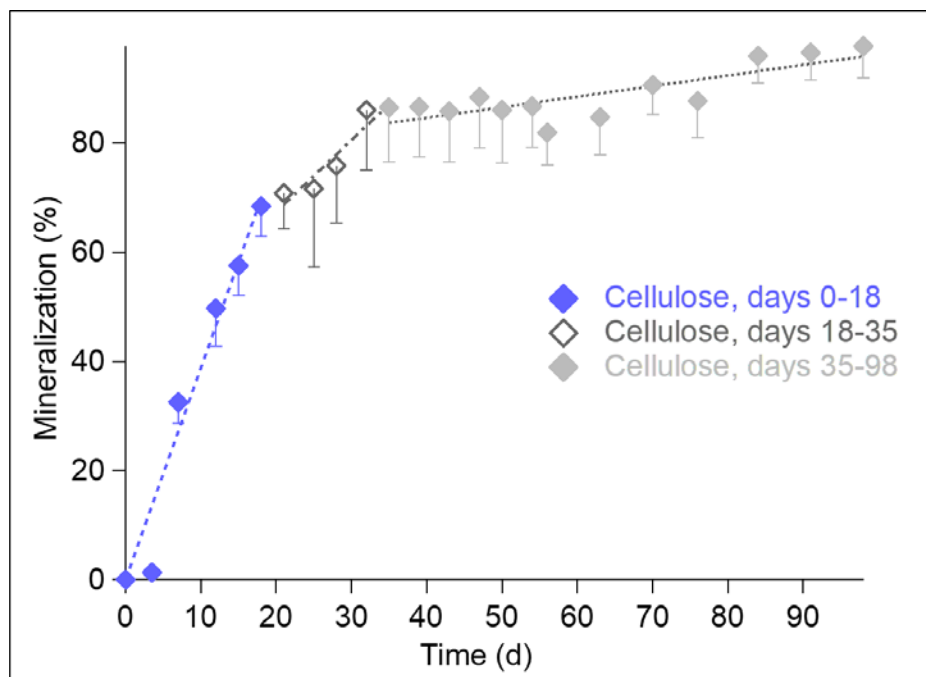
Supplementary Figure 4. The different rates of cellulose mineralization over 98 days of incubation: $\Delta t_{0\text{-}18}$, y = 3.87 x, R^2 = 0.9556; $\Delta t_{18\text{-}35}$, y = 1.31 x + 41.18, R^2 = 0.9024; $\Delta t_{35\text{-}98}$, y = 0.19 x + 76.84, R^2 = 0.6440 .

Cellulose showed a rate of mineralization of 3.9 %/d in $\Delta t_{0\text{-}18}$, reaching 68% mineralization, then 1.3 %/d in $\Delta t_{18\text{-}35}$ and finally it tended to plateau with a rate of 0.19 %/d in $\Delta t_{35\text{-}98}$, reaching 97% on day 98 (Supplementary Figure 4). The final mineralization value, projected over a 6-month incubation period, keeping the rate of $\Delta t_{35\text{-}98}$ (0.19 %/d), would be 100%.

Mineralization

The % of carbon by weight used to compute the mineralization levels (denominator of equation (2) of the main text) can be inferred from the molecular formula of the material, with the assumption that the tested materials are pure (absence of water or inorganic matter not present in the molecular formula). In practice, the extraction process could leave water or inorganic matter (i.e. salts) as residues. Water could also be absorbed in the storage environment. Consequently, we validated such theoretical computations experimentally. The dry solids, the ash content (inorganic matter) and the % of carbon by weight of the materials tested were measured. The ash content is the mass left after heating at 550°C in an oxidative environment and keeping such temperature until constant

mass was reached. It was obtained by means of TGA, entailing a ramp of 10 °C/min until 550°C and then an isotherm at 550°C until the DTG was lower than 0.01 %/min, in air atmosphere. The test was run on 4 samples for SM-E and 2 samples for the other materials.

The % of C by weight was measured by Galbraith laboratories, TN, USA (carbon, hydrogen, and nitrogen determination, average of 2 tests). The amount of inorganic carbon (carbonates) for Sepia Melanin was found to be negligible ($< 0.75\%$ wt.).

For Sepia Melanin, the mass of carbon present was obtained by multiplying the measured C % wt. by the organic matter (i.e. the dry solids after subtraction of the ash content).

The amounts of CO_2 for a complete mineralization (*CO_2(total)* of equation (3) of main text) of the materials tested, the negative control as well as the positive control in the biodegradability test under mesophilic conditions (25°C), test 1, and in the biodegradability test under mesophilic conditions (58°C), test 2, are listed in Supplementary Table 3.

Supplementary Table 3. Physicochemical properties of the materials tested.

Test Materials	Poly(p-phenylene sulphide)	Copper (II) phthalocyanine[4]	Polyethylene	Sepia Melanin	Cellulose
Formula	$(C_6H_4S)_n$	$Cu\ C_{32}H_{16}N_8$	$(CH_2)_n$	$(C_8H_7NO_2)_n$ + $(C_9H_7NO_4)_m$	$(C_6H_{10}O_5)_n$
Dry solids (wt. %)	99.64 ± 0.01	98.9 ± 0.2	100 ± 0	83.1 ± 0.3	94.8 ± 0.1
Theoretical C % in the formula (wt.)	67	67	86	N/A	44
Measured C % of dry solids (wt.)	65.66 ± 0.05	64.16 ± 0.01	N/A	66.1 ± 0.1	43.8 ± 0.1
Ash Content (wt. %)	5.2 ± 0.6	16 ± 1	0 ± 0	2.1 ± 0.4	0 ± 0

---

[4] The amount added was chosen taking into consideration that the dye content in the material as received was 90 % by weight, with the remaining 10 % being inorganic, as stated by the company Sigma-Aldrich.

CO$_2$ if complete mineralization occurred, test 1 (g)	N/D	N/D	N/D	19	13
CO$_2$ if complete mineralization occurred, test 2 (g)	51	51	66	41	32

Considering <u>equation (2)</u> of the main text, the standard error of mineralization, S_e, was computed following paragraph 12.3 of ASTM D5338 [339]:

$$S_e = \sqrt{\frac{s_{mat}^2}{n_1} + \frac{s_{blank}^2}{n_2}} * \frac{100}{CO_2(total)} \qquad \text{(S4)}$$

Where:

- s_{mat} is the standard deviation of the average measured mass of CO$_2$ evolved from the bioreactors containing the test material blended with the compost (average *CO$_2$(material)* of <u>equation (2)</u> of the main text); n_1 is the number of such bioreactors,

- s_{test} is the standard deviation of the average measured masses of CO$_2$ evolved from the bioreactors containing blank compost (average *CO$_2$ (blank compost)* of <u>equation (2)</u> of the main text); n_2 is the number of the bioreactors containing blank compost.

- *CO$_2$(total)* is the theoretical mass of CO$_2$ that would evolve if all the test material were completely respired by the microorganisms (<u>equation (3)</u> of the main text).

Phytotoxicity Test

A natural sandy soil (0.7% clay, 2.0% organic matter, 97.6% sand, 1.6% silt, and pH 5.5–6.0) from Valcartier (QC, Canada) was used as a non-contaminated substratum to conduct the phytotoxicity test [525]. Prior to seeding the sandy soil, its water content was adjusted to 8.3% wt., which is 75% of its water holding capacity. The water content of the compost samples, which were recovered from the bioreactors at end-point (98 d) of the biodegradability test under thermophilic conditions (58°C), was adjusted to 40% wt. Secondly, 77 g of the wet sandy soil was mixed with approximately 23 g of compost + test material, that is a 3.3:1 weight ratio. Twenty (20) seeds of ryegrass (*Lolium perenne*) were sown in 15 cm wide dishes (TC dish, Sarstedt #83-3903) containing 100 g of wet sandy soil with compost + test material. Such TC dishes were incubated

in sealed plastic bags to ensure the maintenance of the soil moisture throughout the duration of the germination test.

The phototoxicity test was conducted on eight samples:

a. Six samples of compost + test material used for the biodegradability in composting conditions test (blank compost, compost + PE, compost + cellulose, compost + Sepia Melanin, compost + PPS and compost + Cu-Pc).

b. Two samples of blank wet sandy soil for reference, of which:

    a. 100 g, for reference of this test

    b. 220 g, for comparison with previous works [526].

The wet sandy soil sample (100 g) shows a seedling emergence of 93% with respect to the wet sandy soil sample (220 g) after seven days. The results from 100 g and 220 g of wet sandy soil are statistically equivalent, therefore the wet sandy soil sample (100 g) was taken as the reference for the other samples.

The test was performed in a temperature and light controlled growth chamber (Conviron Inc., Winnipeg, MB, Canada). Planted seeds were incubated in total darkness for the first 2 d, then they were exposed to a diurnal photoperiod cycle. Such cycle implied dark for 8 h at 20°C and light for 16 h at 25°C with a light intensity of $5,000 \pm 500$ lux. Luminosity level was measured weekly using a photometer, and the light intensity was readjusted when needed. The measurement endpoint, after 19 d, included seedling emergence, shoot wet mass, and shoot dry mass. Shoots were cut just above the soil line, and fresh mass was determined immediately. Total dry mass was determined after drying the plants at 70°C for 24 h.

Methods of Supporting Information

Infrared spectra of the melanin samples were recorded with a resolution of 4 cm^{-1} using a Bruker Optics Vertex 70 FT-IR spectrometer equipped with a DLaTGS detector. The spectra shown in Supplementary Figure were recorded in transmission by dispersing the melanin powders in KBr and pressing them into 7 mm pellets using a Pike Technologies Hand Press (WI, USA). The

spectrum of a pure KBr pellet was subtracted and a concave rubber band baseline correction (a single iteration) was applied. Each spectrum was normalized with respect to the highest band for the sake of comparison.

TGAs were carried out by means of a TGA 2950 thermogravimetric analyser (TA Instruments, Inc.). The atmosphere (argon, nitrogen or air), flow of 90 $cm^3\,min^{-1}$, as well as the thermal history (ramp or isotherm), are specified for each test in the SI.

Nuclear activation analysis was performed with a SLOWPOKE nuclear reactor (Atomic Energy of Canada Limited) and a germanium semiconductor gamma-ray detector (Ortec, GEM55185). The samples were irradiated for 600 s at an average thermal neutron flux of 5 x 10^{11} $cm^{-2}\,s^{-1}$.

The analysis of the amount of C by weight was performed by Galbraith Labs, Inc, USA. A PerkinElmer 2400 Series II CHNS/O Analyzer (Governing SOP: ME-14, Analyte: Carbon, Hydrogen, Nitrogen, Range: > 0.5 % CHN) was used. This instrument burns sample in pure O_2 at 920 – 980°C under static conditions to produce combustion products of CO_2, H_2O, and NO_x. The PE-2400 automatically separates and analyzes these products in a self-integrating, steady state thermal conductivity analyzer.

The Inorganic Carbon test of Sepia Melanin extracted from cuttlefish ink was performed by Galbraith labs, Inc, USA, too. This method determines carbon dioxide, carbonic acid, bicarbonate ion, and carbonate ion. A Carbon Dioxide Coulometer Model CM 5014, Coulometrics, Inc was used. This method liberates CO_2 from the sample through acidification with H_2SO_4 solution and heat. CO_2-free nitrogen gas sweeps the evolved CO_2 through a scrubber and into an absorption cell, which coulometrically titrates.

APPENDIX E – SUPPORTING INFORMATION OF ARTICLE 4

On the Interfaces Between Organic Bio-sourced Materials and Metals for Sustainable Electronics: the Eumelanin Case

Eduardo Di Mauro, Emilie Hebrard, Yasmina Boulahia, Marco Rolandi and Clara Santato

Jpn. J. Appl. Phys., vol. 58, no. 5, p. 051014, May 2019. doi: 10.7567/1347-4065/ab1061.

Table S1: Summary of the occurrence of metal electrode dissolution under bias from the literature and the present work.

Do the metal dissolution and structure growth take place (90% RH)?		
Metal	Synthetic eumelanin, 8% wt. Cl^-	Sepia Melanin, 7% wt. Cl^-
Au	Yes [210]	Yes [210]
Pd	Yes (no if RH < 90%)	Yes (no if RH < 90%)
Cu (treated)	Yes (temp.)	No
Cu (untreated)	Yes (temp.)	N.D.
Fe (treated)	Platelets	Platelets
Fe (untreated)	Platelets	Platelets
Ni (treated)	No	No
Ni (untreated)	No	No

Temp.= temporary current increase

N.D.= not determined, trivial as the treated Cu did not show dissolution.

Table S2: Gibbs Free Energy of the oxidation reaction, $\Delta G° = -(-nFE^0)$, with n being the number of electrons exchanged between the oxidized and reduced species, F the Faraday constant and E^0 the standard reduction potential [527], [528].

Oxidation Reaction	$\Delta G°$ (J/mol)	Equation
$Au + 2\ Cl^- \rightarrow AuCl_2^- + e^-$	1.1.E+05	S1
$AuCl_2^- + 2\ Cl^- \rightarrow AuCl_4^- + 2e^-$	1.8.E+05	S2
$Au + 4\ Cl^- \rightarrow AuCl_4^- + 3e^-$	2.9.E+05	S3
$Pd + 4\ Cl^- \rightarrow [PdCl_4]^{2-} + 2e^-$	1.1.E+05	S4
$[PdCl_4]^{2-} + 2\ Cl^- \rightarrow [PdCl_6]^{2-} + 2e^-$	2.5.E+05	S5
$Cu + Cl^- \rightarrow CuCl + e^-$	1.3.E+04	S6
$2\ Cu + 2\ OH^- \rightarrow Cu_2O + H_2O + 2e^-$	-6.9.E+04	S7
$Fe + 2\ OH^- \rightarrow Fe(OH)_2 + 2e^-$	-1.7.E+05	S8
$2\ Fe(OH)_2 + 2\ OH^- \rightarrow Fe_2O_3 + 3\ H_2O + 2e^-$	-1.6.E+05	S9
$Ni + 2\ OH^- \rightarrow Ni(OH)_2 + 2e^-$	-1.4.E+05	S10
$Ni(OH)_2 + 2\ OH^- \rightarrow NiO_2 + 2H_2O + 2e^-$	-9.4.E+04	S11

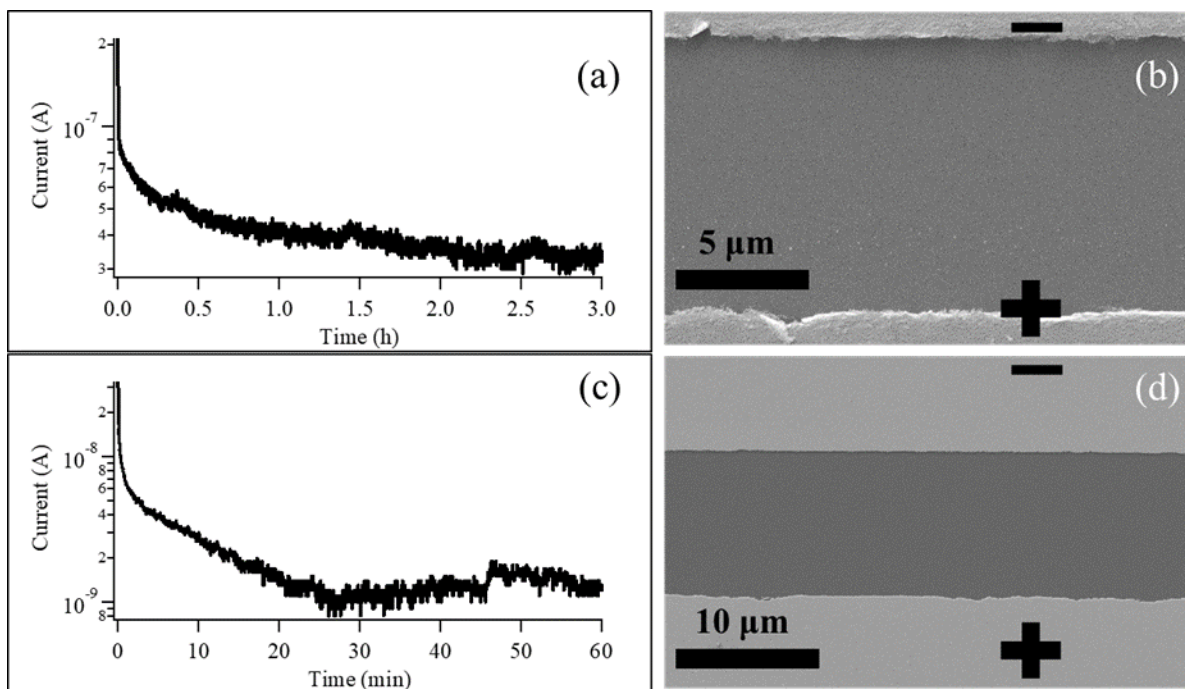**Eumelanin and Palladium Electrodes: effect of RH and Cl⁻ content**

Figure S1. Current vs time plots, and related SEM images of the interelectrode area, obtained with: (a-b) a synthetic eumelanin thin film with 1% wt. Cl⁻, hydrated for 1 hour at 90% RH, spin coated on a substrate patterned with Pd electrodes, bias time of 3 hours; (c-d) a synthetic eumelanin thin film with 8% wt. Cl⁻, hydrated for 1 hour at 70% RH, spin coated on a substrate patterned with Pd electrodes, bias time of 1 hour; 1 V electrical bias; images taken in secondary electron mode, at 10 kV (b) and 5 kV (d).

Eumelanin and Copper Electrodes: effect of Cl⁻ content and Sepia Melanin
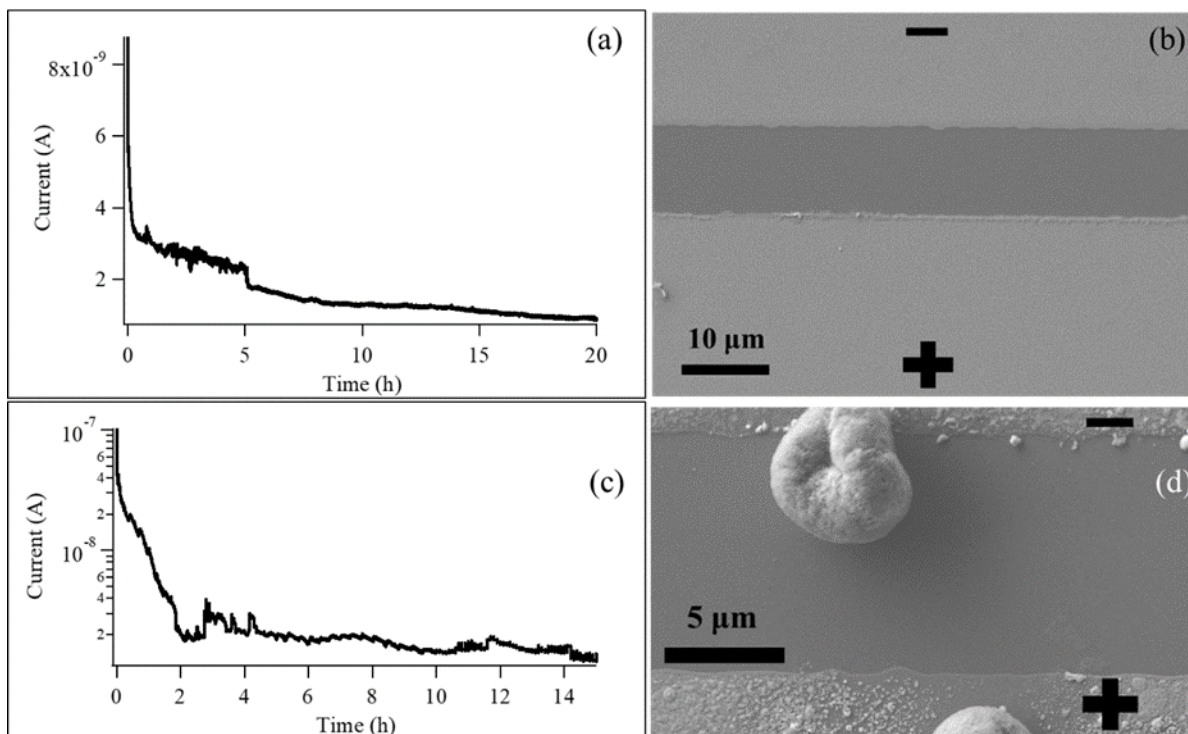
Figure S2. Current vs time plots, and related SEM images of the interelectrode area, of eumelanin films spin coated on treated Cu electrodes: (a-b) synthetic eumelanin film, 1% wt. Cl⁻, bias time of 20 hours; (c-d) Sepia Melanin film, hydrated for 1 hour at 90 % RH, bias time of 15 hours; 1 V electrical bias; images taken in secondary electron mode at 5 kV.

Iron Electrodes: synthetic eumelanin (8% wt. Cl⁻) with untreated and treated electrodes, Sepia Melanin with untreated and treated electrodes
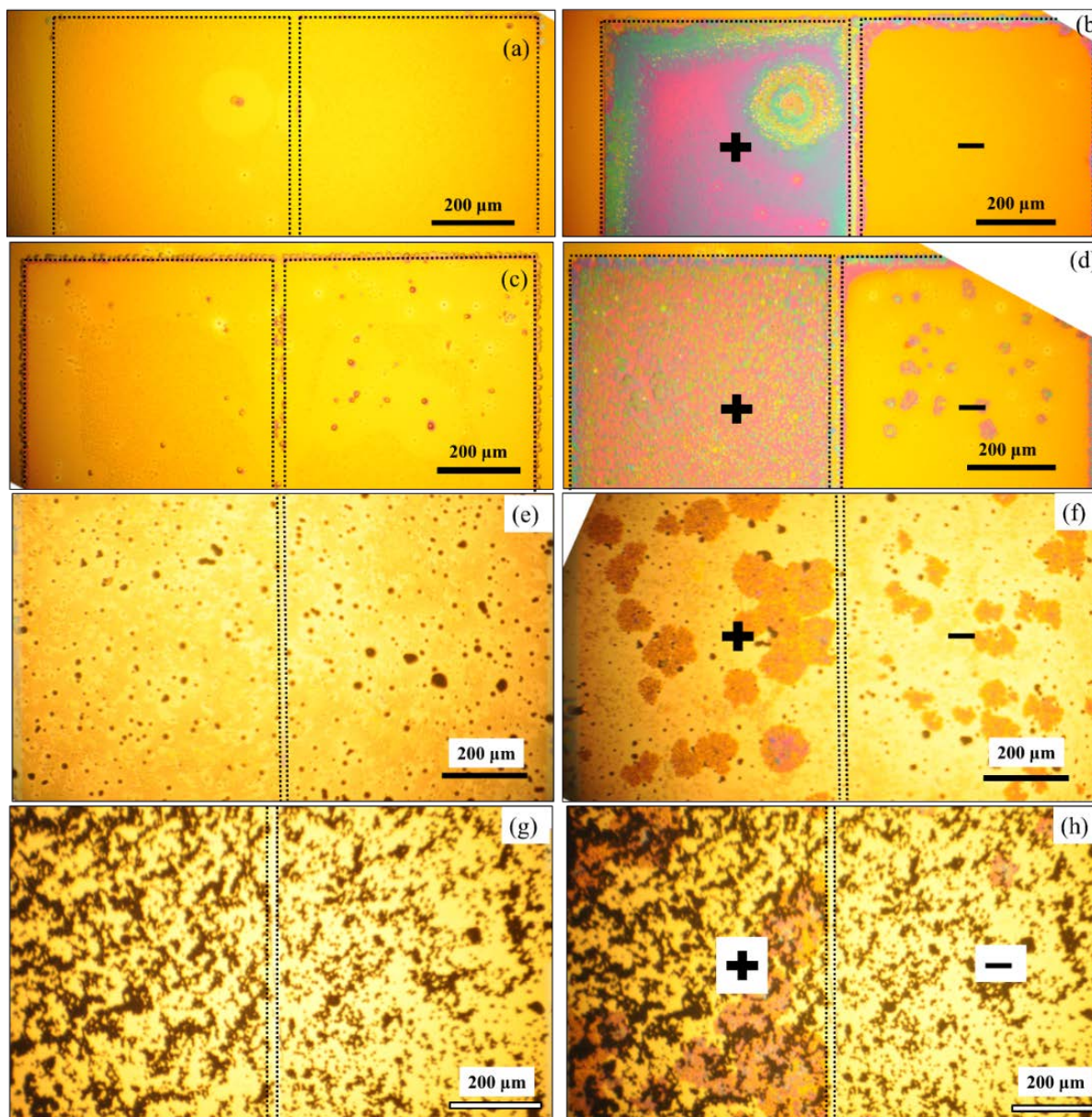
Figure S3. Optical images of eumelanin films hydrated for 1 hour at 90% RH: (a-b) synthetic eumelanin film, 8% wt. Cl⁻, spin coated on substrates patterned with Fe electrodes (untreated), before (a) and (b) after the electrical bias application (19 hours); (c-d) synthetic eumelanin film, 8% wt. Cl⁻, spin coated on substrates patterned with Fe electrodes (treated), before (c) and (d) after the electrical bias application (22 hours); (e-f) Sepia Melanin film, 7%, wt. Cl⁻, spin coated on substrates patterned with Fe electrodes (untreated), before (e) and (f) after the electrical bias

application (18 hours); (g-h) Sepia Melanin film, 7%, wt. Cl⁻, spin coated on substrates patterned with Fe electrodes (treated), before (g) and (h) after the electrical bias application (22 hours); the electrical bias is 1 V; the black dotted line delimits the electrodes in figures (a-d) and the interelectrode area in figures (e-h).

Iron Electrodes: untreated and treated electrodes with synthetic eumelanin (8% wt. Cl⁻), treated electrodes with Sepia Melanin
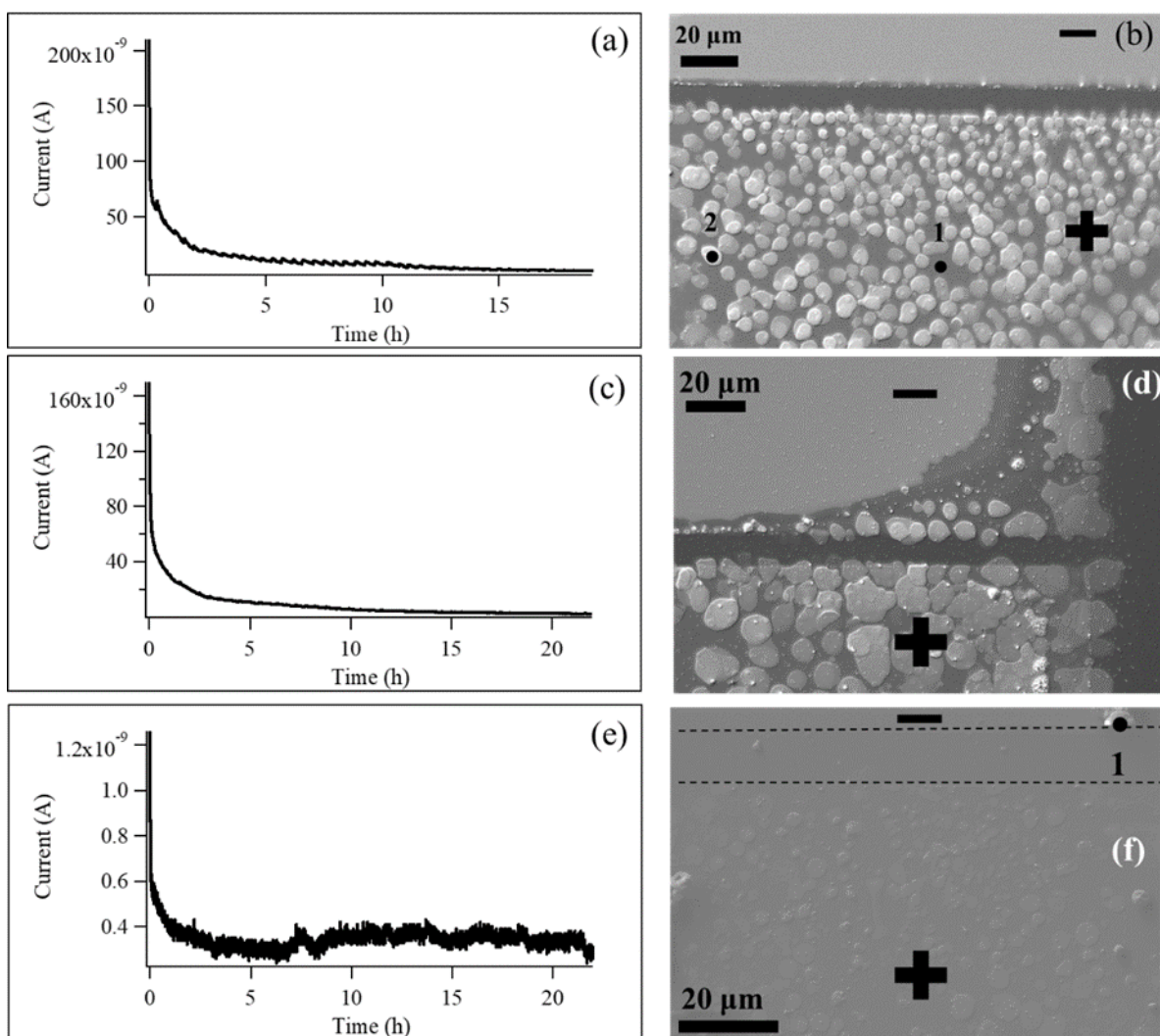

Figure S4. Current vs time plots, and corresponding SEM images, obtained with: (a-b) a synthetic eumelanin film, 8% wt. Cl⁻, spin coated on substrates patterned with Fe electrodes (untreated) and hydrated for 1 hour at 90% RH, bias time of 19 hours; (c-d) synthetic eumelanin film, 8% wt. Cl⁻, spin coated on substrates patterned with Fe electrodes (treated) and hydrated for 1 hour at 90%

RH, bias time of 18 hours; (e-f) Sepia Melanin film, 7% wt. Cl⁻, spin coated on substrates patterned with Fe electrodes (treated) and hydrated for 1 hour at 90% RH, bias time of 22 hours, where the dotted black line delimits the interelectrode area and point 1 corresponds to a Sepia Melanin aggregate that moved while the image was taken; 1 V electrical bias; images taken in secondary electron mode, at 5 kV.

Point 1 of Figure S4(b) is devoid of Fe; it is reasonable to assume that the platelet indicated by point 2 of Figure S4(b) is constituted of iron oxide (at. %: 57% O, 22% Fe, 9% Si, 9% C).

Nickel Electrodes: synthetic eumelanin (8% wt. Cl⁻) with untreated and treated electrodes, Sepia Melanin with untreated and treated electrodes
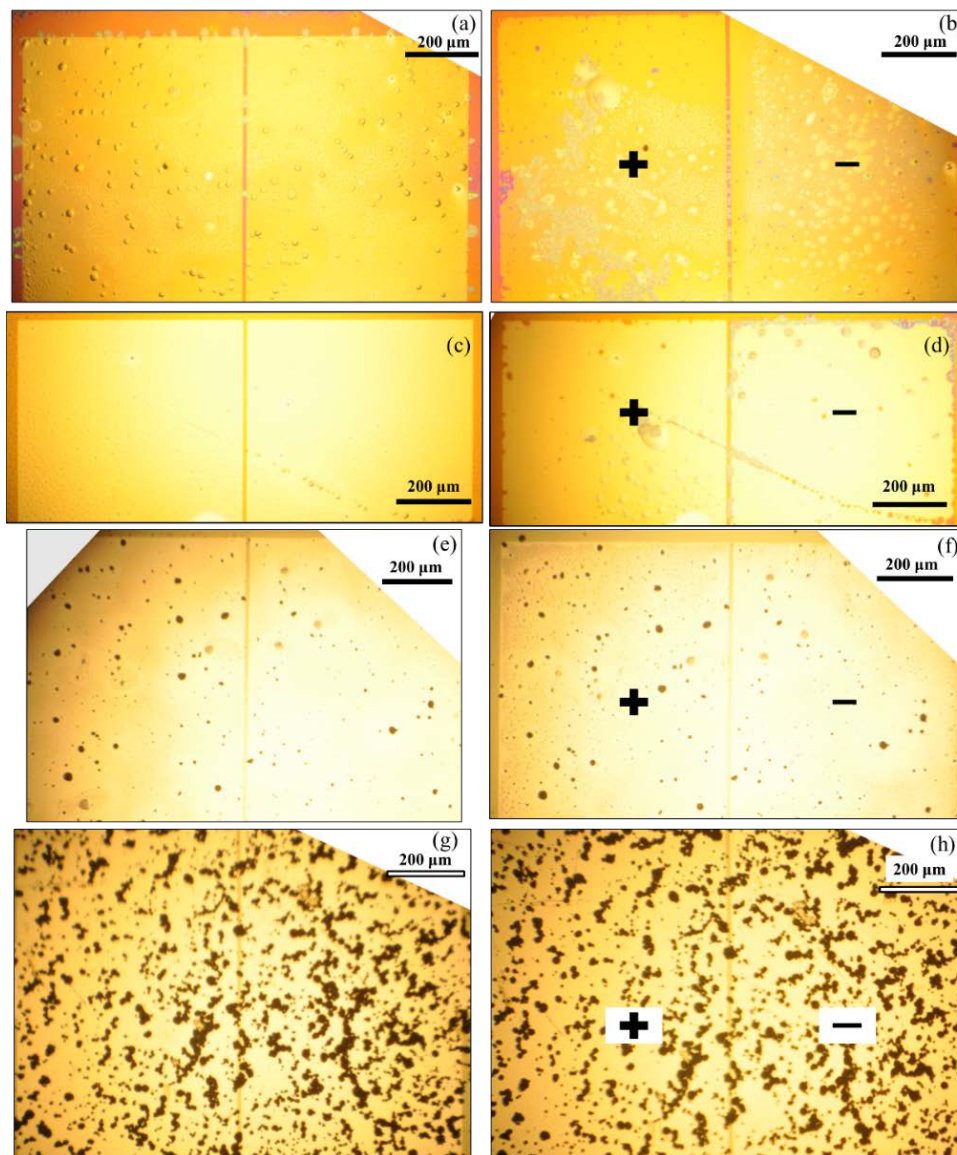

Figure S5. Optical images of eumelanin films hydrated for 1 hour at 90% RH: (a-b) synthetic eumelanin film, 8% wt. Cl⁻, spin coated on substrates patterned with Ni electrodes (untreated), before (a) and (b) after the electrical bias application (27 hours); (c-d) synthetic eumelanin film, 8% wt. Cl⁻, spin coated on substrates patterned with Ni electrodes (treated), before (c) and (d) after the electrical bias application (27 hours); (e-f) Sepia Melanin film, 7%, wt. Cl⁻, spin coated on substrates patterned with Ni electrodes (untreated), before (e) and (f) after the electrical bias

application (17 hours); (g-h) Sepia Melanin film, 7%, wt. Cl⁻, spin coated on substrates patterned with Ni electrodes (treated), before (g) and (h) after the electrical bias application (20 hours); the electrical bias is 1 V.

Nickel Electrodes: treated and untreated electrodes with synthetic eumelanin (8% wt. Cl⁻), treated electrodes with Sepia Melanin
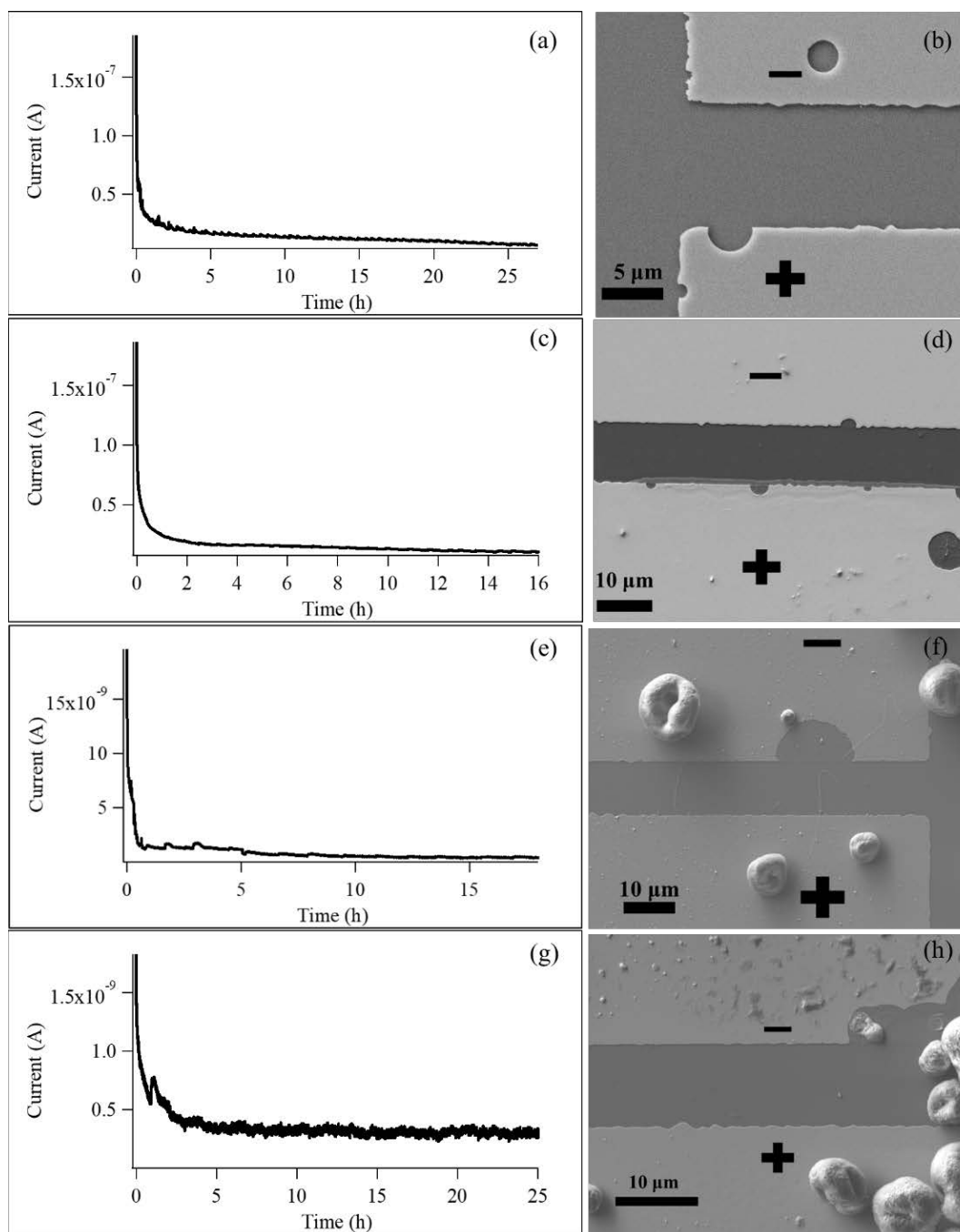

Figure S6. Current vs time plots, and corresponding SEM image of the interelectrode area, obtained with thin film spin coated on substrates patterned with Ni electrodes and hydrated for 1 hour at 90% RH (a, b) synthetic melanin 8% wt. Cl⁻ , untreated Ni electrodes, bias time of 27

hours; (c, d) synthetic melanin 8% wt. Cl⁻, treated Ni electrodes, bias time of 16 hours; (e, f) Sepia Melanin, treated Ni electrodes, bias time of 25 hours; 1 V electrical bias. Images taken in secondary electron mode, at (b) 10 kV and 5 kV (d, f) 5 kV. The spheres are aggregates of Sepia Melanin.

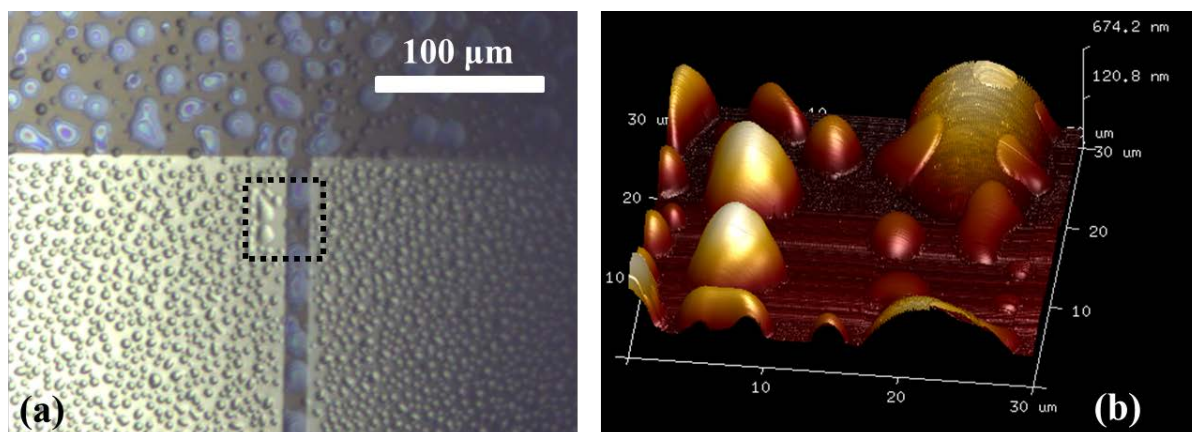**The Surface of Hydrated Eumelanin Films Spin Coated on Au electrodes**

Figure S7. (a) Synthetic eumelanin film spin coated on substrates patterned with Au electrodes, at 86% RH, after 1 hour; (b) AFM 3-D image of the area delimited by the dotted rectangle of figure (a).
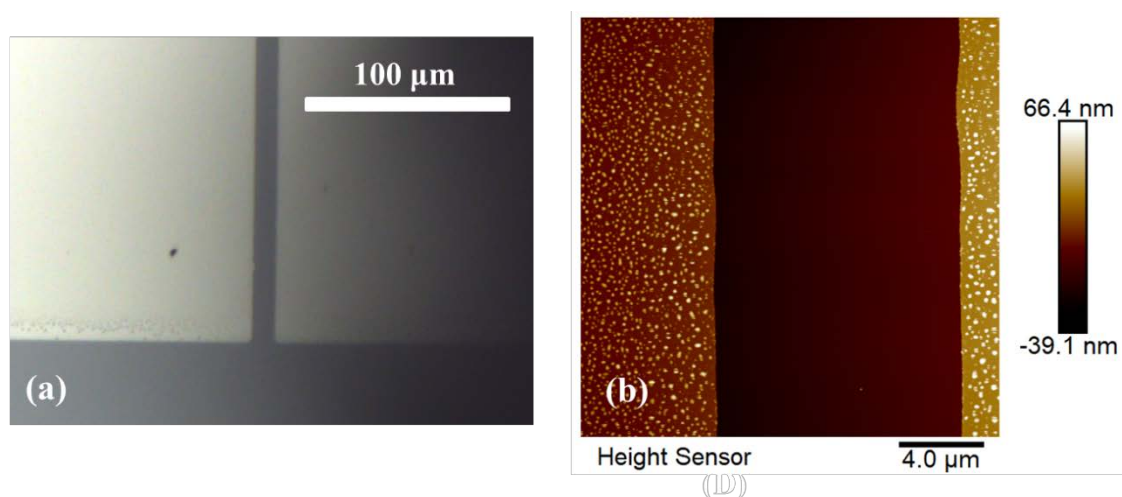

Figure S8. (a) Bare SiO_2 substrates patterned with Au electrodes at 82% RH, after 1 hour; (b) AFM image of the interelectrode distance of blank patterned Au electrodes at 80% RH.

After 60 minutes with RH increasing from 25% to 85%, drops of water with a diameter of up to tens of micrometers form on thin films of synthetic eumelanin spin coated on the patterned substrates (Figure S7); for the sake of comparison, bare patterned Au electrodes at the same RH level present drops with diameters of 2-3 orders of magnitude lower (Figure S8). The system under electrical bias can thus be the one schematized in Figure 2(c) of the main text.
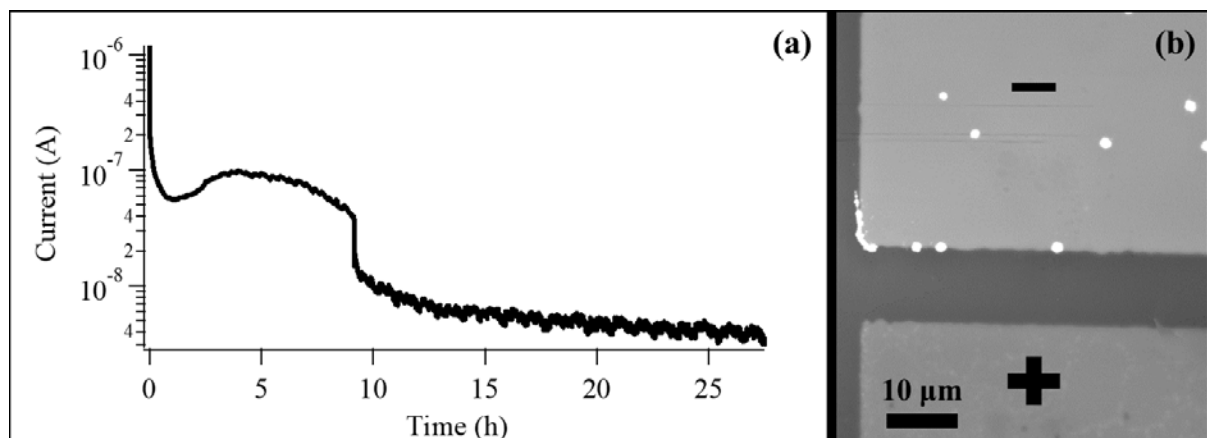

Figure S9. (a) Current vs time plot obtained with a synthetic eumelanin thin film, 8% wt. Cl⁻ content, hydrated for 1 hour at 90 % RH and then buried under a drop-cast chitosan layer (10 mg/ml in DI water, 1% acetic acid, 1 mg/ml NaCl) at 90% RH, 1 V electrical bias for 27 hours and (b) related SEM image of the interelectrode area taken in backscatter electron mode, at 30 kV. The eumelanin thin film was obtained by means of 5 spin coatings on the substrate patterned with Au electrodes, to maximize the filling of the interelectrode distance. The sample was metallized (2 nm Au on the surface) prior to imaging.

In Figure S9, chitosan was used to bury eumelanin films spin coated on a substrate patterned with Au electrodes, to avoid the formation of water drops on eumelanin films (but, at the same time, preventing the dehydration or Cl⁻ depletion of the underlying eumelanin film). Such solution had a concentration of 10 mg/ml in DI water, 1% acetic acid, 1 mg/ml NaCl [145].

APPENDIX F – PARTICIPATION TO CONFERENCES

1. **E. Di Mauro**, X. Ri, D. Boisvert, S. Zhang, P. Kumar, F. Cicoira, C. Santato, "Resistive switching in thin films of the pigment eumelanin in contact with different metal electrodes under bias", 2016 MRS Fall Meeting and Exhibit, Materials Research Society, Oral; Boston, USA, 27/11/2016;

2. **E. Di Mauro**, L. G. S. Albano, F. Cicoira, C. F. Graeff, C. Santato, "The pigment eumelanin and its metal chelation properties: a first screening on a potential candidate for green electronics", Energy Materials Nanotechnology, Oral; Hong Kong, 12/01/2016;

3. **E. Di Mauro**, L. G. S. Albano, O. Carpentier, M. Lalancette-Jean1, S. I. Yáñez Sánchez, N. Ignoumba Ignoumba, F. Cicoira, C. F. Graeff., Clara Santato, "Eumelanin thin films and metal electrodes: nanostructures formation under electrical bias for memory applications", 2015 MRS Fall Meeting and Exhibit, Materials Research Society, Oral; Boston, USA, 28/11/2015.

APPENDIX G – AWARD

01/06/2017, 3rd placed at the contest *Le génie en Images* (presentation of scientific images as art masterpieces and vulgarization of the explanation of their content)